Determination of Pb-210 and Po-210 in aqueous environmental samples

Von der Naturwissenschaftlichen Fakultät der
Gottfried Wilhelm Leibniz Universität Hannover
zur Erlangung des Grades
Doktor der Naturwissenschaften (Dr. rer. nat.)
genehmigte Dissertation
von

M. Sc. Lena Yvonne Johansson

geboren am 13. Oktober 1976 in Frändefors, Schweden

2008

Referentin: Prof. Dr. Carla Vogt
Korreferent: Prof. Dr. Rolf Michel
Tag der Promotion: 28.07.2008

Abstract

The naturally occurring radionuclides Pb-210 and Po-210, arising from the uranium-radium decay series, provide a considerable contribution to the radiation exposure to humans over mobile, aqueous systems. Since environmental compartments are generally not closed systems, the individual radionuclides of a decay series may behave differently due to dissimilar chemical properties, which result in radiochemical disequilibria. Therefore, it is very important to be able to determine the activities both Pb-210 and Po-210 separately.

The chemical separation of lead and polonium is performed by solid phase extraction using the *Pb Resin*. In order to simultaneously retain both lead and polonium, a concentration of $c(\mathrm{HCl}) = 2\ \mathrm{mol\ l^{-1}}$ is chosen for the sample load; Po-210 is selectively stripped from the cartridge with diluted nitric acid ($c\ = 1\ \mathrm{mol\ l^{-1}}$ and $c = 0.1\ \mathrm{mol\ l^{-1}}$, respectively). Moreover, Po-210 and Pb-210 are quantitatively separated from each other; Pb-210 is completely stripped from the cartridge with distilled water.

The activity measurement of Pb-210 in water samples is generally difficult, due to its weak gamma radiation ($E_\gamma = 46.5$ keV with $P_\gamma = 4.05$ %) and its low energetic beta radiation ($E_{\beta\mathrm{max}} = 63$ keV). The determination of Pb-210 via LSC is usually performed subsequent to chemical separation by measuring the beta activity of the daughter Bi-210, after about 30 days of ingrowth. The Pb-210 yield is determined by ICP-MS measurement of the added stable lead carrier and yields > 90 % are reached. Po-210 is a pure alpha emitter and is measured via alpha spectrometry. The polonium fraction can directly be utilized for the making of alpha sources by spontaneous deposition. The overall chemical yield for Po-210 is determined over Po-208 tracer and reaches 75 per cent.

The detection limit for Po-210 is as low as 0.2 mBq kg^{-1}, which is more than adequate for the determination of environmental water samples as well as ground- and drinking water. For Pb-210, decision thresholds and detection limits of 10 mBq kg^{-1} and 20 mBq kg^{-1}, respectively, are reached for sample volumes of 1 l and a measurement time of 24 h.

The newly developed method can be applied for the analyses of all kinds of environmental water samples containing Pb-210 and Po-210; unpolluted natural waters, as well as waters polluted by mining activities, such as the coal mining affected area near Rheinberg (NRW) and uranium mining affected region of Mailuu Suu, Kyrgyzstan. Furthermore, the obtained measurement results lead to a better understanding of the studied disequilibria as well as mobilisation processes and it enable a realistic radiological dose assessment.

Keywords

Pb-210, Po-210, disequilibria

Kurzzusammenfassung

Beim Transport über wässrige Systeme liefern die natürlich vorkommenden Radionuklide Pb-210 und Po-210 aus der Uran-Radium-Zerfallsreihe einen erheblichen Beitrag zur Strahlenexposition des Menschen. Da es sich in der Umwelt oft um nicht abgeschlossene Systeme handelt, können sich die einzelnen Radionuklide einer Zerfallskette wegen ihrer unterschiedlichen chemischen Eigenschaften deutlich uneinheitlich verhalten, wodurch radioaktive Ungleichgewichte entstehen. Daher müssen die Pb-210- und Po-210-Aktivitäten separat gemessen werden.

Die chemische Trennung von Blei und Polonium wird mittels Festphasenextraktion unter Verwendung vom *Pb-Resin* durchgeführt. Die Probenaufgabe erfolgt in salzsaurer Lösung ($c = 2$ mol l^{-1}), um Blei und Polonium simultan zu extrahieren. Polonium lässt sich selektiv mit Salpetersäure ($c = 1$ mol l^{-1} bzw. $c = 0{,}1$ mol l^{-1}) eluieren. Polonium und Blei werden quantitativ voneinander getrennt; das Blei wird mit wenig Wasser von der Säule ausgewaschen.

Die Bestimmung von Pb-210 in Umweltproben ist wegen der schwachen Gamma-Strahlung ($E_{\gamma} = 46{,}5$ keV mit $P_{\gamma} = 4{,}0$ %) und der niedrigen Energie der Betastrahlung ($E_{\beta max} = 63$ keV) schwierig. Die Bestimmung von Pb-210 per LSC erfolgt üblicherweise nach chemischer Trennung über die Messung der Beta-Aktivität des Tochternuklids Bi-210 nach etwa 30 Tagen Einwachszeit. Die chemische Ausbeute von Pb-210 lässt sich mittels ICP-MS anhand der Ausbeute des stabilen Bleis bestimmen und liegt bei > 90 %. Po-210 ist ein reiner Alphastrahler und wird per Alphaspektrometrie gemessen. Die Polonium-Fraktion kann zur Herstellung von Messpräparaten mittels Autodeposition direkt eingesetzt werden. Die gesamte Ausbeute von Po-210 wird über einen Po-208-Tracer bestimmt und liegt bei 75 %.

Die Nachweisgrenze von Po-210 beträgt 0,2 mBq kg^{-1}, niedrig genug für die Bestimmung von sowohl wässrigen Umweltproben, als auch Grund- und Trinkwasserproben. Für Pb-210 liegen die Erkennungsgrenze und die Nachweisgrenze bei 10 bzw. 20 mBq kg^{-1}, bei einem Probenvolumen von 1 Liter und einer Messzeit von 24 h.

Die neu entwickelte Methode kann im Bereich der Radioökologie bei allen Arten von wässrigen Umweltproben zur Anwendung kommen; auf nicht belastete, natürliche Gewässer, sowie bergbaulich belastete Wasserproben, wie z.B. aus der durch Kohlebergbau beeinflusste Region in Rheinberg (NRW) oder der durch Uranbergbau belasteten Gebiet in Mailuu-Suu, Kirgisistan. Die dabei gewonnenen Messergebnisse sollen zu einem besseren Verständnis der betrachteten Ungleichgewichte und Transportvorgänge beitragen und eine Festlegung von realistischen radioökologischen Modellparametern ermöglichen.

Schlagworte

Pb-210, Po-210, Ungleichgewichte

Contents

1 Introduction and Scientific Aim

Lead-210 and polonium-210 are naturally occurring, relatively long-lived radionuclides of the U-238 decay series, with half-lives of 22.3 y and 138.4 d, respectively. They are released into air by the emanation of radon-222 from soil surfaces. Rn-222 is a noble gas and may diffuse through fissures into aquifer layers, where its long-lived decay products (Pb-210 and Po-210) can dissolve. However, both Pb-210 and Po-210 are particle reactive and are rapidly removed from the water column by adsorption onto sinking particulates or they may be co-precipitated with ferric hydroxides and manganese oxides. Due to different chemical properties of Pb-210 and Po-210, the extent of the removal varies independently of each other with the water properties and results in radiochemical disequilibria. If both radionuclides are in equilibrium, it is only necessary to measure either the mother or the daughter, depending on which is easier to determine. However, in environmental water samples, Pb-210 and Po-210 cannot be assumed to be in radioactive equilibrium with each other and therefore it is highly important to be able to determine both separately.

The major sources of technically enhanced natural radioactivity are mining activities (uranium, coal, and mineral sands), combustion of coal and fossil fuels and other energy production such as geothermal energy, and the use of phosphate rock. In industrial processes associated with the extraction and processing of minerals, the hazard arising from radiation is generally small compared to that from other chemical substances. Hitherto very little account has been taken to this technically enhanced natural radiation and the doses which arise thereof. In regions of excessive mining, the contaminations are caused by dissolved radionuclides from the U-238 and Th-232 decay chains which are brought to the surface by the mine water drainage and discharged into the nearby water systems, or the mine wastes are deposited in the close proximity of the mines, which are then exposed to weathering and leaching of radionuclides with water. This technically enhanced natural radioactivity also includes Pb-210 and Po-210, which may lead to elevated radiation exposure to people living in these areas and who may use contaminated water for drinking purposes. Furthermore, the dose coefficients for ingestion of Pb-210 and Po-210 [1] are relatively high. Pb-210 clearly plays an important role in human radiation exposure, since it possesses long residence times in the skeleton and thus highly contributes to the skeletal dose [2]. According to the UNSCEAR Report from 1988 [3], both Pb-210 and Po-210 significantly contribute to the radiation dose of the population, with 8 % of the natural internal radiation dose to man. This stresses the importance of the simultaneous determination of Pb-210 and Po-210 in aqueous samples, as well as measurement techniques with low detection limits, which in turn enables a realistic dose assessment.

In order to achieve low detection limits, a chemical separation is required. Solid phase extraction has found increasing use for the purification of both Pb-210 and Po-210, in particular the strontium extractant based on crown ethers. Horwitz *et al.* [4] have developed an extraction chromatographic resin for the separation of strontium (*Sr Resin*), based on a crown ether (4,4'(5')-bis-(*t*-butyl-cyclohexano)-18-crown-6).

This crown ether also shows a very high selectivity for lead with a maximum distribution coefficient of 10^3. The maximum distribution coefficient for polonium on *Sr Resin* is about 10^2 in nitric acid (c = 0.5–1.0 mol l^{-1}); at higher concentrations it decreases abruptly [4]. The *Sr Resin* was later modified to even better fit the extraction of lead. This new resin was denoted *Pb Resin* and contains the same crown ether, only in a lower concentration and a different solvent [5]. Distribution coefficients for polonium on the *Pb Resin* have not been determined.

Vajda *et al.* [6] found that even under maximum polonium retention in nitric acid solution, lead and polonium could not be efficiently separated by the *Sr Resin*, since polonium was released from the column before bismuth had been eluted. However, a simultaneous separation of lead and polonium was achieved from a hydrochloric acid solution. Lead is retained by the *Sr Resin* to a lesser extent in hydrochloric acid than in nitric acid at the same concentrations, but polonium has a higher distribution coefficient in hydrochloric acid and can be retained, although with recoveries of only 70 %. In the method developed by Vajda *et al.*, the sample load is performed in hydrochloric acid (c = 2 mol l^{-1}), polonium is eluted with nitric acid (c = 6 mol l^{-1}) and lead is subsequently eluted with HCl (c = 6 mol l^{-1}). The lead fraction was evaporated, the chemical yield was determined gravimetrically and finally the Pb-210 activity was determined via liquid scintillation counting (LSC). The high acid concentrations used in this method complicate a direct measurement via LSC, since most scintillation cocktails are sensitive to acid quench: a direct mixing of a larger fraction of the sample with the cocktail is therefore not possible.

Eichrom Technologies has developed a selective method for the determination of Pb-210 in water using the *Pb Resin* [7], based on the 18-crown-6-ether mentioned above. The sample load is performed in diluted nitric acid (c = 1 mol l^{-1}); polonium is eluted with nitric acid (c = 0.1 mol l^{-1}) and lead with 20 ml of distilled water. Bismuth is not retained by the resin at all. By using this method similar problems occurred by the separation of polonium as Vajda *et al.* found for the *Sr Resin*: no separate polonium fraction was obtained.

The activity measurement of Pb-210 in environmental water samples is, however, generally difficult, due to its weak gamma radiation (E_γ = 46.5 keV with P_γ = 4.05 %), its low energetic beta radiation ($E_{\beta,max}$ = 63 keV), and the weak internal conversion electrons (8, 30 and 43 keV). For this reason, the determination of Pb-210 is generally performed after chemical separation by measuring the beta activity of the daughter nuclide Bi-210 ($E_{\beta,max}$ = 1.2 MeV) by LSC. Polonium-210, on the other hand, is a pure alpha emitter and for this reason the determination of Po-210 can only be carried out by alpha spectrometry, most commonly using passivated implanted planar silicon (PIPS) detectors, after proper alpha source preparation, usually taking advantage of the fact that polonium ions in solution spontaneously deposit onto less noble metal surfaces, such as nickel or silver. A yield tracer (usually Po-208) of known activity is added as internal standard. Chemical pre-concentration is not always performed and leaving it out may save time [8], but the presence of interfering ions makes the procedure undependable both by reducing the deposition yield of polonium as well as increasing the thickness of the deposited layer, which in turn will negatively affect the alpha

spectrometric determination. Therefore, a chemical separation of polonium from interfering radionuclides and matrix elements prior to the spontaneous deposition is preferred.

1.1 Aim of study

The purpose of this work is the development of a method for the simultaneous determination of Pb-210 and Po-210 from the same aqueous sample using solid phase extraction. Furthermore, the measurement techniques and sample source preparation shall be optimized, in order to achieve the lowest possible detection limits. The optimization of the measurement techniques generally includes the minimization of the background count rates as well as the determination of the most favourable measurement parameters, for liquid scintillation counting as well as for alpha spectrometry. The sample source preparation for the alpha spectrometric determination of polonium will be optimized, in order to achieve highly reproducible alpha sources with high resolution.

Until now the detection limits reached by the gamma spectrometric determination of Pb-210 in aqueous samples of 0.5 litres were in the order of 100 mBq per litre, which is evidently too high for natural environmental water samples. Low detection limits are important for a realistic dose assessment, especially in regions of technically enhanced natural radiation. If no actual activity concentration can be determined, the detection limits have to be used in the dose assessment instead, which clearly will lead to an overestimation of the radiation dose. Since Po-210 solely emits alpha radiation it cannot be determined via gamma spectrometry. For that reason, Po-210 is usually assumed to be in radioactive equilibrium with Pb-210, which once again undoubtedly leads to an overestimation of the dose.

The newly developed method will be applied on unpolluted, natural waters, as well as waters polluted by mining activities, such as coal mining, but also uranium mining. Additionally, the gained measurement results should lead to a better understanding of the studied disequilibria as well as mobilisation processes and furthermore enable a realistic radiological dose assessment.

2 Radioactivity in the Environment

Radioactivity was discovered by Henri Becquerel in 1896, who investigated the radiation emitted by uranium minerals [9]. Two years later similar properties were discovered for thorium by Marie Curie [10] and by G. C. Schmidt [11]. Marie Curie found differences in the radioactivity of uranium and uranium minerals and concluded that the minerals must contain still other radioactive elements. Together with her husband, Pierre Curie, she discovered polonium and radium in 1898 [12].

Radioactive substances are depending on their origin divided up into two groups; natural and anthropogenic. In nuclear power stations artificial radionuclides, mainly fission products and transuranium elements, are produced. The application of nuclear weapons, by nuclear weapon tests and nuclear accidents, considerable amounts of fission products have been set free and distributed via the atmosphere as radioactive fall-out over large areas, in particular in the north hemisphere.

2.1 Natural radioactivity in the environment

There are about 80 natural radionuclides existing in measurable amounts in the environment [13]. They are, depending on origin, divided up into four groups:

- Primordial radionuclides
  Primordial radionuclides, such as K-40, Th-232, U-235, and U-238, have been produced in the course of nucleogenesis and have been present on earth since the beginning and are not being reproduced, but due to their long half-lives they are not yet completely decayed.
- Radionuclides of the natural decay chains
  There are four natural decay chains, originating from the four primordial radionuclides U-238, U-235, Np-237, and Th-232, which contain 45 of the natural radionuclides. A decay chain consists of a definite sequence of alpha and beta decays. The neptunium chain ends with the stable Bi-209, the other three ends with stable lead isotopes. However, the radionuclides of the natural neptunium decay chain have already decayed, since the half-life of the longest lived radionuclide Np-237 is 2.1×10^6 years, which is short compared to the age of the solar system (4.5×10^9 y).
- Cosmogenic radionuclides
  Cosmogenic radionuclides are produced by nuclear reactions in the atmosphere by the cosmic radiation and at the surface of the lithosphere. They can reach the lower air layers by sedimentation, where they can merge in to the biosphere (for example tritium, Be-7, Be-10, and C-14).

– Nucleogenic radionuclides

  In places, where a neutron flux is present, nuclear reactions can occur to produce radionuclides. For example, Np-237 is reproduced in uranium deposits in small amounts by the reaction:

$$^{238}\mathrm{U(n,2n)}^{237}\mathrm{U} \xrightarrow{\beta} {}^{237}\mathrm{Np} \tag{2.1}$$

2.1.1 Radiation exposure

The largest contribution to the every day radiation dose of the population comes from the concentration of Rn and its daughters in air, as can be seen from Tab. 1 below, where the average equivalent dose rate received from natural radiation sources are listed [14].

The concentration of Rn-222 is relatively high in regions of high uranium concentration in the ground and in poorly ventilated housing built of materials containing small amounts of uranium, radium or thorium. Accordingly, the dose rates vary considerably.

In comparison to natural radiation sources, the radiation exposure originating from artificial sources is in many cases much higher. These doses originate from the application of X-rays and radionuclides for diagnostic and therapeutic purposes, from various radiation sources applied in daily life and from radioactive fall-out. By severe nuclear installation accidents, such as the Chernobyl accident, doses up to several Sv have been transmitted.

2.1.2 Natural deposits

Radioactive substances are found in the atmosphere, but most of them are present in the lithosphere. Most important are the ores of uranium and thorium, but also potassium salts contribute to the natural radioactivity. Uranium and thorium are common elements in nature. High concentrations of uranium are found in granite in Saxony, Germany, which contain up to 20 ppm [15]. Some minerals containing U and Th and their major deposits are listed in Tab. 2. The most important uranium mineral is pitchblende (U_3O_8).

The naturally occurring isotopes of uranium are U-238 (99.27 %), U-235 (0.72 %) and U-234 (0.006 %) [16]. The isotope ratio of U-238 to U-235 in the Earth's crust is constant at 137.5 ± 0.5 [17]. So far the only known exception is found in Gabon in West Africa (Oklo). About 10^9 years ago the U-235 content was in the order of 3 % of the U-238 content. This enrichment was enough to start a chain reaction, which led to a burn-up of U-235, which in turn led to a considerably lower U-235 content today than what is normally found around the world [13].

Tab. 1: Average radiation exposure by natural radiation sources [14]

Kind of exposure	Equivalent dose ($mSv\ y^{-1}$)		
	Whole body and gonads	Bone	Lung
External radiation sources			
Cosmic radiation[(a)] (sea level, 50° north)	0.35	0.35	0.35
Terrestrial radiation[(b)] (K; U, Th and decay products)	0.49	0.49	0.49
Internal radiation sources			
Uptake by ingestion			
Tritium	< 0.00002	–	–
C-14	0.016	0.016	0.016
K-40	0.19	0.11	0.15
Rb-87	0.003	–	–
Po-210	–	0.14	–
Rn-220 + Rn-222	0.02	0.02	0.02
Ra-226 + Ra-228	0.03	0.72	0.05
U-238	0.0008	–	–
Uptake by inhalation			
Rn-220	–	–	1.75[(c)]
Rn-222	–	–	1.30[(c)]
Sum	≈ 1.10	≈ 1.85	≈ 4.10

[(a)] On the ground, locally up to ≈ 2 $mSv\ y^{-1}$. Intensity of cosmic radiation increases by a factor of ≈ 1.6 per 1000 m above sea level.
[(b)] Locally up to ≈ 4.3 $mSv\ y^{-1}$. On average, in the open air ≈ 25 % less than in buildings. Minimum values × 1/10, maximum values × 10 of the values listed.
[(c)] Values for brick buildings and 3.5-fold exchange of air per hour. In concrete buildings without exchange of air the values are higher by a factor of 4–7.

2.1.3 Uranium-radium decay chain

The uranium-radium decay chain starts with U-238, in the course of which Ra-226, Rn-222, Pb-210, and Po-210 are produced. In Fig. 1 this decay chain is depicted. From the mother nuclide of all the members of the uranium family, U-238 (4.468×10^9 years), two short lived isotopes of thorium and protactinium are formed by one alpha and one beta decay. Another uranium isotope, U-234 with a half-life of 2.455×10^5 years, is formed by beta decay from

protactinium. Further alpha decays subsequently produce Th-230 (7.54×10^4 years), Ra-226 (1600 years), and the noble gas Rn-222 (3.825 days). Its decay products include polonium, bismuth and lead isotopes up until Po-214, all short-lived (less than 30 min). The next isotope Pb-210 has a half-life of 22.3 years. By beta decay Bi-210 (5.013 days) is formed, by another beta decay the alpha emitter Po-210 (138.38 days) is formed, until the stable Pb-206 is reached.

Tab. 2: Naturally occurring uranium and thorium minerals [14]

Mineral	Composition	Conc. of U (%)	Conc. of Th (%)	Deposits
Pitchblende	U_3O_8	60–90		Bohemia, Congo, Colorado (USA)
Becquerelite	$2\ UO_3{\cdot}3H_2O$	74		Bavaria, Congo
Uraninite		65–75	0.5–10	Japan, USA, Canada
Broeggerite	$UO_2{\cdot}UO_2$	48–75	6–12	Norway
Cleveite		48–66	3.5–4.5	Norway, Japan, Texas
Carnotite	$K(UO_2)(VO_4){\cdot}nH_2O$	45		USA, Congo, Russia, Australia
Casolite	$PbO{\cdot}UO_3{\cdot}SiO_2{\cdot}H_2O$	40		Congo
Liebigite	Carbonates of U and Ca	30		Austria, Russia
Thorianite	$(Th, U)O_2$	4–28	60–90	Ceylon, Madagascar
Thorite	$ThSiO_4{\cdot}H_2O$	1–19	40–70	Norway, USA
Monazite	Phosphates of Th and Rare Earths		0.1–15	Brazil, India, Russia, Norway, Madagascar

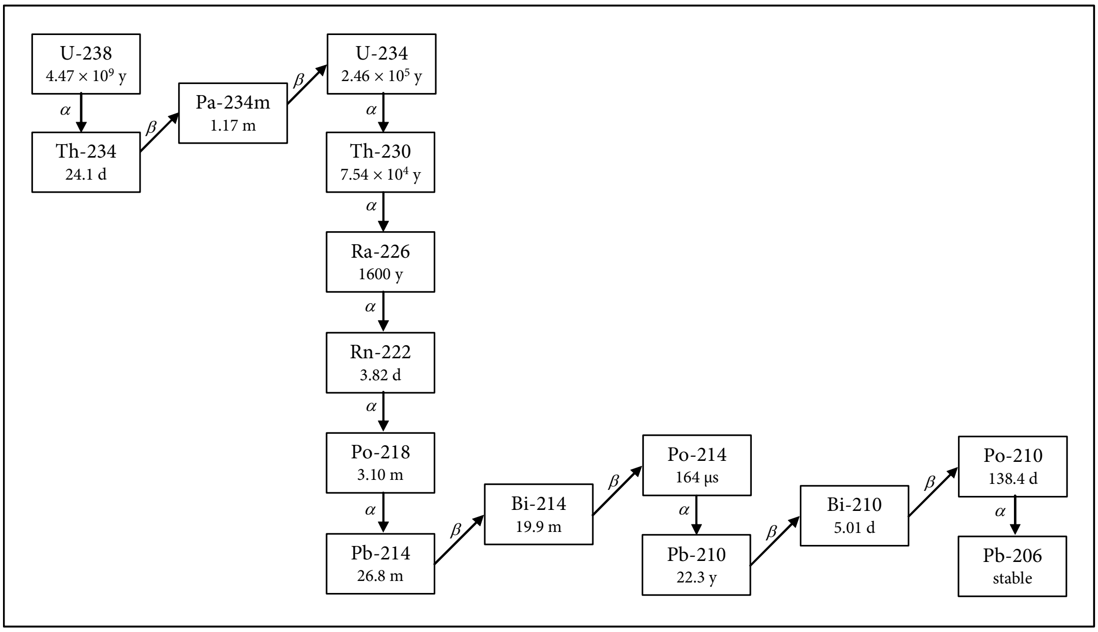

Fig. 1: The U-238 decay chain [16]

2.1.3.1 Lead

Lead (Lat. *Plumbum*, Pb) occurs in nature, but it is rare: only 1.6×10^{-3} % is found in the earth crust [18]. Lead is obtained chiefly from galena (PbS) by a roasting process. Anglesite ($PbSO_4$), cerussite ($PbCO_3$), and minim (Pb_3O_4) are other common lead minerals [25].

The radiochemistry of lead has a history almost as long as the history of radiochemistry itself. In 1899, 3 years after the discovery of radioactivity by Becquerel and only a year after the discovery of polonium and radium by the Curies, Elster and Geitel [19] reported that lead sulphate obtained from pitchblende was very active. This was interpreted at the time as being due to activity induced in stable lead by exposure to the radiation of radium in the ore and was first called "radiolead".

Natural lead is a mixture of four stable isotopes [16]: Pb-204 (1.4 %), Pb-206 (24.1 %), Pb-207 (22.1 %), and Pb-208 (52.4 %) and these isotopes are the end products of each of the three series of naturally occurring radioactive elements: Pb-206 for the uranium series, Pb-207 for the actinium series and Pb-208 for the thorium series. In total 27 other isotopes of lead with mass number from 183–214 (excluding 204, 206, 207, and 208), all of which are radioactive, are recognized [16]. In Tab. 3 the decay data for natural radioactive lead isotopes is listed. Due to its comparatively long half-life, Pb-210 is the most abundant of the radioactive lead isotopes. The existence of convenient radioactive lead isotopes in the natural series brought their early use as tracers in natural processes [20]. Pb-210 is often applied in sedimentation studies and dating of sediments [21].

Some physical properties of lead are shown in Tab. 4.

Tab. 3: Relevant decay data for naturally occurring radioactive lead isotopes [22]

Radionuclide	Half-life	E_β (MeV)	Emission prob. (%)	E_γ (keV)	Emission prob. (%)
Pb-210	22.3 y	0.017	82.0	46.5	4.0
		0.063	18.0		
Pb-211	36.1 min	1.37	90.8	405	3.8
		0.54	6.5	832	3.8
		0.97	1.7	427	1.7
Pb-212	10.64 h	0.33	82.6	239	43.4
		0.57	12.3	300	3.2
		0.16	5.1		
Pb-214	26.8 min	0.68	48.2	352	36.9
		0.74	43.0	295	19.2
		1.03	5.6	242	7.5
		0.19	2.2		

Tab. 4: Some physical properties of lead and polonium[23, 24, 25, 26]

Property	Lead	Polonium
Electron configuration	$4f^{14}5d^{10}6s^{2}6p^{2}$	$4f^{14}5d^{10}6s^{2}6p^{4}$
Ionic radius (pm)	Pb^{2+}: 133 (6) Pb^{2+}: 143 (8)	Po^{4+}: 108 (6) Po^{4+}: 122 (8)
Density (g cm^{-3})	11.34	9.20
Melting point (°C)	327	254
Boiling point (°C)	1751	962

Due to its high density, lead is commonly used as a radiation shield around X-ray equipment and nuclear reactors. Gamma and X-rays are efficiently attenuated by lead shields. On the other hand, the thermal neutron cross section of natural lead is low, and that of the Pb-208 is very low (0.0006 barns) [27].

Lead forms two series of compounds, corresponding to the oxidation states +2 and +4. In contradiction to the other members of the group IV a in the Periodic Table, the most common oxidation state of lead in its compounds is +2. The compounds of lead(IV) are accord-

ingly generally regarded as being covalent in nature, whereas those of lead(II) are considered to be ionic [27].

2.1.3.2 Polonium

Polonium was discovered in 1898 by Marie Curie and her husband as the first element separated from pitchblende, and named after her home country, Poland (*Lat*. Polonia) [12]. It has 25 known radioactive isotopes with mass numbers from 192 to 218, of which only the 208, 209 and 210 isotopes have half-lives longer than 1 day [16], see Tab. 5.

Tab. 5: Relevant decay data for Po-208, Po-209 and Po-210 [22]

Radionuclide	Half-life	Decay modes	E_α (MeV)	Intensity (%)
Po-208	2.898 y	α: 99.99777 %	5.115	99.9956
			4.220	2.4E-4
		ε: 0.00223 %		
Po-209	102 y	α: 99.52 %	4.885	20
			4.883	80
			4.622	0.551
			4.310	1.5E-4
			4.110	5.6E-4
		ε: 0.48 %		
Po-210	138.376 d	α: 100 %	5.304	100
			4.517	1.22E-3

Polonium is a very rare natural element. Uranium ores contain only about 100 micrograms of the element per 10^6 g [28]. It was in 1934 found that when natural bismuth (Bi-209) was bombarded by neutrons, Bi-210, the parent of polonium, was obtained. Milligram amounts of polonium may now be prepared this way, by using the high neutron fluxes of nuclear reactors. The annual production of Po-210 worldwide is estimated to about 100 grams [29]. Isotopes of mass 209 and 208 can be prepared by alpha, proton, or deuteron bombardment of lead or bismuth in a cyclotron [30].

The energy released by the decay of Po-210 is so large (140 W g^{-1}) [23] that a capsule containing about half a gram reaches a temperature above 500 °C. A few Curies (1 Curie = 3.7×10^{10} Bq) of polonium exhibit a blue glow, caused by excitation of the surrounding gas. Because almost all alpha radiation is stopped within the solid source and its container, giving up its energy, polonium has attracted attention for uses as a lightweight heat source for thermoelectric power in space satellites.

Polonium can be mixed or alloyed with beryllium to provide neutron sources. The neutron source, or initiator, is one of the most important elements of a fission weapon. It has only one purpose: to generate and release an initial burst of relatively low energy neutrons at just the right moment to trigger and maximize fission reactions in compressed plutonium or uranium fissile fuel. In early nuclear weapons, most initiators were fragile hemispheres ("golf balls") of Po-210 and Be-9. These "golf balls" were placed in the centre of the fissile core; when crushed by implosion, the intermixing of these two elements caused the Be-9 (α, n) C-12 reaction to occur [31].

Polonium is used in devices for eliminating static electricity in textile mills, in the paper industry and by the manufacturing of sheet plastic. It is also used on brushes for removing dust from photographic films and camera lenses. Static eliminators typically contain from 1–10 GBq of Po-210. The polonium used in these eliminators is combined with silver or other metals in a foil mounted inside a protective cage, in order to minimize hazards to the user [29]. Any attempt to destroy or disassemble the source to extract the polonium would be extremely difficult and would require sophisticated laboratories. Po-210 is very dangerous to handle in even milligram or microgram amounts and special equipment and strict control is necessary.

In Tab. 4 some physical properties of polonium are listed. Polonium is the heaviest element in group VI a of the Periodic Table, the other members of which are sulphur, selenium and tellurium, and it is of interest to compare polonium with these elements. The electron configuration of Po is analogous to the configuration of Se and Te, from which stable oxidation states of –2, +2, +4, and +6 would be expected [23]. The +2 state is unstable in solution in the absence of reducing agents. It is rapidly oxidized to the +4 state under the influence of its own alpha particles. Hence, the +4 state is the most stable state in solution. A number of compounds of Po(IV) have been prepared. The tetrachloride is relatively volatile (boiling point, 390 °C [28]) and, therefore, hydrochloric acid solutions of polonium must be evaporated carefully to prevent loss of polonium.

In slightly acidic to neutral solutions it hydrolyses, forming $PoO(OH)^+$, $PoO(OH)_2$ and PoO_2, and in alkaline solution it forms PoO_3^{2-} [30]. In hydrochloric acid solutions, polonium is complexed, probably as $PoCl_6^{2-}$ or $PoCl_4^{2-}$. In nitric acid solution Po is only partially complexed [28]. As a consequence thereof, storage of polonium is preferred in hydrochloric acid solution, as the losses due to adsorption are reduced.

Elemental polonium is more metallic than tellurium and its physical properties resemble those of thallium and bismuth rather than those of tellurium. In chemical properties, however, polonium follows that of tellurium very closely [23]. Polonium is a low-melting, fairly volatile metal and it distils readily in vacuum. The vapour pressure between 438 and 745 °C is represented by the equation [32]:

$$\log p = \frac{-5377.8}{T} + 7.2345 \tag{2.2}$$

where p is the pressure in mm Hg, T is the absolute temperature. From the above equation the calculated boiling point is 962.04 °C.

Polonium metal exposed to air oxidizes to form the dioxide, PoO_2. The reaction is slow in dry oxygen at room temperature, but is rapid at 300 °C [28]. The polonium dioxide is less volatile than elemental polonium.

Physiological damage arises from the complete absorption of the energy of the alpha particle into tissue. With ingestion of several micrograms of Po-210, gastrointestinal symptoms begin to appear within about a day [33]. Gastrointestinal symptoms will mimic food poisoning; nausea, diarrhoea, vomiting, and general tiredness. This is followed by a “latent” phase and a further decline, including the loss of all hair and a massive depletion in white blood cells. Bone marrow depression will occur with a 5 Gy whole-body single radiation dose. The intestinal lining has rapidly proliferating cells which are sensitive to radiation; gastrointestinal syndrome will occur with acute doses of 5–15 Gy, and necrosis and ulcerations will occur at 40–50 Gy. Within the lining of the gastrointestinal tract, the alpha particles will irradiate the mucosa; this will cause sloughing of the disrupted cells and will affect the inner lining, leading to gastrointestinal bleeding.

Polonium-210 inside the body is not detectable with standard radiation instrumentation used outside the body. Testing urine or faeces for alpha radiation would be the method of detection. For someone to be poisoned with Po-210, a big radiation dose would be needed; a dose not possible with naturally occurring Po-210, only with man-made Po-210. A median survival time of 20 days has been associated with a median dose of about 1.6 MBq (0.0096 μg) per kilogram of Po-210. For a 70-kilogram person, this would only be about 111 MBq (about 0.7 μg Po-210) [33]. Weight for weight Po-210 is about 2.5×10^{11} times more toxic than hydrocyanic acid [34].

2.1.4 Carrier-free radionuclides

Nuclides of instable elements, with no existing inactive isotopes, are so called carrier-free radionuclides. Carriers are elements with identical or very similar chemical properties to the radionuclide, and are added to ensure normal chemical behaviour of radionuclides.

Handling of micro-amounts requires special precautions, because in absence of measurable amounts of carriers the radionuclides are micro-components and their chemical behaviour may be quite different from that observed for macro-components. The percentage of radionuclides sorbed on the walls of a container depends on the chemical form of the nuclide, its concentration and specific activity (activity per mass of element, in Bq g^{-1}), and on the properties of the container material. At high specific activity of a radionuclide in solution, the surface of a glass beaker generally offers an excess of surface sorption sites. Glass surfaces possess an ion exchange capacity of the order of 10^{-10} mol cm^{-2}, which corresponds to about 10^4 ions per cm^{-2} of a glass beaker and similar number of sorption sites is available for chemisorption [14]. By comparison with Tab. 6, it becomes clear that in the absence of carriers, radionuclides in low activity concentrations may easily be sorbed on glass walls by ion exchange. However, the ion exchange and hydrolysis of the container surface is suppressed in acidic solutions (pH < 2), due to the excess of H^+ ions which saturates the glass surface and

creates a repelling positive charge. The surfaces of plastic materials, such as polyethylene, do not exhibit ion exchange, but adsorption may be pronounced, in particular adsorption of organic compounds including organic complexes of radionuclides, which might often be the case for polonium and radon.

With respect to the suitability of the carrier for a carrier-free radionuclide, the chemical state is decisive. For that purpose, they must be in the same chemical state as the radionuclide considered. In the case of radioisotopes of stable elements, such as Co-60 and Na-24, small amounts (traces) of these metals are always present. In the case of isotopes of radioelements, such as Ra-226, Ac-227 or Po-210, however, stable nuclides do not exist. For such radionuclides a non-isotopic carrier can be utilized. The non-isotopic carrier can be an element with similar properties as the considered radionuclide, for example barium is usually used as a carrier for radium, or tellurium or bismuth for polonium.

Tab. 6: Number of atoms and mass of various radionuclides corresponding to 10 Bq

Radionuclide	Half-life	Number of atoms	Mass (g)
Ra-226	1600 y	7.3×10^{11}	2.7×10^{-10}
Ac-227	21.77 y	9.9×10^{9}	3.7×10^{-12}
Co-60	5.272 y	2.4×10^{9}	2.4×10^{-13}
Po-210	138.38 d	1.7×10^{8}	6.0×10^{-14}
Na-24	14.96 h	7.7×10^{5}	3.1×10^{-17}

2.1.5 Age determination from radioactive decay

The basis of age determination by nuclear methods is the laws of radioactive decay. From the variation of the number of atoms with time due to radioactive decay, time differences can be calculated rather exactly. Dating by nuclear methods is applied in many fields of science, but mainly in archaeology, geology and mineralogy. Two kinds of dating by nuclear methods can be distinguished [14]:

- dating by measuring the radioactive decay of cosmogenic radionuclides, such as tritium or C-14;
- dating by measuring the daughter nuclides formed by decay of primordial mother nuclides (various methods, e.g. K/Ar, Rb/Sr, U/Pb, Th/Pb, Pb/Pb).

There are basically three generations of method development in age determination by radioactive decay. Dating methods using K–Ar, Rb–Sr, lead isotopes and cosmogenic C-14 reached importance in the 1960s and early 1970s. A second group of methods reached importance in the late 1970s and early 1980s. Examples are the Sm–Nd method, Rare Gas geochemistry and uranium-series nuclides. These techniques offered new and powerful isotopic tracers for analysing geochemical systems in the mantle and crust. The third group of dating methods, the Re–Os method, became important in the 1990s [35].

All naturally occurring radionuclides can be used for dating. The time scale of applicability depends on the half-life. With respect to the accuracy of the results, it is most favourable if the age to be determined and the half-life of the radionuclide are of the same order. Therefore the long-lived mother nuclides of uranium, thorium and actinium decay series and other long-lived naturally occurring radionuclides such as K-40 and Rb-87 are most important for application in geology and mineralogy. In Tab. 7 some principal radiometric dating methods are listed.

Tab. 7: Principal radiometric dating methods used in geochronology and archaeology [36]

Method	Description	$t_{1/2}$ (y)	Effective dating range	Datable materials
U/Pb Th/Pb	U-238/Pb-206 U-235/Pb-207 Th-232/Pb-208 Pb-207/Pb-206	4.5×10^9 0.71×10^9 13.5×10^9	From 10^7 y to the age of the earth	Zircon, pitchblende, monazite, some whole rock, lava flows, igneous rocks
K/Ar	(1) total degassing (2) K-40/Ar-39 age-spectra analysis	1.31×10^9	From 10^5 y to the age of the earth	Any K-bearing mineral or rock, primarily applicable volcanic rocks
Rb/Sr	Rb-87/Sr-87	47.0×10^9	From 10^7 y to the age of the earth	Rb-containing minerals or rocks, such as muscovite, granite, gneiss
I/Xe	I-129 decay to Xe-129	16.4×10^6	Up to 10^7 y	Meteorites, lunar material
Re/Os	Re-187 decays to Os-187	43×10^6	Up to 10^8 y	Metal sulphides and rare earth minerals, meteorites
C-14	C-14 beta decay and AMS	5730	Up to 4×10^4 y	Wood, charcoal, peat, tissue, bone, cloth
U-series disequilibria	Th-230/U-234 Pa-231/U-235 etc.	7.5×10^4 3.4×10^4	3.5×10^5 y 2×10^5 y	Corals, speleothem, bones, teeth, deep-sea cores, shells, etc.

Dating by means of Pb-210 is of special interest with respect to ages in the range between about 20 and 150 years, in particular for dating of glacier and polar ice, sedimentation rates in lakes, estuaries, and coastal marine sediments. The isolation of Pb-210 is ascribed to its precursor, Rn-222, which escapes from the earth's surface into the atmosphere. Most Rn-222 remains in the troposphere where it decays to Pb-210. The Pb-210 residence time in the troposphere is estimated to range from days to a month before it is removed by precipitation and dry fallout. The atmospheric flux of unsupported Pb-210 is presumed to have remained constant at a given locality, and so Goldberg [37] first proposed dating permanent snow fields by the measured Pb-210 activity.

The age of different horizons in a sediment core can be calculated using eqn. (2.3) from the unsupported Pb-210 activity (Pb-210-excess = Pb-210 – Ra-226) assuming that Pb-210 and Ra-226 are immobile in the core [35]. Two different age calculations can be carried out depending on the choice of two assumptions: constant initial concentration; or constant rate of supply [36]:

The first method assumes that the Pb-210-excess remains constant with time at a particular location. Then, the difference in age between the surface sediment and sediment at depth n is given by

$$t_{\mathrm{n}} = \ln\left((\text{Pb-210-}excess)_0 / (\text{Pb-210-}excess)_{\mathrm{n}}\right) \lambda_{\text{Pb-210}} \tag{2.3}$$

where $(\text{Pb-210-}excess)_0$ and $(\text{Pb-210-}excess)_{\mathrm{n}}$ are excess activities of Pb-210 at the two positions in the core in units of decompositions per minute per gram of dry matter, and is the Pb-210 decay constant. When the accumulation rate is constant the following relation can be applied:

$$\ln(\text{Pb-210})_{\mathrm{n}} = \ln(\text{Pb-210})_0 - \left(\frac{\lambda_{\text{Pb-210}}}{R}\right) M \tag{2.4}$$

where M is the mass depth in grams of dry matter per square centimetre, and R is the accumulation rate of sediment in grams of dry matter per square centimetre per year.

The second method assumes that the flux of Pb-210-excess supply to the sediment is constant with time at a particular location. Thus, the age (t) for a horizon at depth n is calculated from:

$$\sum(\text{Pb-210-}excess)_{\mathrm{n}} = n_{\mathrm{t}}\left(1 - e^{-\lambda_{\text{Pb-210}} t}\right) \tag{2.5}$$

where $\sum(\text{Pb-210-}excess)_{\mathrm{n}}$ is the total excess Pb-210 activity per cm^{-2}, from surface to depth n, and n_{t} is the total Pb-210-excess in the core down to a deposition horizon much older than 100 years.

2.2 Radioactive equilibria and disequilibria

Radioactive decay follows the laws of statistics. If a sufficiently large number of radioactive nuclei N are observed for a sufficiently long time, the law of radioactive decay is found to be

$$-\frac{dN}{dt} = \lambda N \tag{2.6}$$

where $-dN/dt$ is the disintegration rate, and λ is the decay constant (dimension s^{-1}) [14]. It is a measure of the probability of radioactive decay. The integration of eqn. (2.6) gives

$$N = N_0 e^{-\lambda t} \tag{2.7}$$

where N_0 is the number of radioactive nuclei at the time $t = 0$. Instead of the decay constant λ, the half-life $t_{1/2}$ is frequently used. This is the time after which half the radioactive nuclei have decayed: $N = N_0/2$. Introducing the half-life $t_{1/2}$ in eqn. (2.7) it follows that

$$t_{1/2} = \frac{\ln 2}{\lambda} \tag{2.8}$$

The activity A of a radionuclide is given by its disintegration rate:

$$A = -\frac{dN}{dt} = \lambda N = \frac{\ln 2}{t_{1/2}} N \tag{2.9}$$

The dimension is s^{-1}, and the unit is Becquerel (Bq). An older unit is the curie (Ci). The curie is defined as the amount of radioactivity which has the same disintegration rate as 1 g of Ra-226, and is defined as 1 Ci = 3.7×10^{10} s^{-1} = 37 GBq.

Genetic relations between radionuclides, as in the decay series, can be written in the form

$$\text{nuclide 1} \xrightarrow{\lambda_1} \text{nuclide 2} \xrightarrow{\lambda_2} \text{nuclide 3} \tag{2.10}$$

where nuclide 1 is transformed by radioactive decay into nuclide 2 with the decay constant λ_1, and nuclide 2 into nuclide 3 with the decay constant λ_2. At any instant, the net production rate of nuclide 2 is given by the decay rate of nuclide 1 diminished by the decay rate of nuclide 2:

$$\frac{dN_2}{dt} = -\frac{dN_1}{dt} - \lambda_2 N_2 = \lambda_1 N_1 - \lambda_2 N_2 \tag{2.11}$$

With the decay rate of nuclide 1 it follows:

$$\frac{\mathrm{d}N_2}{\mathrm{d}t} + \lambda_2 N_2 - \lambda_1 N_1^0 \mathrm{e}^{-\lambda_1 t} = 0 \qquad (2.12)$$

where N_1^0 is the number of atoms of nuclide 1 at time 0. The solution of the first-order differential equation (2.12) is

$$N_2 = \frac{\lambda_1}{\lambda_2 - \lambda_1} N_1^0 \left(\mathrm{e}^{-\lambda_1 t} - \mathrm{e}^{-\lambda_2 t}\right) + N_2^0 \mathrm{e}^{-\lambda_2 t} \qquad (2.13)$$

where N_2^0 is the number of atoms of nuclide 2 present at time 0. If nuclide 1 and 2 are separated quantitatively at $t = 0$, the situation becomes simpler and two fractions are obtained. In the fraction containing nuclide 2, this nuclide is not produced any more by decay of nuclide 1, and for the fraction containing nuclide 1 it follows with $N_2^0 = 0$:

$$N_2 = \frac{\lambda_1}{\lambda_2 - \lambda_1} N_1^0 \left(\mathrm{e}^{-\lambda_1 t} - \mathrm{e}^{-\lambda_2 t}\right) = \frac{\lambda_1}{\lambda_2 - \lambda_1} N_1 \left(1 - \mathrm{e}^{-(\lambda_2 - \lambda_1)t}\right) \qquad (2.14)$$

Above the radioactive equilibrium between a mother nuclide and a daughter nuclide according to eqn. (2.10) has been considered. For the next successive daughter (nuclide 3), the following equation is obtained:

$$N_3 = \lambda_1 \lambda_2 N_1^0 \frac{\mathrm{e}^{-\lambda_1 t}}{(\lambda_2 - \lambda_1)(\lambda_3 - \lambda_1)} + \frac{\mathrm{e}^{-\lambda_2 t}}{(\lambda_1 - \lambda_2)(\lambda_3 - \lambda_2)} + \frac{\mathrm{e}^{-\lambda_3 t}}{(\lambda_2 - \lambda_3)(\lambda_1 - \lambda_3)} \qquad (2.15)$$

The time necessary to attain radioactive equilibrium depends on the half-life of the daughter nuclide. In the radioactive equilibrium, the ratio N_2/N_1, the ratio of the activities is constant. It should be mentioned that this is not an equilibrium in the sense used in thermodynamics and chemical kinetics, because it is not reversible, and it generally does not represent a stationary state. Three cases can be distinguished:

– Secular radioactive equilibrium ($t_{1/2}(1) >> t_{1/2}(2)$)
  In secular radioactive equilibrium, eqn. (2.14) reduces to

$$N_2 = \frac{\lambda_1}{\lambda_2} N_1 (1 - \mathrm{e}^{-\lambda_2 t}) \qquad (2.16)$$

  After $t >> t_{1/2}(2)$ (in practice, after about 10 half-lives of the nuclide 2), radioactive equilibrium is established and the activities of the mother nuclide and of all the nuclides emerging from it are the same: $A_1 = A_2$. Secular radioactive equilibrium can be used for the determination of a long-lived mother nuclide, if the daughter activ-

ity is easier to measure. Examples are the determinations of Pb-210 via the daughter Bi-210 and Ra-226 via Rn-222 respectively, both using liquid scintillation counting.

- Transient radioactive equilibrium
  After attainment of radioactive equilibrium ($t_{1/2}(1) > t_{1/2}(2)$), the daughter activity is always higher than the mother activity:

$$\frac{A_2}{A_1} = \frac{\lambda_2}{\lambda_2 - \lambda_1} \tag{2.17}$$

- Half-life of mother nuclide shorter than half-life of daughter nuclide
  In this case the mother nuclide decays faster than the daughter nuclide, and the ratio between the two changes continuously, until the mother nuclide has disappeared. No radioactive equilibrium is attained.

2.2.1 Radioactive disequilibria in waters

The decay products of uranium pass over 10 elements, all with very different chemical properties. These elements are transported by groundwater (migrate), the solute composition of which varies with the surrounding rock/soil minerals. The different elements migrate at different rates due to their different chemical properties; dissolving in some areas and precipitating in others.

Radioactive disequilibrium can be a result of geochemical sorting or differentiation processes, whereby one decay series daughter is more mobile than another. These differentiation processes may be physical as well as chemical, and isotopic as well as elemental. When one daughter in a radioactive chain is selectively mobilised from aquifer rock surfaces, disequilibrium is produced in both the solid and the aqueous phases. Precipitation from solution is also elementally selective. In the case of radon, enhanced diffusion is another cause of fractionation and disequilibrium. These processes all depend on elemental geochemistry. The alpha recoil fractionation mechanism, on the other hand, is not element specific. Each daughter in the decay chain is more prone to have been displaced than its immediate parent. In some cases the displacement is across phase boundaries, and disequilibrium is the direct result. In other cases the displacement leads to unstable lattice sites where enhanced vulnerability to leaching, which in time results in disequilibrium [38].

An important determinant of the abundance level of a given radionuclide in solution is its half-life. In the case of unsupported species, shorter-lived radionuclides will decay away while longer-lived sisters will persist. Even though two radionuclides have similar chemical properties, the shorter-lived species, or isotope, will be scarce unless there is a continuing supply contributed by the aquifer rock. Uranium, radium, and radon frequently occur in natural waters at the 10–100 mBq l^{-1} level, and are thought of as geochemically soluble. Tho-

rium and protactinium are seldom detected in solution, and are essentially insoluble in natural waters. Lead, polonium, bismuth, and actinium may be found under certain conditions in solution in natural waters. For those radionuclides which are readily soluble, the factor which limits their occurrence may be their average lifetimes. Radioactive disequilibrium is induced between the nuclides above and below radon in the decay series. Similarly, loss of an intermediate nuclide due to solubility in water (for example radium) may also be a cause of disequilibrium. Many daughters of thorium and uranium, however, are too short-lived to become appreciably fractionated from their immediate parents [38].

2.2.2 Disequilibria of Pb-210 and Po-210 in water and sediments

Disequilibrium between Pb-210 and its parent isotope Ra-226 arises through diffusion of the intermediate gaseous isotope Rn-222. A fraction of the Rn-222 atoms formed by Ra-226 decay in soil escapes into gaps and diffuse through the soil into the atmosphere, where they decay to Pb-210. Lead-210 atoms become readily attached to airborne particulate material and are removed from the atmosphere by precipitation or dry deposition. A part of this natural radioactive fallout is adsorbed onto sedimentary particles in lake waters and seas, deposited on the lake or sea bed, and buried by subsequent accumulations. If diffusion of Rn-222 is negligible, Pb-210 is likely to be in equilibrium with its progenitor Ra-226 because the other four intermediates all have half-lives of only seconds or minutes, see 2.1.3.

The atmospheric flux of Pb-210 (from the decay of Rn-222) has been estimated at 15 atoms min^{-1} cm^{-2} [39]. In oceans and near-shore environments, decay of Ra-226 in solution provides another source of Pb-210. Except for surface ocean waters, dissolved Pb-210 is found to be deficient in the entire water column [40]. Its activity ranges from 15–80 per cent of Ra-226 activity and generally decreases with depth. This indicates that Pb-210 is rapidly removed by adsorption on to sinking particulates and may be co-precipitated with ferric hydroxide and manganese oxides or form insoluble lead sulphides in anoxic waters [41]. As a result, estimates of residence time of Pb-210 in ocean water vary widely, depending on location: less than one month near land, to over 50 years in the deep ocean.

In lake waters, Pb-210 has a relatively short residence time. Residence times depend to a large extent on water depth, but estimates are typically in the order of months [42]. For lakes with relatively short water residence times, of the same order as the Pb-210 residence time, significant losses of Pb-210 from the lake may occur through outflow from the lake.

In the hydrological cycle Po-210 generally follows its precursor Pb-210, but it is often found out of radioactive equilibrium with Pb-210 in the marine environment. Polonium-210 is more readily adsorbed than Pb-210 on to particulate matter and microorganisms in surface layer of the oceans (see Chapter 3). The Po-210 excess in the plankton can account for at least 70 per cent of the surface water deficit, part of which may be removed by sinking particles. However, because of differing chemical properties at greater depths, polonium is easily recycled, whereas lead tends to remain with the sinking particulates [43]. It is also likely that polonium is adsorbed onto colloidal mineral particles (silica, aluminosilicates, iron oxides) as

well as fulvic and humic acids, to a higher extent than lead. It was found that in Finnish groundwater both Pb-210 and Po-210 mainly exist as particles, rather than in ionic forms [44]. Furthermore, disequilibrium between Pb-210 and Po-210 has been observed in Finnish drinking water; the mean activity concentrations of Pb-210 and Po-210 in dug wells were 13 and 7 mBq l^{-1}, respectively [45]. Po-210 is often depleted to a higher extent than Pb-210, except for one example in west Florida, USA. In shallow well waters, near an area of phosphate mineralization, unsupported Po-210 activities of over 1000 min^{-1} l^{-1} were observed in fairly acidic, S^{2-}-bearing waters. Microbial activity was thought to be the cause of this enrichment [46]. In sediments and soils, however, Pb-210 and Po-210 are commonly found in radiochemical equilibrium with one another or close to it [47, 48].

2.3 Technically enhanced natural radioactivity

By mining of natural ores and minerals, considerable amounts of natural radionuclides, in particular members of the thorium, uranium and actinium decay series, are brought up to the surface of the earth and in this way they contribute to the radioactivity in the environment. Also combustion of fossil fuels and the use of phosphate rock make a contribution to the radioactivity, as so called technically enhanced natural radioactivity. In Tab. 8, the releases of some radionuclides from mineral processing installation to air and water, respectively, are listed. The radionuclides released to the atmosphere by large thermal processes, such as those used by the elementary phosphorus production, iron and steel production and the cement industry, are dispersed over great distances. For other mineral processing industries, dusty conditions during handling and shipment of ores are the main reason for the releases of radionuclides to air. The largest releases of radionuclides to water are from the phosphate processing, followed by oil and gas extraction and primary iron and steel production.

2.3.1 Mining and processing of ores, minerals, and coal

The historical development of uranium mining starts with the commercial use of uranium for glass and porcelain colouring during the nineteenth century [49, 50]. Total production for this period is estimated to 300 Mg of uranium. With the discovery of radioactivity and radium (1896 and 1898) uranium became a strategic mineral of global interest. Uranium mining during the colour and radium period was restricted to only a few districts and deposits (e.g. Bohemia, Saxony, Cornwall, Portugal, Colorado Plateau, Great Bear Lake, Canada and Shinkolobwe, Belgian Congo) with limited environmental impact. However, the negative effects on human health of uranium mining and handling soon became obvious. After World War II uranium mining increase rapidly and played an essential role in the nuclear race amongst the superpowers. In 1959 world uranium production peaked at about 48,000 Mg of uranium, which was almost totally assigned to the nuclear weapons programmes.

Tab. 8: Release of radionuclides from typical installation of mineral processing industries [61]

Industry	Ore through-put (kt a^{-1})	Releases to air (GBq a^{-1})				Releases to water (GBq a^{-1})			
		Ra-226	Rn-222	Pb-210	Po-210	Ra-226	Rn-222	Pb-210	Po-210
Elementary phosphorus	570	–	**563**	**66**	**490**	–	–	**24**	**166**
Phosphoric acid	700	0.09	**820**	–	–	**737**	–	**654**	**997**
Fertilizer plant	375	–	**221**	–	–	–	–	0.054	0.057
Iron and steel production	7500	–	**180**	**55**	**90**	–	–	0.51	8
Coal-fired power plants (600 MW_e)	1350	0.11	**34**	0.4	0.8	–	–	–	–
Cement industry	2000	0.2	**157**	0.2	**78**	–	–	–	–
Mineral sands handling	183[a]	0.73	0.73	0.73	0.73	0.066	0.066	0.066	0.066
Titanium-pigment	50	0.001	6.2	0.001	0.001	0.002	0.002	0.003	0.002
Gas-fired power plant (400 MW_e)	600[b]	–	**230**	–	–	–	–	–	–
Oil extraction	3500	–	**540**	–	–	**174**	**174**	**174**	**174**
Gas extraction	72000[b]	–	**500**	–	–	**32**	**32**	**32**	**32**

[a] Zirconium
[b] 10^6 m^3 a^{-1}

At that time the main uranium producing countries were the United States, Eastern Germany, Canada and South Africa.

Total world uranium production until 1994 was about 1.9 million Mg; total reserves of known and at low cost (130 US $ per kg uranium) recoverable resources of uranium are estimated at about 4.7 million Mg in 2005 [51]. The world production in 1994 was 32,000 Mg of uranium, only about half of the present demand which is exclusively for nuclear power generation in worldwide more than 400 reactors [52]. The shortfall in production was covered by inventories and diluted weapon grade uranium available for commercial use. In 2004, the uranium production totalled 40,263 Mg, an increase of almost 12 % over production in 2002 [53]. Australia and Kazakhstan are at the moment the largest producers of uranium in the world, with a market share of 24 and 17 %, respectively, see Tab. 9.

Tab. 9: Uranium production in 2005 by country [51]

Country	Uranium quantity (Mg)	Market share (%)
Australia	1,143,000	24
Kazakhstan	816,000	17
Canada	444,000	9
USA	342,000	7
South Africa	341,000	7
Namibia	282,000	6
Brazil	279,000	6
Niger	225,000	5
Russian Federation	172,000	4
Uzbekistan	116,000	2
Ukraine	90,000	2
Jordan	79,000	2
India	67,000	1
China	60,000	1
Others	287,000	6
World total	4,743,000	

The mining and processing of uranium ores and of other ores, coal, and minerals brings up large amounts of uranium, thorium and members of their decay series to the surface of the earth and initiates mobilisation of radionuclides. Large amounts of radon are released into the air. The residues are stockpiled and slag heaps, as well as waste waters, contain significant amounts of radionuclides and the isotopes of radium continue to emit radon. Although of importance with respect to radiation exposure, natural radioactivity enhanced by mining and milling has only lately found appropriate regard in radiation protection. Through the mining

and processing of uranium ore, the natural environment is extensively altered. As a result, radioactive and toxic substances are released to the atmosphere, to soil, and to surface and groundwaters, see Fig. 2.

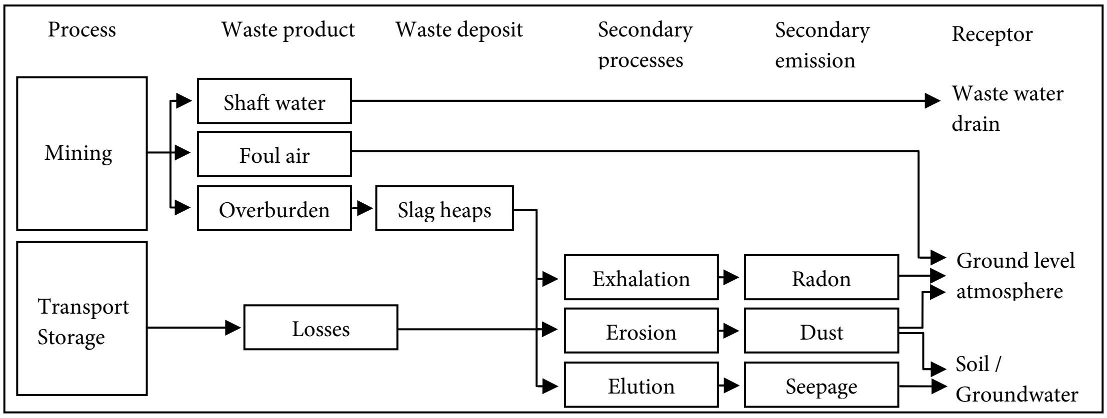

Fig. 2: Schematic diagram of the environmental pollution caused by uranium mining [54]

Waste water from dewatering of mining shafts and open cast mining is contaminated with uranium and other radionuclides, as well as toxic substances, heavy metals and salts (sulphate, chloride, and nitrate). These waste waters are, after purification, released into surrounding water systems (rivers, lakes, etc.). By the ventilation of the shafts, foul air contaminated with radon and radioactive dust is released into the atmosphere. Contaminations, caused by erosion and dust drift from open cast mines and slag heaps, are in dry climate zones of special significance. The open cast uranium mining requires the removal and stock piling of large amounts of rock. The ratio of ore to waste rock usually varies between 1:3 and 1:20, resulting in great amounts of overburden.

Prior to extraction, the ore is milled, in order to uncover the minerals contained in the ore. The subsequent extraction is performed by leaching, either in alkaline or acidic solutions. The purification of the groundwater is unproblematic after alkaline leaching [55]. As for leaching with sulphuric acid, as is and was done in the Czech Republic, Bulgaria, Kazakhstan and Uzbekistan, the groundwater purification proved to be more difficult and could so far in none of the cases successfully be demonstrated [56].

The highest danger potential arising from uranium mining and processing is found in the residues from the uranium processing, the so called tailings. These contain, apart from the used leaching chemicals (sulphuric acid, NaOH, ammonia etc.), the most part of the in the ore existing radium and consequently the entire short-lived radionuclide inventory of the ore. The safe storage of such tailings is of particular importance, and is summarised by the International Atomic Energy Agency (IAEA) [57]. The release of radon to the atmosphere and the drainage of contaminated tailing seepage must be kept as low as possible. In the early years of uranium mining, the safe and environmentally acceptable storage of the produced tailings was not adequately considered and resulted in substantial environmental damage.

The world production of coal was 4.0×10^{12} kg in 2003, a 38 % increase over the past 20 years. The main coal producers are China, USA, India and Australia [58]. Much of the global coal production is used in the country in which it was produced, the rest is exported. For example, in 2003 Germany imported 35×10^9 kg of coal. The biggest market is Asia, which in 2003 accounted for 54 % of the global coal consumption.

Like most materials found in nature, coal contains trace amounts of K-40 and of U-238, Th-232 and their decay products. The average activity mass concentrations of K-40, U-238 and Th-232 in coal were assumed by the UNSCEAR 1993 to be 50, 20 and 20 Bq kg^{-1}, respectively [59]. The main exposure pathways of the population living in coal mining areas are external irradiation and ingestion following deposition of activity on the ground. As in the case of uranium mining, shafts have to be kept clear of water, which is pumped out into the waste water drain and subsequently into the next stretch of water. The population is additionally exposed to the radon present in the exhaust air of the coal mines. The releases of radon were estimated to be between 30 and 800 TBq per year [10].

Mineral sands originate from eroded inland rocks, traces of which were subsequently transported by surface waters towards the sea, where they were deposited by the combined action of wind, waves and sea currents. These mineral sands may occur under water, be part of dunes or occur inland within a few tens of km of the coast [60]. Countries where mineral sands are mined include Australia, Bangladesh, Indonesia, Malaysia, Thailand and Vietnam. The heavy minerals of major commercial importance are ilmenite, rutile, zircon, and monazite. Typical concentrations of Th-232 and U-238 in Australian heavy mineral sands are much greater than the worldwide average concentrations in soils and rocks, see Tab. 10.

Tab. 10: Typical concentrations of Th-232 and U-238 in heavy mineral sands in Australia [61]

Mineral	Th-232 conc. (Bq kg^{-1})	U-238 conc. (Bq kg^{-1})
Ore	60–200	40
Heavy mineral concentrate	1000–1300	< 100
Ilmenite	600–6000	< 100–400
Rutile	< 600–4000	< 100–250
Zircon	2000–3000	200–400
Monazite	600,000–900,000	10,000–40,000

2.3.2 Energy production by combustion

By combustion of coal, the activities of naturally occurring radionuclides are redistributed from underground into the biosphere. About 3×10^9 kg of coal is required to produce 1 GW_e. Coal is burned at a temperature of 1700 °C in order to produce electric energy. In the combustion process, most of the mineral matter in the coal is fused into a vitrified ash. A portion

of the heavier ash, together with incompletely burned organic matter, drops to the bottom of the furnace. Most of the lighter fly ash is collected in the stack, but some, depending on the efficiency of emission control devices, is released to the atmosphere. Depending on its origin, coal contains various amounts of U-238 and Th-232, although an average value of 20 Bq kg^{-1} has been assumed for both [59]. Uranium, thorium, and their daughters are released by combustion. Volatile species, in particular radon, are emitted with the waste gas, Pb-210 and Po-210 are emitted with the fly ash, and the rest, including uranium and thorium, is found in the ash. It is assumed that 100 % of the radon, 10 % of Pb-210 and Po-210, and 1 % of the other radionuclides in coal are released to the atmosphere [62]. The global release of radon is of the order of 10^{14} Bq per year.

Oil has many fuel applications, the most important being for transport vehicles, for the generation of electric energy and for domestic heating. Approximately 2×10^9 kg of oil is needed to produce 1 GW_e. Radium and its daughters are migrating to natural oil and gas reservoirs and constitute the major radioactive contaminants of crude oil. The global activity of radium isotopes brought to the surface by oil production is of the order of 10^{13} Bq per year [59]. Radionuclides released to water in from oil and gas extraction offshore are generally diluted by the large volumes of water involved. Onshore process water is often dumped back into the oilfield. The treatment of process waters before they are released may significantly reduce the radionuclide concentration [63]. External radiation of workers in the oil industry is estimated to give an annual effective dose of less than 5 mSv from separation and storage tanks and scale deposits on inner walls of tubing and pumps. The problem was recognized at the beginning of the 1980s. The accumulation is dominated by radium and its decay products. Activity concentrations of Ra-226 and Ra-228 of up to 1 MBq kg^{-1} have been detected in scale and in thermal brines, consisting mainly of NaCl from gas fields up to 286 Bq l^{-1} have been found [64].

2.3.3 Other energy production

Another example of energy production is the geothermal energy. Geothermal energy is produced in Iceland, Italy, Japan, New Zeeland, Russia, and the US. Geothermal energy makes use of hot steam or water derived from high-temperature rocks deep inside the earth. The water contains natural radionuclides, especially Rn-222, which may be discharged to the atmosphere. In hot springs on Iceland about 2–10 kBq m^{-3} of Rn-222 have been found [65]. From measurements in Italy and in the US, the estimated average discharge of radon was 150 TBq per generated GW_e per year [3].

2.3.4 Phosphate processing and fertilizers

The use of phosphate rock is the starting material for the production of all phosphate products and is the main source of phosphorus for fertilizers. It can be of sedimentary, volcanic or

biological origin. The concentrations of U-238 and its decay products tend to be elevated in phosphate deposits of sedimentary origin. Here, a typical concentration of U-238 is 1500 Bq kg^{-1}. U-238 and its daughters are generally found in close radioactive equilibrium in phosphate ore.

Phosphate processing operations can be divided into the mining and milling of phosphate ore and the manufacture of phosphate products by either wet process or the thermal process. Wet-process plants produce phosphoric acid, the starting material for ammonium phosphate fertilizers: in the process, phosphogypsum is produced as waste or by-product, which is either stored in ponds or stacks or discharged into the aquatic environment. As an example, two phosphoric acid plants in the Netherlands are responsible for some 90 % of all discharges of Pb-210 and Po-210 to water [66]. Large amounts of phosphogypsum discharged in phosphoric acid production may be released into the sea as is the case in the Netherlands. Thermal process plants produce elemental phosphorus, which in turn is used for the production of high-grade phosphoric acid, phosphate based detergents and organic chemicals.

The concentrations of natural radionuclides in phosphate fertilizers vary markedly depending on the origin of the components. Generally, the concentrations of Th-232 and its decay products are always low, but the concentrations of the radionuclides of the U-238 decay chain are 5–50 times higher than in normal soil. Typical values are 4 and 1 kBq per kg P_2O_5 for U-238 and Ra-226, respectively. The global use of phosphate fertilizers constitutes one of the most important sources of mobile Ra-226 in the environment [67].

2.4 Other anthropogenic sources

Anthropogenic sources are sources of man-made character, i.e. no naturally occurring radioactivity sources. Nuclear explosions and nuclear weapon tests are some examples of anthropogenic sources of radioactivity, by which plutonium and fission products have been deposited on the earth, either directly or via the atmosphere in the form of fall-out. Radionuclides released into the air are mainly present in the form of aerosols. From nuclear power plants only limited amounts of radionuclides are allowed to enter the environment. Between 1992 and 2002, an annual average amount of about 6–10 TBq of tritium and 2.7–3.9 GBq C-14, in the form of $^{14}CO_2$, were released from German nuclear power plants with the exhaust air. The aqueous discharges of tritium released from German nuclear power plants in the same period were about 70–160 TBq per year. Under normal operating conditions, only small amounts of fission products, such as Sr-90, Tc-99, I-129, and Cs-137 were released; between 2.5 and 50 GBq per year [68].

Despite safety measures, accidents have happened with nuclear reactors and reprocessing plants, primarily due to human error. By these accidents parts of the radioactive inventory have entered the environment. Mainly gaseous fission products and aerosols have been emitted, but liquid radioactive solutions have also been given off. In the Chernobyl accident in 1986, gaseous fission products and aerosols were transported through the air over large dis-

tances. Even molten particles from the reactor core were carried with the air over distances of several hundred kilometres.

There are, in general, no anthropogenic sources of Pb-210. On the other hand, there are some incidents involving anthropogenic sources of Po-210. The largest accidental release of radioactivity in the British history of the nuclear industry happened on the 10 and 11 October 1957 in a nuclear reactor (Pile No. 1) at Windscale Works, Sellafield in the northwest of England. The fire led to an uncontrolled release of radioactive material to the atmosphere. The background to the fire is described in a publication by Arnold in 1995 [69]. The two reactors at Windscale Works were built for the production of plutonium and other materials for the UK weapons programme, such as Po-210. They were graphite-moderated reactors (electrical power: 180 MW_e), fuelled with a combination of natural and slightly enriched uranium metal. Cooling was done by air. In addition to the production of Pu-239 by neutron irradiation of U-238, the piles were used to produce Po-210 and tritium by irradiating bismuth and lithium, respectively, and to manufacture radionuclides for industrial and medical use (i.e. Co-60). The use of Po-210 in nuclear weapons is mentioned in section 2.1.3.2. The radioactive emissions were dominated by I-131 (900–3700 TBq), Cs-137 (90–350 TBq) and Po-210 (14–110 TBq) [70, 71, 72, 73].

Another source of anthropogenic Po-210 was involved in the polonium-affaire in London 2006, concerning the deceased former Russian agent Alexander Litvinenko (30.08.1962–23.11.2006). This incident has turned the public interest towards "radiological terrorism". Litvinenko unknowingly ingested a lethal amount of Po-210 on the 01.11.2006. The amount needed to kill a 70-kg person has been estimated to 0.7 μg Po-210 [33], also see 2.1.3.2. Since natural Po-210 is very rare in the environment, it is only possible to produce larger amounts (μg to mg) in a nuclear reactor by the irradiation of bismuth (see above). Reasons for choosing Po-210 as a poison include its high toxicity, the difficulties of detection (100 % alpha radiation), which makes Po-210 easy to transport through customs, as well as complicated to detect in a person who ingested it. In the polonium-affaire, a number of people came in contact with the radionuclide and had to be examined, including hospital personnel and hotel staff. The polonium-trail also led to Hamburg and Moscow. Consequently, the need for rapid and reliable Po-210 analyses was demanded. This was realised by the International Atomic Energy Agency (IAEA), which issued a proficiency test on the determination of Po-210 in spiked water in March 2007.

3 Aquatic Radiochemistry

3.1 Mobility of radionuclides

Mobility of radionuclides is the most important aspect when considering the behaviour of radionuclides in the environment. Gaseous species, aerosols and dissolved aqueous species are mobile and easily transported with air or water. Mobility of solid particles, however, may be caused by dissolution or suspension in water or spreading by wind. Solubility and leaching of solids depend on the properties of the solid containing the radionuclide and the properties of the solvent, in general water, in which the various components are dissolved. Redox potential (E_h), pH and complexing agents may be of significant influence.

The inventory of radionuclides on the earth, including surface waters, is mobile, provided that the species are soluble in water. A major part of the relevant radionuclides is of natural origin. K-40 is widely distributed in nature and easily soluble in the form of K^+ ions, which are enriched in clay minerals by sorption. Thorium in minerals is immobile, because chemical species of Th(IV) have a very low solubility in natural waters. However, some of the decay products of Th-232, such as Ra-228, Ra-224 and Rn-220, are mobile. In contrast to Th(IV), U(IV) is oxidized by air to U(VI), which is easily soluble in natural waters containing carbonate or hydrogen carbonate, respectively. The triscarbonato complex ($[UO_2(CO_3)_3]^{4-}$) is found in all rivers, lakes and oceans in concentrations of the order of 10^{-6} to 10^{-5} g l^{-1} [74]. In alkaline systems 75 % of the dissolved uranium is present as $[UO_2(CO_3)_3]^{4-}$ at pH 8, whereas at pH 9 more than 99 % of the uranium can be found as the triscarbonato complex. The daughters of U-238, the long-lived Ra-226 and Rn-222 are also mobile. However, the mobility of radium is dependent on the salinity of the water. In river and groundwaters radium is strongly adsorbed to particles; in sea water it is primarily dissolved. These differences in chemical behaviour are due to a change in the adsorption coefficient of radium between fresh and salt water and to a change in the average particle concentration between terrestrial and ocean waters [75]. Furthermore, Ra-226 is found in relatively high concentrations in mineral springs and salt water spas, and its daughter Rn-222 contributes considerably to the radioactivity in air. Rn-222 and the daughters Po-218, Pb-214, Bi-214, Po-214, Pb-210, Bi-210 and Po-210 are the major sources of the radiation dose received by man under normal conditions.

In the atmosphere, tritium and C-14 are generated continuously by the impact of cosmic radiation. The natural concentration of tritium in the air is about 1.4 mBq m^{-3} and that of C-14 is about 0.15 mBq m^{-3} [61].

From near-surface layers, radionuclides are brought to the surface by natural processes and by human activities, as described in Chap. 2.3. Rn-222 produced by decay of U-238 in uranium ore is able to escape into the air through crevices. Its decay products are found in the air mainly in the form of aerosols. Ions, such as Ra^{2+} and UO_2^{2+}, are leached from ores or minerals by groundwater and may come to the surface. Volcanic activities also lead to the distribution of radionuclides on the surface, where they may be leached out and enter the water cycle.

3.2 Radionuclide reactions in natural waters

3.2.1 General aspects of aquatic radiochemistry

In aqueous solutions, the majority of radionuclides are present in cationic forms, for which primarily the following reactions have to be taken into account [74]:

- Hydration (formation of aquo complexes): By ion-dipole interaction aquo complexes are formed. The energy of the hydration increases with ionic radius and with increasing positive charge of the cations. Accordingly, the energy of hydration is low for Cs^+ and high for Th^{4+}.
- Hydrolysis (formation of hydroxo complexes): If the charge of the cations is high (n > 2), the repulsion of the protons by the cations may lead to the formation of hydroxo complexes. Hydrolysis depends strongly on pH and increases with not only with charge, but also with decreasing ionic radius.
- Condensation (formation of polynuclear hydroxo complexes): Polynuclear complexes are formed by condensation reactions like

  $$2\,(M{-}OH)^{(n-1)+} \rightleftharpoons (M{-}O{-}M)^{2(n-1)+} + H_2O \quad (3.1)$$

  and subsequent condensation reactions. This type of reaction is not only observed with hydroxo complexes of the same metal M, but it takes also place with mononuclear or polynuclear hydroxo complexes of other elements (e.g. polynuclear iron(III) hydroxide, with silic or polysilic acid and with colloids carrying hydroxyl groups.
- Complexation (formation of various complexes with inorganic or organic ligands)
- Formation of radiocolloids (intrinsic or carrier colloids).

Inorganic anions such as Cl^-, CO_3^{2-}, SO_4^{2-} and HPO_4^{2-} and organic compounds containing functional groups compete with the formation of aquo and hydroxo complexes, depending on their chemical properties and their concentrations.

Groundwaters, rivers, lakes and the oceans contain a great variety of substances that may interact with radionuclides. Besides the main component (water), other inorganic compounds have to be considered [74]:

- Dissolved gases, such as oxygen and carbon dioxide, which influence the redox potential E_h and the pH.
- Salts, such as NaCl, $NaHCO_3$ and others, which affect pH and complexation and are responsible for the ionic strength.
- Inorganic colloids, such as polysilicic acid, iron oxides/hydroxides, and finely dispersed clay minerals giving rise to the formation of carrier colloids.
- Inorganic suspended matter (course particles, only found in agitated water).

Organic components in natural water include:

- Compounds of low molecular mass, e.g. organic acids, amino acids and other metabolites
- Compounds of high molecular mass, such as humic and fulvic acids, and colloids formed by these substances or by other degradation products of organic matter
- Suspended coarse particles of organic matter
- Microorganisms

The concentration of these compounds in natural waters varies over a wide range. Coarse particles are observed only in agitated waters and settle down as soon as agitation stops. Even though many of the components listed above may be present in rather low concentrations, their concentrations usually still are many orders of magnitude higher than that of the radionuclides in question and can therefore not be neglected.

Due to the large number of components, natural waters are rather complex systems. The relative concentrations of many components, as well as the pH and E_h, are controlled by chemical equilibria. However, there are also components, in particular colloids and microorganisms, for which thermodynamic equilibrium conditions are not applicable. These are the main reasons for the fact that simulations and model calculations are very difficult to perform.

The species of the radionuclides present in natural waters can be characterized by the chemical form and physical-chemical state (e.g. free ions, complexes, intrinsic colloids, carrier colloids) and speciation has become an important branch of radiochemistry.

3.2.2 Redox potential and pH

The redox potential has a great influence on the behaviour of radionuclides in geomedia, if different oxidation states have to be considered. In this context, the presence of oxygen (aerobic, oxidizing conditions) or of hydrogen sulphide (anaerobic, reducing conditions) in natural waters is significant. H_2S is produced by weathering of sulphidic minerals or by decomposition of organic material in the absence of oxygen. In stagnant surface waters, sediment-water, and soil systems, E_h and pH are especially important variables that are coupled to one another. An increase in E_h is accompanied by a decrease in pH. Solid organic matter as well as heterogeneous redox couples involving the solid phases Mn(III, IV)oxides, Fe(II, III)oxides, and FeS and FeS_2 in soils, sediments, and groundwaters provide important E_h and pH buffering. Redox reactions involving sulphur species in anoxic waters can form aqueous polysulphide ions that can efficiently complex many free metals, such as Fe(II), which can lead to the formation of insoluble pyrite, or Pb^{2+} which can form highly insoluble galena, PbS [76].

Fundamental changes in the water chemistry take place at the O_2/H_2S redox interface where a transition occurs from oxic to anoxic conditions. When organic matter is mineralised, alkalinity and the concentrations of NO_3^- and SO_4^{2-} increase and Fe(II) and Mn(II) be-

come mobilized [76]. Particulate Fe(III) and Mn(III,IV) are reduced to their divalent states and thus solubilized, as the redox potential decreases. At lower E_h values the concentrations of Fe(II) and Mn(II) further increase. At the oxic-anoxic boundaries a rapid turnover of iron takes place. This oxic-anoxic boundary may occur in deeper layers of the water column of fresh and marine waters, at the sediment-water interface or within the sediments. The redox cycling of Fe and Mn has pronounced effects on the adsorption of trace elements and radionuclides onto oxide surfaces as well as on the fluxes under different redox conditions.

In surface waters, dissolved Pb-210 and Po-210 are rapidly scavenged by iron and manganese oxides and biogenic particulates (e.g. plankton) that are then transported downward in the water column by particle settling. In the region above the O_2/H_2S redox interface, where MnO_2 begins aerobic reduction and dissolution, MnO_2-bound Pb-210 and Po-210 also become solubilized. The FeOOH-bound radionuclides will not be released until the O_2/H_2S redox interface is reached. The dissolved Pb-210 and Po-210 can then diffuse into anoxic waters (further downward) where they can be permanently removed from the water column by rapid sulphide (co)precipitation [77].

Both Pb-210 and Po-210 can be remobilized in significant amounts from lake sediments to the water column under reducing conditions [78]. Another remobilization path for polonium may be volatilization and subsequent release from sea sediments by microbial activity [79]. Sulphate-reducing bacteria are known to be able to use the sulphate moiety in gypsum in their normal metabolic activity. It was shown that these bacteria by breaking down the gypsum also reduced and released polonium contained in the gypsum [80].

In some seasonally anoxic lakes, the activity of Po-210 has been found to be higher than the Pb-210 activity. Redox sensitive elements, such as polonium, sulphur, iron, and manganese, appear to diffuse into bottom waters from sediments under summer anoxic conditions by forming reduced soluble species [81].

In general, a strong covariance between the vertical distribution of manganese and lead can be found, suggesting a preference of Pb-210 to manganese, rather than iron oxides. Except in surface water (where the loss of polonium might be explained due to volatilization, see 2.1.3.2), the vertical distribution of dissolved and particulate Po-210 appears to be closely tied to the behaviour of Pb-210 [82].

In general, only aquatic systems were considered in this work, and therefore the redox potential was limited to the redox reactions of water:

$$H^+ + e^- \rightleftharpoons \tfrac{1}{2} H_2 \tag{3.2}$$

$$\tfrac{1}{4}O_2 + H^+ + e^- \rightleftharpoons \tfrac{1}{2}H_2O \tag{3.3}$$

In acidic solution (pH = 0), the corresponding normal potentials are $E_S{}^0 = 0.000$ V for H_2/H^+ and $E_S{}^0 = 1.229$ V for H_2O/O_2, respectively. With increasing pH these potentials decrease according to the Nernst equation, at pH = 14 the $E_S{}^0 = -0.828$ V for H_2/H^+ and $E_S{}^0 = 0.401$ V for H_2O/O_2, respectively [76]. Most of the natural waters lie within these theoretical boundaries of the water redox potential. Typical pH values reach from pH = 4 for some mine waters

and acid rain to pH = 10 for saline and limey waters. The redox potentials of waters in contact with the atmosphere, for instance rain water (pH = 4–6), reach about 0.9 V. The redox potential decreases with increasing water depth or by the influence of reducing bacteria.

The only oxidation state of importance in aqueous solution for lead is +2 state, see also 2.1.3.1. In trace concentrations lead remains mainly as divalent cation and soluble hydrolysed species [18]. Compounds of the +4 plumbic ion are well known but are invariably instable or insoluble in aqueous solution. Due to the dominant stability of the +2 state in aqueous solution oxidation-reduction reactions are of minor importance in lead separations and determinations. The reduction potentials of lead in acidic solutions (pH = 0) at 25 °C are for Pb/Pb(II) –0.126 V and for Pb(II)/Pb(IV) +1.698 V [25]. The potentials are referred to the normal hydrogen electrode.

In Fig. 3 the E_h-pH diagram for lead species of the Pb-S-C-O-H system is shown.

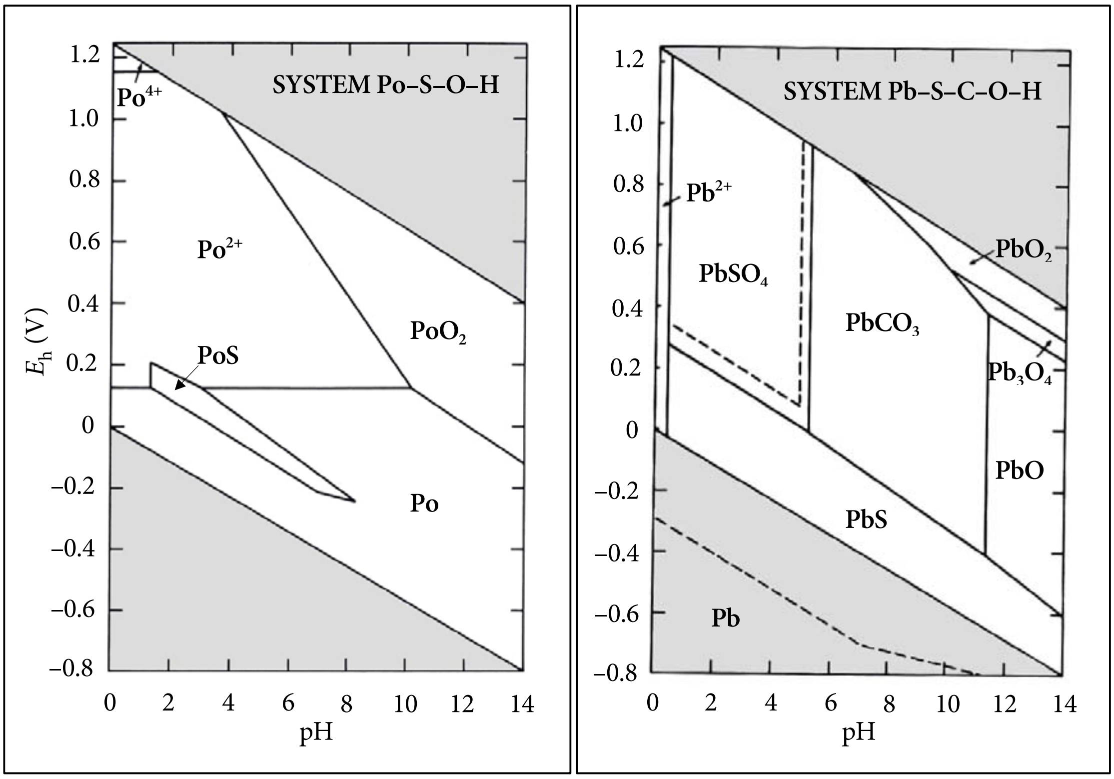

Fig. 3: E_h-pH diagrams for polonium (left) and lead (right) at T = 25 °C and p = 1 bar. Assumed activities for the dissolved species are: Po = 10^{-8} M, Pb = 10^{-6} M, S = 10^{-3} M, C = 10^{-3} M. The redox potential area for water exists within the white field [84].

Under reducing conditions, PbS (galena) occupies the E_h-pH space. Native lead is metastable, as it falls below the lower stability limit of water under sulphur-present conditions. In the absence of sulphur, or at greatly reduced sulphur activity, native lead is stable. When the sul-

phide-sulphate boundary is encountered, S^{2-} is oxidized to S^{4+} but Pb^{2+} remains unchanged. This results in a very small field of Pb^{2+} at pH below 0.4, followed by fields of $PbSO_4$ (anglesite), $PbCO_3$ (cerussite), and PbO (massicot or litharge). Under very oxidizing, near- neutral to basic pH, Pb(II) oxidizes to Pb(III) (i.e. Pb_3O_4; minium) and Pb(IV) (i.e. PbO_2; plattnerite).

In spite of the infinitely small amounts of polonium available for studies, a good deal of evidence was obtained in favour of a value of +0.8 V for the electrode potential Po/Po^{4+} [83]. The electrode potentials of Po are shown in Tab. 11. From the observed values of the electrode potential Po/Po^{4+} it appears that polonium lies between tellurium and silver in the electrochemical series.

Tab. 11: Electrode potentials of polonium [83]

Po/Po(IV)	Po/Po(II)	Po(II)/Po(IV)	Te/Te(VI)	Ag/Ag(I)
+0.8 V	+0.6 V	+1.1 V	+0.7 V	+0.8 V

The prevalent state of polonium is +4, but can in aqueous solution be found as Po^0, Po^{2+} and Po^{6+} (see 2.1.3.2), Po(II) being soluble and Po(IV) insoluble.

The E_h-pH diagram for aqueous polonium species in the Po-S-O-H system [84] is shown in Fig. 3. The diagram shows a large field of native polonium, and a somewhat isolated field of PoS. PoO_2 is important under oxidizing conditions, especially at intermediate to basic pH, while a large field of Po^{2+} occupies most of the acidic, oxidizing E_h-pH space. A small field of Po^{4+} occurs under the most extreme acidic, oxidizing conditions.

3.2.3 Inorganic salts

Inorganic salts affect the behaviour of radionuclides in natural waters in a number of ways. At high salinity the formation of colloids is hindered and colloids already present are coagulated, if salt water enters the system. Therefore, precipitation of colloids carried by rivers occurs in a large scale in the estuaries. Further, dissolved salts influence pH, hydrolysis and complexation. They may act as buffers, e.g. in seawater, where pH is kept constant at about 8.2 by the presence of $NaHCO_3$. Finally, the anions in natural waters form ion pairs and stable complexes with cationic radionuclides and affect solubility, colloid formation and sorption behaviour. Mobility may be enhanced by complexation. Cl^- ions are weak complexing agents, but are able to substitute OH^- ions in hydroxo complexes and to suppress hydrolysis. HCO_3^- ions are also found in significant quantities in natural waters, above all in seawater, and form rather stable carbonato and hydrogen carbonato complexes, as already mentioned for UO_2^{2+}, see section 3.1. The concentration of inorganic ligands in natural waters is given in Tab. 12.

Tab. 12: Concentration range of some inorganic ligands in natural waters (log conc. (M)) [76]

Ligand	Fresh water	Seawater
HCO_3^-	−4 to −2.3	−2.6
CO_3^{2-}	−6 to −4	−4.5
Cl^-	−5 to −3	−0.26
SO_4^{2-}	−5 to −3	−1.55
F^-	−6 to −4	−4.2
HS^-/S^{2-}	−6 to −3	—

The complexation of sulphate ions is rather unspecific and corresponds mostly to electrostatic interactions. HCO_3^- and CO_3^{2-} are of special importance as ligands because they are present in all natural waters at substantial concentrations. While alkali and earth alkali ions form primarily ion pairs with carbonate, metal ions such as Cd, Zn, and Pb form quite stable carbonato complexes. Sulphide becomes an important ligand under anoxic conditions. Both Pb-210 and Po-210 are particle-reactive, implicating a high affinity to bind to particles in solution [43, 44].

In Fig. 4 the inorganic speciation for lead in a representative freshwater composition is shown. In acidic natural waters lead is mostly found as free Pb^{2+} ions. With increasing pH, the aquatic carbonato complex starts to increase and at pH above 8 it is the predominant species.

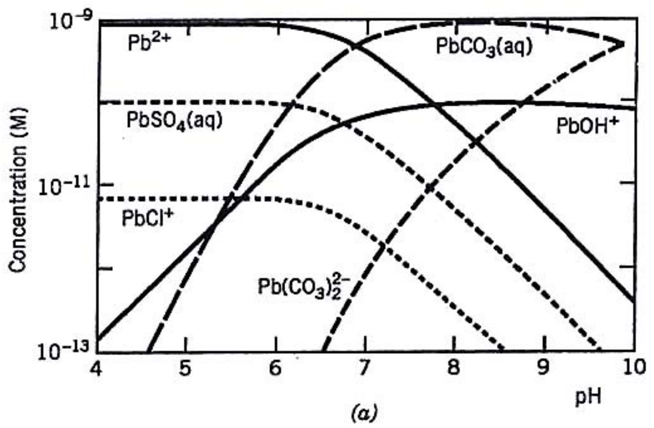

Fig. 4: Speciation of Pb(II) (10^{-9} M) under freshwater conditions. Dotted lines are calculated [76].

For most multi-ligand systems, the calculations can be carried out with the help of computer programmes, for example MINEQL [85] or MICROQL [86]. The total concentrations of the

components and the stability constants of the complex species are the inputs for such programmes.

With suspended inorganic matter (coarse particles of quartz, silicates, clay particles, iron hydroxide and other inorganic substances) radionuclides can also interact by sorption or ion exchange [87]. However, these particles are only observed in flowing natural waters, such as rivers. After transportation over certain distances, the particles settle down in form of sediments which contain the radionuclides bound on these particles.

3.2.4 Organic compounds

Organic compounds are primarily found in surface waters, but also in groundwaters, if these are or have been in contact with organic substances [88]. Compounds of low molecular mass may be of natural origin, such as metabolites (organic acids, amines or amino acids) or anthropogenic, such as detergents. Many of these organic compounds are strong complexing agents and well soluble in water.

Organic compounds of high molecular mass play an important role in natural waters and the knowledge about the behaviour of trace elements in aquatic systems can also be applied to radionuclides [76]. The most important examples of organic compounds of higher molecular mass are humic and fulvic acids, respectively, which both are degradation products of the cellulose of vascular plants. They are mainly composed of a polyaromatic molecular skeleton to which are linked functional groups such as –COOH and –OH. These groups give them their acidic character, as well as ion-exchange properties, make these compounds hydrophilic and enable them to form stable complexes in aqueous solutions. Humic acids are defined as the alkaline-soluble portion of organic material (humus) which precipitates from solution at low pH and are generally of high molecular weight. Fulvic acids are the alkaline-soluble portion which remain in solution at low pH and is of lower molecular weight. Other compounds of high molecular mass are proteins, lipids and carbohydrates. The concentration of dissolved organic matter (DOC) varies considerably in natural waters. Typical DOC values may be 0.7 mg l^{-1} in groundwaters, 2 to 10 mg l^{-1} DOC in rivers and may go up to about 60 mg l^{-1} in swamps.

Interaction of radionuclides with suspended coarse particles of organic matter depends on the nature of the substances and is principally comparable to the interaction with colloidal macromolecular compounds. The suspended particles may stay on the surface of rivers or lake, if their density is low, or they may settle down together with other coarse particles in form of sediments, if the agitation decreases [89].

Microorganisms play an important role in the scavenging of radionuclides, in particular of polonium. The chlorophyll-*a* content of seawater has been used as a measure of the abundance of phytoplankton biomass. The simultaneous measurements of Pb-210 and Po-210 in surface water show a positive correlation between removal rate constant and chlorophyll-*a*. The probability of Po-210 being scavenged by plankton increases in proportion to the abundance of phytoplankton. The ratio of Po-210/Pb-210 in surface waters shows a considerable

deficiency of polonium with ratios ranging between 0.04 and 0.11 [90]. Another study consequently shows that Po-210 is strongly enriched over its parent Pb-210 in plankton samples with an activity ratio generally over 10 and up to 40 [91]. The difference between lead and polonium can be explained by stronger sorption mechanisms for polonium: it has been found that Po-210 is absorbed into the microorganism cell interior, while Pb-210 sorption was a purely extracellular reaction [92]. Additionally, polonium is to a vast extent removed from surface seawaters by zooplankton (*Meganyctiphanes norvegica*) [93]. Through the metabolism of the zooplankton, polonium is excreted with the faeces, rapidly sinking towards the sea bottom where it may be remobilized depending on current redox condition.

3.2.5 Radiocolloids

True radiocolloids are colloidal forms of micro-amounts of radioactive substances. Their formation was first observed by Paneth [94] in his research on the separation of Bi-210 and Po-218. Radiocolloids can be separated from aqueous solutions by ultrafiltration, centrifugation, dialysis and electrophoresis.

In order to understand the nature of radiocolloids, knowledge of the general properties of colloids is needed. Colloids are finely dispersed particles in a liquid phase, a gas or a solid. The size of colloidal particles is in the range between that of molecules or ions, i.e. between about 1 nm and about 0.45 µm [95]. Small particles have a large specific surface area and a relatively large specific surface energy. Therefore, they have a tendency to form particles of lower specific energy, i.e. they are metastable with respect to larger particles. The main feature of colloids is that aggregation to larger particles is prevented by mutual repulsion, for example in water by electric charges of the same sign in the case of hydrophobic colloids or by shells of water the in case of hydrophilic colloids. Like normal colloids, radiocolloids show different behaviour from that of ions or molecules. For instance, they are generally not sorbed on ion exchangers or chromatographic columns [14].

Generally, radiocolloids may be generated in two ways [74]:

- The radionuclide may form an intrinsic colloid ("Eigenkolloid")
- The radionuclide may be sorbed on an already existing colloid which serves as a carrier (carrier colloid, "Fremdkolloid")

Formation of an intrinsic colloid is only possible if the solubility of the radionuclide is exceeded. If an isotopic or a non-isotopic carrier is present, the radionuclide will be incorporated if the solubility of the carrier is exceeded. In this case, a carrier colloid is formed containing the radionuclide in homogeneous or heterogeneous distribution. A carrier colloid is also formed if the radionuclide is sorbed on an already existing colloid.
In aqueous solutions, the generation of radiocolloids is favoured by hydrolysis of the radionuclide considered. Mononuclear hydroxo complexes may form colloids by condensation to polynuclear complexes if their concentration is high enough or they may be sorbed on the

surface of other colloids. The formation of these kinds of radiocolloids can be prevented by a low pH or by addition of a complexing agent.

Many organic molecules, such as humic substances found in natural waters, are large enough to form colloids. Radiocolloids containing organic compounds may be formed in two different ways: By sorption or ion exchange of radionuclides on macromolecular organic compounds or by sorption of organic complexes of the radionuclides on inorganic colloids. These organic complexes may be of low or high molecular mass. In all cases, the surface properties of the resulting colloids are decisive for their behaviour.

3.2.6 Precipitation and co-precipitation

Minerals from rocks dissolve in or react by interaction with water. Under different physico-chemical conditions, minerals are precipitated and accumulate on the ocean floor and in the sediments of rivers and lakes. Natural waters vary in chemical composition: by consideration of solubility relations the understanding of these variations is promoted. The solubilities of many inorganic salts increase with temperature, but a number of compounds of interest in natural waters ($CaCO_3$, $CaSO_4$) decrease in solubility with an increase in temperature.
In the first place those elements are involved in precipitation reactions that are present in sufficiently high concentrations in natural waters, so that the solubility limits are exceeded. For trace elements this condition is in most cases not fulfilled.

Precipitation may occur when species enter a system forming sparingly soluble compounds with the components already present, by change of pH or temperature, redox reactions, loss of volatile components, like CO_2, shift in complexation equilibria or evaporation of water. Examples often observed in natural waters are the precipitation of $CaCO_3$ due to loss of CO_2 and the shift of the equilibrium between $CaCO_3$ and $Ca(HCO_3)_2$, and the precipitate ion of Fe(III) hydroxide due to the oxidation of Fe(II) by access of air. Less common examples are the precipitation of sparingly soluble sulphates by reaction of SO_4^{2-} with group II elements.

Most radium salts are insoluble, particularly the sulphate and the carbonate. Little is known about the chemical properties of polonium because it has no stable isotope and Po-210 in intensely radioactive with a short half-life. Its aqueous chemistry is likely to be dominated by a tendency to hydrolyse to insoluble species or form anionic complexes. Stable lead isotopes are usually found in greatest abundance in association with sulphides but also occur in silicates (particularly potassium feldspar; the ionic radii of K^+ and Pb^{2+} are almost identical) and in apatite. With the exception of nitrate and acetate, lead salts are either insoluble or sparingly soluble in water, often associated with partial hydrolysis to monomeric and polymeric hydroxide species.

If low concentrations of radionuclides are considered, co-precipitation is generally the most important process. Hahn [96] distinguished two possibilities in the case of co-precipitation and these are: co-precipitation by isomorphous substitution and by adsorption, respectively. In the first case solid solutions (mixed crystals) are formed in which the micro-components replace the macro-component in its normal lattice by co-crystallization. In the

second case, the micro-components are incorporated as impurities during formation of amorphous precipitates or crystal growth, respectively.

Co-precipitation of sparingly soluble hydroxides, preferably Fe(III) hydroxide, is frequently used in analytical chemistry for separation of trace elements. Below, the formation of Fe(III) hydroxide by addition of a base to a solution containing Fe(III) ions is described [25]:

$$\left[Fe(H_2O)_6\right]^{3+} \xrightarrow{H^+} \left[Fe(OH)(H_2O)_5\right]^{2+} \xrightarrow{H^+} \left[Fe(OH)_2(H_2O)_4\right]^{+} \qquad (3.4)$$

$[Fe(H_2O)_6]^{3+}$ is only stable at pH below zero and is at pH = 0–2 transformed into $[Fe(OH)(H_2O)_5]^{2+}$. The colour of the precipitation rapidly shifts to yellow:

$\left[Fe(H_2O)_6\right]^{3+}$	pH ≤ 0	colourless
$\left[Fe(OH)(H_2O)_5\right]^{2+}$	pH = 0–2	yellow-brownish
$\left[Fe(OH)_2(H_2O)_4\right]^{+}$		

With a further raise in pH, the complexes condensate into two-core complexes:

$\left[(H_2O)_4Fe(\mu-OH)_2Fe(H_2O)_4\right]^{4+}$	pH = 2–3	yellow-brownish
$\left[(H_2O)_5Fe-O-Fe(H_2O)_5\right]^{4+}$		

The endothermic condensation continues as the H^+-concentration decreases, until 3-dimensional, macromolecular, colloidal condensates are formed:

$\left[Fe_x(OH)_y(H_2O)_z\right]^{w+}$	pH = 3–5	red brown

By further addition of base, the amorphous "iron(III)-hydroxide" $Fe_2O_3 \cdot x\ H_2O$ precipitates in form of a red brown gall-like mass.

The amorphous intermediates that are formed by condensation of mononuclear to polynuclear hydroxo complexes, see above, offer a high specific surface area with hydroxyl groups as reactive sorption sites for many species of trace elements or radionuclides, respectively, in particular cationic hydroxo complexes of metals in the oxidations states +3 and +4, like MOH^{2+}, MOH^{3+}, $M(OH)^{2+}$, $M(OH)_2^{2+}$ and others.

3.3 Biological availability

The radiological impact of radionuclides is usually evaluated with the aid of mathematical models. In such models the pathways of radionuclides to humans are described by transfer between compartments. The radionuclide transfer between compartments is commonly described by transfer parameters. In simple models these transfer parameters represent the ratio concentrations of a radionuclide in two compartments for equilibrium conditions. In more

complex models an attempt is made to represent the time dependent movement of radionuclides between the various environmental compartments.

Equilibrium rarely occurs in natural fresh water ecosystems owing to a variety of reactions (described in section 3.2), but is also influenced by seasonal fluctuations. Equally, the rapid movement of water and suspended sediments in rivers, estuaries and coastal waters may not satisfy the assumption of ecosystem spatial and temporal equilibrium.

In order to properly evaluate radiation exposure to human populations, the average annual dose arising from the naturally occurring levels of radionuclides in the environment and from release due to man-made practices (uranium and coal mining, nuclear power generation etc.) or events (e.g. nuclear accidents) is assessed.

In many countries the radioactivity in the environment is continuously measured by means of monitoring stations, in particular at and in the vicinity of nuclear power plants and other nuclear facilities. The principle objective of radiation protection and monitoring is the achievement of appropriate safety conditions with respect to human exposure. Consequently, radionuclides in those parts of the environment which are of immediate influence on human life (e.g. food stuffs or surroundings) are taken into account by safety regulations and are being monitored. However, the effects of radionuclides in other parts of the environment, particularly in other living things, have not been investigated in detail and the radioactivity in these parts is not kept under surveillance, even though radioactive fall-out has widely been distributed in the natural environment and radioactive waste has been disposed in remote areas, above all into deep sea. Therefore, radiological protection and monitoring of the whole natural environment has found increasing interest over the years.

3.3.1 Radionuclide uptake by plants

The main factor controlling the mineral content of plant material is the nutrient uptake potential for different minerals. The second factor is the availability of plant nutrients in the medium. The rate of nutrient uptake is highly dependent on the concentration in the external nutrient medium. Uptake data for calcium, radium, lead and polonium in different plants, soils and environmental conditions indicate that the plant uptake is a non-linear function of the nutrient concentration. Elements like calcium, radium and lead are taken up by plants increasingly to saturation. However, a different behaviour in uptake is observed for polonium: a threshold value is necessary before uptake of polonium becomes significant [97].

Chelates are known for transforming insoluble cations into soluble complexes and consequently making them available to plants. Multidentate synthetic chelating agents such as EDTA (ethylene diamine tetra-acetic acid), EDDHA (ethylene diamine di-*o*-hydroxyphenylacetic acid), and DTPA (diethylene triamine penta-acetic acid) are extensively used in agriculture to supply micronutrients to plants. In beans (Phaseolus vulgaris *L.*) no significant differences is observed between chelated Pb-210 complexes and ionic Pb-210. The shoot uptake of complexed Po-210 (Po-DTPA and Po-EDDHA) is however significantly increased in comparison to ionic Po-210 [98].

Uptake of radionuclides by plants occurs indirectly through the root system and directly from the deposition of radioactive fall-out on to the plant. The rate of transfer via roots depends on the concentrations of the radionuclides in the soil, while transfer through above-ground parts depends on the rate of radionuclide deposition from the atmosphere. Here Pb-210 and Po-210 play an important role, as they are daughters of Rn-222. Deposited radionuclides can be absorbed into plant tissues or can cause surface contamination. The transfer is also dependent of the shape of the plant, the leaf surface and the vegetative period. Between 60 and 95 % of the total contamination of the above-ground parts of plant is accounted to atmospheric deposition and subsequent incorporation of both Pb-210 and Po-210. Lead-210 is accumulated to a higher extent than Po-210, with Po-210 to Pb-210 ratios varying between 0.3 and 1.0. The concentration factor (or transfer factor) is defined as the ratio of the activity in plant (Bq kg^{-1} dry weight) to the activity in soil at a depth of 20 cm (Bq kg^{-1} dry soil), with no atmospheric deposition. For above-ground vegetables the transfer factors for Pb-210 and Po-210 were in average 7.1×10^{-2} and 4.4×10^{-2}, respectively, and in potatoes (underground parts) 2.5×10^{-2} and 1.4×10^{-2} for Pb-210 and Po-210, respectively [99]. These transfer factors are slightly higher with the factors recommended by the IAEA [100] for vegetables and potatoes (Pb-210: 1.0×10^{-2} and 1.3×10^{-3}; for Po-210 the data was not corrected for atmospheric deposition), respectively, but the trend is the same: the activity in above-ground plants is higher than in underground plants and the transfer factors for Pb-210 are higher than for Po-210.

It has been found that reeds (*Phragmites australis*) can bioaccumulate Pb-210 and Po-210 to a large extent and so help decontaminate water affected by uranium mining. Lead is accumulated to a higher extent than polonium. In the corresponding sediments, Pb-210 and Po-210 were in equilibrium (mining settling pond: 11 kBq kg^{-1} dry weight) and in reed roots (dry weight) activities of 813 Bq kg^{-1} Pb-210 and 674 Bq kg^{-1} Po-210 were found [101].

3.3.2 Radionuclide uptake by fresh water fish

The incorporation of radionuclides into food products derived from the aquatic environment such as fish may contribute to human exposure. Two important element dependent factors for the uptake are adsorption of radionuclides on sediments and suspended matter and the accumulation of radionuclides in fish.

A number of radionuclides (e.g. Pb-210, Po-210 and uranium) were measured in water, sediments and fish from four lakes (Quirke, Whiskey, McCabe, and Elliot Lake) affected by the uranium mining operations at Elliot Lake, Ontario, Canada [102]. Elevated concentrations of Pb-210 and uranium were found in water samples of the study lakes in comparison to control lakes. The activity concentrations of Pb-210 varied between 17 and 1094 mBq l^{-1} and were in general higher than for U. Concentrations in sediments were overall higher than in water. In fish (laketrout (*Salvelinus namaycush*) and whitefish (*Coregonus clupeaformis*)) elevated activities of Pb-210 and Po-210 were found, especially in the bones. In gut samples of whitefish

higher activities of Po-210 were found in one lake, probably due to the fact that whitefish is a bottom-feeding fish. In fish muscle no accumulation of radionuclides was observed.

The concentration ratio of Pb-210 in fish (wet bone/total in water) from Whiskey Lake was 747 in laketrout and 1020 in whitefish, the higher value in whitefish again probably because of its bottom-feeding habits. The bone/gut ratio was for both laketrout and whitefish about 3, indicating a radionuclide accumulation in the bones. In a previous study by Beak [103], the concentration ratio of Pb-210 in fish lay between 8–2500 in wet bone/total in water, and between 0.5–150 in wet muscle/total in water. These values can be compared to the concentration ratio for edible portions of freshwater fish (wet muscle/total in water) recommended by the IAEA, which for lead is 100–300. For polonium the concentration ratio is 10–500, and for radium 10–200 [69]. The range is wide because these include both piscivorous and bottom-feeding fish, the latter, as mentioned above, take up more radionuclides.

The effect of the Gunnar Uranium Mine tailings on the radionuclide concentrations in Langley Bay, Saskatchewan, Canada has been investigated by Waite *et al.* [104]. Water, sediments, and fish were analysed with regard to Pb-210, Ra-226, uranium and thorium. In the water samples there were no elevated radionuclide levels detected, except in samples taken from the principal creek exiting the tailings. The Pb-210 activity concentration was 4.1 Bq l^{-1} and the uranium content 1.3 Bq l^{-1} in average in these samples. The corresponding sediments contained about three orders of magnitude more Pb-210 and two orders of magnitude more U than was found in the water. In samples of fish (pike (*Esox lucius*) and whitefish (*Coregonus clupeaformis*)) elevated concentrations of Pb-210 (wet weight) were found in comparison to control samples, particularly in bones. In the gut content of whitefish high activities were detected, approximately 100-fold more Pb-210 as in the control samples. This was also found in Elliot Lake above. Compared with bone and gut content samples, the muscle and organ samples contained relatively low concentrations of radionuclides.

3.3.3 Radionuclide uptake by humans

The radiotoxicity of a radioactive element depends on the radiation emitted by the radionuclide considered, the mode of intake (e.g. by air, water or food), the size of the ingested or inhaled particles, their chemical properties (e.g. solubility), metabolic affinity, enrichment, effective half-life and ecological conditions. Radium has a very high radiotoxicity (Group I), and polonium and Pb-210 are characterised as highly radiotoxic (Group II) [105]. With respect to radiotoxicity, possible storage in the body and half-lives of radionuclides are very important. Removal from the body is characterized by the biological half-life, and the effective half-life $t_{1/2}(\mathrm{eff})$ is given by the relation [105]:

$$\frac{1}{t_{1/2}(\mathrm{eff})} = \frac{1}{t_{1/2}(\mathrm{b})} + \frac{1}{t_{1/2}(\mathrm{p})} \tag{3.5}$$

where $t_{1/2}$(b) and $t_{1/2}$(p) are the biological and physical half-lives, respectively. Physical half-lives and effective half-lives of some natural radionuclides in the human body are listed in Tab. 13. The latter depend mainly on the part of the body considered.

Tab. 13: Physical half-lives $t_{1/2}$(p) and effective half-lives $t_{1/2}$(eff) of some natural radionuclides absorbed in the human body [105]

Radionuclide	$t_{1/2}$(p)	Part of the body considered	$t_{1/2}$(eff)
U-238	4.47×10^9 y	Lung, kidney	15 d
Ra-226	1600 y	Bone	44 y
Rn-222	3.825 d	Lung	3.8 d
Po-210	138.38 d	Spleen	42 d
Th-232	1.40×10^{10} y	Bone	200 y

Ingestion is generally the most significant route of intake of radionuclides causing radiation exposure to humans. The fractional absorption in the gastrointestinal tract is described by the f_1 value, which is defined as the fraction of an ingested radionuclide that is directly absorbed to body fluids. In nearly all cases, one f_1 value for each age group has been estimated to be appropriate for ingestion of foodstuffs by members of the public [1]. The values used in this work are given in Tab. 14.

Age-specific biokinetic models for lead, bismuth, and polonium are given in [107]. They describe the tissue distribution, retention and excretion of systemic activity. The biokinetic transfer rates for lead are given in Tab. 15. These values show a fast transfer of lead from the plasma to the trabecular and cortical bone surfaces, especially for the younger age groups with still growing skeletons. The skeleton is not mature until about the age of 25 years and in the transfer rate modelling for elements such as lead, adults are taken to be 25 years, in contrast to most other cases where the adult is taken to be of age 20 years [106].

Tab. 14: Fraction of ingested radionuclides directly absorbed in the gastrointestinal tract [107, 108]

Radionuclide	Fraction f_1		
	0–1 year	1–17 years	> 17 years
U-238, U-234	0.04	0.02	0.02
Ra-226	0.6	0.3	0.2
Pb-210	0.6	0.4	0.2
Bi-210	0.1	0.05	0.05
Po-210	1.0	0.5	0.5

Tab. 15: Age-specific transfer rates for lead [107]

Transfer	Transfer rate (d^{-1})					
	3 months	1 year	5 years	10 years	15 years	adult
RBC to plasma	1.39×10^{-1}	1.39×10^{-1}	1.39×10^{-1}	1.39×10^{-1}	1.39×10^{-1}	1.39×10^{-1}
Bone surface to plasma	6.50×10^{-1}	6.50×10^{-1}	6.50×10^{-1}	6.50×10^{-1}	6.50×10^{-1}	5.00×10^{-1}
Nonexch trab vol to plasma	8.22×10^{-3}	2.88×10^{-3}	1.81×10^{-3}	1.32×10^{-3}	9.59×10^{-4}	4.93×10^{-4}
Nonexch cort vol to plasma	8.22×10^{-3}	2.88×10^{-3}	1.53×10^{-3}	9.04×10^{-4}	5.21×10^{-4}	8.21×10^{-5}
Liver 1 to plasma	3.12×10^{-2}	3.12×10^{-2}	3.12×10^{-2}	3.12×10^{-2}	3.12×10^{-2}	3.12×10^{-2}
Liver 2 to plasma	6.93×10^{-3}	6.93×10^{-3}	6.93×10^{-3}	1.90×10^{-3}	1.90×10^{-3}	1.90×10^{-3}
Other kidney tissue to plasma	6.93×10^{-3}	6.93×10^{-3}	6.93×10^{-3}	1.90×10^{-3}	1.90×10^{-3}	1.90×10^{-3}
ST0 to plasma	5.28×10^{0}	6.54×10^{0}	6.75×10^{0}	6.08×10^{0}	5.32×10^{0}	7.39×10^{0}
ST1 to plasma	4.16×10^{-3}	4.16×10^{-3}	4.16×10^{-3}	4.16×10^{-3}	4.16×10^{-3}	4.16×10^{-3}
ST2 to plasma	3.80×10^{-4}	3.80×10^{-4}	3.80×10^{-4}	3.80×10^{-4}	3.80×10^{-4}	3.80×10^{-4}
Plasma to RBC	2.00×10^{1}	2.48×10^{1}	2.56×10^{1}	2.30×10^{1}	2.02×10^{1}	2.80×10^{1}
Plasma to trab bone surf	5.25×10^{0}	3.15×10^{0}	3.11×10^{0}	4.94×10^{0}	7.23×10^{0}	4.86×10^{0}
Exch bone vol to bone surf	1.85×10^{-2}	1.85×10^{-2}	1.85×10^{-2}	1.85×10^{-2}	1.85×10^{-2}	1.85×10^{-2}
Plasma to cort bone surf	2.10×10^{1}	1.26×10^{1}	1.09×10^{1}	1.47×10^{1}	1.87×10^{1}	3.89×10^{0}

Tab. 15: Cont.

Transfer	Transfer rate (d^{-1})					
	3 months	1 year	5 years	10 years	15 years	adult
Bone surf to exch bone vol	3.50×10^{-1}	3.50×10^{-1}	3.50×10^{-1}	3.50×10^{-1}	3.50×10^{-1}	5.00×10^{-1}
Exch bone vol to nonexch vol	4.60×10^{-3}	4.60×10^{-3}	4.60×10^{-3}	4.60×10^{-3}	4.60×10^{-3}	4.60×10^{-3}
Plasma to liver 1	3.50×10^{0}	4.34×10^{0}	4.48×10^{0}	4.03×10^{0}	3.53×10^{0}	4.90×10^{0}
Liver 1 to liver 2	6.93×10^{-3}	6.93×10^{-3}	6.93×10^{-3}	6.93×10^{-3}	6.93×10^{-3}	6.93×10^{-3}
Plasma to kidneys (urinary path)	1.75×10^{0}	2.17×10^{0}	2.24×10^{0}	2.02×10^{0}	1.76×10^{0}	2.45×10^{0}
Plasma to other kidney tissues	1.75×10^{-2}	2.17×10^{-2}	2.24×10^{-2}	2.02×10^{-2}	1.76×10^{-2}	2.45×10^{-2}
Plasma to ST0	1.583×10^{1}	1.963×10^{1}	2.026×10^{1}	1.823×10^{1}	1.596×10^{1}	2.216×10^{1}
Plasma to ST1	5.00×10^{-1}	6.20×10^{-1}	6.40×10^{-1}	5.76×10^{-1}	5.04×10^{-1}	7.00×10^{-1}
Plasma to ST2	1.00×10^{-1}	1.24×10^{-1}	1.28×10^{-1}	1.15×10^{-1}	1.01×10^{-1}	1.40×10^{-1}
Plasma to urinary bladder contents	1.25×10^{0}	1.55×10^{0}	1.60×10^{0}	1.44×10^{0}	1.26×10^{0}	1.75×10^{0}
Kidneys (urinary path) to urine	1.39×10^{-1}	1.39×10^{-1}	1.39×10^{-1}	1.39×10^{-1}	1.39×10^{-1}	1.39×10^{-1}
Liver to small intestine contents	3.12×10^{-2}	3.12×10^{-2}	3.12×10^{-2}	3.12×10^{-2}	3.12×10^{-2}	3.12×10^{-2}
Plasma to ULI	5.00×10^{-1}	6.20×10^{-1}	6.40×10^{-1}	5.76×10^{-1}	5.04×10^{-1}	7.00×10^{-1}
Plasma to sweat	3.00×10^{-1}	3.72×10^{-1}	3.84×10^{-1}	3.46×10^{-1}	3.02×10^{-1}	4.20×10^{-1}
ST1 to excreta*	2.77×10^{-3}	2.77×10^{-3}	2.77×10^{-3}	2.77×10^{-3}	2.77×10^{-3}	2.77×10^{-3}

* Mainly hair, but includes loss in nails and desquamated skin

A urinary to faecal excretion ratio of 1:2 is assumed for polonium that has entered the transfer compartment.

The retention of Ra-226 and Pb-210 in the skeleton leads to an increased exposure of the bone surface and the red bone marrow. Coefficients for the absorbed equivalent doses in various tissues and organs for adults are given in Tab. 16.

Tab. 16: Ingestion dose coefficients for adult members of the public and an integration period of 50 years after intake [1]

Organ/ tissue	Equivalent dose coefficient, $g_{ing, r, j}$ (Sv Bq^{-1})					
	U-238	U-234	Ra-226	Pb-210	Bi-210	Po-210
Adrenals	2.5×10^{-8}	2.7×10^{-8}	4.1×10^{-8}	8.8×10^{-8}	2.0×10^{-11}	2.8×10^{-7}
Bladder Wall	2.5×10^{-8}	2.8×10^{-8}	4.0×10^{-8}	8.9×10^{-8}	5.8×10^{-11}	2.8×10^{-7}
Bone Surface	7.1×10^{-7}	7.8×10^{-7}	1.2×10^{-5}	2.3×10^{-5}	2.0×10^{-11}	1.6×10^{-6}
Brain	2.4×10^{-8}	2.7×10^{-8}	4.1×10^{-8}	8.8×10^{-8}	2.0×10^{-11}	2.8×10^{-7}
Breast	2.4×10^{-8}	2.7×10^{-8}	4.0×10^{-8}	8.8×10^{-8}	2.0×10^{-11}	2.8×10^{-7}
Oesophagus	2.4×10^{-8}	2.7×10^{-8}	4.0×10^{-8}	8.8×10^{-8}	2.0×10^{-11}	2.8×10^{-7}
St Wall	2.5×10^{-8}	2.9×10^{-8}	4.1×10^{-8}	8.8×10^{-8}	4.7×10^{-10}	2.8×10^{-7}
SI Wall	2.7×10^{-8}	3.0×10^{-8}	4.2×10^{-8}	8.8×10^{-8}	1.1×10^{-9}	2.8×10^{-7}
ULI Wall	3.9×10^{-8}	4.4×10^{-8}	6.4×10^{-8}	9.1×10^{-8}	6.0×10^{-9}	2.9×10^{-7}
LLI Wall	6.9×10^{-8}	7.6×10^{-8}	1.5×10^{-7}	9.8×10^{-8}	1.6×10^{-8}	3.2×10^{-7}
Colon	5.2×10^{-8}	5.8×10^{-8}	9.9×10^{-8}	9.4×10^{-8}	1.0×10^{-8}	3.0×10^{-7}
Kidneys	2.5×10^{-7}	2.9×10^{-7}	5.9×10^{-8}	3.7×10^{-6}	5.9×10^{-9}	1.3×10^{-5}
Liver	9.6×10^{-8}	1.1×10^{-7}	1.8×10^{-7}	1.9×10^{-6}	2.0×10^{-11}	6.6×10^{-6}
Muscle	2.4×10^{-8}	2.7×10^{-8}	4.0×10^{-8}	8.8×10^{-8}	2.0×10^{-11}	2.8×10^{-7}
Ovaries	2.5×10^{-8}	2.8×10^{-8}	4.1×10^{-8}	8.8×10^{-8}	2.0×10^{-11}	2.8×10^{-7}
Pancreas	2.4×10^{-8}	2.7×10^{-8}	4.0×10^{-8}	8.8×10^{-8}	2.0×10^{-11}	2.8×10^{-7}
Red Marrow	7.5×10^{-8}	8.1×10^{-8}	8.7×10^{-7}	2.5×10^{-6}	2.0×10^{-11}	2.6×10^{-6}
ET Airways	2.4×10^{-8}	2.7×10^{-8}	4.0×10^{-8}	8.8×10^{-8}	2.0×10^{-11}	2.8×10^{-7}
Lungs	2.5×10^{-8}	2.8×10^{-8}	4.0×10^{-8}	8.8×10^{-8}	2.0×10^{-11}	2.8×10^{-7}
Skin	2.4×10^{-8}	2.7×10^{-8}	4.0×10^{-8}	8.8×10^{-8}	2.0×10^{-11}	2.8×10^{-7}
Spleen	2.4×10^{-8}	2.7×10^{-8}	5.3×10^{-8}	2.8×10^{-6}	2.0×10^{-11}	1.1×10^{-5}
Testes	2.5×10^{-8}	2.7×10^{-8}	4.0×10^{-8}	8.8×10^{-8}	2.0×10^{-11}	2.8×10^{-7}
Thymus	2.4×10^{-8}	2.7×10^{-8}	4.0×10^{-8}	8.8×10^{-8}	2.0×10^{-11}	2.8×10^{-7}
Thyroid	2.4×10^{-8}	2.7×10^{-8}	4.0×10^{-8}	8.8×10^{-8}	2.0×10^{-11}	2.8×10^{-7}
Uterus	2.4×10^{-8}	2.7×10^{-8}	4.0×10^{-8}	8.8×10^{-8}	2.0×10^{-11}	2.8×10^{-7}
Remainder	2.7×10^{-8}	3.0×10^{-8}	4.0×10^{-8}	1.4×10^{-7}	1.0×10^{-10}	6.5×10^{-6}
Effective dose	4.5×10^{-8}	4.9×10^{-8}	2.8×10^{-7}	6.9×10^{-7}	1.3×10^{-9}	1.2×10^{-6}

4 Measurement Instrumentation

4.1 Alpha spectrometry

4.1.1 Alpha decay

By the alpha decay a helium nucleus is emitted, ${}^{4}_{2}He^{2+}$, and the atomic number decreases by two units and the mass number by four units (first displacement law of Soddy and Fajans).

All α-particles originating from a certain decay process are monoenergetic, i.e. they have the same energy. The energy of the decay process is split into two parts, the kinetic energy of the α-particle, E_α, and the kinetic energy of the recoiling nucleus, E_N:

$$\Delta E = E_\alpha + E_N \tag{4.1}$$

From the law of conservation of momentum it follows that

$$m_\alpha v_\alpha = m_N v_N \tag{4.2}$$

where m_α and m_N are the masses and v_α and v_N are the velocities of the α-particle and the nucleus, respectively, and eqn. (4.1) becomes

$$\Delta E = E_\alpha \left(1 + \frac{m_\alpha}{m_N}\right) \tag{4.3}$$

Because the mass of nuclei is appreciable higher than that of α particles ($m_N >> m_\alpha$), E_α is only about 2 % smaller than ΔE.

For some time, the theoretical interpretation of α-decay encountered a fundamental problem: scattering experiments showed that the energy barrier for α-particles entering the nucleus is relatively high (> 9 MeV), whereas α-particles leaving the nucleus have energies of only about 4 MeV. This problem was solved by the concept of quantum mechanical tunnelling [109], according to which there is a certain probability that α-particles are able to tunnel through the energy barrier instead of passing over it.

The range of alpha radiation is limited and depends on the energy of the alpha particle and the density of the absorber, i.e. a high density of the absorber results in a more efficient absorption. The course of an alpha particle is practically neither influenced by collisions with electrons nor is it deflected by collisions with nuclei. Along its way the alpha particle loses its energy by creating ion pairs in the absorber. As the energy decreases by about 3.6 eV per ion pair generated in a silicon semi conductor material, an alpha particle with an initial energy of 3.6 MeV produces about 10^6 ion pairs. At the end of its path it forms a neutral helium atom.

The range of alpha particles in air amounts in general to a few centimetres. The range in various substances for the high energetic Po-214 is listed in Tab. 17.

Tab. 17: Range of alpha particles of Po-214 (E = 7.69 MeV) in different substances [14]

Substance	Extrapolated range in (cm)	Density (g cm^{-3})
Air	6.95	0.001226
Mica	0.0036	2.8
Al	0.00406	2.702
Au	0.00140	19.32
Pb	0.00241	11.34

4.1.2 Alpha spectrometer

Characteristic for the alpha spectrometry measurements of environmental samples is the low activity of a few mBq to some Bq. The measurement requires therefore measurement systems with high counting efficiencies and low background radiation.

For the measurement of alpha radiation the directly ionising effect of alpha particles can be used. The measurements can be performed using gas-filled ionising detectors or semiconductor detectors, in which the electrical pulses released by the ionisation are counted [14, 123]. Another measurement principal commonly used for alpha detection is the liquid scintillation counting (LSC). In Fig. 5 below, the LSC spectrum of the polonium tracer, containing mainly Po-208 (E_α = 5115.2 keV), but also some Po-209 (E_α = 4881 keV), and the analyte Po-210 (E_α = 5304.4 keV) is shown. As can be seen, the energy resolution is obviously insufficient for alpha counting analyses, which require the addition of a tracer, even with an energy difference between Po-208 and Po-210 of almost 200 keV, also see 4.2.2.5. However, further application of the liquid scintillation counting in this work was applied for the measurement of the beta radiation of Pb-210, see 4.2.2. Alpha spectrometric measurements with high resolution were performed solely using semiconductor detectors.

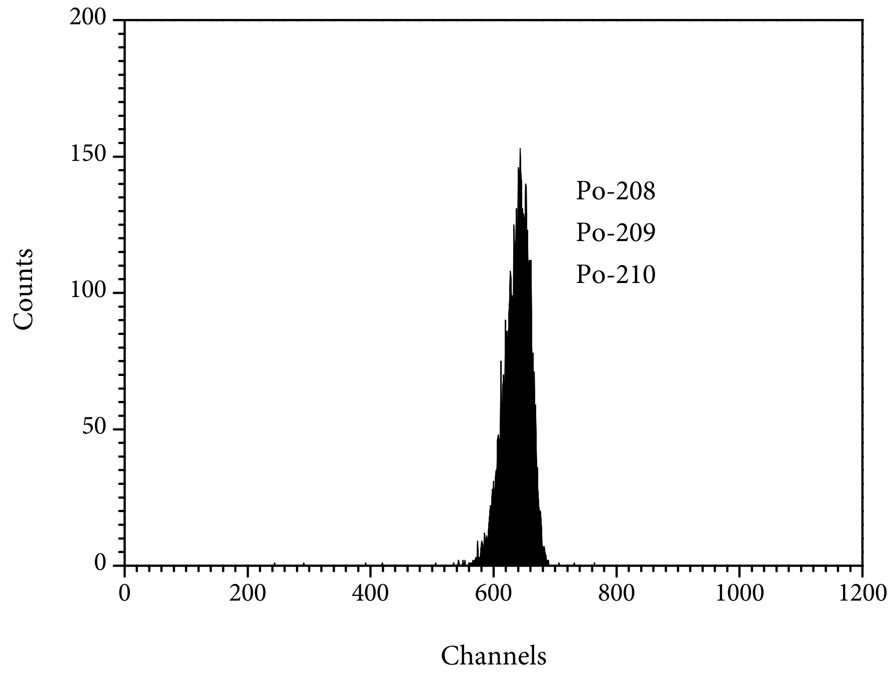

Fig. 5: LSC spectrum of similar activities of polonium tracer (Po-208 and Po-209) and Po-210, demonstrating the insufficient energy resolution of the LSC.

For the alpha counting measurements a commercially available instrument *(Canberra Model 7200 Alpha Analyst Integrated Alpha Spectrometer)*, in which all the necessary electronic components were integrated, was used. The measurements in this work were performed using an alpha spectrometer module *(Canberra Model 7200 Dual Alpha Spectrometer)*, which contained two counting chambers enabling two simultaneous measurements. The counting chambers were made of a stainless steel, which exhibits very low background count rates. The dimensions were 82.6 mm × 60.3 mm × 63.5 mm (H × B × T). Fig. 6 shows two counting chambers of a completely installed alpha spectrometer and the semiconductor detector from underneath.

The air pressure in the counting chambers could easily be adjusted within a range of p = 0.13–2.67 kPa (1–20 Torr) over fixed pipes and controllable valves with the help of a vacuum pump. The reduced air pressure between sample and detector within the chamber considerably lowered the absorption of the alpha radiation.

Fig. 6: An open alpha counting chamber next to a closed one (l). Semiconductor detector (*Canberra Model A300-17AM Alpha PIPS Detector*) (r) with the active surface facing downwards (PIPS = passivated implanted planar silicon).

In the upper part of each chamber was a connection, a so called microdot, where the semiconductor detector was installed. Circular detectors possessing an active surface up to 1200 mm², with an axial-microdot implementation, could be installed in the chambers. In this work detectors with an active surface of 450 mm² were utilised. The commercially available detectors *(Canberra Model A450-18AM Alpha PIPS Detector)* possessed an active diameter of 23.9 mm, a total diameter of 32.0 mm, and a height of 12.3 mm. The height of the microdot connection was 7.1 mm, see Fig. 7.

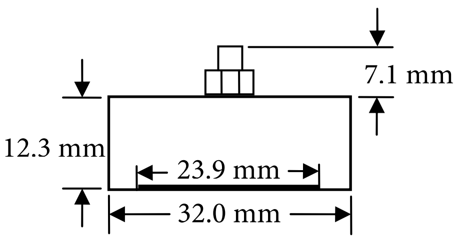

Fig. 7: Schematic figure of a PIPS detector, with the circular active surface facing downwards

The semiconductor detectors employed in this work were the passivated implanted planar silicon (PIPS) detectors. In most applications, this type of detector replaced silicon surface barrier (SSB) detectors and diffused junction (DJ) detectors.

The PIPS detector was fabricated by the planar process using photolithographic techniques for defining device geometries. As for the implanted detectors, the silicon wafer surface was not evaporated with metal (usually gold) as the SSB detectors, but was implanted with boron and arsenic ions to produce the *p*- and *n*-conducting layers [123]. Due to the passivated implanted surface of the PIPS detectors, instead of evaporated metallic contacts, as for the SSB, the PIPS detectors could be touched by hand and even cleaned with a cotton ball damped with isopropyl alcohol.

The low reverse leakage current of the PIPS detectors helped minimize peak shift with temperature variation and translates into low noise contribution. Unlike the SSB detectors, which have raw junction edges that were epoxy sealed to achieve some measure of stability, the PIPS detector junctions were all buried within the silicon wafer.

The entrance window of the PIPS detector was ion-implanted and thinner than conventional SSB detectors, with a thickness of < 500 Å, which improved the resolution.

The sample disc was placed at a distance of 10 mm below the detector in the alpha counting chamber, which was then evacuated. The active side of the sample disc was placed facing up towards the radiation sensitive surface of the detector. In Fig. 6, a sample disc can be seen placed on the height wise adjustable sample tray underneath the detector.

In order to actually detect the alpha radiation, an interaction between the alpha particles and the detector material had to take place. To be able to measure the energy spectrum, the entire alpha energy had to be absorbed within the radiation sensitive area of the detector. The thickness of the silicon wafer used in the semiconductor detector was between 275 and 315 µm. The actual radiation sensitive area was constituted of the depletion zone, which was produced by applying a voltage to the *p*-*n* junction. For the applied working voltage of $U = 40$ V, the depletion depth amounts to at least 140 µm [123], which was enough to completely absorb alpha energies up to 15 MeV. The detection efficiency of alpha radiation, which actually reached the detector, was therefore practically 100 %.

The direct ionizing effect of the alpha radiation created electron–hole pairs in the semiconductor material. These electron gaps were separated in the electric field of the detector. A charge sensitive pre-amplifier generated from this a voltage pulse, where the pulse height depended on the energy of the absorbed alpha radiation. The pulses produced by the preamp were additionally amplified by a linear amplifier and converted into a pulse shape, which was suitable as an incoming signal (i.e. positive polarity and amplitudes between 0–10 V) to an analogue-to-digital converter (ADC). The preset coarse gain factor was chosen so that pulses with the maximum amplitude of 10 V would correspond to a detected alpha radiation of the energy $E_\alpha = 7.00$ MeV. By using an additional fine gain setting of 1.500, the measurement region could be minimized to energies between 0–4.67 MeV, in order to improve the energy resolution. The analogue pulses from the linear amplifier were, corresponding to their pulse height, each assigned to one out of 1024 digital channels of a multi-channel analyser (MCA). The assigning of channels was performed using a conversion gain of 1024; meaning a pulse with the maximum amplitude of 10 V would be sorted into channel 1024. Accordingly, the first channel corresponded to $E_\alpha = 0.00$ MeV and the 1024th channel to $E_\alpha = 4.67$ MeV. The useful region of the analogue-to-digital converter was shifted by a constant value (the so

called ADC offset) of –550 channels, so that finally a measurement region between 2.51–7.17 MeV resulted. In this measurement region all of the alpha emitters relevant to this work could be measured.

The entire signal chain of one alpha counting chamber is schematically depicted in Fig. 8. The spectrometer was connected to a conventional personal computer (PC) using a network connection. The different parameter settings and the viewing of spectra was performed using the commercially available software *(Canberra Genie-2000 Basic Spectroscopy Software – Version 2.0)* [110, 111, 112, 113].

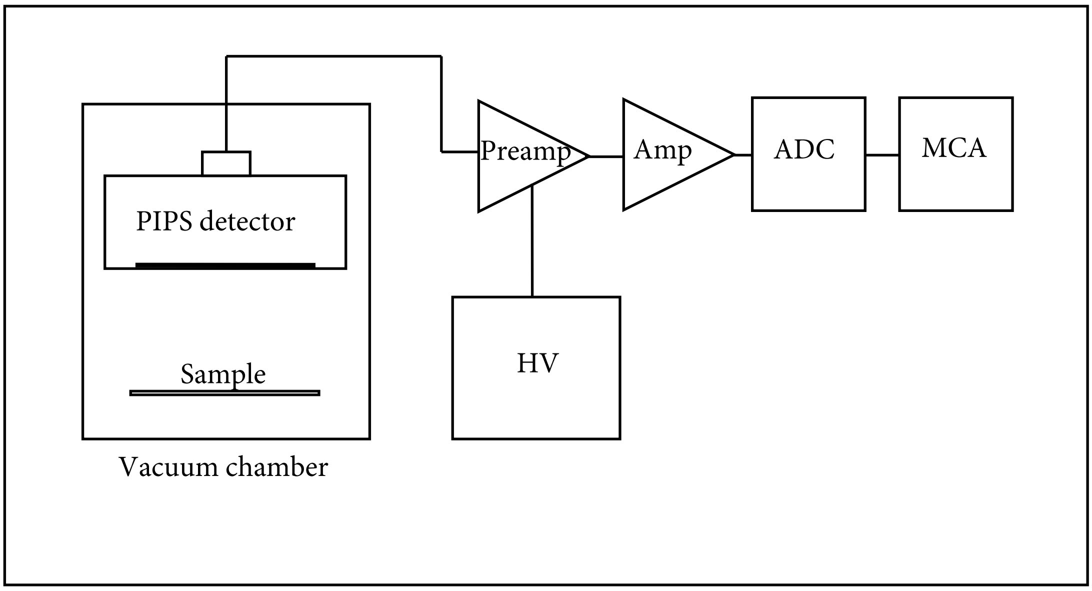

Fig. 8: Schematic figure of the alpha chamber signal chain.

4.1.2.1 Background radiation

Alpha spectrometry is a very useful and sensitive method for detection of alpha emitting nuclides in a variety of materials. One of the main reasons the technique is so sensitive is because of its low background. When new, a typical 450 mm² ion-implanted silicon PIPS detector would have a background count rate in the order of 0.004 impulses per minute for the 3–8 MeV region or less than 0.001 impulses per minute under individual regions of interest, usually about 300 keV wide. Unfortunately, this situation soon changes because of detector contamination dominated by two processes: (i) alpha recoil; and (ii) "volatilization" of polonium.

Alpha recoil contamination occurs when an alpha-emitting nuclide on the source disc decays to an alpha-emitting daughter or chain of daughters. The total decay energy is partitioned into two parts: the kinetic energy of the daughter nucleus and the kinetic energy of the alpha particle. The relatively small alpha particle is carrying away several MeV while the much more massive recoil nucleus is imparted with ≤ 100 keV. Important here is while the

kinetic energy of the recoil daughter small is in relation to the energy of the emitted alpha particle, it is very large in comparison to chemical binding energies which are generally < 5 eV. Thus, the recoil daughter easily breaks all chemical bonds by which it is held to adjacent atoms and it may be ejected from sources prepared for the alpha spectrometry. In the evacuated counting chamber the recoil daughter could reach the detector and, due to its high kinetic energy, it may be implanted deep into the crystal lattice of the detector window. Since the specific activity is inversely proportional to the half-life for a fixed number of atoms, recoil will produce the most background when relatively short-lived daughters are produced. However, if the half-lives in question are very short (up to a few hours), they will decay away quickly enough to be of little concern in alpha spectrometry. Particularly serious are those cases that involve transfer of recoil daughters with half-lives from days to weeks, short enough that a reasonable amount of parent activity will produce a significant amount of recoil contamination, and long enough that decay back to normal background levels will require an inappropriately long time.

Some common examples of decay chains that produce recoil contamination include Th-228 (produces alpha-emitting daughters Ra-224, Rn-220, Po-216, Po-212, and Bi-212), Th-229 (Ac-225, Fr-221, At-217, and Po-213), and Ra-226 (Rn-222, Po-218, and Po-214). Even beta-emitting nuclides ejected by alpha recoil can contribute to alpha background if they subsequently decay to alpha emitters.

Contamination of detectors by polonium isotopes probably occur by some other process than alpha recoil; namely the so called pseudo recoil effect. This is probably due to the inherent volatility of polonium at low pressure (see 2.1.3.2). Polonium activity is transferred from the sample sources to the detectors, a very serious problem with the long-lived Po-210 and even worse when working with Po-209 ($t_{1/2}$ = 102 y) as a yield tracer. For this reason it is better to use a less long-lived tracer, such as Po-208 ($t_{1/2}$ = 2.9 y), so that the contamination may decay within a reasonable amount of time. In order to reduce the pseudo recoil contamination from polonium, the sample disc should be heated on a hotplate for at least 5 minutes prior to measurement [114]. As mentioned in 2.1.3.2, polonium metal is oxidized to PoO_2, which is relatively non-volatile.

4.1.2.2 Prevention of contamination

Because of the large size and energy difference between the alpha particle and the recoil nucleus, it should be possible to put an absorber between the source and the detector which is thin enough to allow the high-energy alpha particles through, while stopping the heavier daughter nuclides. The recoil contamination is reduced a 1000-fold by leaving enough air in the alpha chamber to produce an air thickness of 12 to 16 μg cm^{-2} between the source and detector (air thickness: (μg cm^{-2}) = density (μg cm^{-3}) × distance (cm)) [114]. Air is the preferred material for an absorber because commercial films are either too thick and degrade the alpha spectra or too delicate to handle conveniently. The loss in peak resolution at an air thickness of 12 μg cm^{-2} was observed to be as little as 1–2 keV of the full width at half maximum (FWHM). The effect of air thickness on the apparent energy is depicted in Fig. 9, using

Po-210 as an example. The recoil nuclei, which were retarded by the residual air pressure, continue to drift around in the chamber because of their net positive charge. Hence, they could still reach the detector and cause a possible contamination. In order to further prevent recoil contamination, a negative potential (suppression bias) of $U = 5$ V was applied to the source plate relative to the detector, attracting the daughter nuclei back to where they originated.

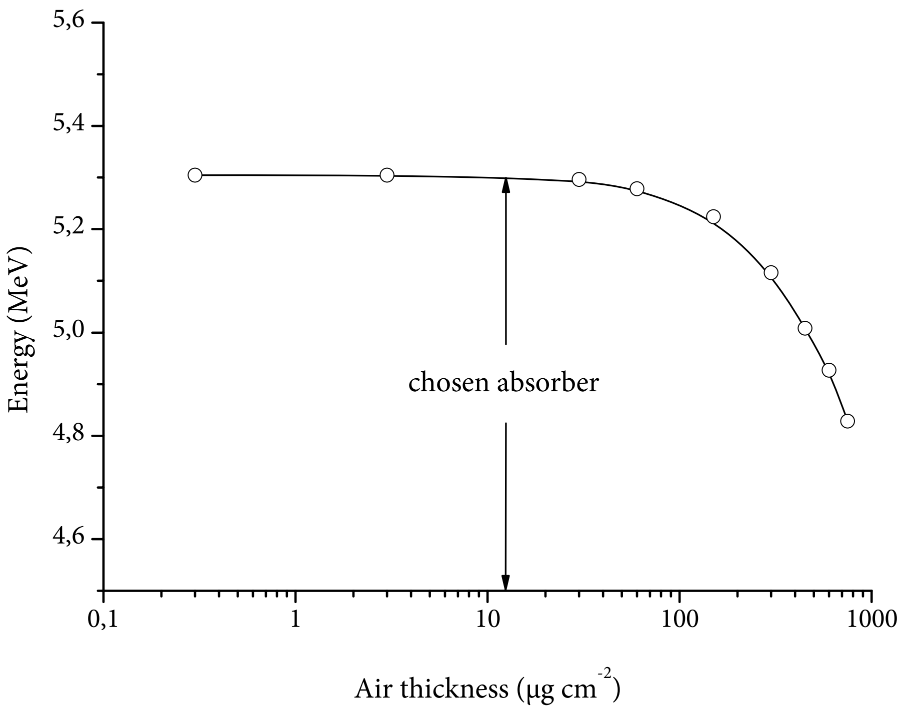

Fig. 9: Effect of air thickness on the apparent energy of Po-210 (E_α = 5304.5 keV). Results are replotted from data presented in [114].

The simplest way of reducing contamination was to reduce the time, in which the samples spent in the chambers. Therefore, the sample should only be measured long enough to ensure good statistics and then be removed from the chamber as soon as the measurement is completed.

Another important contribution to the background was provided by the radionuclides in air, due to the residual air pressure, used for recoil suppression. The most important radionuclide was the noble gas Rn-222 (E_α = 5489.7 keV), originating from the U-238 decay chain, but also to a lesser extent the Rn-220 (E_α = 6288.3 keV), originating from the Th-232 decay chain. The indoor air would contain an average of 55.9 Bq m^{-3} of Rn-222, which at normal pressure would correspond to an activity of 17.7 mBq and at a working pressure of

$p = 0.66$ kPa to an activity of about 0.12 mBq. Additionally, the activity of the Rn-222 alpha emitting daughters, such as Po-218, At-218, Rn-218, Po-214, and Po-210, had to be taken into account. Due to the short half-lives of the radon daughters, a radioactive equilibrium was relatively quickly established, with Po-218 ($t_{1/2} = 3.0$ min) as the rate-determining species. After waiting about 30 min (10 half-lives) the activity of Po-218 would have decayed enough to start the measurement with reasonably low background.

An additional way to reduce or eliminate the introduction of radon and moisture into the alpha counting chambers was by installing a so called clean vent, which allowed for the chambers to be vented with dried bottled air or nitrogen, which is free of radon and its progeny. All chambers were connected to a common vent manifold, which was supplied with low pressure nitrogen. When the counting chambers were vented for sample loading and unloading the chambers were backfilled with the supplied gas and continuously purged while the chambers were open. When using the clean vent feature, the 30 min waiting time before starting the measurement could be ignored.

The observed background for brand-new detectors arose mainly from radioactivity existing in the detector material and from radon in the air. The typical background amounted to about 0.05 h^{-1} cm^{-2} (referring to the detector surface) between the energies 3–8 MeV, which corresponded to 5.4 d^{-1} for the employed detector size of 450 cm^2.

The background was measured every 6 months throughout this work, in order to determine any changes in the background count rate. The results are shown in Fig. 10.

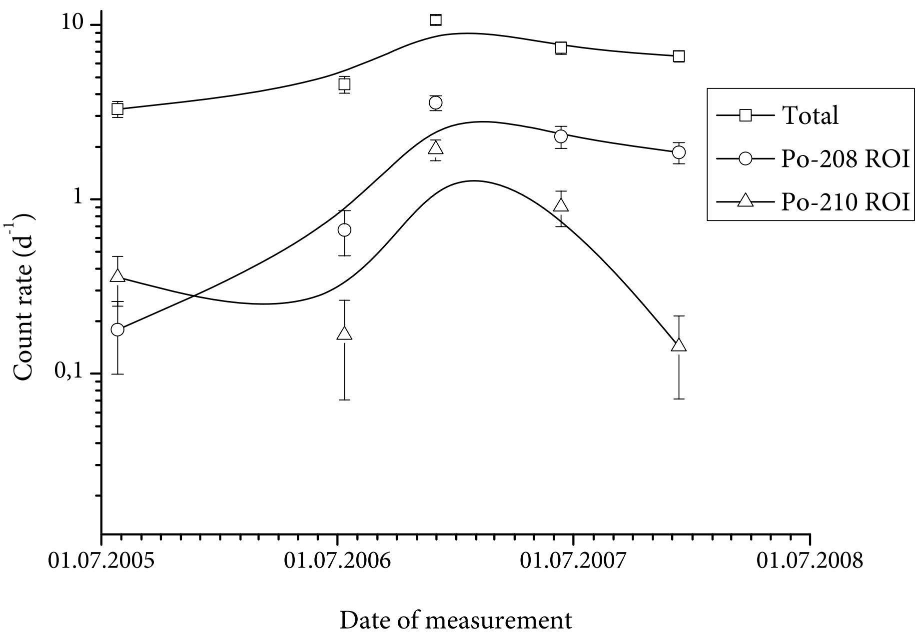

Fig. 10: Change of background count rate with time for detector 3A. Total count rate between all channels 1–1024 ($E_\alpha = 2.5$–7.1 MeV), the selected Po-208 region of interest (ROI) between channels 525–575, and Po-210 ROI between channels 580–630.

For the newly installed detector, the count rate amounted to 3.3 d^{-1}, increasing with usage, reaching a maximum of 10.7 d^{-1} after about 1.5 years in use. The main contaminations were attributed to Po-208 and Po-210, respectively, which could be observed in form of broadened peaks in the background spectra, accounting for about half of the total background count rate (in the measurement from 30.11.2006). The increase in background was a result of a number of measurements containing high activities. In the following year the total background count rate decreased to 6.6 d^{-1}. Since the relevant peaks only take up a minor region of the whole alpha spectrum, usually a region of interest (ROI) is set in order to limit the background count rate that region. In Fig. 10, the count rates for the Po-208 and Po-210 regions of interest, between channels 525–575 and 580–630, respectively, are depicted together with the total background count rate. As can be seen, the background count rates in both Po-208 and Po-210 ROIs decrease with time. The fact that polonium is volatile may result in atom implantation in the detector window, which will cause an increase in the background, see section 4.1.2.1. These implanted atoms decay with the corresponding half-life. The decrease in total background corresponded well to the decay of Po-208 ($t_{1/2}$ = 2.9 a), as well as to Po-210 ($t_{1/2}$ = 138.4 d).

4.1.3 Calibrations

The experimental energy calibration can be performed using a source, which contains at least two known alpha emitters. The calibration source should possess similar geometry and self absorption compared to the actual samples.

In this work a certified, commercially available calibration source (*AEA Technology QSA QCRB2500 Alpha reference source*), which contained about 1 kBq ± 30 % of each Pu-239, Am-241, and Cm-244, was used. The source was manufactured by deposition of the radionuclides from chemically pure solutions onto a stainless steel disc with a diameter of 25 mm and a thickness of 0.5 mm. Subsequently, a thermal treatment of the disc took place, in order to improve the mechanical fixation and chemical passivation.

4.1.3.1 Energy calibration

For the energy calibration the detector to sample distance was chosen to 50 mm. This rather large distance was chosen to spare the detectors from unnecessary contamination, which could arise from the calibration source, but also to reduce the effect of the different sample geometry.

In Fig. 11 the measured alpha spectrum of the calibration source is shown. The energy calibration was performed with the help of such spectra, using the most important alpha energy of Pu-239 (E_α = 5156.2 keV; P_α = 73.3 %), Am-241 (E_α = 5485.6 keV; P_α = 85.2 %), and Cm-244 (E_α = 5804.96 keV; P_α = 76.98 %), respectively.

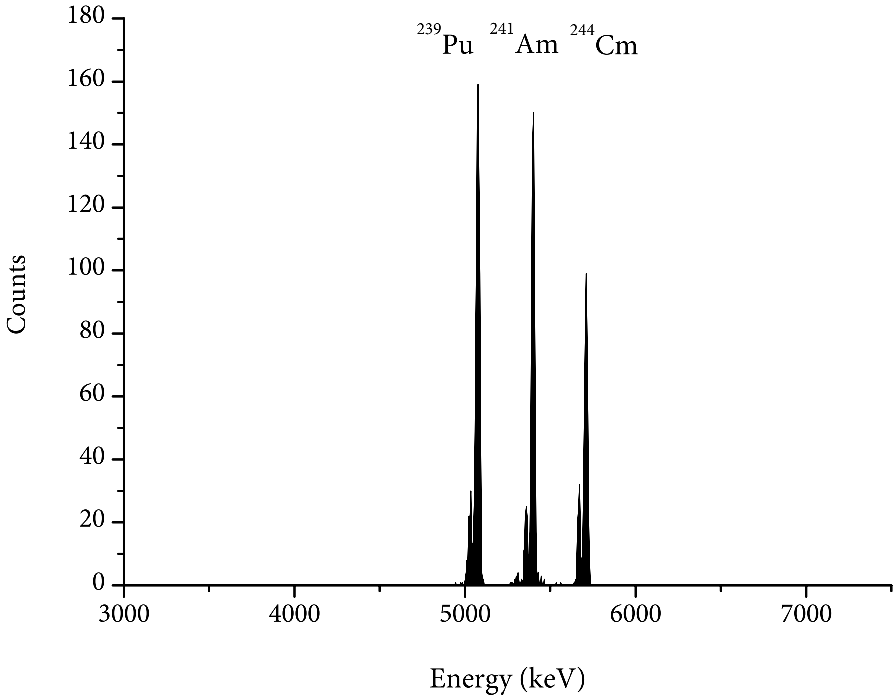

Fig. 11: Measured alpha spectrum of the calibration source *(AEA Technology QSA QCRB2500 Alpha reference source)*

4.1.3.2 Efficiency calibration

The calibration of the counting efficiency ε of an alpha spectrometer was necessary for the conversion of the observed count rates into the corresponding activities. However, the determination of the activity ratio of the radionuclides within an alpha spectrum was possible without knowing the counting efficiency.
The experimental efficiency calibration could be performed using calibration sources with known alpha activities. Since the efficiency was nearly independent of the alpha energy, it was sufficient to use only one calibration source. In this work the efficiency calibration was performed using the same source as was used for the energy calibration (*AEA Technology QSA QCRB2500 Alpha reference source*). However, the activities of the three radionuclides (Pu-239, Am-241, and Cm-244 each of 1 kBq) were given with a relatively high uncertainty of ± 30 % (k = 2; p = 95 %), which would not be accurate enough for the efficiency calibration. On the other hand, the certified uncertainty of the total alpha activity was with ± 5 % (k = 2; p = 95 %) markedly lower, and could therefore be used for the calibration.

The alpha radiation from the sample source was emitted evenly in all directions, so that only a part of the radiation reached the radiation sensitive surface of the detector. The maxi-

mum theoretical efficiency was $\varepsilon = 50$ %, which was achieved at a direct detector contact ($d = 0$). With increasing sample distance from the detector the efficiency would decrease. The counting efficiency for the alpha detectors 3A and 3B was determined at the distance $d = 10$ mm and the result thereof is shown in Tab. 18. The empirical efficiency for both detectors used in this work was about 15 %.

Tab. 18: Counting efficiency of the alpha detectors at a detector distance of 10 mm

Detector	Empirical efficiency ε (%)	Simulated efficiency ε (%)
3A	15.0 ± 0.8	14.7
3B	15.2 ± 0.8	14.7

The detector efficiency could also be simulated using a Monte-Carlo simulation, when parameters such as sample diameter, sample–detector distance, and diameter of the radiation sensitive surface of the detector were known. In Fig. 12 below, the theoretical detector efficiency ε depending on the detector distance is graphically presented. The theoretical efficiency for a 450 mm^2 PIPS detector at the sample–detector distance of 10 mm was 14.7 %. This corresponded well with the empirical value for the same detectors.

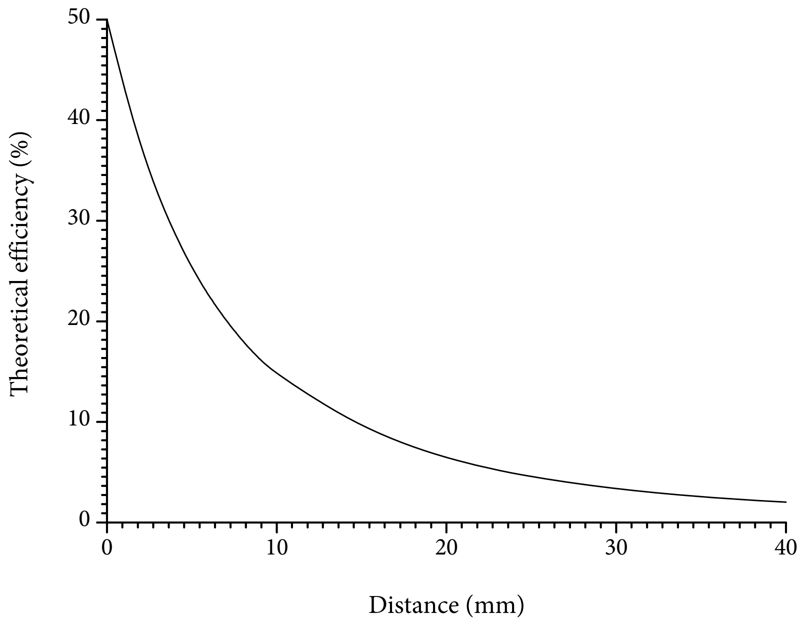

Fig. 12: Theoretical detector efficiency (simulated) for a 450 mm^2 PIPS detector and a source diameter of 21.3 mm.

4.2 Beta spectrometry

4.2.1 Beta decay

Nuclides with an excess of neutrons experience β^- decay. By the beta decay, a neutron is converted into a proton, an electron and an electron antineutrino. The atomic number increases by one unit, whereas the mass number remains the same (second displacement law of Soddy and Fajans). Nuclides with an excess of protons exhibit β^+ decay. A proton in the nucleus is converted into a neutron, a positron and an electron neutrino. The atomic number decreases by one unit, and the mass number remains unchanged. The equations (4.4) and (4.5) are valid for β^- and β^+ decay.

$$\beta^- : \quad {}_0^1\text{n(nucleus)} \rightarrow {}_1^1\text{p(nucleus)} + {}_{-1}^{\ 0}\text{e}^- + {}_0^0\overline{\nu}_\text{e} \tag{4.4}$$

$$\beta^+ : \quad {}_1^1\text{p(nucleus)} \rightarrow {}_0^1\text{n(nucleus)} + {}_1^0\text{e}^+ + {}_0^0\nu_\text{e} \tag{4.5}$$

As an alternative to β^+ decay is electron capture (EC, symbol ε). Electrons are available from the electron shell of the nuclide, and the transformation of an excess proton into a neutron can also proceed by taking up of an electron. As the K electrons have the highest probability of being close to the nucleus, they have also the highest probability of being captured. The result is the same as in the case of β^+ decay. But instead of positrons, characteristic X-rays are emitted, because the empty K shell of the atom is filled up with electrons of higher shells, a process that is associated with the emission of characteristic X-rays. These X-rays from the K shell are monoenergetic, and therefore radionuclides exhibiting electron capture are of practical interest as X-ray sources. Electron capture is described by the following equation:

$$\varepsilon : \quad {}_1^1\text{p(nucleus)} + {}_{-1}^{\ 0}\text{e}^-\text{(shell)} \rightarrow {}_0^1\text{n(nucleus)} + {}_0^0\nu_\text{e} \tag{4.6}$$

In contrast to alpha particles, beta particles do not have a distinct energy, but they show a continuous energy distribution. The energy of the emitted electrons varies between zero and the maximum energy, E_{max}, since this is divided between the electron and an electron antineutrino:

$$E_{\text{max}} = E_\text{e} + E_\nu \tag{4.7}$$

where E_e is he energy of the electron and E_ν the energy of the electron neutrino or antineutrino, respectively. The neutrino has no charge and an extremely small mass. The energy ΔE is split up:

$$\Delta E = E_\text{e} + E_\nu + E_\text{N} \tag{4.8}$$

where E_e is the energy of the electron or positron, respectively, E_v that of the electron antineutrino or the electron neutrino, respectively, and E_N the recoil energy of the nucleus.

The interaction of beta radiation with matter is much weaker than that of alpha radiation. Whereas a 3 MeV alpha particle has a range of about 1.7 cm in air and produces several thousand ion pairs per millimetre, a beta particle of the same energy covers a distance of about 10 m in air and produces only about 4 ion pairs per millimetre. On the other hand, the electrons are markedly deflected by collisions with other electrons, in contrast to the heavy alpha particles, and they therefore exhibit a zigzag course.

Beta radiation interacts with matter in three different ways:

- Interaction with electrons, which leads to ionization. The important parameter is the electron density in the absorber, given by Z/A; more electrons give better absorbing properties.
- Interaction with atomic nuclei increases with the beta radiation energy. In the electric field of a nucleus high-energy electrons emit X-rays of continuous energy distribution (bremsstrahlung) and lose their energy in steps.
- Backscattering depends on the energy E_{max} of the beta radiation and the atomic number Z of the absorber.

With respect to radiation protection, absorbers of low atomic numbers Z are most useful for absorption of beta radiation, for instance aluminium of about 1 cm thickness (Bremsstrahlung may be produced when electrons (beta radiation) interact with materials of high atomic numbers).

4.2.2 Liquid Scintillation Counting

4.2.2.1 Comparison of beta spectrometry methods

For the measurement of beta radiation three methods exist: gas flow proportional counting (GF-PC), Čerenkov counting and liquid scintillation counting (LSC) with alpha/beta discrimination. For the simultaneous measurement of alpha and beta emitting radionuclides in the same sample, only the GF-PC and the LSC can be considered.

A typical gas flow detector consists of a tube with a high conductivity copper body, an anode wire, and a thin Mylar window [14]. The detector is filled with a mixture of argon and methane gas. Alpha and beta particles penetrate the window and ionize the gas. This ionization results in further ionizations because of the potential applied between the anode and cathode. Ultimately, the ionization accumulates on the anode wire and produces an electrical pulse. The separation of the alpha from the beta emitters is based on the pulse height. This can be accomplished because the alpha emitters produce a pulse which is about 40 times higher than that of the beta pulse. The sample preparation for the GF-PC involves evapora-

tion of the sample to dryness on a planchet. This will lead to higher amounts of solid material deposited onto the planchet. The presence of even milligram quantities of material will greatly affect the counting efficiencies for alpha [115] and, to a lesser extent, beta emitters. For a typical GF-PC source, the self-absorption correction was found to be as high as 8 % for the beta emitting Tl-204 [116]. Typical counting efficiencies are 30 % for alphas and 40 % for betas. The detection limit lies in the range of a few Bq per litre [117].

A second method for detecting beta radiation is through the Čerenkov radiation. The intense blue radiation was first discovered by P. A. Čerenkov and appears when charged particles travel with a higher velocity than the velocity of light in a transparent medium [118]. Alpha radiation, however, does not produce Čerenkov radiation. The Čerenkov radiation is observed if beta particles passes through a transparent substance, such as water, because the condition $v \geq c / n$ (n = refractive index of the medium) is already fulfilled for beta particles at relatively low energies. The minimum kinetic energy that the beta particle needs to produce Čerenkov radiation in water is E_{kin} = 216 keV. Therefore, low-energy beta emitters cannot be detected and a chemical separation to remove interfering beta emitters is often not necessary. For instance can Pb-210 (E_{max} = 63 keV) be discriminated from Bi-210 (E_{max} = 1.2 keV). For the Čerenkov measurement no scintillation medium is required, any transparent medium will be sufficient. However, the counting efficiency is relatively low, for Bi-210 in the range of 10 %, which will lead to higher detection limits.

The third and most commonly used method for simultaneous quantitation of alpha and beta particles is the liquid scintillation counting using pulse shape analysis (PSA). As early as 1937, Professor H. P. Kallmann noted that certain organic materials fluoresced under ultraviolet light [119]. Kallmann also showed that aromatic solvents with certain dissolved solutes were efficient scintillation sources when subjected to nuclear radiation and from here on the LSC detection method was further developed. The LSC as we know it today is a widely used method for the detection of beta emitting radionuclides. The radionuclides are usually dissolved in a scintillation cocktail, but in some cases suspensions or whole filters are mixed with the cocktail and measured. Due to the close contact of the radionuclide to the detector medium high efficiencies can be achieved, so that even nuclides with low energy beta radiation, such as tritium and Pu-241, can be measured with high efficiencies. Counting efficiency is nearly 100 % for alpha emitters. Generally, the detection limits are low, markedly under 1 Bq per litre. Due to its higher efficiencies for alpha as well as beta emitters, the lower detection limits, and the wider range of measurement flexibility the further work will be focussed on the LSC.

4.2.2.2 LSC counting vials

The beta radiation of the usual radionuclides in solutions has a range of about one centimetre. This allows for small dimensions of counting vials, a few centimetres would be enough even for high energy beta radiation. The most common types of counting vial materials are summarised in Tab. 19. The vials could be made of low potassium borosilicate glass or poly-

ethylene (PE), the latter with the lowest background radiation. Vials made of quartz and Teflon, respectively, are also available, exhibiting lower background. The advantage of Teflon vials is that they can be re-used.

Tab. 19: Different types of scintillation counting vials [118]

Type	Main advantage	Main disadvantage	
Glass (borosilicate)	Low cost	High background, absorption in near UV	
Low K glass	Reduced background from K-40	Absorption in near UV, expensive	
Quartz	Increased transmission in the UV	Expensive	
Plastic (polyethylene)	Low background, low cost, higher efficiency	Some solvent loss	
Nylon	Low background	Cost, solvent loss	
Teflon	Low background, can be re-used, high efficiency	Cost, has to be machined	

The mentioned materials are available for vials which range in volume from mini-vial categories (approximately 7 ml), to conventional vial of approximately 18–22 ml capacity. Mini-vials show a 3–5 % counting efficiency increase at any given quench compared to the larger vials [120]. The better counting efficiency is due to the more central position between the two photomultipliers. Disadvantageous is the lower sample volume that can be measured, increasing the limit of detection.

4.2.2.3 Scintillation solutions

The quest for optimum efficiency has prompted the development of a wide variety of liquid scintillation counting solutions. A scintillator solution (usually called cocktail) is composed of one or more solvents and one or more solutes (scintillators). The solvent acts as a medium for absorbing energy of the nuclear radiation and for dissolving the sample. The solute acts as an efficient source of photons after accepting energy from the excited solvent molecules.

The base for the scintillation cocktail is an aromatic solvent; commonly used earlier were toluene, dioxane, xylene, or 1,2,4-trimethylbenzene (pseudocumene). A growing concern of health risk handling these scintillation cocktails led to the introduction of new scintillation

cocktails. The common solvents today are less toxic and possess higher flash points; examples are phenyl-xylylethane (PXE) and di-isopropylnaphthalene (DIPN), see Tab. 20.

Tab. 20: Some commonly used solvents in the LSC [118]

Solvent	Structure	Relative scintillation yield	Flash point (°C)
Toluene	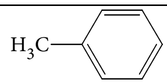	100	4
Dioxane	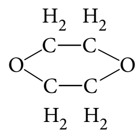	65	11
p-Xylene	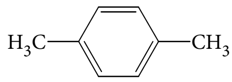	110	25
1,2,4-Trimethylbenzene (Pseudocumene)	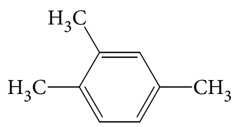	112	50
Phenyl-xylylethane (PXE)	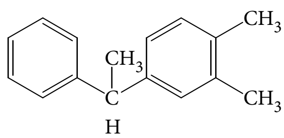	110	150
Di-Isopropylnaphthalene (DIPN)	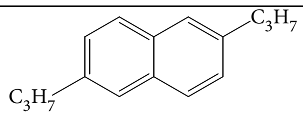	112	150

Naphthalene and its derivates, such as DIPN, will in general raise the scintillation yield, because they possess properties of a primary scintillator (i.e. they emit light with wavelengths < 400 nm). However, the scintillation yield is the energy produced as photons by the scintillator solution upon excitation by a particle, and should not be confused with the counting efficiency, which is a measure of the fraction of particles that produce a measurable pulse [118].

The alpha or beta particles excite the solvent molecules and these excited solvent molecules give part of their excitation energy to a scintillation molecule, which gets excited. The scintillation molecule then relaxes under emission of photons. As scintillation materials are often organic compounds with phenyl-, naphtyl-, biphenyl-groups, oxazole and oxadizole in

small amounts (a few per cent) used [15]. The most common one is diphenyl oxazole (PPO). This and other examples are listed in Tab. 21. These so called primary scintillators emit light in the ultraviolet range, varying between 334 and 385 nm.

Tab. 21: Properties of a few primary scintillators [118]

Scintillator	Structure	Peak fluorescence (nm)	Decay time (ns)
2,5-Diphenyloxazole (PPO)	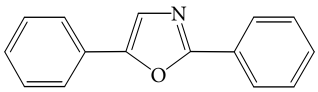	375	1.4
p-Terphenyl	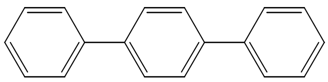	342	1.0
Butylphenylbiphenyl-oxadiazole (Butyl-PBD)	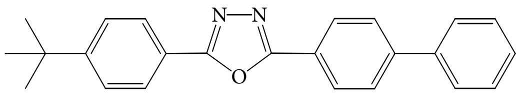	385	1.0
Naphthalene	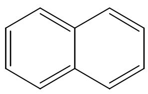	334	96.0

The photocathode in the photomultiplier is not able to detect UV light (wavelength < 400 nm) and consequently secondary scintillators are added (a few per mille) to ensure the adaptation of the wavelength from UV to visible light (blue; wavelength just over 400 nm). The addition of secondary scintillators will also reduce the absorption of the emitted UV-light, since most aromatic compounds also absorb light in the UV-range. Common secondary scintillators are bis-MSB and POPOP, see Tab. 22 below.

Tab. 22: Some commonly used secondary scintillators [118]

Compound	Structure	Average wavelength (nm)
Diphenyloxazolylbenzene (POPOP)	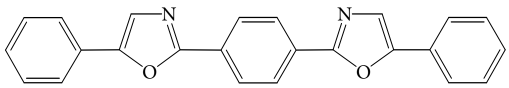	415
1,4-Bis(2-methylstyryl)benzene (bis-MSB)	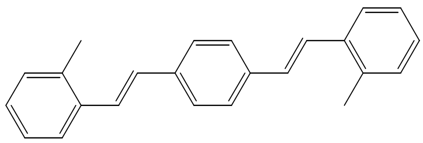	425
2-(1-Naphthyl)-5-phenyloxazole (α-NPO)	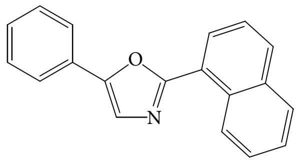	400

4.2.2.4 Surfactants

The problem of the incorporation of water or aqueous samples in aromatic solvents is solved by introducing surface-active compounds such as surfactants. The application of a non-ionic/anionic surfactant combination, whatever the solvent is, shows that the sample load capacity is relatively independent of temperature and will achieve a higher quench resistance [121]. The introduction of combined surfactants results in higher sample load capacities for water, enabling a stable micro emulsion to be formed when aqueous samples are present. Surfactants are also necessary for ensuring stable conditions over the whole counting period. Examples of surfactants used in scintillation cocktails are alkyl phenol ethoxylates (non-ionic), succinates, carboxylates and sulphonates (anionic) [121].

4.2.2.5 Principle of liquid scintillation counting

The scintillation process and light that is produced are different for the alpha and beta decay processes. When alpha decay occurs in a liquid scintillation cocktail, the alpha particles interact with the scintillation cocktail to produce light (about 1 photon/keV of original decay energy). The emitted photons from the sample will be led over reflectors to a photo multiplier

tube (PMT), where the detection will take place. Approximately 10 photons per keV of beta-particle decay energy are produced in a liquid scintillation process [122].The schematic principle of the liquid scintillation process is shown in Fig. 13.

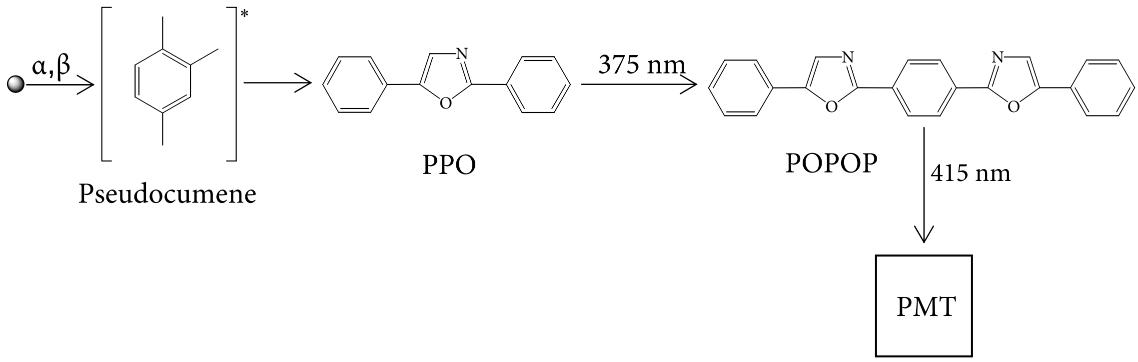

Fig. 13: Principle of the liquid scintillation counting

Liquid scintillation detectors, as all detectors based on scintillation processes, have a poor energy resolution, leading to broad pulses [123]. This is brought about principally because of the relatively large amount of energy required to produce a single photon at the PMT photocathode and, to a much lesser extent, because of the inefficient light production by alpha particles relative to betas, see Tab. 23.

Tab. 23: Relative scintillation yield for different types of ionizing particles [118]

Type of particle	Fraction of particle energy converted to photons compared to electrons
Electrons (> 80 keV)	1.0
Protons (1–10 MeV)	0.20–0.50
Alphas (4–6 MeV)	0.08–0.12

The liquid scintillation counting efficiency for beta particles is dependent on the original energy of the beta decay. For most beta particles with a decay energy above 100 keV, the counting efficiency is 90–100 %, but for lower energy beta decays the efficiency is normally in the range of 10–60 % depending on the degree of quench in the sample. The counting efficiency is approximately 100 % for almost all alpha decays using a liquid scintillation cocktail. Because of the slower pulse decay time, alpha particles can be distinguished from most other nuclear decay radiations with the liquid scintillation analyser.

4.2.3 Background radiation

There are many sources of background events in liquid scintillation counting. The main division of these sources is into those produced in the LS solution and those which result from events that have no connection with the LS solution. Tab. 24 summarises many of the common sources.

Tab. 24: Sources of background radiation in liquid scintillation counting [118]

Source	Contributors
Liquid scintillator cocktails	Natural radioactivity in the scintillator cocktails (tritium, C-14)
	Chemiluminescence and phosphorescence of certain solvents enhanced by the presence of the solutes
Sample	Natural radioactivity in the sample which may be the same or different from the radionuclide to be assayed
	Contamination with the same or other radioactive material
	Chemiluminescence and phosphorescence produced by the sample or impurities in the sample
Vial	Natural radioactivity in the vial walls or cap (K-40, Th-232, Be-7)
	Cosmic-ray-induced background – Čerenkov and secondary electrons and γ-rays
	Chemiluminescence and phosphorescence produced by sun light or impurities on the vial walls
	Static charge build-up during movement in the sample charger
PMT	Natural radioactivity in materials which make up the PMT (K-40, Th-232 and its daughters, uranium)
	Cosmic rays which produce Čerenkov radiation, secondary electrons and γ-rays
	Thermionic and secondary electron emission from photocathode and dynodes – in coincidence systems this is mostly eliminated, because of its randomness
	Cross talk from electric discharges and/or Čerenkov radiation
Other radioactive sources	Radioactive sources (usually γ rays) in the area of the liquid scintillation counter

Important contributions to the background are luminescence effects. The luminescence mechanisms have in common that single photons are produced. These can be detected by the photomultiplier and could lead to high count rates in the low energy part of the beta spectrum, up to 6 keV. Two kinds of luminescent effects are distinguished: chemiluminescence and photoluminescence.

The chemiluminescence is a result of chemical reactions in the scintillator solution, mostly reaction with oxygen or hydrogen peroxide impurities. Decreasing the temperature of the sample may reduce the chemiluminescence, but a complete elimination is not possible.

Photoluminescence concludes all processes which occur by the influence of light (i.e. sunlight, room light etc.). This effect can occur in the solution as well as in the vial. The photoluminescence mostly decays within minutes and therefore this effect can be reduced by storing the samples cold and in the dark.

Counting to the radioactive impurities in scintillation cocktails are tritium and C-14, therefore should only materials containing low activities of these two radionuclides be used.

Furthermore, the counting vial materials may contribute to the background radiation. Commonly used vials consist of glass (low-potassium borosilicate or quartz) or polyethylene (PE). The background count rate is for PE vials lower than for glass vials. The reason therefore is the lower content of K-40, Th-232 along with its daughters or Be-7 in the polymer material compared to glass. Blank samples in counting vials of various materials were measured, see Fig. 14.

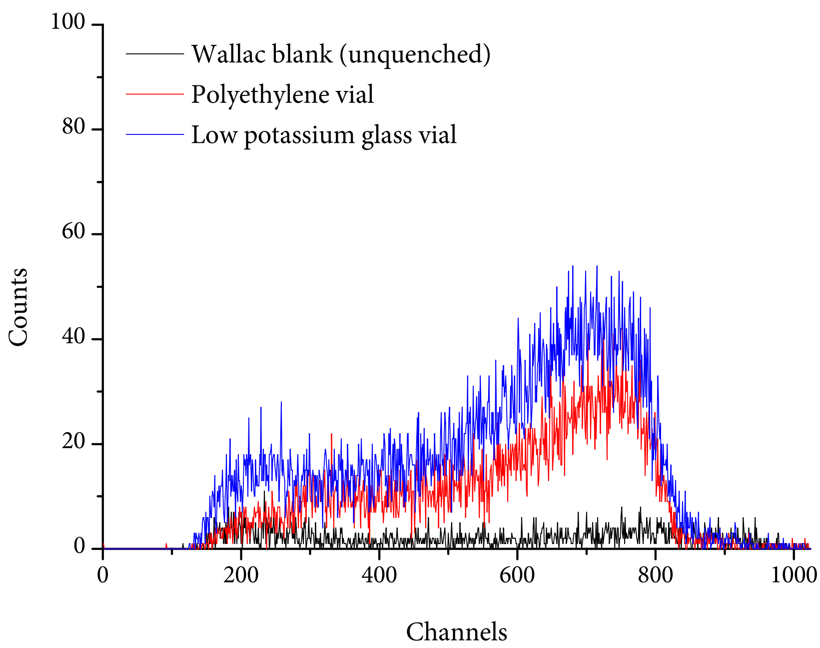

Fig. 14: Reagent blank samples in various vials measured and a Wallac blank 12 h via LSC

The Wallac blank consisted of an unquenched organic cocktail contained in a quartz vial. This blank sample showed practically no background. For identical samples, the vials consisting of PE showed a lower background count rate compared to the low potassium glass vials, see Fig. 14. In the further work, vials made of PE were preferred. Teflon and quartz were not tested.

Further sources of background radiation could come from the chemicals used in sample preparation, for instance carrier-, tracer-, or acid solutions. In Tab. 25, the effect of the amount of added lead carrier on the background is shown.

Tab. 25: Count rates arising from various amounts of lead carrier

Lead carrier (mg)	Count rate (min^{-1})
1.0	5.5 ± 0.1
2.5	5.1 ± 0.1
5.0	5.2 ± 0.1
7.5	5.2 ± 0.1
10.0	5.4 ± 0.1

The used lead carrier may contain impurities arising from atmospheric Pb-210 or from trace levels of U-238 in the lead carrier. Different amounts of lead carrier solution were transferred to PE vials and mixed with scintillation cocktail and measured for 24 hours via LSC. As can be seen in Tab. 25, there was no significant increase in the background count rates due to various amounts of added lead carrier.

4.2.4 Quench effects

As a consequence of the complex processes involved in the energy transfer in the liquid scintillation detector, various disruptions in the energy transfer can occur. These mechanisms are described as quench effects. These quench effects all contribute to a spectral shift to lower energies and to a decrease in the total count rate.

The main quench effects are:

- Chemical quench: The energy transfer between solvent molecules can be disrupted by a foreign substance. This can occur by direct reactions between the foreign substances and the scintillator (e.g. proton transfer reaction of the scintillator by acids), or a part of the energy is through dipole-dipole interactions transferred to a foreign substance (e.g. NO_3^- ions), which will relax without emitting radiation.

- Colour quench: Due to coloured compounds, such as iron complexes or organic pigments, a part of the emitted photons can be absorbed by the scintillator solution.
- Concentration quench: The scintillation yield initially increases with the concentration of scintillator; at higher concentrations the photons are absorbed by the scintillators.
- Phase quench: Arises by the occurrence of several phases in the scintillation solution.

4.2.5 Quench corrections

There are several ways to correct quench effects; with an internal standard, the sample channels ratio method and with the external standard technique [118].

The oldest method for quench correction is the internal standard technique. It involves the addition of a known amount of the nuclide in high specific activity to the same sample that is being measured. The efficiency is calculated by taking the difference of the count rates before and after the addition. The main disadvantages with internal standard techniques are that they require additional sample manipulation and precision addition of an accurately labelled standard of the same material as the sample.

The sample channels ratio (SCR) method was applied often during the early generations of liquid scintillation counters. In the SCR method two counting windows are assigned for the radionuclide of interest, followed by the measurement of two differently quenched standards. By monitoring the ratio of counts in the two windows, it is possible to measure the amount of quench. The SCR methods of quench determination is limited to a relatively narrow quench range, especially in the case of dual labelled samples (two radionuclides determined in the same measurement, i.e. C-14 and H-3, or Pu-239 and Pu-241), and decreases in accuracy with low count rates.

The most commonly used quench correction method involves the use of external γ-ray sources, such as Ra-226, Ba-133 or Eu-152, which irradiate the samples to create a Compton spectrum in the scintillation cocktail [122]. The sample in its vial is counted first in the absence and subsequently in the presence of the external gamma source. This gamma source is located within the instrument and it is positioned in the proximity of the counting vial when needed. The general interaction of the gamma rays with the scintillation vial and cocktail is by Compton electrons, produced via Compton effect. By the Compton effect, a gamma ray photon gives off only a part of its energy to an electron, which is emitted. According to the law of conservation of momentum, the gamma ray photon changes its frequency and its direction [14]. The Compton process will produce a continuum of electrons (somewhat like a beta continuum) with energies from zero to a maximum E_{max}, which is only dependent of the original γ-ray, $E_{\gamma 0}$ [118]:

$$E_{\max} = \frac{2E_{\gamma o}^2}{2E_{\gamma o}^2 + 0.51} \tag{4.9}$$

where all energies are expressed in million electron volts and 0.51 is the rest mass energy equivalent of an electron. The produced Compton electrons result in scintillations which can be detected by the PMT and which undergo the same quench effects as the scintillations arising from the beta decay in the sample. With the help of the Compton spectrum the degree of quench can be determined.

The most common measure of the quench is the Spectral Quench Parameter of the External standard (SQP(E)), i.e. endpoint of the Compton electron spectrum. The SQP(E) is measured with Ra-226 or Eu-152 as external standard sources. An MCA with 1024 logarithmic channels is used to determine the position of 99th percentile of the endpoint of the external standard spectrum to define SQP(E) [122]. In Fig. 15 below is the external standard spectrum of the Ra-226 gamma source used in this work shown, measured with a Wallac Quantulus1220™. The determined SQP-value was 831.18 for this measurement.

When measuring differently quenched samples a quench calibration must be performed. A series of differently quenched samples are measured to create a quench curve. This quench curve is a measure for how the counting efficiency varies with the SQP value (i.e. quench). The quench is increased from vial to vial by adding a quenching agent. A quenching agent is any chemical or colour substance which would cause a shift in the spectrum to lower energy and a subsequent decrease in the counting efficiency of the radioactive standard, see 4.2.4 above. Commonly used quenching agents for the quench standards are chloroform ($CHCl_3$), nitromethane (CH_3NO_2), carbon tetrachloride (CCl_4) and acetone (CH_3CH_3CO). Usually, a set of 6 to 10 quench standards are prepared per radionuclide.

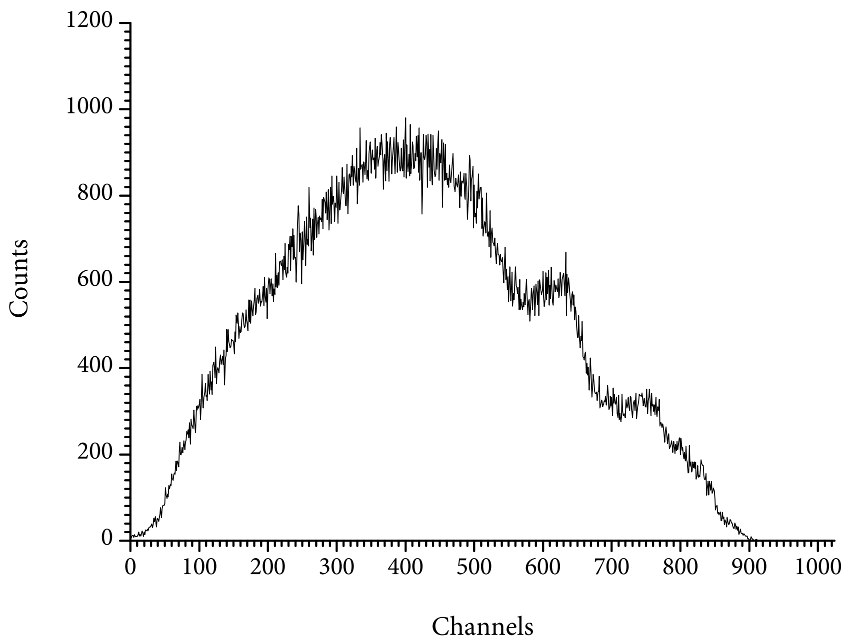

Fig. 15: The external standard spectrum of Ra-226, measured with a Wallac Quantulus 1220™

For H-3 and C-14, there are factory-stored quench samples commercially available from the LSC manufacturers (e.g. PerkinElmer). When purchasing a quench standard series it is important to consider what solvents are used. For cocktails based on toluene, xylene, pseudocumene or LAB (see 4.2.2.3) as solvent, toluene quench standards should be used. For cocktails based on DIPN or PXE, *Ultima Gold*™ quench standards should be used. If the wrong quench standard is used, this may lead to incorrect count rate, in worst case up to 18 % inaccuracy for low energy isotopes such as tritium in samples with high quench [124].

4.2.6 Pulse Shape Analysis

A simultaneous determination of alpha and beta activity is solely by using counting windows not possible. The alpha particle scintillation yield is low compared to that of an electron, see Tab. 23 above, making it difficult to separate alpha and beta decay solely on the basis of the decay energy, in spite the fact that alpha particles have a much higher energy than beta particles. An alpha particle in a liquid scintillation solution will on average produce the same number of photons per MeV of energy as an electron with about one-tenth of its energy, i.e. a 5 MeV alpha particle and a 0.5 MeV electron will produce the same number of photons emitted from the same liquid scintillation [118]. This is due to the fact that nearly 90 % more of the excited molecules produced along the alpha particle track, compared to those along an electron track, are quenched by competing reaction before they have an opportunity to transfer their excitation energy to the scintillating molecules which will emit photons. Electrons have a uniform, low specific ionization, except at the very end of the track. Therefore, the different species produced along the track are usually at a low concentration, and the probability of interactions between the species is low. On the other hand, alpha particles have a non-uniform, high specific ionization, except there is a very high specific ionization at the end of the alpha track. The concentration of various species (ions, radicals, excited molecules and fragments) along the alpha track is much higher, compared to an electron track, and the probability of reactions is greater. Part of these reactions will involve excited molecules and will therefore not be able to lead to the emission of photons [118]. This accounts for the considerable overlap of alpha spectra and high energy beta spectra in LSC and as a consequence thereof the alpha/beta discrimination through pulse shape analysis is essential.

The simultaneous determination of alpha and beta particles can be performed by closer observation of the pulse shape of the particular decays. For the pulse shape is the most significant factor the specific energy transfer of the particular particle. The intensity of photons from a scintillation event as a function of time can be divided into at least two components, fast (prompt) and slow (delayed), see Fig. 16. The fast component has a decay time equal to the fluorescence lifetime of the fluorescing species (the fluorescence solute), a few ns. The slow component has a decay time which is diffusion controlled; at room temperature in an aromatic solvent the decay is about 200–300 ns [125].

The total emission intensity–time equation as a function of the decay time τ_n of each component is given by the expression [126, 127]:

$$I(t) = I_1 \exp(-t/\tau_1) + I_2 \exp(-t/\tau_2) \cdots I_n \exp(-t/\tau_n). \tag{4.10}$$

Normally only the two first decay components are observed, $\tau_1 \approx 1$–3 and $\tau_2 \approx 200$–300 ns.

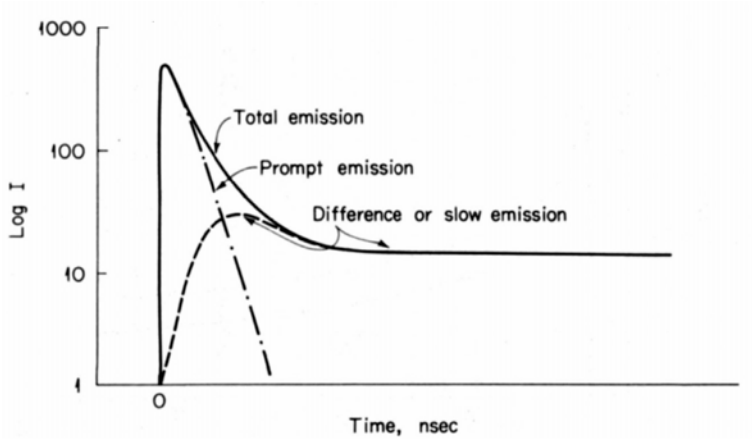

Fig. 16: The scintillation intensity shown as a function of time, showing the division of the total intensity into the prompt and slow components [118].

The diffusion-controlled component, hence the slower component, has been shown to be due to the annihilation of two triplet excited molecules [128]:

$$T_1 + T_1 \rightarrow S_1 + S_0. \tag{4.11}$$

Since the transfer from the excited triplet state T_1 to the singlet state S_0 is forbidden, the triplet state possess a comparatively long lifetime. The energy transfer process results in the formation of a ground-state molecule S_0 and a singlet by excited molecule S_1. The S_1 molecule will fluoresce with the emission of photons which are of the same energy distribution as those produced directly:

$$S_1 \rightarrow S_0 + h\nu. \tag{4.12}$$

The initial portion (the prompt component) of the light pulse produced by an alpha particle contains a great deal of ionized species which are not converted to light. The tail portion (the delayed component) of the pulse is larger relative to the initial portion than for beta produced pulses. The net effect is that alpha pulses have longer decay lifetimes than beta pulses. The longer decay lifetime for alpha pulses forms the basis of alpha/beta pulse shape analysis.

The pulse shape analysis uses special pulse decay time discrimination electronics to differentiate alpha pulses from beta pulses basically on the basis of the time it takes for the pulse to decay in a liquid scintillator. It is performed by comparing the ratio of the area of the tail of a pulse, beginning at 50 ns after pulse initiation to the total pulse area for each pulse [122]. This value is compared to a previously set numeric parameter (the PSA level) and with the help of this comparison it is possible to decide whether a pulse originates from an alpha decay, or from beta decay. The liquid scintillation counter, which is equipped with pulse shape discrimination (PSD) for α–β analysis, is therefore equipped with two MCAs. All the pulse events originating from scintillation photon emissions with a decay time longer than the PSD setting are sent to the α-MCA and those events which have a shorter lifetime are sent to the β-MCA. It is necessary to find the optimum PSA setting to get the best separation of α- and β-radionuclide activities from mixtures into separate MCAs. At the optimum PSD setting there is a minimum spill of alpha counts into the beta spectrum and beta counts into the alpha spectrum. The determination of the spill-over requires two samples: one pure alpha and one pure beta sample. For the most accurate results, the samples should have the same chemical properties, volume, and geometry as the unknown samples to be counted.

The addition of a few per cent naphthalene to the scintillation cocktail (or by using a cocktail based on di-isopropylnaphthalene) generally increases the pulse decay time, which leads to an even better α–β discrimination, see 4.2.2.3 above [129].

4.2.7 The Liquid Scintillation Counter

The Liquid Scintillation Counter used for the measurements was the Wallac Quantulus 1220™ from PerkinElmer Life and Analytical Sciences, see

Fig. **17**. Also seen in

Fig. **17** is the logarithmic presentation of the spectrum, which spreads the spectra out over a larger channel range than the linear multi channel analyser (MCA) spectra, therefore, when optimization of the measuring conditions are done, the counting window limits can be set in smaller steps giving better resolution.

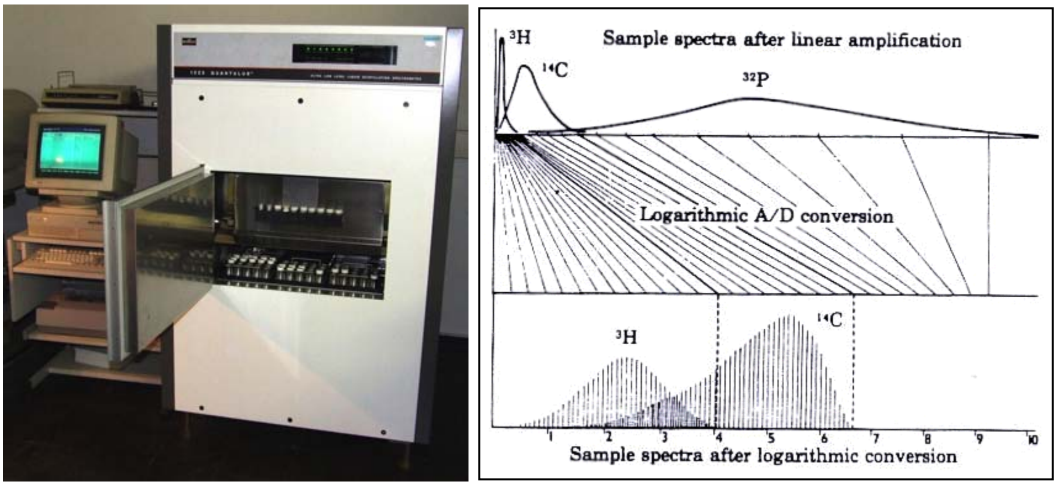

Fig. 17: The Wallac Quantulus 1220™ (PerkinElmer Life and Analytical Sciences): frontal view with open lid, showing the auto sampler trays (l). Logarithmic AD conversion of the linear amplification (r).

The Wallac Quantulus 1220™ is a device for low-level measurements; due to its unique detector shielding, consisting of a passive and an active shield, low background levels are achieved. The schematic system setup is shown in Fig. 18.

The passive shield consists of three layers; first a lead shield (630 kg), asymmetrically placed around the detector, with a maximum thickness of 20 cm above the measuring position. The lead shield will absorb high energy cosmic radiation (mostly coming from above) and gradually transform it to low energy radiation, which will not disturb the LSC measurements. The second layer consists of cadmium, which absorbs low energy (thermal) neutrons and X-rays produced in the lead shield by fluorescence reactions. Any X-ray fluorescence produced in the cadmium is shielded by a third layer, made of copper. The active shield consists of a tank, filled with a mineral oil based scintillator solution. Two photomultiplier tubes (G-PMT, circuited in coincidence), are used to detect scintillations in the tank. The sample itself is also surrounded by two photomultipliers (β-PMT, also circuited in coincidence). Ionizing radiation moving through the active guard creates scintillations, which are detected by the photomultiplier tubes of the guard detector. The pulse activates a logical signal. If this signal is coincident with a pulse in the β-PMT it can be used to inhibit the analogue to digital conversion of the pulse. If a quantum from the outside reaches the guard scintillator tank, it will create a scintillation event which is coincidently detected by both of the G-PMT. If this quantum creates a scintillation event in the sample as well, which is detected by the β-PMT, the anti-coincidence circuit will inhibit this signal, and consequently reducing the background radiation. The voltage pulse from the β-PMT will then be supplied to an analogue to digital converter (ADC) and a multi channel analyser (MCA). The Quantulus incorporates two dual programmable MCA:s. This enables the simultaneous measurement of four spectra, each with 1024 channel resolution. The pulse amplifiers yield a linear pulse height spectrum.

The analogue to digital conversion is logarithmic. The data storage is managed by a personal computer using the provided Quantulus software. For spectrum plots the computer software *Origin* was used. The external standard used for the determination of the quench value (SQP(E)) is a $^{226}RaSO_4$ source wrapped in a gold wire. The activity is 10 µCi (May 1st 1991).

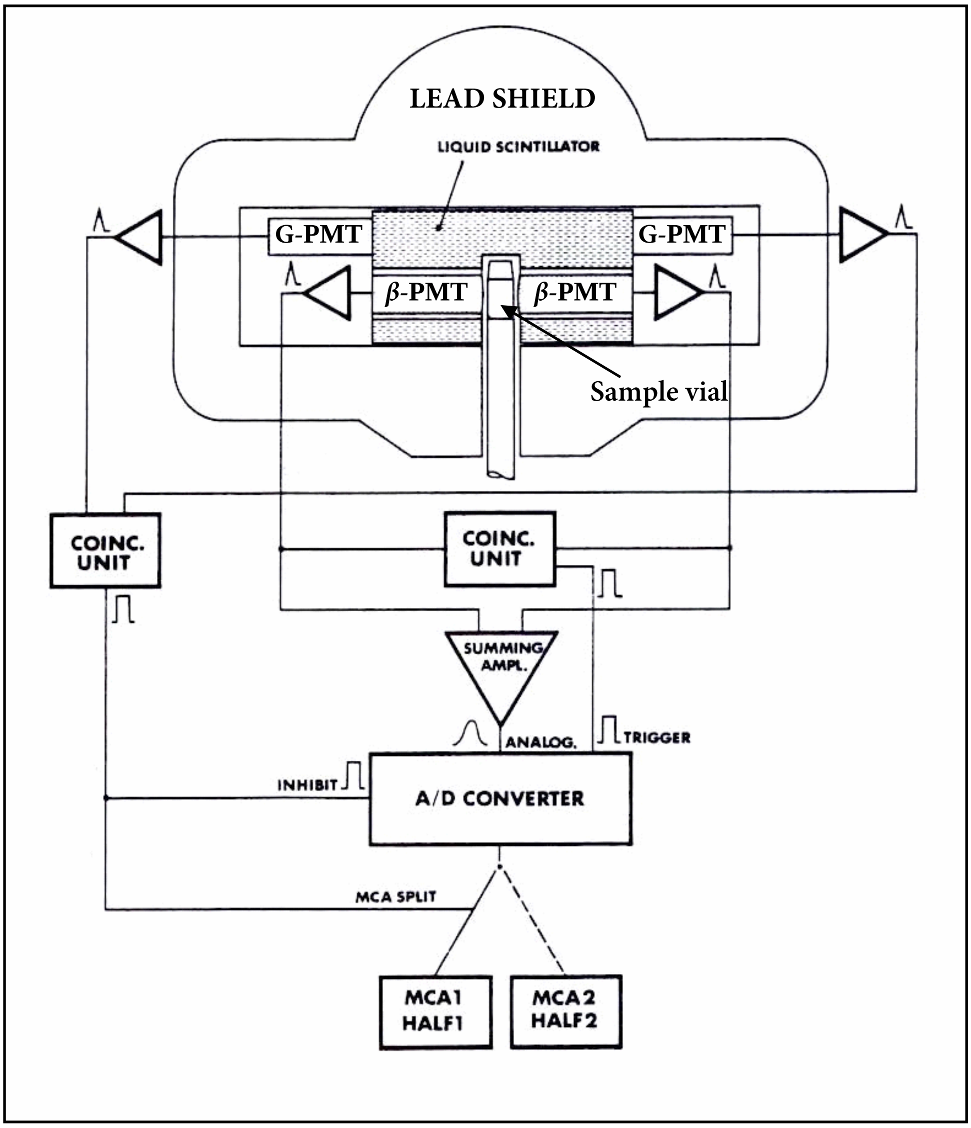

Fig. 18: Wallac Quantulus 1220™ schematic system setup

5 Method development

5.1 Overview

Lead-210, bismuth-210 and polonium-210 are all members of the natural uranium-238 decay series, see Fig. 1. The reasons for measuring Pb-210/Bi-210/Po-210 are mainly radiological considerations: attention has been paid to their analysis in drinking water and in air [130, 131], and they can be used as tracers of rates and mechanisms of environment processes, also see 2.1.5. A detailed decay scheme for Pb-210 is illustrated in Fig. 19 below.

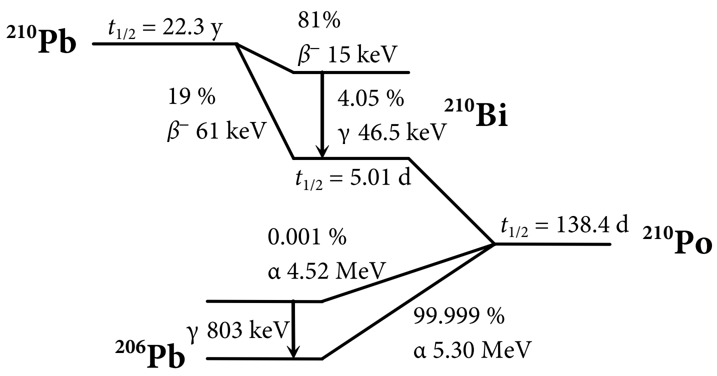

Fig. 19: Decay scheme for Pb-210, Bi-210 and Po-210 [16]

There are three basic approaches to the measurement of Pb-210 activity: (i) by gamma spectrometry, measuring the gamma radiation from Pb-210 directly; (ii) by beta spectrometry either counting the Pb-210 activity directly or after ingrowth of its daughter Bi-210; and (iii) by alpha spectrometry of the granddaughter Po-210, assuming radioactive equilibrium exists between the two nuclides.

5.1.1 Direct counting by gamma spectrometry

The direct measurement of Pb-210 can be accomplished by counting the 46.5 keV gamma photon emissions using an N-type High Purity Germanium (HPGe) detector. The difficulty in this is the comparatively low counting efficiency of HPGe detectors combined with the low absolute intensity of the 46.5 keV gamma photon (about 4 %) and the high self absorption of the gamma rays in the sample. The self absorption depends on the sample quantity, composition, density, and distance from the detector. The main limitations of Pb-210 determinations in water samples by gamma spectrometry lie in the higher detection limit, mainly due to the

self absorption [132], compared to other measurement techniques, which will be discussed below. The advantage of gamma spectrometry lies in the fast determinations, in which samples often can be measured without chemical separation. However, long measurement times are needed and/or large sample volumes. Furthermore, environmental analysis frequently requires simultaneous determination of other isotopes of interest, which in some cases do not emit detectable gamma radiation, such as Po-210 or Sr-90. Their determination usually requires pre-concentration and chemical separation from the sample, before measurement.

5.1.2 Beta spectrometry measurements

Rapid determinations of Pb-210 via LSC have been performed for sediments samples directly after chemical separation from the daughter Bi-210 [133]. Secular equilibrium with Bi-210 is not awaited. However, the counting efficiency determination for Pb-210 alone is difficult, since the available Pb-210 standards usually are in secular equilibrium with the daughters Bi-210 and Po-210. The immediate measurement also implies a limitation in the number of samples that can be analysed, as the ingrowth of Bi-210 must be avoided within the sample.

The German measurement instructions for environmental radioactivity (Messanleitungen für die Überwachung der Radioaktivität in der Umwelt und zur Erfassung radioaktiver Emissionen aus kerntechnischen Anlagen, Bundesministerium für Umwelt, Naturschutz und Reaktorsicherheit) describes a method for the determination of Pb-210 in drinking water and groundwater (Pb-210-TWASS-01-01) [134]. After ingrowth of Bi-210, the sample preparation, which involves several wet-ashing steps using concentrated nitric acid as well as perchloric acid, is performed. Bi-210 is spontaneously deposited onto a nickel disc from a hydrochloric solution for 18 h and subsequently counted by gas-flow proportional counting. Besides bismuth, other elements, which are electrochemically nobler than bismuth, including polonium and thallium, will also be deposited. Problematic is also inactive bismuth carrier, which is deposited as well, resulting in a lower yield and a higher detection limit. The simultaneous determination of Po-210 by alpha spectrometry would be likely, however under the deposition conditions used, the yield of polonium is low, see 5.4.1, and major activity losses during the sample preparation are probable.

In order to simultaneously determine Pb-210, Bi-210 and Po-210, a chemical separation is required. Several methods have been developed for the separation of lead including

- precipitation (e.g. $PbSO_4$),
- solid-phase extraction (e.g. Sr and Pb resin),
- liquid-phase extraction (e.g. Polex™ extractive scintillator),
- ion exchange, and
- combinations of these techniques.

In the method RP280 proposed by the US Department of Energy (DOE) [135], the indirect determination of Pb-210 is achieved by measuring the daughter Bi-210. Lead-210 is concentrated from a water sample by iron hydroxide co-precipitation. After dissolution, lead is selectively extracted on a *Sr Resin* form Eichrom. The purified lead fraction is evaporated onto a counting planchet. After allowing for Bi-210 ingrowth, the planchet is counted by gas-flow proportional counting. This method is optimized for the determination of Pb-210 and it is not possible to use this method for the simultaneous determination of Pb-210 and Po-210, at least when using polonium tracer for the yield determination, due to poor energy resolution of gas-flow proportional counters.

The determination of Pb-210 in environmental water samples was performed by Al-Masri *et al.* [136] by adding stable lead carrier as a yield tracer, followed by precipitation as a sulphate and dissolution in alkaline EDTA. Bismuth-210 was allowed to grow in and the activity was measured via Čerenkov photon counting, thereby avoiding potential interferences from alpha and soft beta emitters (energies < 216 keV, see 4.2.2), although the counting efficiency with this method was low (20 %).

The major advantage afforded by liquid scintillation is the high counting efficiency. Beta emitters with energies above 100 keV and alpha emitters, such as Bi-210 and Po-210 respectively, can be analysed with almost 100 % counting efficiency by LSC. Vajda *et al.* simultaneously determined Pb-210 and Po-210 in a range of matrices including soils, sediments, and biological samples by solid phase extraction using Sr resin [6]. The analysis of Po-210 was performed by alpha spectrometry, using Po-208 as yield tracer while Pb-210 was determined by LSC after ingrowth of Bi-210. Katzlberger *et al.* [130] determined Pb-210, Bi-210 and Po-210 in natural drinking water by removing Pb-210 from water sample via sulphide-precipitation of the inactive lead carrier and subsequent liquid-liquid extraction using Polex™, an extractive liquid scintillation cocktail, from a phosphoric acid solution. Bismuth and polonium were extracted with the cocktail (extraction yield about 90 %), leaving lead in the aqueous phase. No polonium yield tracer can be added using this method. Additionally, the bismuth yield was sensitive to chloride ions and very sensitive to nitrate.

5.1.3 Indirect measurement of Po-210 by alpha spectrometry

In sediments, Pb-210 and Po-210 are often found in equilibrium and the activity of Pb-210 can be estimated from that of Po-210. The Po-210 is typically analysed by alpha spectrometry following pre-concentration and spontaneous deposition onto silver discs. However, in the upper water column, equilibrium between Pb-210 and Po-210 is rarely achieved and separate Pb-210 and Po-210 determinations are required. Vesterbacka *et al.* have optimized the Pb-210 determination via spontaneous deposition of Po-210 on silver discs [137]. A polonium tracer is added to the sample (Po-208 or Po-209), Po-210 must then by quantitatively removed for analysis after which the sample is re-spiked with the polonium yield tracer and stored for several months to allow ingrowth of Po-210. Miura *et al.* have determined Pb-210 and Po-210 in environmental samples, after solid extraction using *Sr Resin* [138]. The lead fraction was

stored for 3–6 months to allow ingrowth of Po-210, and then re-spiked with Po-208. Polonium was electroplated on stainless steel discs for 2.5 h at 20 mA cm^{-2} and subsequently counted via alpha spectrometry. The determination of Pb-210 over Po-210 via alpha spectrometry will be further discussed in chapter 5.6.

5.1.4 Mass spectrometry

A possible alternative to radiometric counting for the determination of Pb-210 is offered by inductively coupled plasma-mass spectrometry (ICP-MS). ICP-MS has been used for the determination of long-lived radionuclides, such as Pu-239/240, U-238, Th-232, Ra-226, and Tc-99, based on their mass instead of their radioactive properties [139, 140, 141]. For radioactive isotopes with short half-lives, radiometric methods generally offer analyses with lower detection limits than ICP-MS. On the other hand, radiometric determination of Pb-210 is usually involving long ingrowth and measurement times, respectively, see above. Larivière *et al.* have determined Pb-210 in water by ICP-MS [142]. The obtained detection limit with this method was 90 mBq l^{-1} (10 pg l^{-1}). It was achieved after a 300-fold pre-concentration with yields between 63–73 %. However, in many natural waters, drinking water as well as groundwater, the Pb-210 activity is substantially lower than the detection limit achieved via ICP-MS.

5.2 Sampling procedure and sample preparation

The sampling of environmental waters was performed according to DIN 38402 A-15 [143]. Preferably three times one litre of water was sampled; due to the constantly changing composition (e.g. dissolved oxygen, particles, organic matter, dissolved ions etc.) of flowing water and the thereof resulting difficulty in achieving reproducible environmental water samples. It was important to additionally measure the changeable parameters specific for the weather conditions and the time of day that the sampling was performed. These parameters were water temperature, pH, conductivity, and redox potential. On-site the samples were filtered (0.45 μm membrane filter) and transferred to suitable containers, mostly one litre polyethylene bottles. The water samples were subsequently acidified to a pH below two, in order to terminate biological activity (algae) and to stabilize the samples. This was also preventing the radionuclides from sorbing to the container wall surface (see 2.1.4).

A stable (non-radioactive) lead carrier (5 mg) was added. After the lead carrier has been added, the sample was left to equilibrate. In the laboratory the sample preparation continued. First the water sample was transferred to a one litre glass beaker and the exact weight of the samples was noted. The weight was noted, because the accuracy of a scale is usually much higher than for any volumetric instrument. An aliquot (1 ml) was taken for the chemical yield determination via ICP-MS. This sample would reflect the total content of the lead available in the sample at this point. For the chemical yield determination, see section 5.5.5.

Depending on the radionuclides of interest, an appropriate amount of tracer was added. The tracer was added in order to pursue (trace) the fate, transport or chemical reaction of a certain element in that system and in order to determine the chemical yield. Radioactive tracers are preferable used, because they can be detected and measured in very low concentrations and with high sensitivity. The tracer radionuclide should be in the same chemical form as the species to be investigated. The same chemical behaviour can be assumed in the case of isotopic tracers. The tracer used for the analysis of Po-210 was Po-208 ($t_{1/2}$ = 2.9 y), but also Po-209 ($t_{1/2}$ = 102.1 y) is commonly used. The added tracer activity should lie in the same range as the activity of the radionuclide of interest, but should be high enough to ensure reasonable measurement times: for environmental water samples about 100 mBq was satisfactory.

Existing in the sample were the radionuclides of interest, the carrier and the tracer, but also other naturally occurring ions found in environmental waters, such as Na^+, K^+, Ca^{2+}, Mg^{2+}, etc. A separation from these matrix components was performed by precipitation. However, a direct precipitation was mostly not possible for radionuclides, since the solubility product cannot be exceeded. Co-precipitation was therefore performed after addition of a suitable carrier: isotopic or non-isotopic carriers can be used. A non-isotopic carrier does not lower the specific activity of the radionuclide, must co-precipitate the radionuclide efficiently and must be separable from the radionuclides after the co-precipitation. The co-precipitation of lead has been studied more thoroughly than most other elements [144]. This was due to the availability of carrier-free Pb-212 from thorium ores and due to the relatively short half-life and decay characteristics of Pb-212 ($t_{1/2}$ = 10.64 h, E_γ = 239 keV). In this case, iron (Fe^{3+}) was successfully used as a non-isotopic carrier and the radionuclides of interest were co-precipitated by adsorption, see section 3.2.6. The added iron carrier (20 mg) was precipitated with an excess of ammonium hydroxide at elevated temperatures. The elevated temperature of the precipitation process enabled a bulky precipitation with a large specific surface area with negative hydroxyl groups as reactive sorption sites. Lead and polonium were quantitatively co-precipitated with iron hydroxide, but ions of low valency, such as Na^+ and K^+, were not adsorbed onto the iron hydroxide and therefore remained in the solution. Possible calcium and magnesium ions in the water samples were not co-precipitated with the iron hydroxide, but directly precipitated as hydroxides. The solution was subsequently decanted and the precipitation was centrifuged and washed several times with distilled water. The solubility constant for iron(III)hydroxide is $L(Fe(OH)_3) = 5 \times 10^{-38}$ mol^4 l^{-4} [25], but it varies with pH: at pH = 7, the solubility lies in the range of 10^{-18} mol^4 l^{-4}, which ensures no unwanted dissolution of the hydroxide during the washing step.

For the further separation of the precipitated elements, the precipitation had to be dissolved. Dissolving the precipitation with diluted HCl was faster than with diluted HNO_3, due to the complexing ability of Cl^--ions. The attained solution had a yellow colour due to the formed chloro-complexes, for example:

$$[FeCl_2(H_2O)_4]^+$$
$$[FeCl_4(H_2O)_2]^-$$

The precipitations in the further work were therefore dissolved in 10 ml diluted hydrochloric acid (c = 2 mol l^{-1}). Less than 10 ml would not be sufficient to dissolve the whole amount of precipitation. The choice of acid concentration will be discribed in the next section.

5.3 Chemical separation

The chemical separation involves the removal of existing inactive matrix components (such as calcium, magnesium, and ferric ions), interfering radionuclides, and it serves as a sample volume reduction and of course the separation of the individual radioelements of interest. In cases where the radioactive equilibrium is taken advantage of, the radionuclide to be measured has to be completely removed before the ingrowth can start. This is usually performed via a chemical separation step.

There is a wide variety of separation methods available, including solvent extraction, using TOPO in toluene [145, 146], TIOA in xylene [147], and “Aliquat 336” in benzene [148], ion exchange chromatography [149, 150, 151, 152, 153] and extraction chromatography. The solid phase extraction, especially by crown ethers adsorbed on an inert polymer (e.g. Amberchrom), has found increasing use in the separation of Pb-210 and Po-210. Horwitz *et al.* have developed two solid phase extraction resins, mainly for the exceedingly selective extraction of strontium [4] and lead [5], using the 4,4’(5’)-bis-(t-butyl-cyclohexano)-18-crown-6, abbreviated DtBuCH18C6, see Fig. 20.

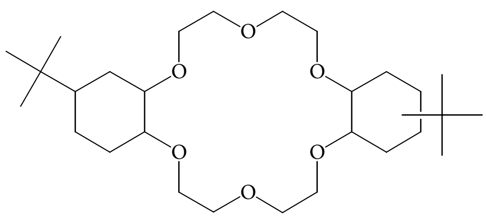

Fig. 20: 4,4’(5’)-bis-(t-butyl-cyclohexano)-18-crown-6

The characteristic properties of several solid phase extraction resins are listed in Tab. 26. As can be seen, the only differences between the *Sr Resin* and the *Pb Resin* are the concentration of the crown ether (lower in *Pb Resin*) and the solvent. The extraction of strontium by the dicyclohexano-18-crown-6 is directly related to the solubility of water in the solvent [154]. For a given solvent family (e.g. alcohols), this solubility, in turn, was found to decrease with increasing solvent molecular weight. Therefore, strontium extraction was found to decrease, when n-hexanol was replaced by n-octanol. In order to ease the elution of lead, which is strongly sorbed onto the *Sr Resin*, a new resin was prepared from a 0.75 M solution of DtBuCH18C6 dissolved in isodecanol yielded as much as four times lower distribution ratios

than those obtained with the *Sr Resin* [4]. These features were used in preparing a new resin, the *Pb Resin* [5].

Tab. 26: Characteristics of the different extraction chromatographic materials [4, 5, 155]

Bulk material:	*Pb Resin*	*Sr Resin*	*TEVA*® resin
Stationary phase	0.75 M D*t*BuCH18C6 in isodecanol	1.0 M D*t*BuCH18C6 in 1-octanol	Undiluted Aliquat™ 336
Support		Amberchrom™ CG–71	
Particle diameter (μm)		50–100 (cartridges) 100–150 (columns)	
Extractant loading, $L_{ex, resin}$		40 % (w/w)	
Density of extractant-loaded beads, ρ_{resin}	1.16 g/ml	1.12 g/ml	1.09 g/ml
Packed columns:			
v_s, ml/ml of bed	0.16	0.146	0.158
v_m, ml/ml of bed (also FCV)	0.68	0.71	0.68
Conversion factor, *f*	1.47	1.74	1.58

The ions in the sample solution, in this case Pb^{2+}, Bi^{3+} and Po^{4+}, form stable neutral complexes with the crown ether, D*t*BuCH18C6, along with a suitable counter ion provided by the acid solution (e.g. Cl^-, NO_3^-, or Br^-), here with the chloride ion as counter ion:

$$Pb^{2+} + 2\ Cl^- + \mathrm{D}t\mathrm{BuCH18C6} \rightarrow [Pb(\mathrm{D}t\mathrm{BuCH18C6})]Cl_2 \tag{5.1}$$
$$Bi^{3+} + 3\ Cl^- + \mathrm{D}t\mathrm{BuCH18C6} \rightarrow [Bi(\mathrm{D}t\mathrm{BuCH18C6})]Cl_3 \tag{5.2}$$
$$Po^{4+} + 4\ Cl^- + \mathrm{D}t\mathrm{BuCH18C6} \rightarrow [Po(\mathrm{D}t\mathrm{BuCH18C6})]Cl_4 \tag{5.3}$$

The stability of the complexes varies with the counter ion and its concentration. There is also a sterical selection of the crown ether; only ions of a certain size are able to form stable complexes with the crown ether.

The nitric acid dependence of the capacity factor k' for selected metal ions on the *Pb Resin* has been investigated [5]. The k'_{Pb} exceeds that of each of the other metal ions by a wide margin over the entire range of concentrations, with k'_{Pb} of about 1000 at $c(HNO_3) = 1$ mol l^{-1}. In several cases, e.g. K^+ and Na^+, the ion is hardly retained by the resin at

all, with k' of < 1 for $c(HNO_3) = 1$ mol l^{-1}. The excellent selectivity over sodium is important, due to the ubiquitousness of this element. Also significant is the low capacity factor of the resin for calcium, an element present in high quantities in environmental samples.
In order to selectively extract polonium from lead, the *TEVA*® (TEtraValent Actinides) resin could come into use. Some of the resins characteristics are listed in Tab. 26. It functions basically like a strong base anionic exchange resin, due to the resin's active component, a quaternary amine, the Aliquat™336 [155], see Fig. 21.

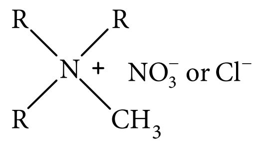

Fig. 21: The quaternary amine used in the *TEVA*® resin. R = C_8H_{17} and $C_{10}H_{21}$

The difference from a classic anionic exchange resin is that the amine is not fixed to a polymer, but exists in liquid form, which enhances the flexibility to coordinate around the extracted anions. Additionally, the resin capacity is higher compared to a classic anionic exchange resin due to the higher density of functional groups. The *TEVA*® resin has been widely used for the extraction of tetravalent ions, such as Pu(IV), Th(IV) and Np(IV), in form of their anionic complexes, but also Tc(VII) has been successfully separated using the *TEVA*® resin. However, so far it has not been investigated how the tetravalent polonium isotopes are retained by the resin.

5.3.1 Resin distribution coefficients for lead and polonium

In order to achieve the best possible separation of both lead and polonium simultaneously, first of all the distribution coefficients on different resins and in various matrices and matrix concentrations of interest were determined for both lead and polonium, and from these results the optimal separation conditions could be set. The distribution coefficients can be determined in batch experiments, where a known activity or concentration of the elements is shaken together with a known amount of resin in different matrices (in this case HNO_3, HCl, and HBr acids, respectively) in various concentrations. The distribution coefficients can also be attained from elution experiments, which is, however, more time consuming.

Two different resins were investigated for the purpose of selectively separating lead and/or polonium from surrounding matrix elements and interfering radioelements: the *Pb Resin* and the *TEVA*® resin (both available from Eichrom Environment, France). Similar investigations have already been performed for lead and polonium on the *Sr Resin* [6, 138].

The separation of lead in meteorites and chondrites has been performed by using anion exchange columns, where the sample load was performed in $c(HBr) = 1$ mol l^{-1} [156].

The extraction behaviour of lead and polonium by the *Pb Resin* in HBr was therefore also investigated.

5.3.1.1 Experimental performance

All samples were spiked with a tracer solution containing known activities of Pb-210 in equilibrium with its daughters. This was done in order to simultaneously determine the distribution coefficients for lead, bismuth and polonium on the *Pb Resin* by activity measurements of the radionuclides via LSC. Another possibility would be using inactive species (not possible for polonium, however) and to determine the distribution coefficients by mass spectrometry measurements. The distribution coefficients for polonium on the *TEVA®* resin was determined by using a known activity of Po-208. The amount of the resin was held constant in all experiments, only the matrix solution and its concentration were varied. In addition, background samples, which contained no activity, and tracer samples, which had not been in contact with the resin, hence containing maximum activity, A_{max}, were made. By these experiments it was possible to determine the activity of the radionuclides which were not retained by the resin, instead of determining the actual retained activity. This non-retained activity was subsequently compared to the maximum activity samples in order to determine the activity which had been held back by the resin.

The background samples were prepared by shaking 100 mg of the resins in 5 ml of HNO_3, HCl and HBr solutions of different concentrations, respectively. The samples were shaken for 2 hours at 65 rpm at room temperature [6], the solutions were then filtered through a 0.45 µm membrane filter, using a plastic syringe, and finally one-ml aliquots were taken and 19 ml *Ultima Gold™ AB* scintillation cocktail (from PerkinElmer) were added. The samples were measured 24 h via LSC.

To prepare the maximum activity samples tracer solution of known activity was transferred to glass LSC vials and evaporated to dryness using a heating lamp. The samples were dissolved in 1 ml of the different acid solutions (HNO_3, HCl and HBr), mixed with 19 ml LSC cocktail and analysed via LSC. The quench parameters for different matrices were determined by measuring the maximum activity samples 10 minutes at different PSA settings. For the activity determination the samples were measured 30 minutes.

The distribution ratio samples were prepared in the same manner as the background samples, but spiked with a tracer of known activity. The added tracer solutions were evaporated to dryness and dissolved in the different acid solutions. The total volume was 5 ml per sample. Approximately 100 mg of each resin were added to each sample and the vials were shaken for 2 hours, like above. The solutions were filtered and one-ml aliquots were taken and transferred to LSC glass vials and 19 ml of the *Ultima Gold™ AB* cocktail were added. The samples were measured 12 h via LSC.

The following equation was used for calculating the weight distribution ratios [4, 5]:

$$D_{\mathrm{w}} = \left(\frac{A_{\max} - A_{\mathrm{s}}}{m_{\mathrm{resin}}} \right) \Bigg/ \frac{A_{\mathrm{s}}}{V} \tag{5.4}$$

Tab. 27: Distrubution ratio variables

Symbol	Description
D_{w}	Weight distribution ratio
D_{v}	Volume distribution ratio
$A_{\max}$	Aqueous phase activities before equilibration (min^{-1})
A_{s}	Aqueous phase activities after equilibration (min^{-1})
m_{resin}	weight of the resin (g)
V	Aqueous phase volume (ml)
k'	Number of free column volumes (FCV) to peak maximum (capacity factor)

In Tab. 27, the used symbols are listed. The D_{w} values were converted to the number of free column volumes (FCV) to peak maximum, k', by dividing with a conversion factor, f, see eqn. (5.8). This factor includes the conversion of D_{w} to D_{v} (a volume distribution ratio) and the ratio of the number of stationary phase to volume of mobile phase $v_{\mathrm{s}}/v_{\mathrm{m}}$, see Tab. 26. The volume distribution factor is shown in eqn. (5.5) below. The number of free column volumes to peak maximum, k', is shown in eqn. (5.6) and (5.7) and the relation between k' and D_{w} is depicted in eqn. (5.8). The conversion factors for the different resins are found in Tab. 26.

$$D_{\mathrm{v}} = \left(\frac{A_0 - A_{\mathrm{s}}}{\frac{m_{\mathrm{resin}} L_{\mathrm{ex,resin}}}{\rho_{\mathrm{resin}}}} \right) \Bigg/ \frac{A_{\mathrm{s}}}{V} = \frac{D_{\mathrm{w}} \rho_{\mathrm{resin}}}{L_{\mathrm{ex,resin}}} \tag{5.5}$$

$$k' = D_{\mathrm{v}} \left(v_{\mathrm{s}} / v_{\mathrm{m}} \right) \tag{5.6}$$

$$k' = \frac{D_{\mathrm{w}} \rho_{\mathrm{resin}}}{L_{\mathrm{ex,resin}}} \cdot \frac{v_{\mathrm{s}}}{v_{\mathrm{m}}} \tag{5.7}$$

$$k' = D_w / f \tag{5.8}$$

5.3.1.2 Results

The number of free column volumes to peak maximum, also known as the capacity factor, k', was calculated using the Eq. (5.4) and (5.8) above. The results for both the *Pb Resin* and the *TEVA®* resin are shown in Tab. 28 below.

In both nitric acid as well as hydrochloric acid, the capacity factor for bismuth was very small, mostly $k'_{Bi} < 1$ over the whole acid concentration range. Hence, Bi-210 was not retained by the *Pb Resin* at all.

Tab. 28: Capacity factor, k', for *Pb Resin* and *TEVA®* resin

Matrix	*Pb Resin*		*TEVA®*
	Pb(II)	Po(IV)	Po(IV)
0.1 M HNO_3	659 ± 18	22 ± 3	2720 ± 105
0.5 M HNO_3	2120 ± 102	26 ± 3	1660 ± 49
1.0 M HNO_3	1900 ± 91	23 ± 3	1950 ± 70
2.0 M HNO_3	1770 ± 76	81 ± 3	1110 ± 34
4.0 M HNO_3	1040 ± 46	45 ± 3	1490 ± 52
8.0 M HNO_3	–	–	106 ± 3
0.1 M HCl	1100 ± 77	85 ± 3	6470 ± 440
0.5 M HCl	696 ± 31	132 ± 4	21600 ± 3010
1.0 M HCl	1630 ± 157	144 ± 4	64200 ± 29000
2.0 M HCl	412 ± 16	216 ± 5	29340 ± 7030
4.0 M HCl	49 ± 2	240 ± 5	6090 ± 515
9.0 M HCl	–	–	238 ± 4
0.1 M HBr	302 ± 71	66 ± 7	–
0.5 M HBr	3040 ± 963	1050 ± 56	–
1.0 M HBr	1190 ± 166	3350 ± 316	–
2.0 M HBr	470 ± 32	6500 ± 943	–
4.0 M HBr	47 ± 9	1680 ± 120	–

Fig. 22 shows the nitric acid dependence as well as the hydrochloric acid dependence of the capacity factor for lead and polonium on the *Pb Resin*. As can be seen, k'_{Pb} exceeds 10^3 over most of the range of nitric acidities examined, with a maximum at about $c(HNO_3) = 1$ mol l^{-1}. Lead is also readily sorbed from hydrochloric acid solution. Although the maximum k'_{Pb} ob-

served is approximately a factor of two lower than that obtained from nitric acid, the lead retention is still more than adequate for many applications.

The tetravalent polonium is in nitric acid solution not very well retained by the *Pb Resin*. The maximum k'_{Po} does not exceed 10^2 in the whole range of nitric acid concentrations. In nitric acid a complete separation of both lead and polonium can be achieved, but since the capacity factor for polonium is so low, the separation from bismuth is incomplete. However, in hydrochloric acid solutions useful capacity factors are achieved for polonium. The maximum k'_{Po} of 240 is found at c(HCl) = 4 mol l^{-1}. However, at c(HCl) = 4 mol l^{-1} the capacity factor for lead is too low to achieve a satisfactory separation of both radionuclides. Therefore, in the further work the extraction of both lead and polonium were performed in c(HCl) = 2 mol l^{-1}, where k'_{Pb} = 412 and k'_{Po} = 216. Polonium was eluted in diluted nitric acid, where lead still possessed a high capacity factor. The lead was finally eluted by lowering the nitric acid concentration, by adding a sufficient amount of distilled water.

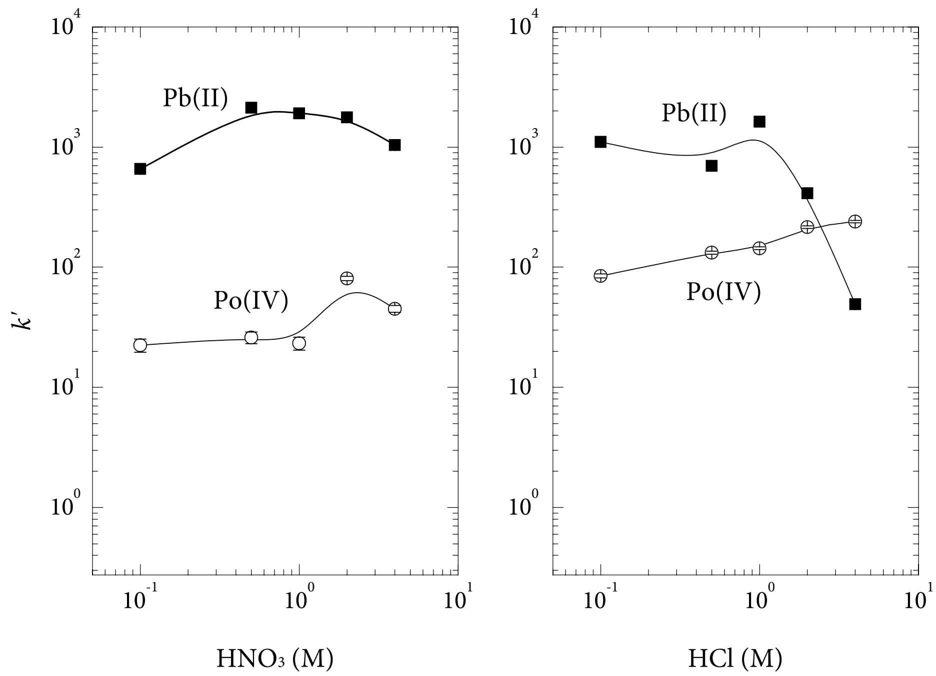

Fig. 22: Capacity factor k' for lead and polonium in HNO_3 and HCl solutions on *Pb Resin*. Particle size of resin: 50–100 µm

The capacity factors for lead and polonium in hydrobromic acid (HBr) were investigated and the results are shown in Fig. 23. Overall, the retention in diluted hydrobromic acid was clearly stronger than in nitric and hydrochloric acid, respectively, especially for polonium. The maximum k'_{Po} was obtained in c(HBr) = 2 mol l^{-1}, reaching over 6000, and for lead the maxi-

mum k'_{Pb} is over 3000 at c(HBr) = 0.5 mol l^{-1}. The maximum in distribution coefficient for lead in hydrobromic acid observed in the anion extraction columns is found at just under c(HBr) = 1 mol l^{-1}, which corresponds well to what was obtained in this work. However, such high capacity factors over the wide range of acidities made the stripping of polonium from the column complicated hence separate polonium and lead fractions were not achieved. Due to the stripping difficulties and the unpleasant handling of the very corrosive hydrobromic acid, the further use of this acid in the solid phase extraction of lead and polonium was refrained from.

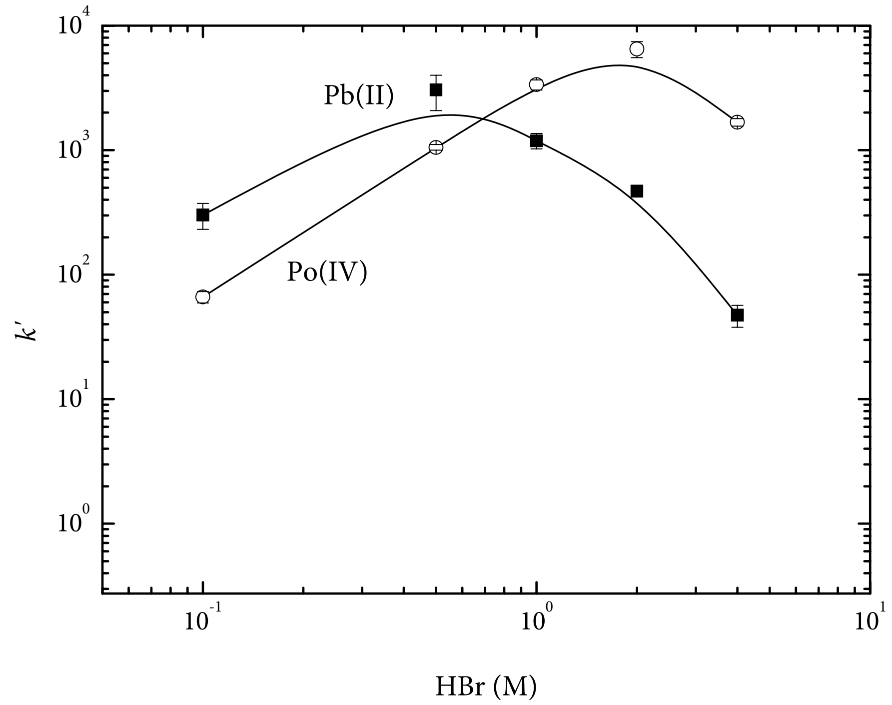

Fig. 23: Capacity factor k' for lead and polonium in hydrobromic solutions on *Pb Resin*. Particle size of resin: 50–100 µm

The extraction of polonium by the *TEVA*™ resin is remarkably high in HCl solutions, with maximum k'_{Po} values > 5 × 10^4 in c(HCl) = 1 mol l^{-1}, see Fig. 24. The extraction in diluted nitric acid solutions is weaker than in HCl solutions, with a maximum capacity factor obtained at $c(HNO_3)$ = 1 mol l^{-1}. The elution of Po(IV)-ions from the *TEVA*™ resin seem rather difficult. The lowest k'_{Po} value in nitric acid is found at about 10^2, but at a relatively high acid concentration ($c(HNO_3)$ = 8 mol l^{-1}). In hydrochloric acid the lowest k'_{Po} value lies at about

200, at a concentration of $c(HCl) = 9$ mol l^{-1}. The handling of high acid concentrations is inconvenient and therefore this resin will not be used further in this work.

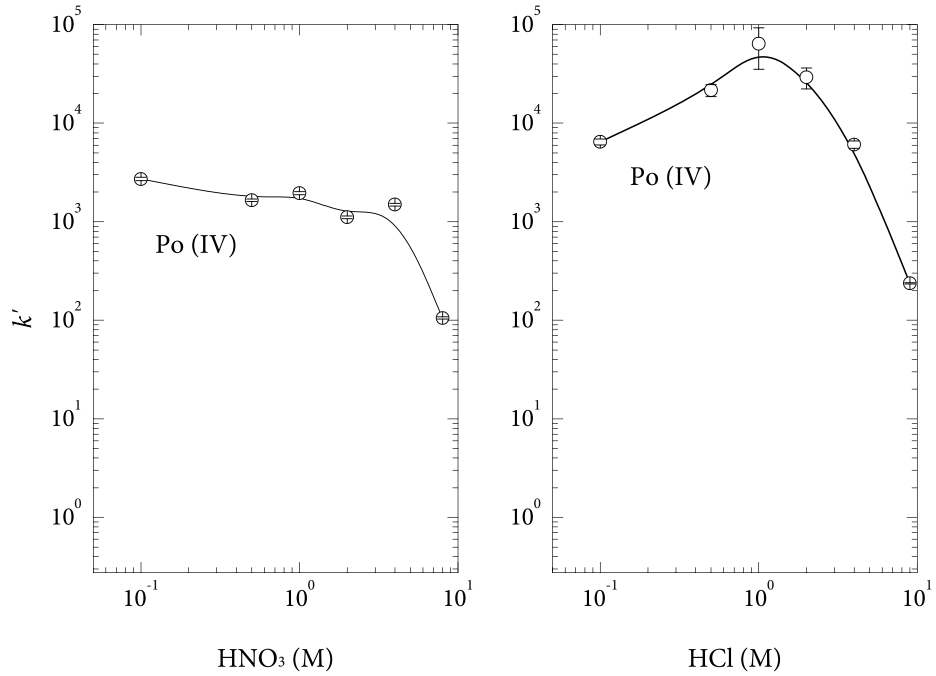

Fig. 24: Acid dependency of k' for polonium in HNO_3 and HCl solutions on *TEVA*™ resin. Particle size of resin: 100–150 µm

5.3.2 Chemical separation using the *Pb Resin*

The solid phase extraction was performed using the *Pb Resin* with a particle size of 50–100 µm. This relatively small particle size reduces the peak broadening of the components to be separated and as a consequence thereof the separation efficiency of the column is raised. To achieve a reasonable flow rate with columns of such small particle size vacuum had to be applied. For this a so called vacuum box (*Eichrom vacuum box system AC-24-BOX*) with pressure gauge for regulation of the flow rate, was utilized. With this box system up to 24 samples can be separated simultaneously.

The extraction column was constituted of 2 ml polyethylene cartridges filled with the *Pb Resin* (*Eichrom Pb Resin cartridge PB-R50-S* or *PB-R200-S*). The cartridges were provided with a luer lock system, which enables the fitting of compatible components without further fixing [157]. The complete set up can be viewed in Fig. 25.

A syringe barrel (without the needle) was luer-locked to the upper seal of the extraction cartridge. The barrel functioned as a reservoir for the different solutions used. The volume of

the barrel was chosen to fit the proper amount of solution needed for the particular step. Optionally, a pre-filter, consisting of a hydrophilic cellulose acetate membrane filter of pore size 0.45 µm, could be luer-locked between the cartridge and the syringe barrel. The filter would protect the column from any solid matter in the sample and could be removed after completed sample load and subsequent rinsing.

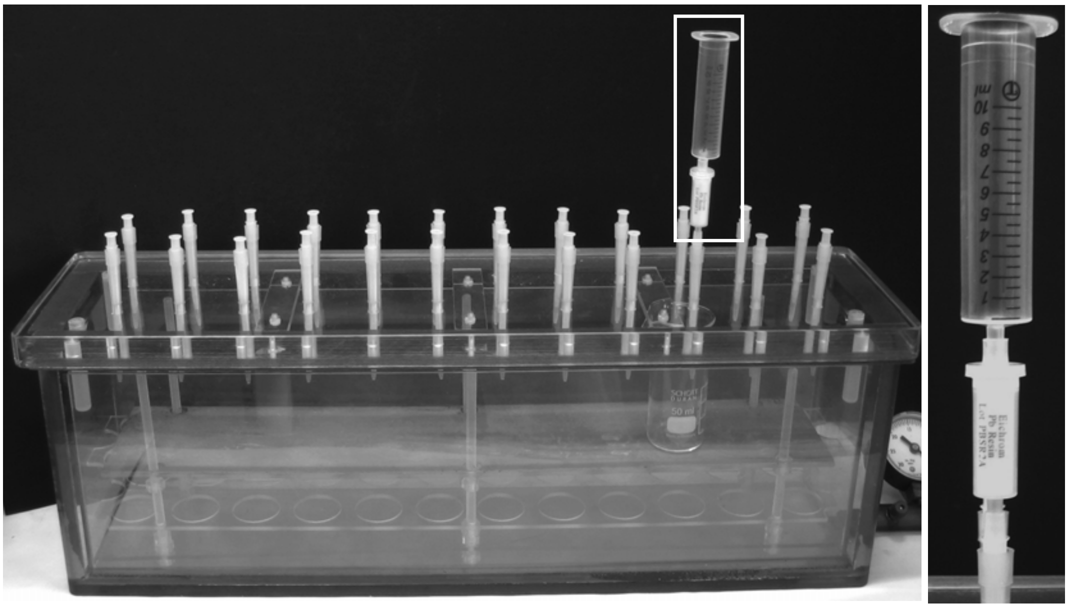

Fig. 25: The vacuum box system *AC-24-BOX* from Eichrom. To the right: a close up of the 2 ml *Pb Resin* cartridge, luer-locked to a syringe barrel.

The extraction cartridge was conditioned with 10 ml diluted HCl ($c = 2$ mol l^{-1}), which were transferred to the syringe barrel. The flow rate was set to 3 ml min^{-1}. After concluded conditioning, the prepared sample was loaded on the column by adding it to the syringe barrel. The flow rate was adjusted to 1 ml min^{-1}. The sample container was rinsed with 5 ml diluted hydrochloric acid ($c = 2$ mol l^{-1}) and transferred to the barrel. This addition would completely remove iron and bismuth from the column. The time and date of this addition was noted. This time will be used to calculate the ingrowth of Bi-210. The eluent was discarded, or if required kept for further analysis (e.g. uranium).

A clean labelled 20 ml LSC glass vial was placed underneath each cartridge and the barrel was removed and replaced with a clean one. To elute polonium from the column 10 ml of diluted nitric acid ($c = 1$ mol l^{-1}) were added to the barrel. The flow rate was kept at one ml min^{-1}. Another 5 ml diluted nitric acid ($c = 0.1$ mol l^{-1}) were added, to completely remove polonium and to lower the nitrate concentration in the column prior to the lead elution. A new clean labelled 20 ml LSC glass vial was placed underneath each cartridge. A clean syringe barrel replaced the former. The elution of lead was performed by transferring 20 ml of bi-distilled water to the barrel; the flow rate kept to 1 ml min^{-1}. One aliquot of the lead frac-

tion was used to prepare a LSC counting sample, see chapter 5.5 below. Another aliquot was used to determine the chemical yield via ICP-MS measurement of the added stable lead carrier, see chap. 5.5.5. The rest of this fraction could be used for the determination of Pb-210 after spontaneous deposition of Po-210, after ingrowth, see chapter 5.6 below. The determination of Pb-210 over Po-210 would lower the detection limit for Pb-210 at least by a factor of 10, with the restriction of the long waiting time required for the ingrowth of Po-210 (six months to one year).

The optimum acid and acid concentration for the sample load was determined from the capacity factor *k*', see Fig. 22. The sample load was performed at high *k*' values, the elution however at low *k*' values. The optimum acid in the case of a simultaneous separation of Pb-210 and Po-210, hydrochloric acid appeared most advantageous. From Fig. 22 can be deduced, that the optimum acid concentration for extracting both lead and polonium quantitatively was at $c(HCl) = 2\ mol\ l^{-1}$). Although nitric acid has commonly been used for the separation of lead from matrix elements [5], the *k*' values for polonium in nitric acid were in all acid concentrations very low, which excluded the use of nitric acid. Hydrobromic acid, see Fig. 23, on the other hand, would extract lead and polonium to a much higher extent than HCl, but the elution was found to be more difficult, due to the high capacity factors. No quantitative separation of Pb-210 and Po-210 was achieved in HBr.

The optimum volumes of the acid solutions presented above were determined by performing a series of elution experiments. A known activity of Pb-210 solution in equilibrium with Bi-210 and Po-210 was together with lead carrier (5 mg) evaporated to dryness. The residue was dissolved in 10 ml of HCl, $c = 2\ mol\ l^{-1}$. The solution was passed through a preconditioned *Pb Resin* cartridge, and the nuclides were eluted sequentially using hydrochloric acid, $c(HCl) = 2\ mol\ l^{-1}$, nitric acid, $c(HNO_3) = 1\ mol\ l^{-1}$ and $0.1\ mol\ l^{-1}$, and distilled water for bismuth, polonium, and lead, respectively. The eluate was collected in a series of 5-ml fractions. Each fraction was mixed with scintillation cocktail (*Ultima Gold AB*) and measured for 30 min by LSC. The percentage recovery of each nuclide in each aliquot was determined by relating the count rate in each fraction eluted to the count rate derived for an aliquot of each yield tracer equivalent to that added to the *Pb Resin* cartridge. The optimum elution diagram for *Pb Resin* is shown in Fig. 26. As can be seen, bismuth was readily eluted by the sample load and the following rinse step (0–20 ml). Bismuth was quantitatively separated from polonium, but about 25 % of the polonium was lost in the rinsing step with HCl, $c = 2\ mol\ l^{-1}$, leaving 75 % in the following polonium fraction (20–40 ml). Polonium and lead were quantitatively separated from one another; lead was completely eluted with 20 ml distilled water.

The separation of Pb-210 and Po-210 has mainly been performed with *Sr Resin* using the method developed by Vajda et al. [6]. The optimum volumes obtained for the *Pb Resin* were additionally tested on the *Sr Resin*. The results are shown in Fig. 27. *Sr Resin* showed a higher retention of polonium, yielding over 95 %. The complete elution of lead required a slightly larger eluate volume (5 ml) than used for the *Pb Resin*. However, the main reason for not using the *Sr Resin* is the price: one *Sr Resin* cartridge costs about 30 €, compared to 20 € for the *Pb Resin*.

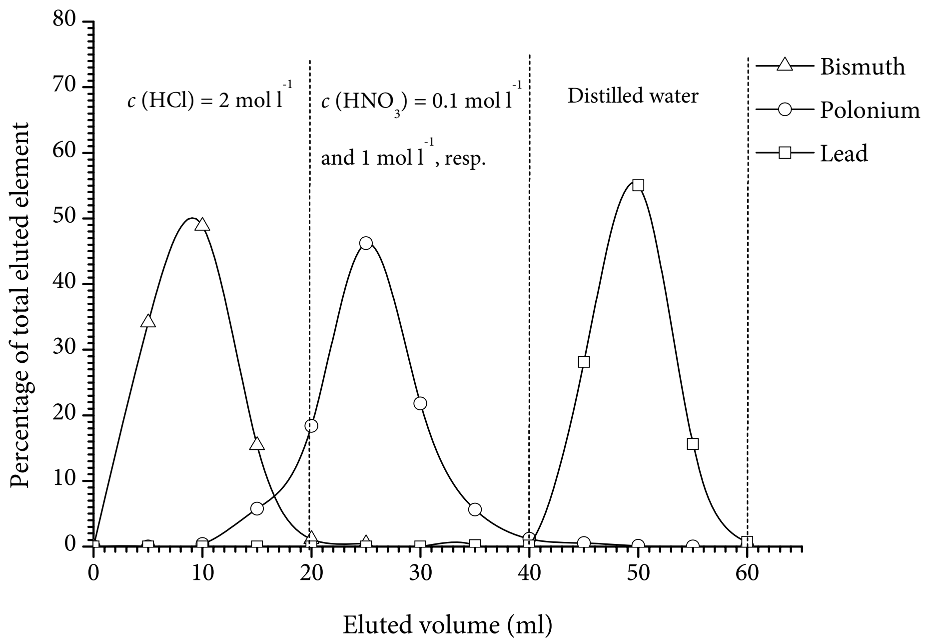

Fig. 26: Elution diagram for *Pb Resin* using the described method in fractions of 5 ml. Dotted lines mark the optimum fractions.

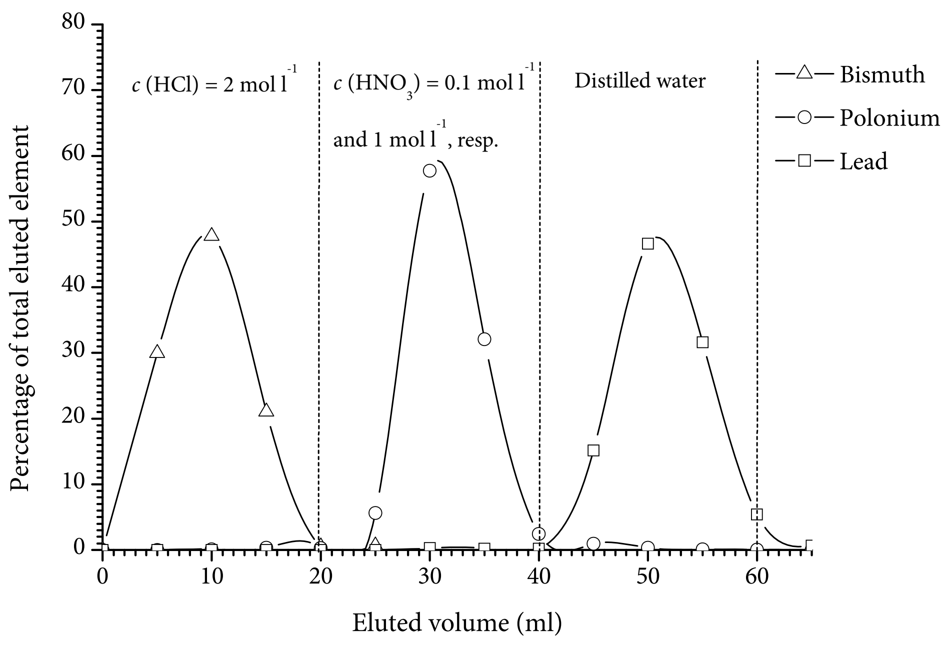

Fig. 27: Elution diagram for *Sr Resin* using the described method in fractions of 5 ml. Dotted lines mark the optimum fractions.

5.3.2.1 Reuse of extraction columns

In general, the solid phase extraction columns can be reused. Vreček *et al.* [101] showed that the reuse of *Sr Resin* columns is possible for the purpose of separating lead and polonium, if no lead carrier was added [47]. In the presence of lead carrier, the lead capacity of the *Sr Resin* column decreased with use. After four repetitions the column capacity for lead decreased by half.

The *Pb Resin* stability was studied by Horwitz *et al.* [5] by making elution profiles with a Sr-85 tracer. Column washing was accompanied by a shift in peak maximum to higher elution volumes, due to loss of solvent (isodecanol) and an increase in peak width. In addition, the stripping of lead from the column was tested. With a used column the stripping was only slightly more difficult.

However, the reuse of extraction columns could lead to cross-contaminations. This is particularly problematic when handling carrier free radionuclides, such as polonium, since different adsorption effects show the highest relative consequences. Therefore, the reuse of extraction columns was refrained from in this work.

5.3.2.2 Effect of high ion concentrations

The effect on the scavenger precipitation as well as the extraction capability of the *Pb Resin* at high ion concentrations was investigated. This was performed using seawater (North Sea at Wilhelmshaven, Germany).

The salt dissolved in seawater has very constant major constituents (Tab. 29): Cl^-, SO_4^{2-}, Mg^{2+}, K^+, Ca^{2+}, and Na^+ dominate sea salt. Their ratios one to another are constant. The salinity, *S* (‰), is defined as the weight in grams of the dissolved inorganic matter in 1 kg of seawater after all $Br^-$and I^- have been replaced by the equivalent quantity of Cl^- and all HCO_3^- and CO_3^{2-} are converted to oxide. In over 97 % of the seawater in the world, the salinity *S* is between 33 ‰ and 37 ‰.

Tab. 29: Major constituents of seawater [76]

Constituent	Seawater at S = 35 ‰ (g kg^{-1})	Constituent	Seawater at S = 35 ‰ (g kg^{-1})
Na^+	10.77	Cl^-	19.354
Mg^{2+}	1.29	SO_4^{2-}	2.712
Ca^{2+}	0.4121	HCO_3^-	0.1424
K^+	0.399	Br^-	0.0673
Sr^{2+}	0.0079	F^-	0.0013

Two samples were prepared: one contained 50 % seawater and the other one contained 100 % seawater. These were prepared using the method described in 5.2. The divalent cations in the seawater (mainly Ca^{2+} and Mg^{2+}) also precipitate by addition of ammonium hydroxide. This will lead to a rather voluminous precipitation, with a change in colour (from rusty brown to light yellow), due to the white calcium- and magnesium-hydroxides. With increasing amount of seawater, the dissolution of the precipitation was difficult. The added acid concentration was no longer the initial (c(HCl) = 2 mol l^{-1}), since the additional hydroxides to various extent had neutralised the acid. Therefore, the samples containing large amounts of salt were dissolved in concentrated HCl and evaporated to dryness and subsequently dissolved in diluted HCl (c(HCl) = 2 mol l^{-1}).

The chemical separation was performed by using the method described in 5.3.2. Aliquots of 5 ml were taken by the separation and subsequently mixed with LSC cocktail and measured via LSC. The results of the chemical separations are shown in Fig. 28. As can be seen, the chemical yield is quantitative for both lead and polonium, even at high dissolved ion concentrations, demonstrating the robustness of the method.

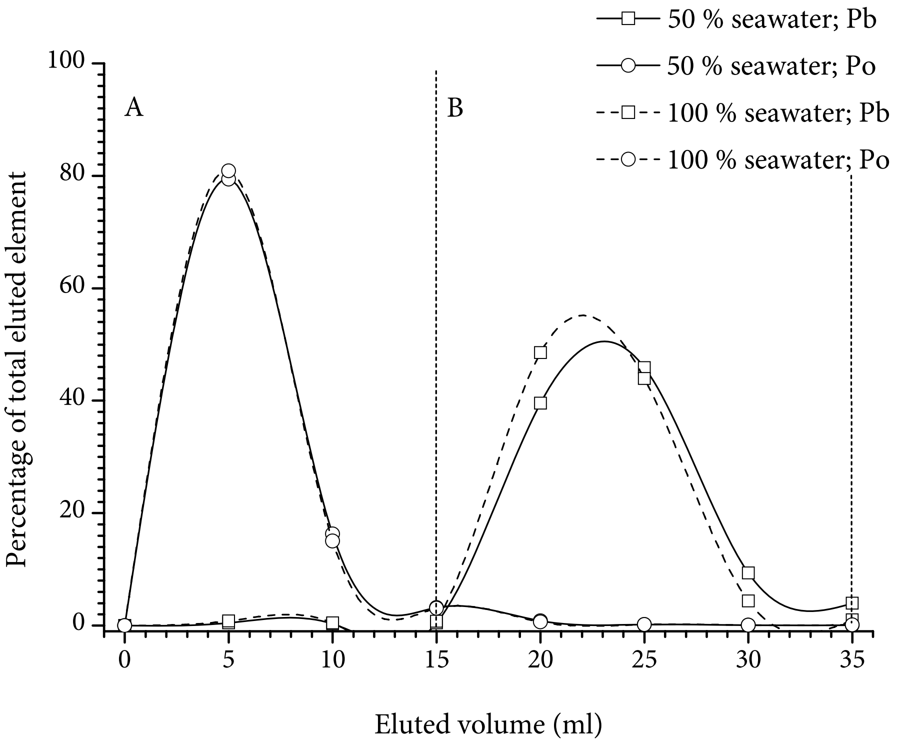

Fig. 28: Pb resin elution diagram for Pb-210 and Po-210. A: Elution of polonium in HNO_3: c = 1 mol l^{-1} (0–10 ml) and c = 0.1 mol l^{-1} (10–15 ml). B: Elution of lead in distilled water (15–35 ml).

5.4 Measurement of Po-210 via alpha spectrometry

5.4.1 Source preparation for the alpha spectrometry

For the alpha source preparation it is important to have the analyte in a purified solution, in order to obtain a source which is practically »massless«, otherwise the alpha radiation would partially or even completely be absorbed within the sample material. A pure sample solution will enable the preparation of an alpha source with high measurement resolution (i.e. low tailing). Prior to the source preparation, a chemical separation is therefore necessary, where not only radioactive species, but also inactive interferences are removed. For this reason, source preparation by precipitation or co-precipitation is usually not preferable, but there are exceptions. For example by the alpha spectrometric determination of Ra-226 a precipitation with barium is used [158, 159]. More convenient are methods which involve a chemical or physical deposition of the radionuclides onto smooth, inactive surfaces [160]. Most commonly used are methods involving electrodeposition and spontaneous deposition onto polished metal surfaces in aqueous solutions.

Noble metals, such as polonium ($E_S^0 = +0.8\,V$ for Po/Po^{4+}) can in solution when in contact with a less noble metal surface (i.e. nickel or silver) be reduced and consequently deposited onto the metal surface; a so called spontaneous deposition, since no current is applied.

In this work, the source preparation for the alpha spectrometry was performed by spontaneous deposition with equipment commercially available from Tracerlab GmbH, consisting of a combined hot plate/magnetic stirring plate (*RCT basic safety control IKAMAG®* from IKA) with contact thermometer (*ETS-D 4 fuzzy IKATRON®* from IKA), a water bath (a normal 2 litre glass beaker, shortened by cutting to proper height), 250 ml glass beakers with a line marking 200 ml, and a special Teflon sample disc holder, fitting the 250 ml beakers, see Fig. 29. The Teflon disc holder was improved for better performance, with a thread-cut fitting instead of the "snap-to-fit" fitting from Tracerlab GmbH, see Fig. 30.

The used method was a modification of an existing method. The basic method was developed by Tracerlab GmbH [161], for the determination of Pb-210 over Bi-210 in water. In this method no chemical separation is performed, but 1 l water is evaporated to dryness at 170 °C. Perchloric acid is added to the residue, in order to remove interfering nitrates, and evaporated to dryness once more. The residue is dissolved in 8 ml HCl, c = 12 mol l^{-1}, then transferred with distilled water to a 400 ml glass beaker, giving a total volume of 200 ml and a HCl concentration of 0.5 mol l^{-1}. Ascorbic acid (100 mg) is added to reduce iron(III). By permanent 18 hour stirring at 85 °C using the Tracerlab equipment, polonium is deposited onto a nickel disc. After terminated deposition, the disc is removed from the sample solution, rinsed with water and dried in air.

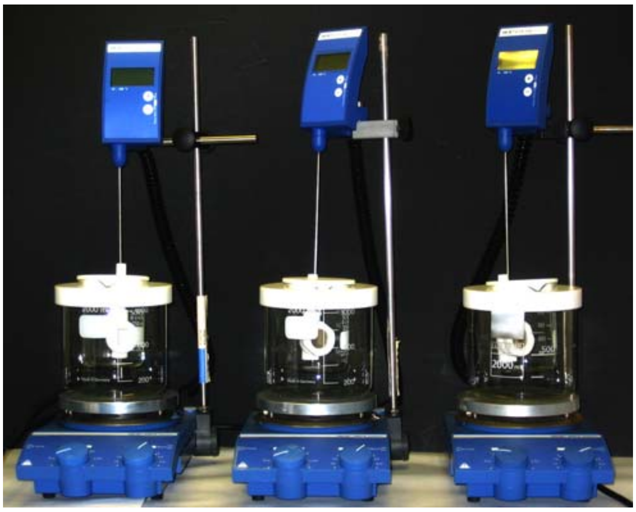

Fig. 29: Three sets of spontaneous deposition equipment

Fig. 30: Teflon disc holders from Tracerlab (l) and the improved disc holder (r).

To improve the method a series of experiments were undertaken. In the literature was found that the deposition of polonium proceeds more smoothly and is more efficient from HCl solutions than from HNO_3 or H_2SO_4 [162]. Therefore, in the following work a hydrochloric solution of 0.5 mol l^{-1}, as described in the Tracerlab method, was applied. First of all, the deposition time was investigated. To a glass beaker 200 ml HCl of c = 0.5 mol l^{-1} and 100 mBq Po-208 tracer were added. In the first series no ascorbic acid was added. The deposition times investigated were 2, 3, 5, 10, and 18 hours, onto nickel discs. A second series was undertaken, with 100 mg of ascorbic acid added to each sample; results are shown in Fig. 31.

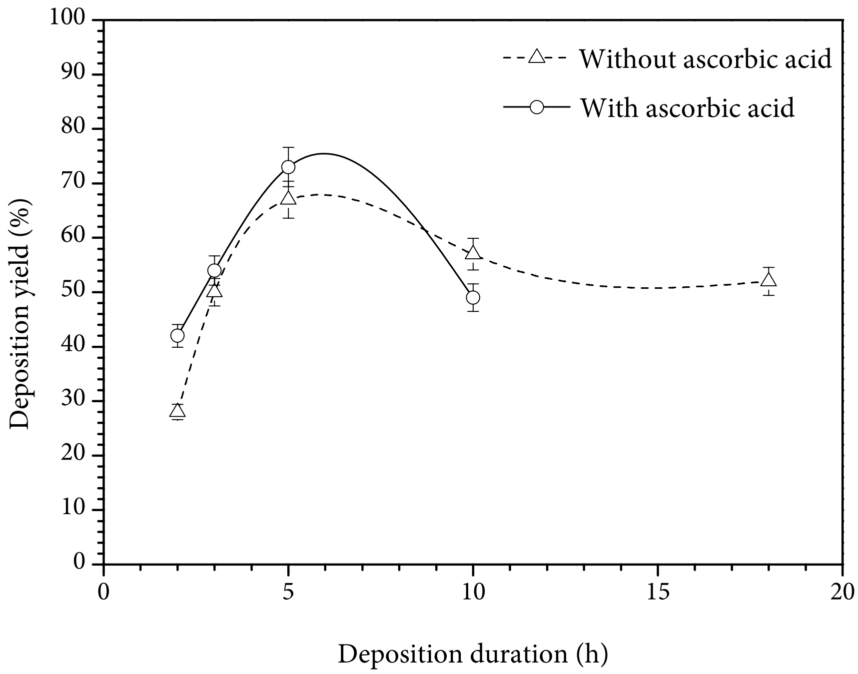

Fig. 31: Effect of deposition time as well as reducing agent (100 mg ascorbic acid) on the deposition yield. The temperature was held at 85 °C in all experiments. The lines are drawn using the spline function (no fits).

The maximum in deposition yield (73 %) on nickel discs was found after about five hours, decreasing with longer duration. The decrease in yield with time could be due to slow dissolution of the nickel disc. Already after five hours the sample solution had a significant pale green colour arising from dissolved Ni^{2+} ions. The suggested deposition time of 18 hours on nickel seemed unnecessary. Therefore, it was hereafter reduced to five hours. With ascorbic acid, as reducing agent, the deposition yield was higher and the deposition more efficient, if the duration was kept short. The ascorbic acid reduced not only the interfering Fe^{3+}, but it was probably also supporting the reduction of polonium. Other reducing agents were found in the literature, for example hydroxylamine hydrochloride and/or sodium citrate [146, 147, 151, 163]. However, Smith and Hamilton [164] found ascorbic acid to be more effective than hydroxylamine hydrochloride in reducing Fe(III). For these reasons, in the further work the addition of 100 mg ascorbic acid was used.

The effect of different deposition temperatures was investigated in three experiments, each with a deposition time of three hours. The results can be seen in Tab. 30, experiments no. 1–3. The deposition yield increased with increasing temperature. Higher temperatures than 85 °C were not investigated, due to the volatility of polonium and since the handling of the sample beaker would be more difficult.

Tab. 30: Method development of the spontaneous deposition

Experiment No.	Deposition time (h)	Disc material	Temp. (°C)	Yield (%)	Matrix composition
1	3	Nickel	50	38	Po-208 tracer (100 mBq) carrier free + 100 mg ascorbic acid
2	3	Nickel	65	47	
3	3	Nickel	85	57	
4	5	Nickel	85	51 (50–52)	Po-208 tracer (100 mBq), 50/50 of HCl/HNO_3 (both $c = 0.5$ mol l^{-1}). No ascorbic acid.
5	5	Nickel	85	61 (57–65)	Like above, but with 100 mg ascorbic acid
6	5	Nickel	85	76 (86–70)	Po-208 tracer (100 mBq) carrier free + 100 mg ascorbic acid
7	5	Stainless steel	85	56	Po-208 tracer (100 mBq) carrier free + 100 mg ascorbic acid
8	5	Silver	85	80	Po-208 tracer (100 mBq) carrier free + 100 mg ascorbic acid
9	18	Silver	85	98	
10	5	Silver	85	41	Pb-210 tracer in equilibrium with Bi-210 and Po-210 (35 mBq) + Pb carrier
11	18	Silver	85	69	

In the suggested method from Tracerlab, interfering nitrates were removed with perchloric acid. It has been reported, that nitrates would interfere with the deposition of polonium onto bismuth discs [30], but otherwise not. Häsänen [165] proved that nitric acid had no effect on the deposition of polonium. Nevertheless, experiments were conducted mixing 100 ml HCl, $c = 0.5$ mol l^{-1}, and 100 ml HNO_3, $c = 0.5$ mol l^{-1}, with 100 mBq Po-208 tracer, see Tab. 30; experiments 4–5. In exp. 4 no reducing agent was added. There was a minor, but no dramatic effect observed in comparison to the depositions without nitrates. In exp. 5, ascorbic acid was added, which seemed to increase the yield to some extent, compared to exp. 4. However, in the further work the nitrate content was kept low, but the use of perchloric acid was refrained from.

The next parameter to be investigated was the disc material. In the literature most common is the use of silver discs [6 163, 164, 166]. Benedik and Vreček [167] are employing copper discs for the plating of polonium with a yield of about 90 % in four hours. Nickel is used by some [23, 168], although Ehinger [169] found that other metals than silver were more susceptible to interferences as some Bi-210 and Pb-210 also may be deposited. As an alternative to spontaneous deposition, electroplating has also been employed for Po-210 analyses. Stainless steel discs are used with plating times of 5 h at 20 mA cm^{-2} [138].

As an alternative to nickel, discs made of stainless steel and silver, respectively, were investigated. The content of the materials are shown in Tab. 31. All discs had a diameter of 25 mm (1.0") and a thickness of 0.5 or 1.0 mm. They were all polished and one side was covered by a thin protective polyethylene foil (100 µm). Immediately before deposition the foil was removed and the disc was rinsed with water, then ethanol and subsequently acetone, before mounted in the Teflon holder.

Tab. 31: Materials used for spontaneous deposition and their composition

Material	Content	Price	Obtained from
Nickel	Ni (99.97 %)	1.00 €/disc	Eichrom Environment
		6.80 €/disc	Tracerlab
Stainless steel	Austenite, Cr (18 %),	0.60 €/disc	Eichrom Environment
	Ni (10 %)	1.20 €/disc	Tracerlab
Silver	Ag (92.8 %), Cu	2.50 €/disc	Eichrom Environment

A carrier free activity of 100 mBq Po-208 was used in exp. 6–9, Tab. 30. On nickel, an average deposition yield of 76 % was reached in five hours. With stainless steel the deposition yield after 5 h was lower, 56 %. The surface of the stainless steel disc had during the deposition turned black, probably due to the formation of chrome and/or nickel oxides. The further use of stainless steel was not employed, since the yield was low. The advantage with stainless steel would be the reduction of costs.

Depositions on silver discs exhibited a higher yield; after 5 h the yield was 80 %. A longer deposition time of 18 h resulted in a yield of 98 % (Tab. 30, exp. 9). In exp. 10 and 11 this was confirmed, using a Pb-210 tracer in equilibrium with its daughters Bi-210 and Po-210 (35 mBq). The added tracer solution also contained a small amount of lead carrier. The deposition yields were in both experiments lower than in those using a carrier free, pure Po-208 tracer. It is for this reason essential to employ a chemical separation prior to the spontaneous deposition, in order to reduce the interferences from carriers and other radionuclides. In the further work, both nickel and silver discs were employed. The advantage of nickel was the price and of silver the better deposition yield, which was necessary for low detection limits in low-level analyses. Two deposited discs are shown in Fig. 32; to the left a nickel disc and to the right a silver disc. The nickel disc was deposited for 5 hours. The polished surface of the disc has been altered as a result of the oxidation of Ni metal to Ni^{2+}, where H^{+}, from the hydrochloric acid, is reduced to H_2. Longer deposition times than 5 hours would affect the alpha resolution in a negative way. On the other hand, the silver disc was deposited for 18 hours, exhibiting very little surface etching and consequently possessing a better alpha resolution.

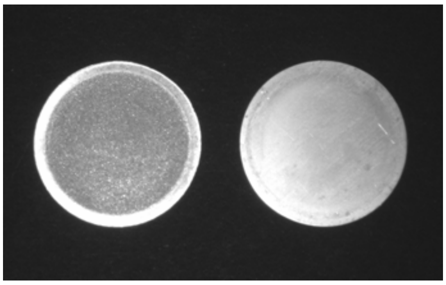

Fig. 32: Nickel (l) and silver (r) discs after spontaneous deposition of polonium

The reproducibility of the spontaneous deposition was investigated. Identical depositions, ten each on nickel and silver, respectively, were performed, using a batch solution containing 90 mBq Po-208. The results are shown in Tab. 32. The average deposition yield on nickel was 61 %, with a standard deviation of 18 %. On silver the average yield was higher than on nickel; 99 % with a standard deviation of 9 %. The reproducibility was significantly higher on silver and the fluctuation in yield lower.

Tab. 32: Reproducibility of spontaneous depositions and activity loss by heating experiments. Added Po-208 activity was in all experiments 90 mBq. Deposition time for nickel was 5 h and for silver 18 h. Average values are shown in bold. The discs were heated 30 min on a hotplate at > 300 °C.

Nickel yield (%)	Yield after heating	Loss (%)	Silver yield (%)	Yield after heating	Loss (%)
70	44	37	102	101	2
47	30	36	104	102	2
43	35	19	98	87	11
77	49	37	98	93	5
86	53	38	104	96	8
48	33	31	103	102	1
41	28	31	105	98	6
71	64	10	99	97	2
42	33	22	102	93	10
85	62	27	76	73	4
61 ± 18	**43 ± 13**	**29 ± 9**	**99 ± 9**	**94 ± 9**	**5 ± 4**

As mentioned in section 4.1.2.2, in order to minimize the detector contamination arising from polonium, the discs should be heated prior to measurement. During this procedure there might be losses of polonium activity. A series of experiments were undertaken to determine the extent of these losses, using the same discs as for the reproducibility test. The results are shown in Tab. 32 as well. The losses of polonium deposited on nickel were markedly higher than on silver. Average loss on nickel was 29 ± 9 per cent compared to before heating. On silver, the average loss was only 5 ± 4 per cent, indicating a high thermal stability of the silver discs.

5.4.1.1 Summary of source preparation

The spontaneous deposition of polonium in the further work was performed in a constantly stirred (using a magnetic stirrer) hydrochloric solution, c = 0.5 mol l^{-1}, kept at 85 °C in a water bath. To the hydrochloric solution 100 mg ascorbic acid were added. The polonium fraction (15 ml) from the chemical separation (see 5.3.2) was added, giving a total volume of 200 ml. The preferred disc material was silver, but also nickel was used. The optimum deposition yield on silver discs was achieved after 18 h deposition and on nickel discs after 5 h, respectively. After completed deposition, the disc was removed from the sample solution, rinsed with water, ethanol and acetone. The disc was allowed to dry in air. Subsequently, the disc was put on a hotplate at > 300 °C for 20–30 min, to oxidize elemental polonium to PoO_2, in order to reduce possible detector contaminations due to volatilisation of polonium in the evacuated alpha chamber. The disc was measured via alpha spectrometry for an appropriate amount of time.

The deposition reproducibility was higher using silver discs than using nickel. The average yield on silver was 99 ± 9 per cent, varying between 73 and 102 per cent. On nickel, the average yield was 61 ± 18 per cent, varying between 41 and 86 per cent. The heating losses after 30 min at 300 °C on silver were diminutive: 5 ± 4 per cent. On nickel, the losses varied between 10 and 38 %, with an average of 29 ± 9 %. For very low-level samples, the silver discs were preferred, since a higher deposition yield resulted in lower detection limits.

5.4.2 Evaluation of the alpha spectra

A polonium alpha spectrum with Po-208 used as a yield tracer is shown in Fig. 33. The spectrum is simple, consisting of three peaks. The presence of Po-209 is due to a contamination in the tracer production, but does not interfere with the evaluation of the alpha spectra. Commonly, channel counts are integrated over regions of interest (ROIs) based asymmetrically around the peaks. The same ROI is used in the sample spectra as well as in the blank spectra. Tailing of Po-210 into the tracer peak needs to be allowed for. The tailing contribution of the tracer peak should only be a small fraction of the count rate in the Po-210 peak, but if the count rate for the Po-210 is much greater than that for the tracer peak, then this tailing may

be significant. As the tracer has a lower energy than that of Po-210, the effect of tailing can be minimized by spiking each sample with a higher activity of tracer than the expected Po-210 activity.

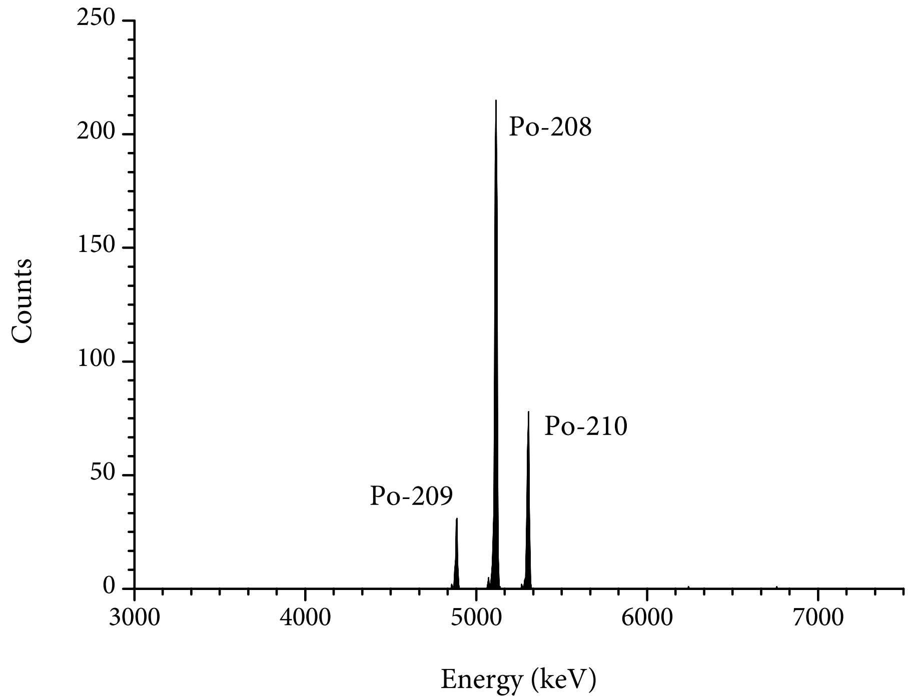

Fig. 33: Typical alpha spectrum of polonium tracer (Po-208 and Po-209) and Po-210

In order to evaluate the spectra received from ionizing radiation measurements, a mathematical model of evaluation was determined. This is a set of mathematical relationships between the measurand and other quantities involved in the evaluation of the measurements [170]. Subsequently, the confidence limits, the decision threshold and the detection limit are determined, using a Bayesian statistical approach.

With the number of registered counts for the tracer peak N, along with the measurement time t and the procedure related calibration factor φ (formed by the measurement efficiency ε of the alpha spectrometer and the total chemical yield η of the radiochemical procedure, for example scavenger precipitation, chemical separation and spontaneous deposition) and the decay correction factor K (implemented for radionuclides with relatively short half-lives), a general equation of the activity can be put to together:

$$A = \varphi K \frac{N}{t} \tag{5.9}$$

$$\varphi = \frac{1}{\varepsilon \eta} \tag{5.10}$$

The measurement time t was attained directly from the α-spectrometer with negligible uncertainty. In all cases the live time was used. The live time is the dead time corrected real time. In nearly all detector systems, there is a minimum amount of time required to separate two events as two separate pulses. The limiting time is may be set by processes in the detector itself or may arise from the associated electronics [123]. This minimum time separation is usually called the dead time of the counting system. The dead time losses can be rather severe when high counting rates are encountered (usually not the case in this work), and any accurate counting measurements made under such conditions must include a correction for these losses.

The procedure related calibration factor φ had to be attained from the separate calibrations of the measurement efficiency ε and the chemical yield η. Considerable fluctuations in the chemical yield could lead to large uncertainties for the procedure related calibration factor.

In order to eliminate the uncertainties of the calibration factor, all the samples were calibrated using an internal standard. The calibration factor was given according to the general equation (5.11) by the known activity A_T of the added tracer (T), the decay correction factor K_T and the number of registered counts of the tracer peak N_T:

$$\varphi = \frac{A_T K_T t}{N_T} \tag{5.11}$$

The calibration factor φ is independent of the alpha energy and can therefore be used for all other radionuclides, to which the tracer is representative. Since the measurement time is inevitably the same for all peaks in the α-spectrum, the activity A_x and K_x for the radionuclide (x) and the number of registered counts N_x for the corresponding peak, was given as:

$$\frac{A_x K_x}{N_x} = \frac{A_T K_T}{N_T} \tag{5.12}$$

The activity A_x could be determined without knowledge of the calibration factor, the measurement efficiency ε or the chemical yield η and the corresponding uncertainties u(φ), u(ε) and u(η) could for this reason remain unconsidered. The activity A_x can be written as:

$$A_x = \frac{N_x A_T K_T}{K_x N_T} \tag{5.13}$$

Equation (5.13) corresponds to the general model of evaluation.

The input quantities necessary for the evaluation are listed in Tab. 33. The index »S« denotes the measurement of a sample, the index »B« that of a background measurement. The

addition »0« refers to the corresponding blank measurement. In the alpha spectrum the peaks are held apart using the indices »x«, for the radionuclide to be measured and »T« for the tracer respectively.

Tab. 33: Designation of input quantities

Measurement	Measurement time	Number of registered counts (sample peak)	Number of registered counts (tracer peak)
Sample	t_S	$N_{x,S}$	$N_{T,S}$
Background (to sample)	$t_{S,0}$	$N_{x,S,0}$	$N_{T,S,0}$
Blind sample	t_B	$N_{x,B}$	$N_{T,B}$
Background (to blind sample)	$t_{B,0}$	$N_{x,B,0}$	$N_{T,B,0}$

As for all other nuclear measurements it is necessary to consider and correct for the background radiation. The background arising from the spectrometer itself is proportional to the measurement time *t*. A separate blank measurement was performed under the same conditions (same detector chamber, same air pressure, same geometry) with a clean metal disc (silver or nickel). Only the measurement time could differ (preferably a longer *t* was used), all other parameters should stay the same. The background radiation from possible radioactive impurities in the tracer solution or in other used chemicals was determined with a separate measurement of a blind sample (reagent blank). Here a known amount of the tracer (no contribution of the radionuclide x) was deposited onto a disc and measured under the same conditions as above. By this measurement again the spectrometer background had to be taken into account and measured, although most of the time the background to sample was used as background to blind sample. In total there were four independent alpha measurements necessary for the evaluation of one sample.

After the background correction was performed, the net counts were compared to a decision threshold. For a significant contribution arising from the measured sample the net count has to be larger than the decision threshold. If there is a significant contribution from the sample the activity can be calculated using the specific mathematical model of evaluation:

$$A_x = A_T \cdot \left(\frac{\exp\left(-\ln 2 \cdot \frac{t_{w,T}}{^{\text{Po-208}}t_{1/2}}\right) \cdot \frac{^{\text{Po-208}}t_{1/2}}{\ln 2 \cdot t_{c,T}} \cdot \left(1-\exp\left(-\ln 2 \cdot \frac{t_{c,T}}{^{\text{Po-208}}t_{1/2}}\right)\right)}{\exp\left(-\ln 2 \cdot \frac{t_{w,x}}{^{\text{Po-210}}t_{1/2}}\right) \cdot \frac{^{\text{Po-210}}t_{1/2}}{\ln 2 \cdot t_{c,x}} \cdot \left(1-\exp\left(-\ln 2 \cdot \frac{t_{c,x}}{^{\text{Po-210}}t_{1/2}}\right)\right)} \right) \cdot \left(\frac{N_{x,S} - N_{x,S,0}\frac{t_S}{t_{S,0}}}{N_{T,S} - N_{T,S,0}\frac{t_S}{t_{S,0}}} \right) \tag{5.14}$$

with A_x and A_T being the activity of the sample peak and tracer peak respectively, $t_{c,x}$ and $t_{c,T}$ being the counting time for the sample and tracer respectively, and with $t_{w,x}$ and $t_{w,T}$ being the waiting time before measurement for the sample and tracer respectively, $t_{1/2}$ is the half-life of the specific radionuclide.

The measurement uncertainty is based on the ISO Guide to the Expression of Uncertainty in Measurement (GUM) [171]. It is based on the methods of Bayesian statistics, in order to be able to consider uncertain quantities and influences which do not behave randomly in repeated measurements. Random variables are assigned as estimators to all incompletely known physical quantities. The probability distributions of these estimators must in general not be interpreted as frequency distributions of events in frequently repeated measurements, as is done in conventional statistics. In Bayesian statistics, the probability $(1-\gamma)$ represents the degree of incomplete knowledge of the confidence interval, whose limits are calculated from the measured data and from other information to contain the true value of the measurand.

The uncertainty of the alpha spectrometry measurement of Po-210, $u^2(A_x)$, is shown in eqn. (5.15) below:

$$u^2(A_x) = u^2(A_T)\left(\frac{N_{x,S} - N_{x,S,0}\dfrac{t_S}{t_{S,0}}}{N_{T,S} - N_{T,S,0}\dfrac{t_S}{t_{S,0}}}\right)^2 + A_T^2\left(\frac{N_{x,S} - N_{x,S,0}\dfrac{t_S}{t_{S,0}}}{\left(N_{T,S} - N_{T,S,0}\dfrac{t_S}{t_{S,0}}\right)^2} + \frac{\left(N_{x,S} - N_{x,S,0}\dfrac{t_S}{t_{S,0}}\right)^2 N_{T,S} - N_{T,S,0}\dfrac{t_S^2}{t_{S,0}^2}}{\left(N_{T,S} - N_{T,S,0}\dfrac{t_S}{t_{S,0}}\right)^4}\right) \tag{5.15}$$

In order to characterize the performance and suitability of the chosen evaluation procedure, it is necessary to know the decision threshold and the detection limit. According to Bayesian theory, the true value $\tilde{\alpha}_x$ is zero if the element or the radionuclide is not present in the sample. The decision threshold and the detection limit are defined on the basis of statistically testing the null hypothesis H_0: $\alpha_x = 0$ against the alternative hypothesis H_1: $\tilde{\alpha}_x > 0$. For the determination of the decision threshold and the detection limit, the standard uncertainty of the decision quantity has to be calculated as a function of $\tilde{u}(\alpha_x)$ of the true value α_x of the measurand. The decision threshold A_x^* is given by [172]:

$$A_x^* = k_{1-\alpha} \cdot \tilde{u}(0), \tag{5.16}$$

with $k_{1-\alpha}$ being the $(1-\alpha)$ quantile of the standardised normal distribution, $\tilde{u}(0)$ is the uncertainty of the measurand if the true value equals zero. The specific decision threshold for the alpha spectrometry measurement of Po-210 is shown in eqn. (5.17). The value for the statistical confidence was chosen to $k_{1-\alpha} = 1.645$.

$$A_x^* = k_{1-\alpha} \cdot \widetilde{u}(0) = k_{1-\alpha} \frac{A_T}{N_{T,S} - N_{T,S,0} \frac{t_S}{t_{S,0}}} \sqrt{N_{x,S,0} \frac{t_S}{t_{S,0}} \left(1 + \frac{t_S}{t_{S,0}}\right)} \tag{5.17}$$

The detection limit α_x^* is the smallest true value of the measurand detectable with the chosen measurement system. The detection limit is given by

$$\alpha_x^* = A_x^* + k_{1-\beta} \cdot \widetilde{u}(\alpha_x^*)\,, \tag{5.18}$$

with $k_{1-\beta}$ being the $(1-\beta)$ quantile of the standardised normal distribution. The specific detection limit for the alpha spectrometry measurement of Po-210 is shown below.

$$\alpha_x^* = A_x^* + k_{1-\beta} \sqrt{u^2(A_T)\left(\frac{\alpha_x^*}{A_T}\right)^2 + A_T^2 \left[\frac{\alpha_x^*}{A_T N_{T,S} - N_{T,S,0} \frac{t_S}{t_{S,0}}} + \frac{N_{x,S,0} \frac{t_S}{t_{S,0}} \left(1 + \frac{t_S}{t_{S,0}}\right) + \left(\frac{\alpha_x^*}{A_T}\right)^2 \left(N_{T,S} - N_{T,S,0} \frac{t_S}{t_{S,0}}\right)}{\left(N_{T,S} - N_{T,S,0} \frac{t_S}{t_{S,0}}\right)^2} \right]} \tag{5.19}$$

The value for the statistical confidence was chosen to $k_{1-\alpha} = k_{1-\beta} = 1.645$. As can be seen, the eqn. (5.19) is implicit. The detection limit can be calculated from this equation by iteration, using the Microsoft computer programme *Excel*[1]. The equations for the model of evaluation, confidence limit, decision threshold and detection limit came to use in the chapters 6.1 and 6.2.

5.5 Measurement of Pb-210 via Liquid Scintillation Counting

For the preparation of a LSC sample, an aliquot (5 ml) of the lead fraction obtained from the chemical separation (see above) is transferred to a counting vial made of polyethylene (Zinsser Analytics) and thereafter mixed with 15 ml of scintillation cocktail. For aqueous samples the *Ultima Gold™ AB* cocktail from PerkinElmer is preferred. This cocktail is based on the diisopropylnaphthalene solvent and consequently possesses outstanding alpha/beta discrimination properties, also see 4.2.2.3.

[1] In Excel under: Tools – Options – Calculation, the option „Iteration" can be activated

5.5.1 Ingrowth of Bi-210

Immediately after the chemical separation of the previously existing Bi-210 in the sample, the ingrowth of Bi-210 from the Pb-210 is commenced. The ingrowth of Bi-210 can be described by the following equation, derived from the law of radioactive decay described in chapter 2.1.3:

$$A_{\mathrm{Bi}} = \frac{\lambda_{\mathrm{Bi}}}{\lambda_{\mathrm{Bi}} - \lambda_{\mathrm{Pb}}} A_{0,\,\mathrm{Pb}} \exp\left(-\lambda_{\mathrm{Pb}} t\right)\left(1 - \exp\left(-(\lambda_{\mathrm{Bi}} - \lambda_{\mathrm{Pb}})t\right)\right) \tag{5.20}$$

The equation includes an unknown parameter ($A_{0,\,\mathrm{Pb}}$), which can be gained by fitting an appropriate curve to the measured values of A_{Bi}. The maximum activity is reached after 53 days. Fig. 34 shows a fitted curve of LSC activity measurements of Bi-210 subsequent the chemical separation of a Pb-210 standard solution. As can be seen, the measured values correspond very well with the theory. With this experiment also the long term stability of the prepared LSC samples is shown to be sufficient.

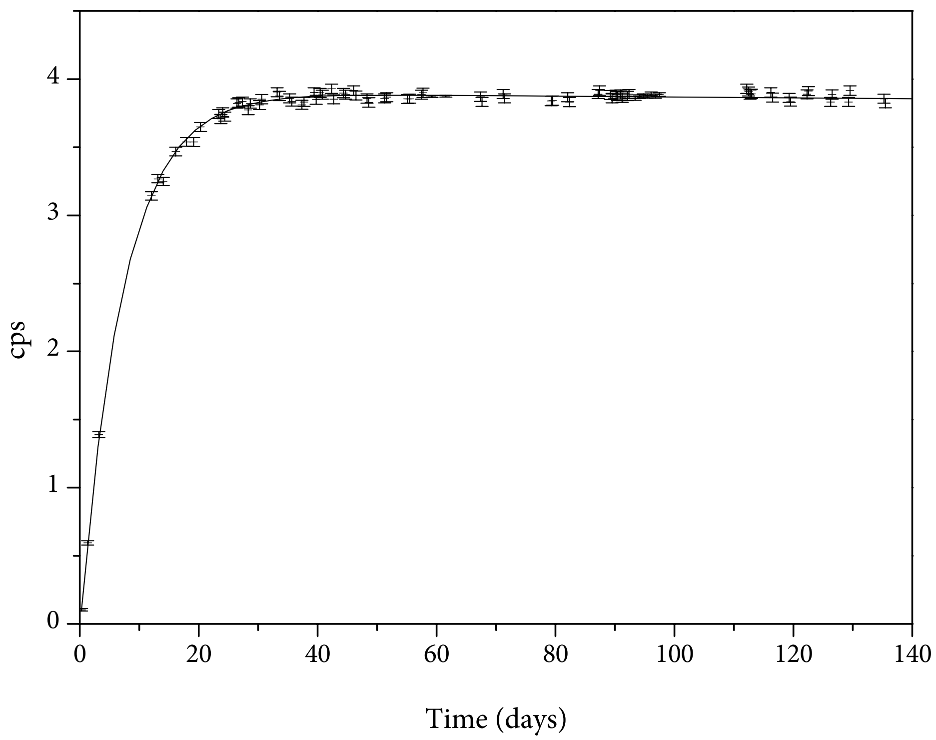

Fig. 34: The fitted ingrowth curve of Bi-210 after chemical separation

5.5.2 Pulse shape setting

With the purpose of finding the optimal pulse shape analysis (PSA) setting, a Pb-210 tracer sample was measured at different PSA values. The sample was prepared in a similar way as the real samples to be measured, containing 5 ml spiked aqueous solution and 15 ml *Ultima Gold™ AB* cocktail, with a quench value at SPQ = 833. In Fig. 35 can be seen, that the spectrum shifts to the right if the PSA is set too low, this corresponds to PSA 10–90. For the lower PSA values more of the beta pulses are misclassified as alpha pulses and will therefore appear in the alpha spectrum. On the other hand, at a too high PSA setting alpha pulses are misclassified as beta pulses and will appear in the beta spectrum. This can be observed for PSA value 120, where at approximately channel 650 a peak contribution of a different shape can be seen. This contribution arises from the misclassified alphas. The optimal PSA setting was chosen to 110, where the misclassification of both alpha and beta pulses was at a minimum; less than 1 % for both alpha and beta pulses. The pulse shape discrimination was utilizing even after chemical separation of Pb-210, because with time the alpha emitting Po-210 is growing in to equilibrium and therefore may add to the count rate in the Bi-210 counting window, which would ultimately lead to an error in activity, unless PSA was used.

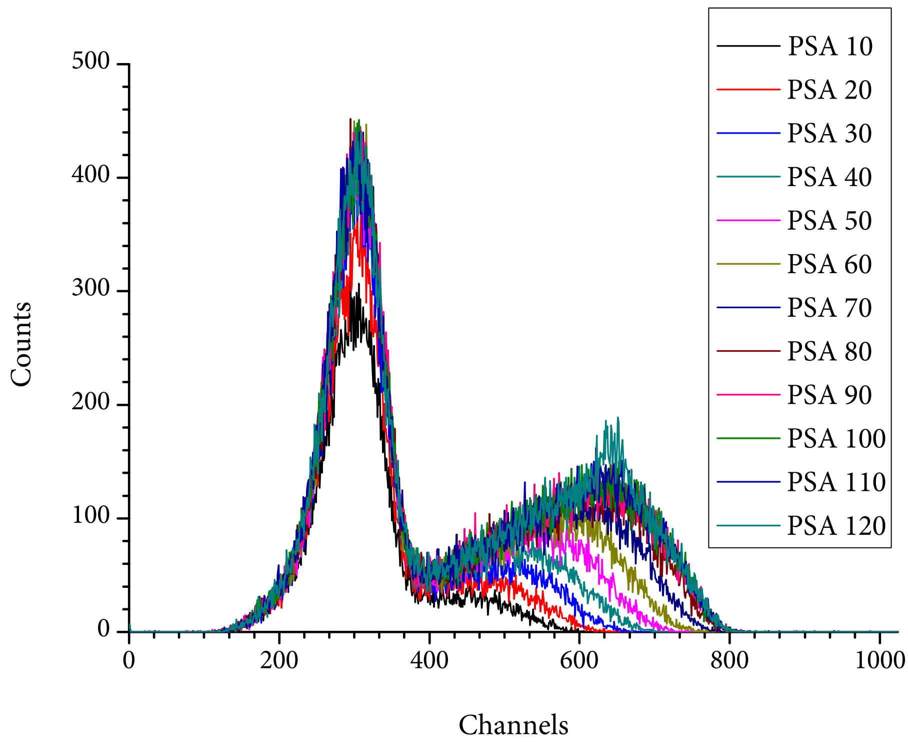

Fig. 35: LSC spectra of a Pb-210 spiked sample measured at different PSA settings

5.5.3 Quench calibration

For strongly quenched samples the measured beta spectrum would shift to lower energies. This may result in false registration of counts in the preset counting windows, as these are static and would not move with the quench, see 4.2.5. A decrease in counting efficiency is also caused by quenching. However, the analysed samples in this work all have the same quench, due to the chemical separation step which delivers equal chemical properties to all lead fractions, the preparation and measurement of a quench curve was refrained from.

5.5.4 Efficiency calibration

In order to determine the counting efficiency, ε, of the liquid scintillation measurement of Bi-210, a known activity of Pb-210 tracer in equilibrium with its daughters was repeatedly measured. Two representative samples were prepared, with an activity of each 36.3 Bq, and measured twenty times via LSC at a PSA setting of 110; the counts in the Bi-210 counting window were compared to the added activity, and from this the counting efficiency was determined to:

$$\varepsilon = 0.802 \pm 0.011 \tag{5.21}$$

As mentioned in 4.2.2.5, the counting efficiency for beta particles with energies > 100 keV is nearly 100 %. The determined efficiency for Bi-210 is only about 80 %, which is due to the overlapping spectrum of Pb-210, where 20 % of the Bi-210 spectrum has to be cut off, see 5.5.6 below. The direct determination of Pb-210 via LSC is also possible, but the counting efficiency of the weak beta emitter Pb-210 ($E_{\beta,\max}$ = 63 keV) is low.

5.5.5 Determination of the chemical yield

The chemical yield η is measure of the performance of a chemical procedure, i.e. how much of the analyte is actually recovered at the end of the procedure, or how much is lost in comparison to what was there from the beginning. It is determined for each sample, since differences in sample composition may have influence on the chemical yield.

The determination of the chemical yield for Pb-210 was performed via inductively coupled plasma-mass spectrometry (ICP-MS) at the Institute for Analytical Chemistry, in the work group led by Prof. Dr. Vogt, at the Leibniz University of Hanover, by measuring the added lead carrier (the stable isotope Pb-208). Two ICP-MS samples were analysed per water sample; one before the sample preparation was begun and one aliquot was taken from the lead fraction obtained after the chemical separation. The reason for taking a "before" sample was, although the amount of added lead carrier was known, the possibility of Pb existing in the sample before adding the carrier, since these were environmental samples and therefore

might contain a number of different dissolved elements, including Pb. After proper dilution (1:1000 for "before" samples and 1:10,000 for "after" samples) the samples were measured using a quadropole (Q) ICP-MS Thermo Elemental X-7 from *Thermo Fisher*. The experimental parameters for the measurement of Pb-208 are shown in Tab. 34.

The calibration was performed using a Pb standard (High Purity Standards) 1000 mg l^{-1}, diluted with ultra-pure water to appropriate concentrations between 1 and 25 ppb. In addition, all samples contained 2 % v/v nitric acid (AnalaR Normapur for trace analysis of Cd, Hg and Pb: ProLabo VWR). The 5 ppb calibration sample was repeatedly measured, in order to detect and correct any background changes during the measurement.

The lead concentrations before and after sample preparation and chemical separation, respectively, were compared; see eqn. (5.22):

$$\eta = \frac{C_{Pb,\,after}}{C_{Pb,\,before}} \tag{5.22}$$

The chemical yield was in general high, between 90–100 %.

Tab. 34: Experimental parameters for the Thermo Elemental X-7 ICP-QMS used for the measurement of Pb-208

Parameter	Setting
Forward power	1200 W
Coolant gas (Ar)	14.0 l min^{-1}
Auxiliary gas (Ar)	1.0 l min^{-1}
Nebulizer gas (Ar)	1.7 l min^{-1}
Sampling cone	1.0 mm nickel
Skimmer cone	0.7 mm nickel
Mode	Normal
Mass monitored	208

5.5.6 Evaluation of the LSC spectra

In order to successfully determine the activity of Pb-210 by measuring the daughter Bi-210, counting windows have to be used. This is due to the spectrum overlap of the two radionuclides, which can be seen in Fig. 36. The Bi-210 window is set so that only the beta events arising of Bi-210 will be measured. This suggests that about 20 % of the low energy part must be cut off, since these counts overlap with the counts arising from the beta events of Pb-210 in the low energy part of the spectrum (since all beta decays have an energy distribution from zero to E_{max}). Consequently, in the high energy window Bi-210 appears and in the low energy

window Pb-210 and about 20 % of the Bi-210 peak. The alpha events arising from the daughter Po-210 (E_α = 5304.5 keV) are not detected in the beta spectrum, due to the alpha/beta discrimination. The LSC counting windows used are listed in Tab. 35.

Tab. 35: LSC counting windows

Radionuclide	Channels	MCA/HALF
Pb-210	100–400	1/1 (Beta spectrum)
Bi-210	410–800	1/1 (Beta spectrum)
Po-210	460–730	1/2 (Alpha spectrum)

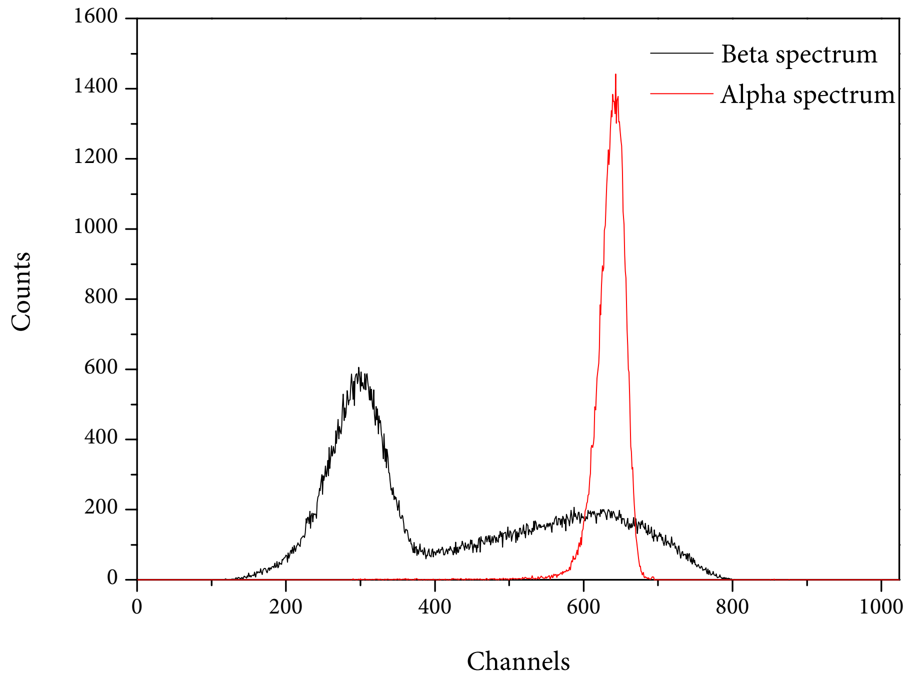

Fig. 36: Typical LSC spectrum of Pb-210 in equilibrium with its daughters. The beta counting window was set between channels 401 to 800, at a PSA value of 110.

The evaluation of the LSC spectra was performed in the same manner as for the alpha spectra, using the GUM and ISO 11929-7, see chapter 5.4.2. The input quantities used for the LSC evaluation are listed in Tab. 36. The equations below were used in the determinations of real samples, see chapters 6.1 and 6.2.

Tab. 36: Input quantities used in the LSC evaluation

Quantity	Symbol	Unit	Uncertainty symbol
Number of gross counts	N_g	–	$u(N_g)$
Time of gross measurement	t_g	s	
Gross count rate	R_g	s^{-1}	$u(R_g)$
Number of background counts	N_0	–	$u(N_0)$
Time of background measurement	t_0	s	
Background count rate	R_0	s^{-1}	$u(R_0)$
Counting efficiency	ε	$Bq^{-1}\ s^{-1}$	$u(\varepsilon)$
Chemical yield	η	–	$u(\eta)$
Sample volume	V	l	$u(V)$
Aliquot correction factor	f_a	–	$u(f_a)$
Volume of aliquot of the Pb fraction	v_a	l	$u(v_a)$
Volume of the total Pb fraction	v_{Pb}	l	$u(v_{Pb})$
Waiting time	t_w	s^{-1}	
Decay correction factor, due to waiting time	K_w	–	
Decay constant	λ	s^{-1}	
Activity	A	Bq	$u(A)$
Decision threshold	A^*	Bq	
Detection limit	α^*	Bq	

The general model of evaluation can be written as:

$$A = \frac{R_g - R_0}{\varepsilon \eta V f_a} \cdot K_w , \tag{5.23}$$

where $f_a = \dfrac{v_a}{v_{Pb}}$ and (5.24)

$$K_w = \frac{\lambda_{Bi}}{\lambda_{Bi} - \lambda_{Pb}} \exp(-\lambda_{Pb} t_w)(1 - \exp(-\lambda_{Bi} - \lambda_{Pb})t). \tag{5.25}$$

Due to the long waiting time for the ingrowth of Bi-210 before measurement, a decay correction factor, K_w, was applied. Since the sample measurements were short in comparison to the half-life of Pb-210, there was no measurement time decay correction performed. The uncertainty for the decay correction factor K_w was assumed to be negligible.

Using the input quantities from Tab. 36, the specific model of evaluation can be formulated as:

$$A = \left(\frac{N_\mathrm{g}}{t_\mathrm{g}} - \frac{N_0}{t_0} \right) \left(\frac{\frac{\lambda_\mathrm{Bi}}{\lambda_\mathrm{Bi} - \lambda_\mathrm{Pb}} \exp(-\lambda_\mathrm{Pb} t_\mathrm{w})(1 - \exp(-\lambda_\mathrm{Bi} - \lambda_\mathrm{Pb}) t_w)}{\varepsilon \eta V f_\mathrm{a}} \right). \tag{5.26}$$

The uncertainty of the LSC measurement is shown in:

$$u^2(A) = \left(\frac{N_\mathrm{g} \frac{1}{t_\mathrm{g}^2} + N_0 \frac{1}{t_0^2}}{\left(\frac{n_\mathrm{g}}{t_\mathrm{g}} - \frac{n_0}{t_0} \right)^2} + \frac{u^2(\varepsilon)}{\varepsilon^2} + \frac{u^2(\eta)}{\eta^2} + \frac{u^2(V)}{V^2} + \frac{u^2(\nu_\mathrm{a})}{\nu_\mathrm{a}^2} + \frac{u^2(\nu_\mathrm{Pb})}{\nu_\mathrm{Pb}^2} \right) \left(\left(\frac{N_\mathrm{g}}{t_\mathrm{g}} - \frac{N_0}{t_0} \right) \frac{K_\mathrm{w}}{\varepsilon \eta V f_\mathrm{a}} \right)^2 \tag{5.27}$$

The decision threshold can be written as:

$$A^* = k_{1-\alpha} \cdot \tilde{u}(0) = k_{1-\alpha} \sqrt{\frac{N_0}{t_0} \left(\frac{1}{t_\mathrm{g}} + \frac{1}{t_0} \right)} \cdot \frac{K_\mathrm{w}}{\varepsilon \eta V f_\mathrm{a}}, \tag{5.28}$$

and the detection limit can be expressed as:

$$\alpha^* = A^* + k_{1-\beta} \left(\sqrt{ \frac{ \frac{\alpha^*}{\left(\frac{K_\mathrm{w}}{\varepsilon \eta V f_\mathrm{a}} \right)} + \frac{N_0}{t_0} }{t_\mathrm{g}} + N_0 + \frac{ \frac{u^2(\varepsilon)}{\varepsilon^2} + \frac{u^2(\eta)}{\eta^2} + \frac{u^2(V)}{V^2} + \frac{u^2(\nu_\mathrm{a})}{\nu_\mathrm{a}^2} + \frac{u^2(\nu_\mathrm{Pb})}{\nu_\mathrm{Pb}^2} \cdot \alpha^{*2} }{ \left(\frac{K_\mathrm{w}}{\varepsilon \eta V f_\mathrm{a}} \right)^4 } } \right) \left(\frac{K_\mathrm{w}}{\varepsilon \eta V f_\mathrm{a}} \right) \tag{5.29}$$

5.6 Determination of Pb-210 by measuring Po-210 after ingrowth

The activity of Pb-210 was additionally determined by measuring the ingrown activity of the daughter Po-210 using alpha spectrometry. An aliquot of the lead fraction from the chemical separation was used in the spontaneous deposition with subsequent alpha spectrometric measurement, as described in 5.4.

5.6.1 Ingrowth of Po-210

The ingrowth of Po-210 from Pb-210 can be described by the following equation, derived from eqn. (2.15) described in chapter 2.2:

$$A_{\mathrm{Po}} = \lambda_{\mathrm{Po}} \lambda_{\mathrm{Bi}} A_{0,\mathrm{Pb}} \frac{\exp(-\lambda_{\mathrm{Pb}} \Delta t)}{(\lambda_{\mathrm{Bi}} - \lambda_{\mathrm{Pb}})(\lambda_{\mathrm{Po}} - \lambda_{\mathrm{Pb}})} + \frac{\exp(-\lambda_{\mathrm{Bi}} \Delta t)}{(\lambda_{\mathrm{Pb}} - \lambda_{\mathrm{Bi}})(\lambda_{\mathrm{Po}} - \lambda_{\mathrm{Bi}})} + \frac{\exp(-\lambda_{\mathrm{Po}} \Delta t)}{(\lambda_{\mathrm{Bi}} - \lambda_{\mathrm{Po}})(\lambda_{\mathrm{Pb}} - \lambda_{\mathrm{Po}})}, \quad (5.30)$$

where A_{Po} is the measured activity of Po-210, and Δt is the time passed between chemical separation and time of measurement.

The ingrowth of the daughter Bi-210, as well as the granddaughter Po-210, is shown in Fig. 37 as an activity ratio of the decaying mother Pb-210 over time. Radiochemical equilibrium between Pb-210, Bi-210 and Po-210 is achieved after about 800 days (2.2 y), not depicted in Fig. 37.

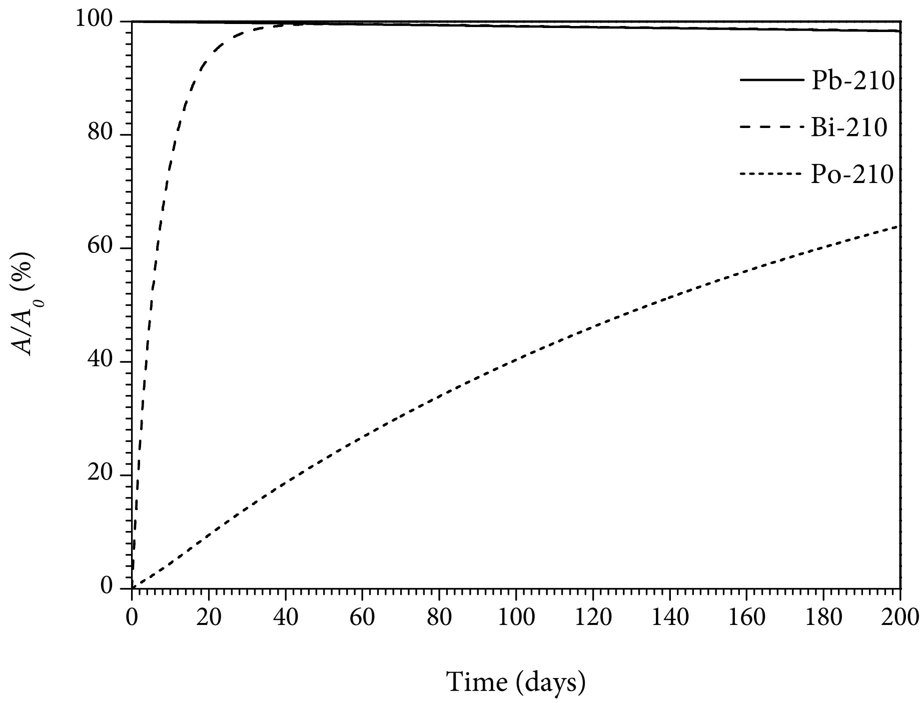

Fig. 37: Ingrowth of Bi-210 and Po-210 from Pb-210 as a function of time

5.6.2 Determination of the Pb-210 activity

In order to determine Pb-210 over Po-210 enough time had to pass between the chemical separation and the subsequent spontaneous deposition of the ingrown polonium. To the aliquoted Pb-210 fraction, a known amount of Po-208 tracer was added, usually about 45 mBq. The deposition was performed as described in 5.4.1. The sensitive measurement of polonium via alpha spectrometry yielded low detection limits for the Pb-210 determination, which occasionally was required for the environmental and groundwater samples. The Pb-210 activity, $A_{0,\,\mathrm{Pb}}$ was calculated using eqn. (5.31), derived from eqn. (5.30):

$$A_{0,\mathrm{Pb}} = \frac{A_{\mathrm{Po}} \cdot f_{\mathrm{a}}}{\lambda_{\mathrm{Po}}\lambda_{\mathrm{Bi}}\left(\frac{\exp(-\lambda_{\mathrm{Pb}}t)}{(\lambda_{\mathrm{Bi}}-\lambda_{\mathrm{Pb}})(\lambda_{\mathrm{Po}}-\lambda_{\mathrm{Pb}})}+\frac{\exp(-\lambda_{\mathrm{Bi}}t)}{(\lambda_{\mathrm{Pb}}-\lambda_{\mathrm{Bi}})(\lambda_{\mathrm{Po}}-\lambda_{\mathrm{Bi}})}+\frac{\exp(-\lambda_{\mathrm{Po}}t)}{(\lambda_{\mathrm{Bi}}-\lambda_{\mathrm{Po}})(\lambda_{\mathrm{Pb}}-\lambda_{\mathrm{Po}})}\right)}, \quad (5.31)$$

where f_{a} is the aliquot correction factor (see eqn. (5.24) and Tab. 36).

The disadvantage with the determination of Pb-210 over Po-210 was the long ingrowth waiting time (usually between 6 months and one year; with an ingrowth of 60 % or more) required for the measurement.

5.7 Validation

For the purpose of validation, the proposed method was tested with the help of certified reference materials. The reference materials were treated in the same way as any other sample consisting of the same matrix (water), using the proposed method. The measurement results were compared to the certified reference activity. If the activities were not significantly dissimilar, the method was considered to be valid, providing true and accurate results.

Reference materials, for many different radionuclides and for all kinds of matrices can be purchased from the IAEA, NIST and PTB. The round robin tests for gamma emitting radionuclides and gross alpha in water from the BfS are released annually (registration required) and proficiency tests from the IAEA are released occasionally (registration required). However, there are very few reference materials available for naturally occurring radionuclides in water matrices. Lately, two relevant proficiency tests from the IAEA on Po-210 in water and from the French Commissariat à l'Energie Atomique (CEA) involving Pb-210, Po-210, and Ra-226 among others have become available.

5.7.1 IAEA Proficiency test

The validation of the proposed method for Pb-210 and Po-210 in aqueous samples was performed using samples from proficiency tests from the International Atomic Energy Agency (IAEA).

In Tab. 37, the measurement results from the IAEA-CU-2007-09 proficiency test on the determination of Po-210 in spiked water are presented. After chemical separation using the *Pb Resin*, the alpha counting sources were prepared using spontaneous deposition onto silver discs, with subsequent measurement via alpha spectrometry. Measurement time was 24 h for samples 1 and 3, 12 h for samples 2 and 4, and 72 h for sample 5. The added Po-208 tracer activity was 190 mBq $^{-1}$. Sample 5 was intended as a blank, with an activity of < 0.1 Bq kg^{-1}. The evaluation of trueness and precision of the results obtained with the proposed method are shown in Tab. 38.

Tab. 37: Results from the IAEA-CU-2007-09 proficiency test on the determination of Po-210 in spiked water

	Sample 1 (Bq kg^{-1})		Sample 2 (Bq kg^{-1})		Sample 3 (Bq kg^{-1})		Sample 4 (Bq kg^{-1})		Sample 5 (Bq kg^{-1})	
	Value	*Unc*	*Value*	*Unc*	*Value*	*Unc*	*Value*	*Unc*	*Value*	*Unc*
Lab	48.3	1.7	100.2	6.3	54.5	1.8	94.7	5.8	0.025	0.006
IAEA	52.8	1.4	101.6	2.8	52.8	1.4	101.6	2.8	< 0.1	

Tab. 38: Evaluation of trueness and precision of the results from the IAEA-CU-2007-09 proficiency test on the determination of Po-210 in spiked water

	Rel. Bias (%)	z-Score	*A1*	*A2*	Trueness	*P* (%)	Precision
Sample 1	−8.52	−0.85	4.50	5.68	A	4.41	A
Sample 2	−1.38	−0.14	1.40	17.79	A	6.86	A
Sample 3	3.22	0.32	1.70	5.88	A	5.88	A
Sample 4	−6.79	−0.68	6.90	16.61	A	6.71	A

As can be seen in Tab. 38, the results were true and precise and all samples were assigned the final score “Acceptable” (A). The trueness is assigned “Acceptable” if

$$A1 \leq A2 \tag{5.32}$$

where

$$A1 = \left| Value_{\mathrm{IAEA}} - Value_{\mathrm{Lab}} \right| \tag{5.33}$$

$$A2 = 2.58\sqrt{Unc_{\mathrm{IAEA}}^2 + Unc_{\mathrm{Lab}}^2} \tag{5.34}$$

For evaluation precision estimator P is calculated according to the following formula:

$$P = \sqrt{\left(\frac{Unc_{\mathrm{IAEA}}}{Value_{\mathrm{IAEA}}}\right)^2 + \left(\frac{Unc_{\mathrm{Lab}}}{Value_{\mathrm{Lab}}}\right)^2} \times 100\ [\%] \tag{5.35}$$

The precision estimator P directly depends on the measurement uncertainty. The acceptance limit for precision (LAP) for the analyte Po-210 was 15 per cent and given by the IAEA. The results are scored as "Acceptable" for precision when $P \leq LAP$.

In the final evaluation, both scores for trueness and precision are combined. A result must obtain "Acceptable" score in both criteria to be assigned the final score "Acceptable".

The relative bias (RB) is determined with the equation:

$$RB = \frac{Value_{\mathrm{Lab}} - Value_{\mathrm{IAEA}}}{Value_{\mathrm{IAEA}}} \tag{5.36}$$

5.7.2 CEA Proficiency test in water

In March 2008, a proficiency test for Pb-210 and Po-210 along with Ra-226 in water became available from the French Commissariat à l'Energie Atomique (CEA). The proficiency test was composed of three samples:

Sample A: "Niger water spiked with Sr-90",
Sample B: "Finland water" and
Sample C: "French water spiked with Ni-63".

Only the Samples A and B contained Pb-210 and Po-210. Additionally, all three samples contained Ra-226. Sample A also contained Sr-90 and Sample C was spiked with Ni-63. However, in this work only Pb-210 and Po-210 were analysed.

A number of aliquots of each sample were analysed using the proposed method. After chemical separation, the Pb-210 samples were measured after a period of about 30 days, to assure the ingrowth of Bi-210. The Po-210 samples were measured via alpha spectrometry, after spontaneous deposition onto nickel. The measurement results for Pb-210 and Po-210 are shown in Tab. 39 below. The measured activity concentrations have been submitted, but the correct CEA values for the samples were at the time of writing not yet announced.

Tab. 39: Measurement results of the validation of Pb-210 and Po-210

	Aliquot 1 (Bq l^{-1})	Aliquot 2 (Bq l^{-1})	Aliquot 3 (Bq l^{-1})	Aliquot 4 (Bq l^{-1})	Aliquot 5 (Bq l^{-1})	Average (Bq l^{-1})
Sample A						
Po-210	1.72 ± 0.08	1.60 ± 0.08	1.56 ± 0.08	1.50 ± 0.06	1.61 ± 0.06	1.60 ± 0.07
Pb-210	5.13 ± 0.41	5.08 ± 0.36	5.84 ± 0.40	4.28 ± 0.32	5.95 ± 0.51	5.26 ± 0.40
Sample B						
Po-210	4.54 ± 0.19	5.12 ± 0.20	4.80 ± 0.20	4.52 ± 0.17	4.87 ± 0.17	4.77 ± 0.18
Pb-210	3.51± 0.23	3.39 ± 0.23	3.17 ± 0.23	4.72 ± 0.37	–	3.70 ± 0.24

6 Method application

6.1 Coal mining at Rheinberg (Nordrhein-Westfalen)

In the year 2003, the Association for the Protection of the Mining-affected Rheinberg (Schutzgemeinschaft Bergbaubetroffener Rheinberg, SBG) found elevated levels of natural radioactivity around certain water systems, e.g. the Große Goorley, Fossa Eugeniana, Moersbach, Issumer Fleuth, Hoerstgener Kendel, Eyllscher Kendel and Rheinberger Altrhein, compared to other nearby regions. The Material Examination Office (Materialprüfungsamt) in the Federal State of Nordrhein-Westfalen confirmed this statement. The cooperative society (Linksniederrheinische Entwässerungsgenossenschaft, LINEG), which was responsible for the maintenance of the water systems in question, immediately took the first preventive actions by removing certain "hot-spots". In the beginning of 2004, the city of Rheinberg commissioned the LINEG to put together an independent consultant committee to analyse and evaluate the radiological situation in the water system "Fossa Eugeniana". The consultant committee consisted of Dr. R. Gellermann from the HGN Hydrogeologie GmbH Magdeburg, Prof. Dr. R. Michel from Centre for Radiation Protection and Radioecology (ZSR) at the University of Hanover, Prof. Dr. W.-U. Müller from the University of Duisburg-Essen and PD Dr. J. Wiegand from the University of Würzburg.

The main water contaminations came from the mine water discharges from the Mine Works West (Bergwerk West). This mine works belongs to the Deutsche Steinkohle AG and is an aggregation of several independent mine works, including the Friedrich-Heinrich, the Rheinland und the Niederberg. One of the pits of the Rheinland mine works is the Rossenray, located just north of the town of Kamp-Lintfort.

The contaminations were caused by dissolved radionuclides from the U-238 and Th-232 decay chains which were brought to the surface by the mine water drainage and discharged into the nearby water systems. The dissolved radionuclides could precipitate, depending on the concentration of other dissolved ions present in the water. The precipitates were then deposited either directly in the discharge area or together with other suspended matter in areas with low water turbulence, with risk of causing elevated doses to the people spending time nearby these water systems. Different scenarios were proposed in order to predict the effective annual dose. For realistic dose assessment a measurement programme was developed, including local dose rate and radon exhalation measurements, along with analyses of sediments (also sediment profiles), biological samples (grass, fish, small animals), groundwater and surface water.

The sampling of water was performed during three days in September 2005 in Rheinberg and surroundings. The description and exact location of the water sampling stations are listed in Tab. 40 and these are shown as well in Fig. 38. The sampling of the groundwater samples was performed by the LINEG, and the rest of the water samples were sampled according to DIN 38402 A-15.

Tab. 40: Location and description of the sampling stations in and around Rheinberg (NRW)

Station No.	Location	Gauß-Krüger	
		Lat.	Long.
1	Hoerstgener Kendel. Right side of the sewage treatment plant	5709770	2532683
2	Hoerstgener Kendel. Discharger to the mine shaft Hoerstgen	5709572	2533163
3	Eyllscher Kendel. Right side of the bridge, 1.5 m from the bank	5707088	2535547
4	Discharger to the settling pond at Rossenray	5709156	2538511
5	Groundwater well 2217. Depth 9.0 m	–	–
6	Settling pond at Rossenray.	5709142	2538537
7	Groundwater well 1102. Depth 4.6 m	5714820	2540926
8	Groundwater well 1017. Depth 6.5 m	–	–
9	Groundwater well 1929H. Depth 9.0 m	–	–
10	Groundwater well 1647. Depth 8.5 m	–	–
11	Rossenray, outlet to the Fossa Eugeniana	5709617	2538525
12	Altrhein sluice, at Ossenberg, right side	5715246	2540996
13	Moersbach at Jenickes Gatt, right side	5713272	2541628
14	Fossa Eugeniana, Fossa Street in Rheinberg	–	–
15	Fossa Eugeniana, outlet Krummensteg	5710275	2539154

The samples from stations 1–3, and 12–15 were surface waters from flowing stretches of water. Water from stations 4, 6, and 11 were sampled within the Rossenray mining area, including one of the mine water settling ponds. Samples from station 4 were taken from the discharger into the settling pond, which came directly from the mines and which contained large amounts of particulate carbon. The carbon residues were completely removed by filtering. Water from station 6, sampled from the middle of one side of the settling pond, contained less particulate matter than was found in station 4, but still an amount visible to the eye. Station 11 represented water leaving the settling pond, which was discharged into the nearby channel, Fossa Eugeniana. The amounts of carbon were markedly lower, no longer visible to the eye. All other samples were groundwater samples, used for drinking water.

Changeable parameters, e.g. pH, temperature, conductivity and redox potential, were measured directly in the field, see Appendix 10.6.1. All samples were filtered directly after sampling, acidified, and an appropriate amount of lead carrier was added in connection with the sampling. The samples were stored cold until sample preparation and subsequently analysed according to the method proposed in this work (see Appendix 10.4).

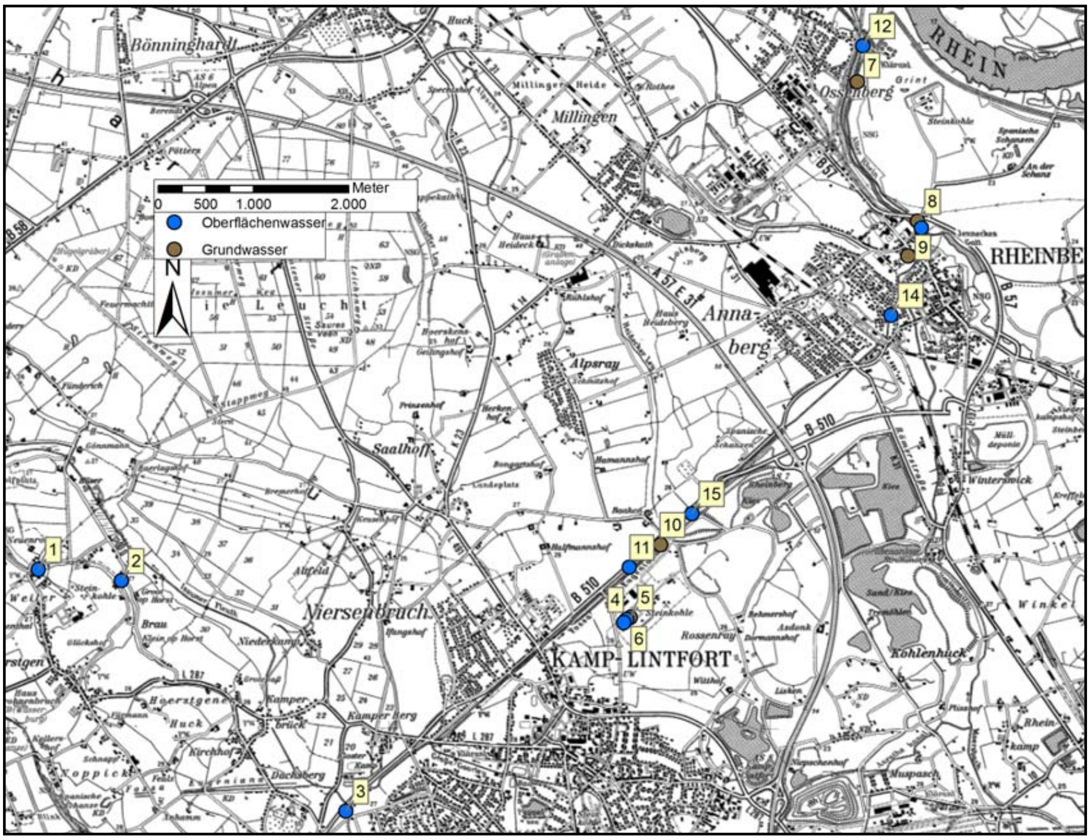

Fig. 38: Map of sampling locations in and around Rheinberg (NRW). Blue dots represent groundwater sampling stations and brown dots surface waters.

6.1.1 Measurement results and discussion

Three samples per sampling station were analysed and the average of the three was determined. In Tab. 41, the measured activity concentrations of Pb-210 and Po-210 are shown. Measurands below the decision threshold are presented as »< detection limit«, and measurands between decision threshold and detection limit are presented in italics. The Pb-210 and Po-210 activities are decay corrected to the date of sampling.

In all samples the activities of both Pb-210 and Po-210 were low. For Pb-210 all measurands were below detection limit. The fluctuations in detection limit between the different samples were due to slightly different sample volumes and chemical yields. Lead-210 was determined via LSC, measured in LSC vials of low-potassium glass. The high detection limits were mainly due to short measurement times and the aliquotation of the lead fraction, where only one forth of the whole fraction was used for the measurement. For the further study of Pb-210 in natural waters longer measurement times were required. The activities measured

for Po-210 varied between 0.2–5.0 mBq kg^{-1}. Po-210 was determined via alpha spectrometry, after spontaneous deposition onto nickel discs.

Tab. 41: Results from the determination of activity concentration of Pb-210 and Po-210 in water. Measurands below the decision threshold are presented as »< detection limit«, and measurands between decision threshold and detection limit are presented in italics. The Pb-210 and Po-210 activities are decay corrected to the date of sampling.

Sample	Sampling Date	Pb-210 (mBq kg^{-1})	Po-210 (mBq kg^{-1})
Station No. 1	05.09.2005	< 35.4	1.3 ± 0.4
Station No. 2	05.09.2005	< 41.6	2.0 ± 0.7
Station No. 3	05.09.2005	< 41.9	*1.3 ± 0.8*
Station No. 4	06.09.2005	< 36.0	1.3 ± 0.4
Station No. 5	06.09.2005	< 40.5	–
Station No. 6	06.09.2005	< 41.1	*0.2 ± 0.2*
Station No. 7	06.09.2005	< 43.6	–
Station No. 8	06.09.2005	< 35.1	1.2 ± 0.3
Station No. 9	06.09.2005	< 40.4	–
Station No. 10	06.09.2005	< 38.2	–
Station No. 11	06.09.2005	< 41.9	0.8 ± 0.3
Station No. 12	07.09.2005	< 44.6	1.3 ± 0.5
Station No. 13	07.09.2005	< 49.6	*0.9 ± 0.4*
Station No. 14	07.09.2005	< 46.4	5.0 ± 0.7
Station No. 15	07.09.2005	< 46.7	4.3 ± 0.7

In samples from stations 4, 6, and 11 higher activities of Pb-210 and Po-210 were expected, particularly in samples from station 4, due to the large amounts of particulate carbon, see above. However, the activities remained low, because the radionuclides were probably not dissolved, but adsorbed onto the particulate matter and therefore removed from the sample along with the carbon during the filtering. There was a slight decrease in activity in the samples from station 6, probably due to the lower turbulence of the water in the middle of the pond.

The detection limits for the analyses of Pb-210 and Po-210 were determined using the evaluations explained in 5.5.6 and 5.4.2. The typical detection limits for the Rheinberg sampling series are shown in Tab. 42. The sample volume was in all cases one litre. The measurement time for Pb-210 samples was 8 hours and for Po-210 about three days.

Tab. 42: Typical detection limits for Pb-210 and Po-210 with the applied methods

Radionuclide	α* (mBq kg^{-1})	Mean range (mBq kg^{-1})
Pb-210	42	29–65
Po-210	0.8	0.5–2.0

In the investigated groundwaters, the Po-210 activity was determined to 1.2 mBq kg^{-1}. This can be considered normal compared to other drinking waters in Germany, but it is lower than the reference values from the UNSCEAR 2000, see the overview of median activity concentrations of some natural radionuclides in drinking water in Tab. 43. For Pb-210, the measurands were all below the detection limits. The average detection limit for Pb-210 of 42 mBq kg^{-1} was factor of 4 higher than the estimated activity concentration in drinking water from the UNSCEAR.

Tab. 43: Median activity concentration of some natural radionuclides in drinking water. Numbers in parenthesis are the number of samples analysed.

Radionuclide	Median activity concentration in mBq l^{-1}		
	Germany [173]	Finland* [45]	UNSCEAR 2000** [61]
Pb-210	5.7 (46)	8 (184)	10
Po-210	1.6 (67)	5 (184)	5
Ra-226	4.8 (1734)	4 (184)	0.5
U-238	15.8 (87)	180 (184)	1

* Values taken for dug wells
** Reference value for the Northern Hemisphere

In Tab. 43, the activities of Pb-210 and Po-210 in German drinking water are slightly lower than compared to the UNSCEAR 2000 reference values. However, the activity concentrations for Ra-226 and U-238 are elevated. The Ra-226 survey included 1734 drinking water samples from 13 of 16 Federal States and is considered to be representative for Germany [173]. The 87 samples of U-238 were primarily taken in the mining polluted areas in the Federal States of Saxony and Thuringia, and that might explain the elevated U-238 value. The Pb-210 and Po-210 samples were taken in the same areas as the U-238 samples, but for these radionuclides there are no influences of the mining pollution to be seen. In Finland, the activity concentrations of Pb-210, Po-210 and Ra-226 correspond well with those found in Germany, only the U-238 activity is very high in Finnish dug wells. The higher uranium content in Fin-

nish water is explained by the higher uranium content in granite bedrock. Finnish bedrock waters are alkaline, containing calcium bicarbonate [45], with which uranium forms soluble carbonato complexes, resulting in highly mobile uranium species.

6.1.2 Summary

The water sampling in the area of Rheinberg (NRW) was performed in order to evaluate the radiological situation, which was considered to be worsened by the technical enhancement of natural radioactivity from the nearby coal mining industry.

By determining Pb-210 via LSC, the detection limits were decreased by a factor of 2–3, compared to the detection limits achieved in the gamma spectrometry for the same kind of water samples, but still a factor of 4 higher than compared to the reference activity concentrations from UNSCEAR. The detection limits from the LSC measurements were used in the dose assessment, see chapter 7.1. In order to lower the detection limits for Pb-210 longer measurement times will be used in the further work.

The radiation measurement of Po-210 cannot be performed via gamma spectrometry, since it emits only alpha particles. In previous work, the polonium activity was assumed to be in radiochemical equilibrium with the mother, Pb-210, and the dose was consequently considerably overestimated. In order to make a realistic dose assessment of the situation in Rheinberg, polonium was determined via alpha spectrometry, with detection limits of less than 1 mBq kg^{-1}.

6.2 Uranium mining in Mailuu Suu, Kyrgyzstan

Kyrgyzstan (Kyrgyz: Кыргызстан, German: Kirgisistan), officially the Kyrgyz Republic, is a country in Central Asia, bordering Kazakhstan to the north, Uzbekistan to the west, Tajikistan to the southwest and the People's Republic of China to the southeast. The city of Mailuu Suu is located about 70 km northwest of Kok-Yangak and about 25 km from the border of Uzbekistan, in an adjacent valley of the Fergana basin, see Fig. 39. It is a tectonically active region, with frequent earthquakes and heavy seasonal rainfalls.

Fig. 39: Map of Kyrgyzstan

Uranium ore mining and milling in the Mailuu Suu District was performed during 1946–1968. The uranium ores were processed by alkaline leaching and ion exchange, by which most of the uranium was extracted and the waste (rock, uranium and its daughters) was put on tailings. The tailings, consisting of residues from the ore processing and waste rocks from mining, were deposited in the proximity of the Mailuu Suu River and its tributaries Kara Agach, Kulmen Sai and Aylampa Sai Rivers. The people living in this area are exposed to several kinds of risks, including major landslides, earthquakes and radioactive pollution from the tailings. In the frame of the EC-TACIS funded project [174, 175] different disaster scenarios were investigated to minimize the radiological exposure of population and to prevent environmental pollution by radionuclides and heavy metals.

In the frame of a current World Bank project for the hazard mitigation in the Mailuu Suu area, the Federal Institute for Geosciences and Natural Resources (BGR) is carrying out hydrological investigations with respect to the planned geotechnical sanitation of the radioactive waste deposits. A part of the project includes the establishment of a programme for long-term groundwater monitoring. In order to understand the situation an investigation of the current contaminant distribution, including the radiological parameters is necessary.

The water sampling in and around the city of Mailuu Suu was performed by the BGR in four different campaigns; in January 2006, July 2006, September 2006, and in March 2007. A

list of the locations as well as descriptions of the sampling stations is given in Tab. 44, and in Fig. 40 below, the sampling stations of the Mailuu Suu area are depicted.

Tab. 44: Location and description of the sampling stations sampled by the BGR

Station No.	Location	UTM (WGS84) Lat.	Long.
1	Community water supply plant Mailuu Suu: catchment basin, pre-filter system, 4–5 km N' of Mailuu Suu town	0293155	4578253
2	Outflow, leakage in water supply pipe, approximately 1 km south of water supply plant	0292334	4577810
3	Artesian well, Street of Pioneers; used for drinking water; very weak smell of H_2S	0290221	4576615
4	Spring in urban area, outflow close to Mailuu Suu River, Street No. 4, east riverbank. Used for drinking water	0290272	4576064
5	Seepage from tailing no. 3: west riverbank; sampling of outflow close to the base of tailing 3 onto tailing 18	0288576	4573192
6	Kulmen Sai River, tributary to Mailuu Suu River; sampling close to inflow (west bank), high stream velocity	0288079	4571945
7	Spring south of ISOLIT at the level of Mailuu Suu River, nearby leakage of oil; water foams due to degassing of H_2S	0288132	4572488
8	Well from ISOLIT factory; sampling from collecting basin; south of the town centre	0285908	4578412
9	Sampling at run-off from sewage treatment plant Mailuu Suu, south of town centre; water sill very dirty	0284706	4567509
10	Private dug well in village Kok Tash; eastern riverbank, 5–7 km south of Mailuu Suu town centre; used for drinking water	0281626	4562656
11	Seepage at the base of tailing no. 5; collected by a well at the southern end of the tailing towards the Mailuu Suu River	0288749	4574643
12	Pore water from tailing No. 3, sampled out of well 2 of 4 (the closest to Mailuu Say); Depth of pore water level at 3.40 m; minor water volume	0288673	4573147
13	Small creek dewatering the southern area shaft no. 10; runs into Kulmen Sai	0290374	4571738

Tab. 44: Cont.

Station No.	Location	UTM (WGS84)	
		Lat.	Long.
14	Seepage at tailing no. 16; collected by a horizontal well at the south western end of the tailing towards the Aschwar River	0286777	4572103
15	Seepage from tailing no. 13, into the Aylampa Sai River	0284595	4569424
16	Spring in the vicinity of ISOLIT, running eastwards to the Mailuu Suu River	0288564	4573227
17	Artesian well water near mosque, could be used for drinking water; cords of oil and CH_4 gas bubbles; no smell of H_2S	0287184	4569789
18	Creek behind tailing no. 6	–	–
19	Mailuu Suu River, down of tailing no. 5, 7, 6	–	–
20	Private spring in Kara-Agach, not used as drinking water	–	–
21	Kara-Agach River at the end of the village	–	–
24	Dug well east of Mailuu Suu town	–	–
35	Artesian water well east of Mailuu Suu	–	–
36	Spring in the village Kok Tash	–	–
37	Spring in the village Kok Tash	–	–
38	Artesian well in the village Kok Tash	–	–
39	Mountainous spring, east of Njefteprom	–	–

As the samples were not filtered on site, the sample should be considered to contain not only dissolved, but also particulate radionuclides. On site measurements performed by the BGR include water temperature, pH, redox potential, conductivity and dissolved oxygen. Other analyses, such as ICP-MS for the elemental composition of the water samples, were also performed by the BGR. The ICP-MS results for uranium are of particular interest to the radiological evaluation and were used to calculate the activity concentration in Bq kg^{-1} from the measured µg l^{-1}, see Tab. 45 below.

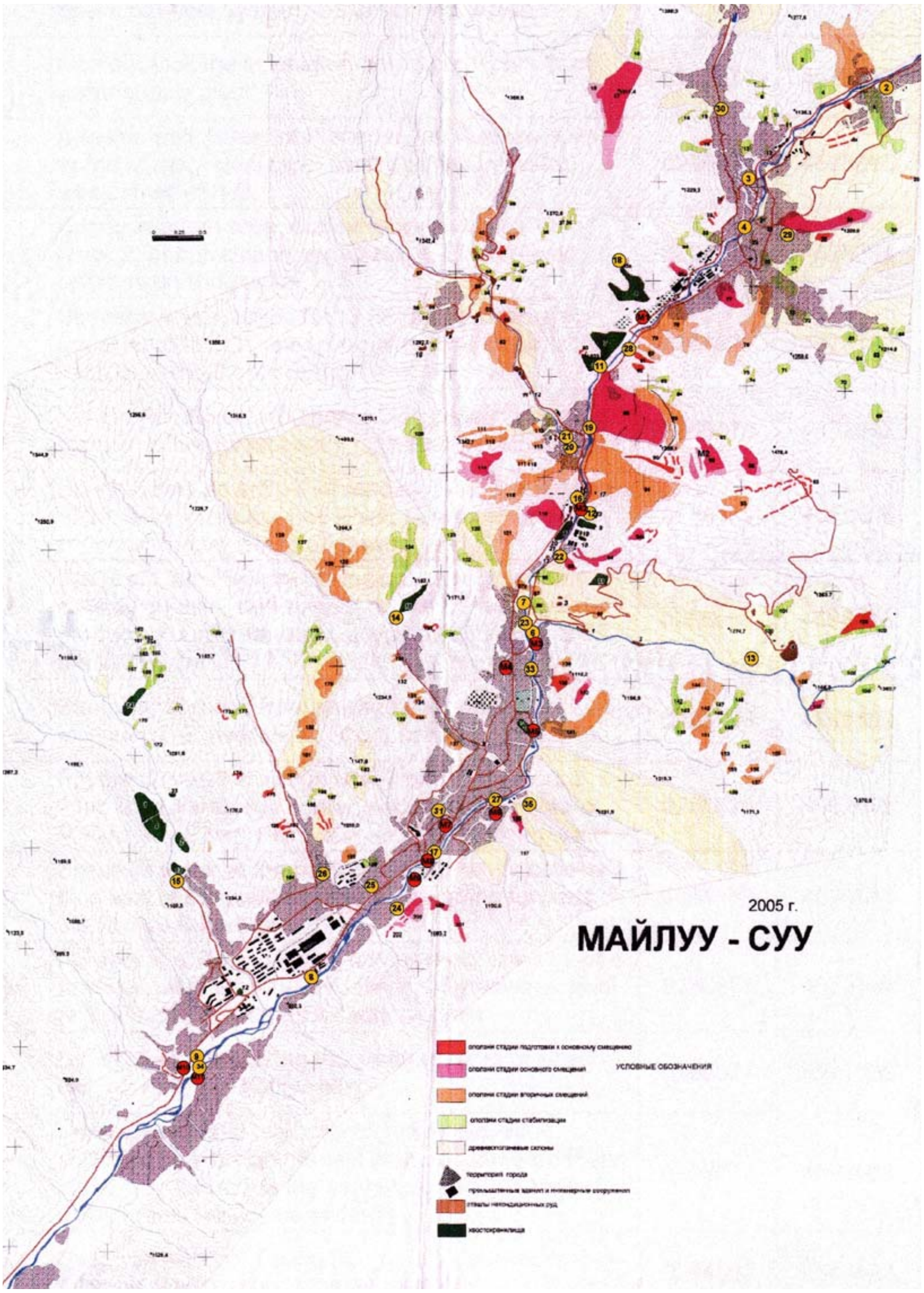

Fig. 40: Map of sampling stations in the Mailuu Suu region. Dark green field are tailings. Dark brown areas are uranium mining shafts and light brown areas are mine waste dumps.

6.2.1 Measurement results and discussion

The results of the LSC and alpha measurements of Pb-210 and Po-210, respectively, are shown in Tab. 45, as well as the results of the uranium analyses. Measurands between decision threshold and detection limit are presented in italics. Bold Pb-210 values were measured by alpha spectrometry via Po-210. The Pb-210 and Po-210 activities are decay corrected to the date of sampling. The U-238 and U-234 derive from the same decay chain and are considered to be in radiochemical equilibrium. Also Pb-210 and Po-210 are included in the U-238 decay chain, but do not necessarily have to be in equilibrium with uranium, mainly due to the radioactive noble gas radon, Rn-222, which can emanate from the soil. The analysis procedure for Pb-210 and Po-210 in water described in chapter 10.4 was followed.

Tab. 45: Results from the determination of activity concentration of Pb-210 and Po-210 in water from Mailuu Suu area. Measurands between decision threshold and detection limit are presented in italics. Bold Pb-210 values were measured by alpha spectrometry via Po-210. The Pb-210 and Po-210 activities are decay corrected to the date of sampling.

Sample	Sampling Date	U-238 Calc. activity ($mBq\ kg^{-1}$)	Pb-210 Measurand ($mBq\ kg^{-1}$)	Po-210 Measurand ($mBq\ kg^{-1}$)
Station 1–1	15.01.2006	4.3	743 ± 215	19 ± 4
Station 2–1	15.01.2006	3.9	857 ± 228	18 ± 3
Station 3–1	15.01.2006	0.6	*343 ± 177*	23 ± 3
Station 3–2	15.09.2006	0.7	*33 ± 18*	10 ± 2
Station 4–1	15.01.2006	27	825 ± 213	36 ± 5
Station 4–2	01.07.2006	51	99 ± 26	8 ± 1
Station 5–1	15.01.2006	21×10^3	**325 ± 24**	26 ± 5
Station 6–1	15.01.2006	2.2×10^3	**170 ± 13**	16 ± 4
Station 6–2	01.07.2006	2.8×10^3	99 ± 28	6 ± 1
Station 7–1	15.01.2006	1.4×10^3	1274 ± 223	53 ± 6
Station 7–2	01.07.2006	2.2×10^3	570 ± 54	127 ± 6
Station 8–1	15.01.2006	360	**210 ± 15**	17 ± 3
Station 8–2	01.07.2006	360	103 ± 31	5 ± 1
Station 9–1	15.01.2006	6.1	**710 ± 40**	30 ± 5
Station 9–2	01.07.2006	9.3	174 ± 33	18 ± 2
Station 10–1	15.01.2006	79	1012 ± 248	21 ± 3
Station 10–2	01.07.2006	64	130 ± 29	16 ± 2
Station 11–1	01.07.2006	1.1×10^5	534 ± 49	323 ± 10
Station 11–3	15.09.2006	1.1×10^5	298 ± 26	364 ± 25

Tab. 45: Cont.

Sample	Sampling Date	U-238 Calc. activity (mBq kg^{-1})	Pb-210 Measurand (mBq kg^{-1})	Po-210 Measurand (mBq kg^{-1})
Station 12–1	01.04.2007	–	5774 ± 193	2614 ± 134
Station 13–1	01.07.2006	1.6×10^3	*93 ± 32*	13 ± 2
Station 14–1	01.07.2006	3.6×10^5	*88 ± 31*	71 ± 5
Station 14–2	15.09.2006	4.5×10^5	77 ± 20	55 ± 13
Station 15–1	01.07.2006	4.1×10^3	**77 ± 4**	11 ± 2
Station 15–3	15.09.2006	4.0×10^3	*40 ± 17*	8 ± 3
Station 16–1	01.07.2006	1.4×10^3	156 ± 44	23 ± 2
Station 17–1	01.07.2006	89	201 ± 42	9 ± 1
Station 17–2	01.04.2007	–	**14 ± 2**	14 ± 2
Station 18–1	15.09.2006	540	**33 ± 2**	4 ± 1
Station 19–1	15.09.2006	60	**47 ± 3**	8 ± 3
Station 20–1	15.09.2006	1.8×10^3	136 ± 20	63 ± 9
Station 21–1	15.09.2006	480	*32 ± 18*	13 ± 3
Station 24–1	15.09.2006	190	**53 ± 4**	11 ± 3
Station 35–1	01.04.2007	425	**14 ± 2**	146 ± 10
Station 36–1	01.04.2007	260	**18 ± 2**	36 ± 4
Station 37–1	01.04.2007	240	**13 ± 2**	28 ± 3
Station 38–1	01.04.2007	140	**14 ± 2**	11 ± 1
Station 39–1	01.04.2007	240	**6 ± 2**	29 ± 3

The measurement results of the sampling campaign in January 2006 are all higher than the rest. This could be due to the small sample volumes and the risk of also measuring dissolved particulate radionuclides. When the unfiltered samples are acidified, the radionuclides attached to particulate matter are released into solution. The difference could also be due to different sampling techniques or sampling personnel, since this could affect the amount of particulate matter in the samples. In the further evaluations, the samples from the first sampling campaign were not considered.

In order to better evaluate the radiological situation using the above determined activities, the sampling stations were divided up into four groups; (1) seepage samples (stations 5, 11, 12, 14, and 15), originating directly from tailings and hence containing high activities, especially of uranium, (2) river surface waters (stations 6, 13, 18, 19, and 21), including larger rivers, such as the Mailuu Suu River, Kara Agach River and Kulmen Sai River, but also smaller creeks, (3) groundwaters (stations 7, 8, 16, 20, and 35–39), such as artesian wells and springs, which were not used as drinking water, and (4) drinking water (3, 4, 10, 17, and 24).

The seepage samples from stations 5 (tailing 3), 11 (tailing 5), 14 (tailing 16) and 15 (tailing 13), all contained high levels of uranium (4–450 Bq kg^{-1}). Nevertheless, the Pb-210 and Po-210 activities were significantly lower, but higher than compared to groundwater levels, with the exception of water from station 15, where both the lead and polonium activities were comparable to groundwater levels. Tailing pore water from station 12 (tailing 3) contained markedly elevated activities of Pb-210 (5.8 Bq kg^{-1}) and Po-210 (2.6 Bq kg^{-1}). Comparing the pore water activities with the seepage activities of the same tailing (tailing 3; stations 5 and 12), it becomes obvious that the Pb-210 and Po-210 activities decrease during the transport through the tailing.

Water from stations 6, 19, and 21 was sampled from larger rivers, whereas water from stations 13 and 18 came from small creeks, dewatering shafts and tailings, respectively. Water from station 19 was taken from the Mailuu Suu River south of tailings 5, 6, and 7, north of the village Kara Agach. In the water sample from station 19, the activities of uranium, Pb-210 and Po-210 were low and could be considered as uncontaminated, even though the Mailuu Suu River runs past several tailing. Sample 21 contained water from the Kara Agach River before it enters Mailuu Suu River, running through Kara Agach. This village is partially situated on a former mine waste dump. The uranium content of sample 21 was slightly raised compared to station 19: 0.5 Bq kg^{-1}, probably because the river runs directly through a strongly uranium polluted area, whereas the Mailuu Suu River does not come in direct contact with tailings or mine waste heaps. Water from the Kulmen Sai River, north of Mailuu-Suu, was sampled at station 6. The Kulmen Sai River transports water from a uranium mining area with several mining shafts, east of Mailuu Suu town, where a small creek dewaters into the Kulmen Sai at shaft no. 10. The river water could therefore be expected to contain more dissolved uranium. The U-238 activity at station 6 ranged between 2–3 Bq kg^{-1}, whereas the Pb-210 activity was about 200 times lower, ranging between 100–170 mBq kg^{-1}. The Po-210 activity was lower than the Pb-210 activity, with approximately 10 mBq kg^{-1}. Furthermore, station 13 was located at the small creek, south of mining shaft no. 10. The activity concentrations at sampling station 13 were comparable to those further down the Kulmen Sai at station 6: the uranium, Pb-210 and Po-210 activities were 1.6 Bq kg^{-1}, 93 mBq kg^{-1} and 13 mBq kg^{-1}, respectively. Water from station 6 contained more uranium than water from stations 19 and 21. This might be explained by the generally lower uranium content in the tailings, since these were the waste material deposits produced from the uranium extraction. Moreover, at the sampling station 18, located at a creek immediately behind tailing 6, the activities of uranium, Pb-210 and Po-210 were very similar to those measured at station 21, i.e. a uranium activity of 0.5 Bq kg^{-1}, but with low Pb-210 and Po-210 activities of 33 and 4 mBq kg^{-1}, respectively.

A number of groundwaters, in form of artesian wells and springs, were sampled, including stations 7, 8, 16, 20, and 35–39. These waters were, however, not used as drinking water. Stations 16 and 20 were located in Kara Agach, north of Mailuu Suu. The influence of tailings and mine wastes was obvious; stations 20 and 16 contained 1.8 and 1.4 Bq kg^{-1} U-238, respectively. These values were higher than compared to the results obtained for the Kara Agach River (station 21). It seems that the radionuclides were transported with seepage through the tailing material into the groundwater, rather than into the nearby river. The corresponding Pb-210 activity for both station 20 and 16 was 150 mBq kg^{-1}; a factor 10 less than the ura-

nium activity. The Po-210 activity was 63 and 23 mBq kg^{-1} for station 20 and 16, respectively. Sampling station 7 was located south of station 16 and of the tailings 3 and 8, at the northern border of Mailuu Suu town. The uranium activity was comparable to stations 16 and 20, with an average U-238 activity of 1.8 Bq kg^{-1}. The Pb-210 and Po-210 activities were significantly elevated; between 570–1274 mBq kg^{-1} and 53–127 mBq kg^{-1}, respectively. The water conditions at station 7 were reducing, with a redox potential of –340 mV, see App. 10.6.2. In reducing environments, both lead and polonium may remobilise from sediments (see 3.2.2). Additionally, degassing of H_2S was observed at station 7, see Tab. 44. However, at the existing water conditions (pH = 7.9; E_h = –340 mV) and in the presence of sulphide, it is more likely that lead forms solid PbS (see 3.2.2), than that it remobilises. The elevated Pb-210 activity can therefore not be associated with the water parameters. On the other hand, polonium may have been remobilised by sulphate-reducing bacteria. Further south along the Mailuu Suu River, groundwater samples from stations 35 and 8 were taken. At these stations the uranium activity was still elevated, at a value of 0.4 Bq kg^{-1} at both stations, even though there were no tailings in immediate proximity. The Pb-210 activity at station 35 was low, 14 mBq kg^{-1}, however the Po-210 was about 10-fold that of Pb-210, 146 mBq kg^{-1}. The result is comparable to that of station 7, but unfortunately some field parameters (e.g. redox potential) were not measured at station 35, which makes a comparison difficult. At station 8, the Pb-210 and Po-210 activities were about 0.1 Bq kg^{-1} and 0.01 Bq kg^{-1}, respectively. Further sampling was performed in the village of Kok Tash, 5–7 km south of Mailuu Suu town, corresponding to stations 36–39. At these stations, the uranium content was two-times lower than in the groundwater from Mailuu Suu town, ranging between 140–260 mBq kg^{-1}. The Pb-210 activities were not elevated, ranging between 6–18 mBq kg^{-1}. On the other hand, at stations 36, 37 and 39, the Po-210 activities were slightly higher than the corresponding Pb-210 activities. Possible explanations for this could not be made, since the redox potentials were lacking.

Water from sampling stations 1, 3, 4, 10, 17, and 24 were used as drinking water; stations 1, 3 and 4 were located north of Mailuu Suu, 17 and 24 in the city centre and 10 in the village of Kok Tash, south of Mailuu Suu. The uranium concentration in these samples were low, varying between about 1–190 mBq kg^{-1}. The uranium activities were lower than the corresponding Pb-210 activities and in some samples also lower than the Po-210 activities. The Pb-210 activities lay between 14 and 130 mBq kg^{-1} and the Po-210 activities varied between 8–16 mBq kg^{-1}, indicating disequilibrium between Pb-210 and Po-210. These were waters with presumably natural levels of the uranium decay chain radionuclides. The low uranium concentration in the groundwater in and south of Mailuu Suu town used for drinking water may be a consequence of deeper wells. Artesian wells consist of shallower groundwater aquifer and the uranium from the tailings and mine waste heaps may have migrated into those, but not into deeper wells.

The typical detection limits for the LSC measurements of Pb-210 and for the alpha spectrometry measurements for Po-210 are shown in Tab. 46. Obviously, the detection limit is depending on the sample volume – the larger the sample volume the lower the detection limit. The detection limit is also depending on measurement time, chemical yield and detector efficiency. For Pb-210, as well as Po-210, the overall yield lay in the range of 70–100 %.

Tab. 46: Typical values for the detection limits for Pb-210 and Po-210

Radionuclide	α^* (mBq kg^{-1}) V ≈ 100 ml	Mean range (mBq kg^{-1})	α^* (mBq kg^{-1}) V ≈ 500 ml	Mean range (mBq kg^{-1})
Pb-210	577[a]	459–681	89[a] and 59[b]	80–94
Po-210	2.8	2.2–3.5	0.7	0.3–1.2

[a] 8 h measurement in low-potassium glass vials; [b] 24 h measurement in polyethylene vials

For a better understanding of the radiological situation in the Mailuu Suu mining district, it is necessary to compare the determined activities in this work with prior investigations at Mailuu Suu, as well as with other areas with similar mining activities, as for instance in Slovenia. In the area around the uranium mines an increase in the uranium concentration in the waters of the Mailuu Suu River has already been observed. Vandenhove *et al.* analysed water and sediment samples as a part of an EC-TACIS funded project in 2003 [175] and made further investigations in 2006 [176]. The uranium content in sediments from five different locations along the Mailuu Suu River varied between 1.6 and 3.4 Bq g^{-1}. In water, the uranium activity ranged from 24 to 88 mBq kg^{-1}. These results are fairly comparable with river water samples measured by the BGR, see Tab. 47. It should be noticed, that the sampling locations are approximately the same, but not the exact ones. The uranium concentration in sediments was by a factor of 10^4 higher than in the corresponding water samples.

Tab. 47: Comparison of the average U-238 activity concentration in sediments and water at locations along the Mailuu Suu River

Location		Sediment U-238 (mBq kg^{-1})	Water U-238 (mBq kg^{-1}) Vand. *et al.*	Water U-238 (mBq kg^{-1}) BGR
Vandenhove *et al.* [176]	BGR			
Water reservoir	Station 1	3.4×10^6	24	4.3
Confluence of Kara Agach and Mailuu Suu (M-S) rivers	Station 19	2.6×10^6	45	60
After T3, T9, T10…	Station 7	2.3×10^6	52	1.8×10^3
Confluence of Kulmen Sai and M-S	Station 6	2.6×10^6	66	2.4×10^3
Confluence of Aylampa Sai and M-S	Station 9	1.6×10^6	88	7.7

Not only sediments and water samples were analysed by Vandenhove *et al.*, but also samples of tailing material. Material from four boreholes from tailing 3 was examined. The results for uranium and Pb-210 are shown in Tab. 48 and compared with the results of the water analyses from the BGR and from this work. There was about 100 times more uranium in the tailing material than in the seepage. In general, there was less uranium than Pb-210 in the borehole material from tailing 3.

Tab. 48: Comparison of the average U-238 activity concentration from four boreholes (solid material) and seepage water at tailing 3, Mailuu Suu (average ± standard deviation)

	Borehole material U-238 (Bq kg^{-1})	Seepage[a] water U-238 (Bq kg^{-1})	Borehole material Pb-210 (Bq kg^{-1})	Seepage[b] water Pb-210 (Bq kg^{-1})
Average of four boreholes	$(2.9 \pm 2.0) \times 10^3$	21	$(30 \pm 34) \times 10^3$	0.3 ± 0.02
Most contaminated borehole	$(3.6 \pm 2.4) \times 10^3$		$(62 \pm 35) \times 10^3$	

[a] ICP-MS measurement at the BGR, station 5; [b] LSC measurement at the ZSR, station 5. Borehole material was analysed by Vandenhove *et al.* [176].

In average about 90 % of the uranium was extracted, which corresponds to the estimations made by Križman *et al.* for the uranium mine at Žirovski vrh in Slovenia [177]. The Pb-210 activity concentration in borehole material was about 4×10^4 higher than in the seepage. The seepage from tailing 3 showed elevated levels of uranium, but under these conditions the radioactive daughters did not seem to leach from the tailing material.

The measured activity concentrations of Po-210 were in almost all groundwater and river samples lower than for Pb-210, see Tab. 45. In one groundwater sample from the village Kok Tash the Po-210 activity exceeded the Pb-210 10-fold, and in one seepage sample from tailing 5 (sampling station 11), the Po-210 activity was slightly higher than for Pb-210. Vreček *et al.* compared activities of Pb-210 and Po-210 in sediments and water [101]. This examined area had been contaminated by mine waste from the uranium mines at Žirovski vrh in Slovenia. Some of the results from the above mentioned work are summarised in Tab. 49.

As can be seen in Tab. 49, the Pb-210 and Po-210 activities in sediments were high, especially in the settling pond. Another sample was taken about 100 m downstream from the deposit site. Here the sediment activities were about 100 times lower (190 ± 10 Bq kg^{-1}, not shown in Tab. 49). In the sediment samples, Pb-210 and its daughters were in radiochemical equilibrium. The activities in water were all lower than corresponding sediments, in the settling pond as much as 10^6 times lower. The water content of Po-210 was about one order of magnitude lower than for Pb-210 in all samples, except in the settling pond, where lead and

polonium activities were in equilibrium. This corresponds well with the results shown above in Tab. 45.

Tab. 49: Sediment and water activities of Pb-210 and Po-210 at the Žirovski vrh mine in Slovenia [101]

Pb-210	Sediment (Bq kg^{-1})	Water (Bq kg^{-1})
At the U mine	–	$(68 \pm 12) \times 10^{-3}$
Settling pond	$(11.0 \pm 0.5) \times 10^{3}$	$(81 \pm 10)^{a} \times 10^{-3}$
		$(63 \pm 10)^{b} \times 10^{-3}$
River after all inflows from mine	63 ± 5	$(19 \pm 2) \times 10^{-3}$
Po-210	Sediment (Bq kg^{-1})	Water (Bq kg^{-1})
At the U mine	–	$(33 \pm 6) \times 10^{-3}$
Settling pond	$(11.8 \pm 0.3) \times 10^{3}$	$(66 \pm 7)^{a} \times 10^{-3}$
		$(41 \pm 9)^{b} \times 10^{-3}$
River after all inflows from mine	67 ± 5	$(3.9 \pm 0.4) \times 10^{-3}$

[a] Settling pond inflow, [b] Settling pond outflow

6.2.2 Summary

Drinking water, groundwaters, river waters and seepage samples were collected by the Federal Institute for Geosciences and Natural Resources (BGR) in the uranium mining region of Mailuu Suu, Kyrgyzstan, with the purpose of evaluating the existing radiological situation. Radionuclides such as U-238, Pb-210 and Po-210 were analysed, using different techniques.

In general, there was no radiochemical equilibrium between uranium and its daughters observed. The uranium mining at Mailuu Suu was terminated in 1968, since then about 38 years have passed, which is not enough time for the equilibrium adjustment. Furthermore, between Pb-210 and its daughter Po-210 there was no radiochemical equilibrium present. In water samples this seemed to be normality. Lead and polonium possess different chemical properties and therefore behave differently in solution, as discussed in chapter 3.2.

The produced tailing materials generally contained higher amounts of radionuclides than the corresponding water. Tailing 3 contained about 3 kBq kg^{-1} U-238 and about 10 times more Pb-210, 30 kBq kg^{-1} [176]. This was plausible, since the uranium was selectively extracted from the ore and the daughter nuclides not. Pore water sampled from within tailing 3 (BGR station 12) contained 5.8 Bq kg^{-1} Pb-210, which was a considerable reduction in activity compared to the total tailing content of Pb-210. Uranium was unfortunately not determined for station 12. Seepage water exiting the same tailing 3 (BGR station 5) showed elevated amounts of U-238 (21 Bq kg^{-1}), but still about 150 times lower than the total tailing content of

U-238. The measured Pb-210 activity in the seepage was 0.3 Bq kg^{-1}. In the seepage, the Pb-210 the activity was significantly lower than in both tailing material (10^5 times lower) and the tailing pore water (about 15 times lower). Obviously, uranium was, due to the formation of strong carbonato complexes, such as $[UO_2(CO_3)_3]^{4-}$, see 3.1, very mobile, more so than for instance lead, as was seen at most sampling stations south of the tailing and mine waste areas, where the uranium levels were elevated even at larger distances (km) from tailing areas. High activities of uranium (2–3 Bq kg^{-1}) were found along the Kulmen Sai River (BGR station 6), east of Mailuu Suu town. The river runs past several uranium mining shafts, which were drained into the river. However, no elevated activities of Pb-210 and Po-210 in the nearby rivers systems were confirmed. This may be because both Pb-210 and Po-210 are easily scavenged by particulate matter (inorganic and/or organic matter, see 3.2.3 and 3.2.4) present in the water and transported through the water column into sediments. In a mining area in Slovenia, some sediment samples were analysed. These showed high activities of Pb-210 and Po-210 (both about 11 kBq kg^{-1}, hence in equilibrium) in sediments in the settling pond at the uranium mine (see Tab. 49), but markedly lower activities in the water (< 100 mBq kg^{-1}). In order to remediate water and in particular sediments from radionuclides, such as Pb-210 and Po-210, the use of vegetation, for instance reed, could be applied. Radionuclide uptake by the plants has extensively been studied. It has been found, that lead is accumulated to a higher degree than polonium, see 3.3.1.

A number of groundwaters were sampled in Mailuu Suu town, but also in villages around; e.g. Kara Agach in the north and Kok Tash in the south. In Kara Agach groundwater, the U-238 activity was high (1.8 Bq kg^{-1}), probably due to the fact that the village was built on top of a former mine waste dump. The influence of tailings and uranium mining became obvious, when looking at the groundwaters south of the larger tailings T5, T6, T7, T9, and T3. The World Health Organisation (WHO) has proposed a guideline value for U-238 of 15 µg l^{-1} (corresponding to 185 mBq kg^{-1}) in drinking water [181]. All the groundwater samples, which were not used for drinking water, contained elevated activities of uranium, exceeding the WHO guideline. The Pb-210 and Po-210 activities, on the other hand, were in some samples raised, but not alarmingly high. The sampling station 35 exhibited elevated unsupported Po-210 activity, which could not be explained. In the village Kok Tash, south of Mailuu Suu town, the uranium content in groundwater was only slightly elevated; 140–260 mBq kg^{-1}. It seems that with a large distance from the mining area, the uranium content in groundwater decreases. The Pb-210 and Po-210 activities in Kok Tash were both low: < 36 mBq kg^{-1}.

The analysed drinking water samples all showed low U-238 activities, less than 100 mBq kg^{-1}, hence not exceeding the WHO guideline for drinking water. Compared to drinking water in Finland, see Tab. 43 above, these U-238 activities were normal, although UNSCEAR 2000 estimated a median U-238 activity in drinking water of 1 mBq l^{-1}. In some samples, the Pb-210 activity was slightly raised. Since the Mailuu Suu district is an area of rather high natural uranium content, hence the mining, it could be expected to have elevated levels of Pb-210 and Po-210. Due to the emanation and diffusion of radon from soil into water, higher levels of its radioactive daughters may be found in water. This could be the explanation for the elevated Pb-210 activity found in the drinking water, since the uranium content in all the water samples was low. In chap. 7.2 below, the dose assessment can be found.

7 Dose assessment

The German Commission for Radiological Protection (SSK) made in 1998 (revised in 1999) a recommendation of the calculation principles for the determination of radiological exposure to humans as a result of mining activities of environmental radioactivity (BGB) [178]. This recommendation was used in this work in order to estimate the radiation exposure to the people originating from radionuclides in food stuffs (in this case: drinking water).

The effective annual dose was calculated, using the following equation:

$$E = \sum_{\mathrm{n}} p_{\mathrm{n}} U_{\mathrm{n,\,j}} \sum_{\mathrm{r}} \left(C_{\mathrm{n,\,r}} - C_{\mathrm{n,\,r}}^{\mathrm{b}} \right) \cdot g_{\mathrm{ing,\,r,\,j}} \tag{7.1}$$

Herein after referred to as:

E	effective annual dose for the reference person j by ingestion of locally produced food stuffs in Sv y^{-1}
$C_{\mathrm{n,\,r}}$	specific activity in Bq kg^{-1} and Bq l^{-1} respectively of the radionuclide r in food stuff n
$C_{\mathrm{n,\,r}}^{\mathrm{b}}$	Specific natural background – activity in Bq kg^{-1} and Bq l^{-1} respectively of the radionuclide r in food stuff n
n	index for labelling the food stuffs, in this case n = w for water
p_{n}	fraction of the annual production of the locally produced food stuff n
$U_{\mathrm{n,\,j}}$	Annual consumption of the food stuff n by reference person j in kg (in l for n = water)
$g_{\mathrm{ing,\,r,\,j}}$	ingestion dose coefficient for radionuclide r and reference person j in Sv Bq^{-1}

The age dependent dose coefficients are available from ICRP, and the number of age groups considered can be expanded to six: 0–1 year, 1–2 years, 2–7 years, 7–12 years, 12–17 years, and > 17 years. For most purposes one can consider the age categories of infants, children, and adults and use the available dose coefficients corresponding to 1–2 year, 7–12 years, and > 17 years respectively, for these categories.

The dose coefficients for Po-210 are in almost all of the six age groups higher than for Pb-210, indicating the necessity of actually measuring Po-210, instead of assuming radiochemical equilibrium with Pb-210. The clearly lower dose coefficients for Bi-210 on the other hand allow ignoring the initial Bi-210 activity. The higher dose coefficients of Pb-210 relate to the high energy alpha emission of Po-210 (5.4 MeV, 100 % alpha) and the relative short half-life of 138.38 days. The dose coefficients for Ra-226 are in general lower than those for Pb-210 and Po-210, respectively, but higher than for U-238.

Tab. 50: Age-specific ingestion dose coefficients for an integration period to age 70 years [1]

Radionuclide	Effective dose coefficient, $g_{ing, r, j}$ (Sv Bq^{-1})					
	0–1 year	1–2 years	2–7 years	7–12 years	12–17 years	> 17 years
U-238	3.4×10^{-7}	1.2×10^{-7}	8.0×10^{-8}	6.8×10^{-8}	6.7×10^{-8}	4.5×10^{-8}
U-234	3.7×10^{-7}	1.3×10^{-7}	8.8×10^{-8}	7.4×10^{-8}	7.4×10^{-8}	4.9×10^{-8}
Ra-226	4.7×10^{-6}	9.6×10^{-7}	6.2×10^{-7}	8.0×10^{-7}	1.5×10^{-6}	2.8×10^{-7}
Pb-210	8.4×10^{-6}	3.6×10^{-6}	2.2×10^{-6}	1.9×10^{-6}	1.9×10^{-6}	6.9×10^{-7}
Bi-210	1.5×10^{-8}	9.7×10^{-9}	4.8×10^{-9}	2.9×10^{-9}	1.6×10^{-9}	1.3×10^{-9}
Po-210	2.6×10^{-5}	8.8×10^{-6}	4.4×10^{-6}	2.6×10^{-6}	1.6×10^{-6}	1.2×10^{-6}

For the calculation of the annual effective dose arising from radionuclides in drinking water, the yearly water consumption of the population has to be estimated. In the BGB, the drinking water consumption in Germany has been estimated for six different age groups, see Tab. 51.

Tab. 51: Estimated annual drinking water consumption

Source	Estimated annual consumption of drinking water in litres, $U_{n, j}$					
	0–1 year	1–2 years	2–7 years	7–12 years	12–17 years	> 17 years
BGB [178]	55*	65	250	440	440	440
StrlSchV [179]	55*	100	100	150	200	350
UNSCEAR 2000 [61]	150	–	–	350	–	500
European Union [180]	–	–	–	–	–	730

* If dried milk is used for babies, then additionally 148 litres of drinking water have to be taken into account.

To be able to evaluate a radiological situation, it is necessary to compare the assessed doses with current regulations, directives or similar. In 1998, the European Union (EU) presented a new council directive for the quality of water intended for human consumption, 98/83/EC [180]. For radioactivity in water, natural as well as artificial, a Total Indicative Dose (TID) of 0.1 mSv a^{-1} has been set. However, it excludes tritium, K-40, radon and radon decay products, such as Pb-210 and Po-210. Due to the high level of exposure to the public by radon in water

it was recommended in 2001 that the Commission should also involve radon and its decay products in the directive. So far the EU Member States are not required to monitor the nuclide specific radioactivity in drinking water, as long as the calculated TID from other monitoring results are well below certain parametric values; an indication of an elevated TID can be derived from gross alpha activities exceeding 0.1 Bq l^{-1}, or gross beta activities exceeding 1 Bq l^{-1}. If these values are exceeded, each radionuclide has to be specifically determined.

For the limitation of radiation exposure to the public caused by ingestion of drinking water with increased levels of radon and its long-lived daughters Pb-210 and Po-210, the EU recommended in 2001/928/Euratom "for the public radiation protection against radon in drinking water" reference values. If these are exceeded, it should be investigated whether countermeasures are necessary for the protection of public health. For Pb-210 and Po-210 these reference values are: 0.2 Bq l^{-1} and 0.1 Bq l^{-1}, respectively. The reference activities will each on their own not reach an effective annual dose of the recommended 0.1 mSv. For this estimation, the EU used a drinking water consumption of 730 litres per year, see Tab. 51 above.

In 2003, the World Health Organisation (WHO) proposed a provisional guideline of 15 µg l^{-1} for U-238 in drinking water, which is based on the chemical toxicity of uranium [181]. This guideline value would correspond to 185 mBq l^{-1}.

7.1 Coal mining area of Rheinberg (NRW)

The dose assessment was performed using the procedure mentioned above, see page 139. The effective annul dose was determined for all age groups (ICRP: 0–1 year, 1–2 years, 2–7 years, 7–12 years, 12–17 years, and > 17 years) for the ingestion of water. The specific activities of Pb-210 and Po-210 used for the calculations are found in Tab. 41. The specific natural background was not subtracted, in order to determine the total effective annual dose. It was assumed, that all the consumed drinking water was taken from local sources; $p_w = 1$.

In Fig. 41 the effective annul doses for children aged 7–12 years are shown for the different sampling stations. The doses for Pb-210 were in all samples distinctly higher than for Po-210, ranging in the order of between 30–40 µSv per year. This was due to using the detection limits for Pb-210, since no actual activities could be determined. The actual activities lay probably in the order of 5–10 mBq per litre, which would have resulted in even lower doses. For Po–210, the doses ranged between 0.2 and 6 µSv annually. The determined doses for Pb-210 and Po-210 did not reach the total indicative dose (TID, see above) of 0.1 mSv per year in any of the samples. In two samples, 14 and 15, the doses were slightly higher than for the rest. These were both sampled from the channel Fossa Eugeniana, which runs through the town of Rheinberg.

The effective annual dose for adults arising from Pb-210 and Po-210 in the water in and around Rheinberg is depicted in Fig. 42.

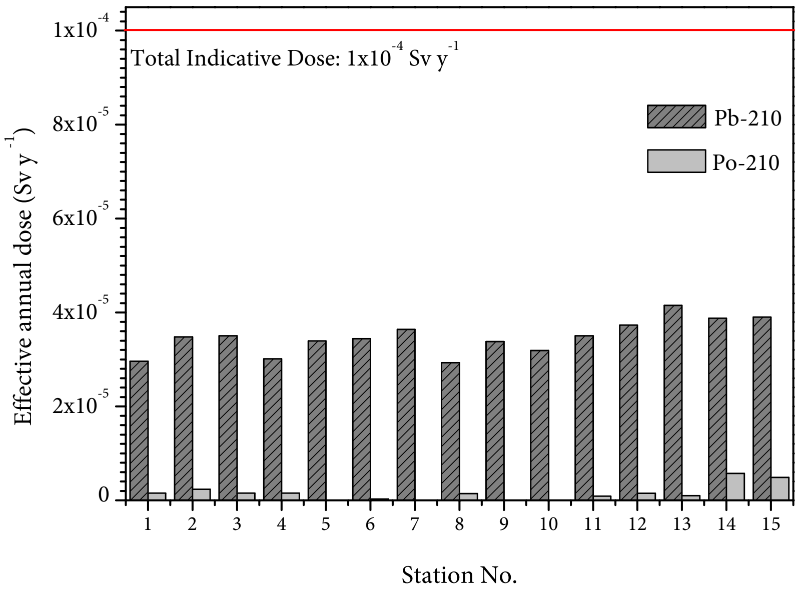

Fig. 41: Effective annual dose for children (7–12 years) due to ingestion of water containing Pb-210 and Po-210. The estimated drinking water consumption was 440 l per year. The total indicative dose is indicated at 0.1 mSv y^{-1}.

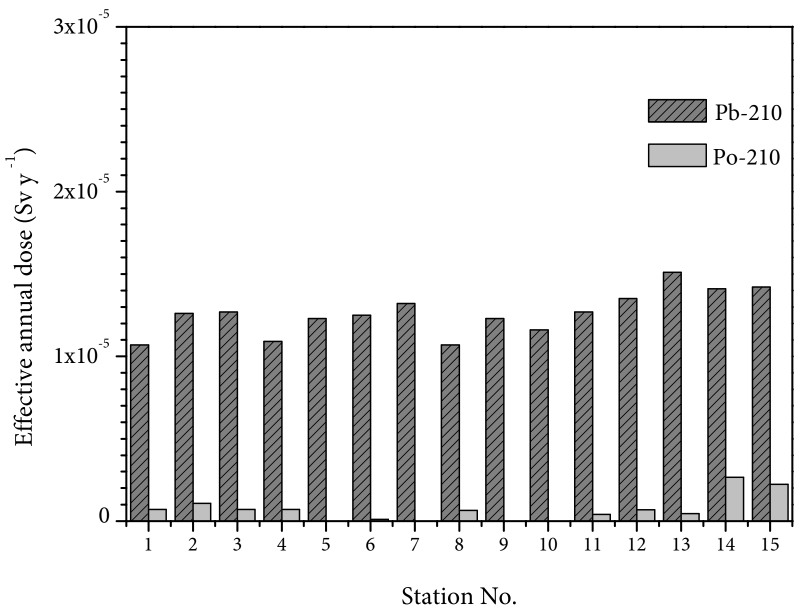

Fig. 42: Effective annual dose for adults (> 17 years) due to ingestion of water containing Pb-210 and Po-210. The yearly drinking water consumption was estimated 440 l. The total indicative dose (0.1 mSv y^{-1}) not indicated.

The determined doses were lower for adults than for children, due to lower dose coefficients used, since adults are less sensitive to radiation than children are. The doses arising from Pb-210 ranged between 10–15 µSv per year, and for Po-210 between 0.1–3 µSv per year. In none of the samples the TID was reached.

The total effective annual dose arising from Pb-210 and Po-210 together for the age groups is shown in Tab. 52. The largest contribution to the dose was obviously Pb-210. The doses arising from Po-210 were in all samples low, so that even after adding the doses from Pb-210 and Po-210, the total effective annual dose did not exceed the TID of 0.1 mSv per year.

Tab. 52: Total effective annual dose arising from Pb-210 and Po-210 in drinking water

Age group	Total dose (µSv per year)
Children (7–12 years)	30–45
Adults (> 17 years)	11–17

7.1.1 Conclusions

A considerable decrease in the doses arising from Pb-210 was achieved, compared to previous measurements via gamma spectrometry. The calculated total effective annual dose for children in the Rheinberg area caused by Pb-210 and Po-210 lay in the range of 30–45 µSv per year, and for adults about three times lower; 11–17 µSv per year. These doses alone were not detrimental compared to the European Union drinking water directive, the Total Indicative Dose, of 0.1 mSv per year. However, the other natural radionuclides in the uranium and thorium decay chains had to be considered as well, before the complete radiological situation could be entirely evaluated [182].

7.2 Uranium mining district of Mailuu Suu, Kyrgyzstan

Lead-210 and polonium-210 significantly contribute to the radiation dose of the population according to UNSCEAR [3], as much as 8 % of the natural internal radiation dose to man originates from these two nuclides. To get an idea of how harmful the radiation contribution of Pb-210 and Po-210 in the Mailuu Suu water is, the activities were converted into doses using the dose assessment described above, see page 139. For the specific activity $C_{n,r}$, the measured values for Pb-210 and Po-210, respectively, were taken from Tab. 45. The specific natural background was not subtracted, since the total effective annual dose was assessed, including the dose from the natural background radiation. It was assumed that the consumed

water was taken from local sources, giving $p_w = 1$. In this work two age groups were considered for the dose assessments; one group of children aged 7–12 years and one group of adults (> 17 years). The annual consumption of drinking water in the area of Mailuu Suu has already been estimated to 630 l for children and 750 l for adults [176].

Children are generally more sensitive to the damage caused by incorporated radionuclides. For certain radionuclides and pathways it is therefore necessary to distinguish between adult and child. This is particularly true for I-131, but also for Pb-210 and Po-210. To get an overview over the radiological situation arising from ingestion of water in the Mailuu Suu area, only the relevant sampling stations were looked at in detail, with special focus on the drinking water stations (3, 4, 10, 17 and 24), but also other groundwater stations (8, 16, 20, 35–39) were studied. Station 7 was excluded from the further study, due to the degassing of H_2S. The dose assessment results for the drinking water and the other groundwater samples for children are shown in Fig. 43.

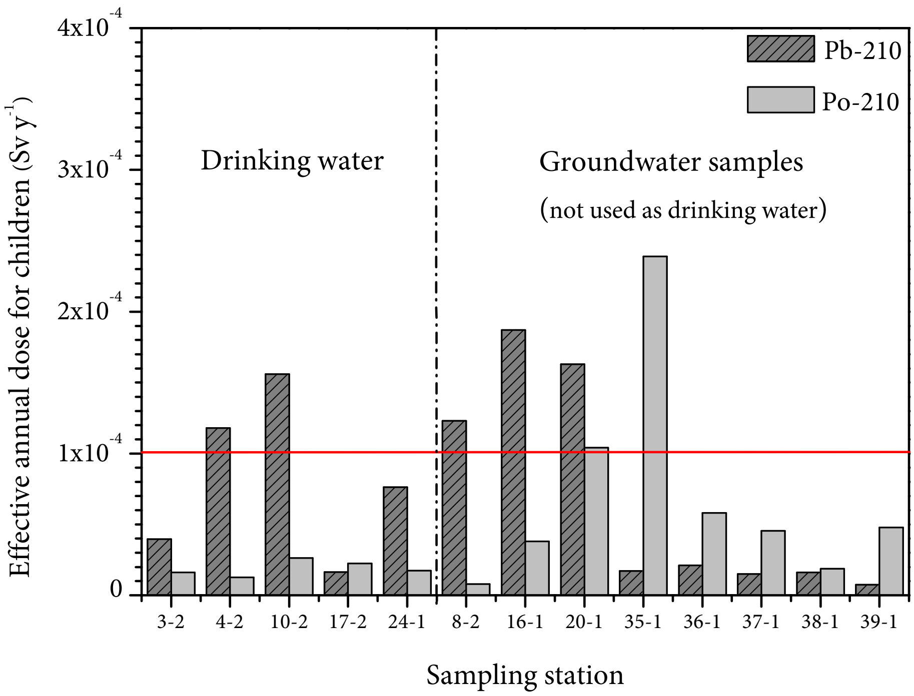

Fig. 43: Effective annual dose for children (7–12 years) from ingestion of water containing Pb-210 and Po-210. Estimated drinking water consumption was 630 l per year. Water from sampling stations 3, 4, 10, 17 and 24 was used as drinking water, whereas 8, 16, 20, and 35–39 were groundwater samples not used as drinking water. The horizontal line indicates the total indicative dose (TID) of 0.1 mSv y^{-1}.

In order to get an idea of the extent of the radiological impact of Pb-210 and Po-210 to the people drinking the water in Mailuu Suu, the doses were compared to the EU drinking water directive with its total indicative dose (TID, see above), since no Kyrgyz drinking water regulations were known. The comparison of the Pb-210 doses for children with the TID made it clear that the drinking water samples from station 4 and 10 exceeded the TID value of 0.1 mSv y^{-1}. The Pb-210 doses for children varied between 16 µSv y^{-1} and 0.16 mSv y^{-1}. The Po-210 doses were all lower than TID in the drinking water samples, varying between 13–26 µSv y^{-1}. In the other groundwater samples, the Pb-210 doses calculated for children ranged between 8 µSv y^{-1} and 0.19 mSv y^{-1}, whereas the TID was exceeded at stations 8, 16 and 20. At station 20, the Po-210 dose (0.1 mSv y^{-1}) also slightly exceeded TID. The sampling station 20 is located in Kara Agach, a village partially situated on a former mine waste dump, which might explain the elevated doses there. Water from station 35 contained elevated amounts of Po-210, which gave rise to the comparatively large dose (0.24 mSv y^{-1}) seen in Fig. 43. The reason for the elevated dose could not be clarified. In Fig. 44, the effective annual dose arising from the intake of water by adults is shown.

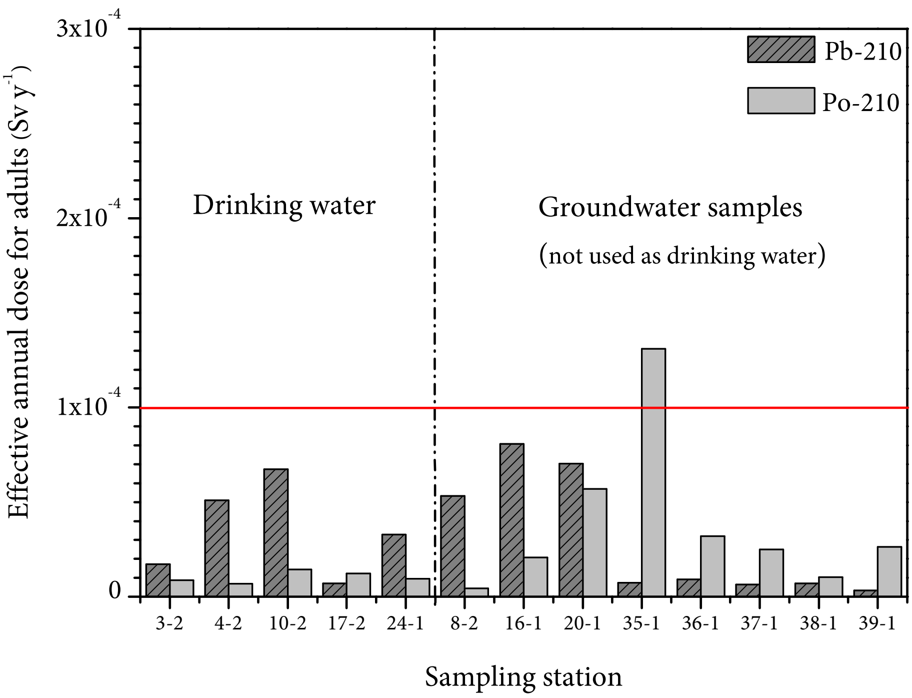

Fig. 44: Effective annual dose for adults (> 17 years) from ingestion of water containing Pb-210 and Po-210. Estimated drinking water consumption was 750 l per year. Water from sampling stations 3, 4, 10, 17 and 24 was used for drinking purposes, whereas stations 8, 16, 20, and 35–39 were groundwaters not used as drinking water. The horizontal line indicates the total indicative dose (TID) of 0.1 mSv y^{-1}.

Only at station 35, the effective annual dose exceeded the TID, in all other samples the doses were lower than TID. The Pb-210 doses for adults arising from drinking water varied between 7–50 μSv y^{-1} and hence all lower than the TID. For Po-210, the effective annual doses were lower than the corresponding Pb-210 dose for the same drinking water sample, as a result of the generally lower Po-210 activity measured in the samples. For the groundwater samples 35–39, the trend was reverse; the Po-210 doses were all higher than the corresponding Pb-210 doses. It seems that for adults the drinking water and groundwater in Mailuu Suu could be ingested without elevated radiological risk, if only the radionuclides Pb-210 and Po-210 were considered.

In Tab. 53, the average assessed doses for both children and adults are displayed. The doses were in general higher for children than for adults in all types of samples, due to the higher dose coefficients for children. The doses arising from river waters were comparable to those from drinking water and groundwater. Generally, the doses in drinking water, groundwaters and river waters were below the TID. For seepage, the doses were all higher than TID. That the doses were not higher would imply that Pb-210 as well as Po-210 are fairly immobile in tailing material.

Tab. 53: Average assessed doses for children and adults. Total indicative dose: 1×10^{-4}.

Type of sample	Average assessed doses, children (Sv y^{-1})		Average assessed doses, adults (Sv y^{-1})	
	Pb-210	Po-210	Pb-210	Po-210
Drinking water	6.6×10^{-5}	1.6×10^{-5}	2.8×10^{-5}	8.7×10^{-6}
Groundwater	6.9×10^{-5}	7.0×10^{-5}	3.0×10^{-5}	3.8×10^{-5}
River water	7.3×10^{-5}	1.4×10^{-5}	3.1×10^{-5}	7.9×10^{-6}
Seepage	9.0×10^{-4}	7.1×10^{-4}	3.9×10^{-4}	3.9×10^{-4}

7.2.1 Conclusions

The high dose coefficient by ingestion of Po-210, especially for children, has stressed the importance of measuring the specific activity of Po-210. In many studies radiochemical equilibrium between Pb-210 and Po-210 has been assumed, but it is in water clearly not the case. In order to make a realistic and non-conservative dose assessment, each radionuclide activity should be independently determined.

In order to understand the radiological impact of Pb-210 and Po-210 in drinking water to the people living in the Mailuu Suu area, the dose assessment for these radionuclides was performed for two age groups; children (7–12 years) and adults (> 17 years), using different dose coefficients, see Tab. 50. The drinking water consumption was estimated to 630 litres for children and 750 litres for adults [176]. The results were compared to the European drinking

water directive, guided by a total indicative dose (TID) of 0.1 mSv y^{-1}, since no Kyrgyz drinking water regulations were known.

In the drinking water samples from the BGR sampling stations 3, 4, 10, 17 and 24, the effective annual dose for children arising from Pb-210 varied between 16 μSv and 0.16 mSv, where two samples (station 4 and 10) slightly exceeded the TID. The Po-210 doses were all below the TID, ranging between 13–26 μSv per year. For adults, all assessed doses were below the TID, for both Pb-210 and Po-210.

The conclusion that can be drawn for the consumption of drinking water in the Mailuu Suu area is that there is, at least not for adults, no elevated radiological risk, if only the radionuclides Pb-210 and Po-210 are considered. However, for children slightly elevated doses are possible. The complete radiological evaluation of the Mailuu Suu situation can be found in [183]. Nevertheless, it is highly important to keep monitoring the drinking water, as well as groundwater and river systems in the area of Mailuu Suu, in order to protect the population from upcoming radiological hazards.

8 Summary and Outlook

8.1 Summary

A selective method for the simultaneous determination of both Pb-210 and Po-210 in aqueous samples has been developed. The chemical separation of the two radionuclides was performed using a lead specific solid phase extraction resin; the *Pb Resin*, pre-packed in cartridges (2 ml, particle size: 50–100 µm) available from Eichrom Environment. The weight distribution ratios were determined for both lead and polonium on the *Pb Resin* in different concentrations of nitric and hydrochloric acid by batch experiments. Lead was very well retained by the resin over a wide range of nitric acid concentrations. However, the retention of polonium was poor. The batch experiments in hydrochloric acid demonstrated a high retention of lead by the resin from moderately concentrated HCl solutions, but lower than compared to nitric acid at the same concentrations, therefore allowing an easier elution from the column. Polonium showed increased retention with increasing hydrochloric acid concentration. In order to simultaneously retain both lead and polonium, a concentration of $c(\mathrm{HCl}) = 2\ \mathrm{mol\ l^{-1}}$ was chosen for the sample load. Bismuth was not retained at all in any of the acid solutions.

Furthermore, the separation properties of lead, bismuth and polonium were studied in column elution experiments. The sample load (Pb-210, Bi-210 and Po-210 activities in equilibrium, and 5 mg lead carrier) was performed in $c(\mathrm{HCl}) = 2\ \mathrm{mol\ l^{-1}}$, as already mentioned. Bi-210 was not retained by the *Pb Resin*; it was found in the effluent and the rinsing eluent. The optimum elution of Po-210 was found by stripping the polonium in two steps with diluted nitric acid; $c(\mathrm{HNO_3}) = 1\ \mathrm{mol\ l^{-1}}$ (10 ml) and $c(\mathrm{HNO_3}) = 0.1\ \mathrm{mol\ l^{-1}}$ (5 ml). However, about 25 % of the polonium was lost already in the rinsing step, indicating that the distribution factor at $c(\mathrm{HCl}) = 2\ \mathrm{mol\ l^{-1}}$ was not high enough for a complete separation. Moreover, Po-210 and Pb-210 were quantitatively separated from each other; Pb-210 was completely stripped from the cartridge with 20 ml of distilled water.

The chemical separation of lead and polonium, including loading, elution and stripping, is fast; it can be performed within 2 h for up to 24 samples simultaneously with flow rates of $1\ \mathrm{ml\ min^{-1}}$, using the vacuum-box system available from Eichrom Environment.

The obtained fractions from the chemical separation were used to prepare suitable measurement sources. The polonium alpha sources were prepared by the selective method of spontaneous deposition from a $0.5\ \mathrm{mol\ l^{-1}}$ HCl solution under constant agitation at 85 °C. To the solution ascorbic acid was added in order to reduce interfering Fe(III) and to expedite the reduction of polonium. Subsequent to deposition, the disc was heated at 300 °C, with the purpose of oxidizing elemental polonium to $\mathrm{PoO_2}$, which reduced the detector contaminations due to volatilisation of polonium within the alpha counting chamber. The preferred disc material was silver, but also nickel was used. The optimum deposition yield on silver discs was achieved after 18 h deposition and on nickel discs after 5 h, respectively. The deposition reproducibility was higher using silver discs than using nickel. The average yield on silver was

99 ± 9 per cent. On nickel, the average yield was 61 ± 18 per cent. The heating losses after 30 min at 300 °C on silver were diminutive: 5 ± 4 per cent. On nickel, the losses varied between 10 and 38 %. For very low-level samples, the silver discs were preferred since a higher deposition yield resulted in lower detection limits. The discs were subsequently measured via alpha spectrometry at a sample–detector distance of 10 mm, which corresponded to a detector efficiency of 14.7 per cent and a low background of about 0.5 counts per day.

The determination of Pb-210 was performed by measuring the high-energy beta-emitter Bi-210 ($E_{\beta,max}$ = 1.2 MeV) via liquid scintillation counting (LSC) after ingrowth into radioactive equilibrium subsequent to chemical separation. This allowed a high counting efficiency of 80 %. The LSC sample source was prepared by adding a 5 ml-aliquot of the lead fraction from the chemical separation in a polyethylene LSC vial and mixing it with scintillation cocktail, in this case the *Ultima Gold™ AB*, based on di-isopropylnaphthalene, available from PerkinElmer. The polyethylene vials provided the lowest background and in addition, no diffusion of cocktail solvent was observed. The measurements were performed by a low-background Wallac Quantulus™ 1220 from PerkinElmer. The optimal pulse shape analysis (PSA) value was chosen to 110, where the misclassification of both alpha and beta pulses was at a minimum.

The overall chemical yield for Po-210 was determined over Po-208 tracer and reached 75 %, including chemical separation and spontaneous deposition onto silver. The yield for Pb-210 was determined by ICP-MS measurement of the added stable lead carrier and yields > 90 % were reached for most of the analysed samples.

High chemical yields as well as low backgrounds were important in order to reach low detection limits. The detection limits were calculated using a Bayesian statistical approach. The alpha spectrometry provided very low detection limits due to extremely low backgrounds. For Po-210 the detection limit was as low as 0.2 mBq kg^{-1}, which was more than adequate for the determination of environmental water samples as well as ground- and drinking water. Decision thresholds of 10 mBq kg^{-1} Pb-210 and a detection limit of 20 mBq kg^{-1} Pb-210 were reached via LSC for sample volumes of 1 litre and a measurement time of 24 h, using only an aliquot of a quarter of the whole lead fraction. Using the whole fraction after evaporation would decrease the detection limits further and the measurement time may be shortened. The method can be used for aqueous samples containing a large range of Pb-210 and Po-210 activities; ranging from a few mBq per kg up to 100 Bq per kg. Furthermore, the method was validated by performing the IAEA *Proficiency test on the determination of Po-210 in spiked water* (IAEA-CU-2007-09). The precision and accuracy of the method were both assigned acceptable by the IAEA. The stability of the method was tested with seawater samples with high ionic strength and found satisfactory. Moreover, the reproducibility was confirmed by analysing a series of identical proficiency test samples from the CEA.

The developed and validated method was successfully applied to the analyses of aqueous samples from areas polluted by mining. Until now water samples have been analysed by gamma spectrometry with detection limits of > 100 mBq kg^{-1}. For a realistic dose assessment, the sensitivity of the gamma spectrometry was not sufficient, since the assessment has to be

based on the detection limits when the measured activities were below the decision threshold, usually leading to significant overestimations.

The water sampling in the coal mining affected area around Rheinberg (NRW) was performed in order to evaluate the radiological situation, which was presumably worsened by technically enhanced natural radioactivity caused by the coal mining. The analysed water samples contained low activities of both Pb-210 and Po-210. The Pb-210 activity was below detection limit in all samples. Even in samples taken from a mine waste water settling pond, the activities were low. The calculated total effective annual dose for children in the Rheinberg area caused by measured activities of Pb-210 and Po-210 lay in the range of 30–45 μSv per year, and for adults between 11–17 μSv per year. A considerable decrease in the doses arising from Pb-210 and Po-210 was achieved, compared to previous measurements via gamma spectrometry.

Moreover, drinking water, groundwaters, surface waters and seepage samples were collected by the Federal Institute for Geosciences and Natural Resources (BGR) in the uranium mining region of Mailuu Suu, Kyrgyzstan, with the purpose of evaluating the present radiological situation. Uranium was mined there between 1945 and 1968. The determined Pb-210 and Po-210 activities were compared to U-238 activities determined by the BGR, whereas no radioactive equilibrium could be confirmed between U-238 and Pb-210. Furthermore, no equilibrium was observed between Pb-210 and its daughter Po-210 in aqueous samples, probably as a result of different chemical behaviour of the two radionuclides in solution. In general, the water samples contained low activities of Pb-210 and Po-210, even after influences of tailings seepage. This was an indication of a very low mobility of Pb-210 and Po-210 and no leaching from the tailing material and mine wastes at the current water properties could be confirmed. The uranium activities were in most water samples elevated, indicating a high mobility, probably caused by the highly mobile uranyl carbonato complexes. The calculated total effective annual dose for children in the Mailuu Suu region caused by measured activities of Pb-210 and Po-210 in drinking water was in average 92 μSv per year, and for adults 37 μSv per year. These doses were about 3 times higher than compared to Rheinberg, which could be a result of the higher natural radiation in the area, independent of the mining activities. Compared to the total indicative dose of 100 μSv per year, the consumption of drinking water in the Mailuu Suu area would not lead to any elevated doses, as long as only Pb-210 and Po-210 were considered. However, at a few sampling stations, for children slightly elevated doses were possible.

8.2 Conclusion

A novel method for the simultaneous determination of Pb-210 and Po-210 in aqueous samples has been developed. It is a reliable and relatively fast method, with high chemical yields and low detection limits. By using this method for the analyses of all kinds of environmental water samples containing Pb-210 and Po-210, a realistic dose assessment is achieved.

8.3 Outlook

The achieved sensitivity of the proposed method makes it ideal for further measurements in environmental materials, especially where no elevated activities are presumed. In order to further lower the detection limit for Pb-210 via LSC, studies of the volume reduction of the stripping of lead, e.g. using citric acid, ammonium citrate or EDTA, in the chemical separation can be performed. Furthermore, the LSC measurement efficiency may be raised by adding the counting window of Pb-210 to that of Bi-210.

It appears worthwhile to extend the studies to other environmental matrices, for example solid rock, sediment or plants. The adaptation of the proposed method would require additional work on sample preparation and chemical separation. This would offer a promising possibility to investigate the mobility of Pb-210 and Po-210 in the environment, particularly to evaluate transport rates and transfer factors.

In addition, there is a general demand for chemical separation methods for other radionuclides. It is therefore attractive to investigate modifications of the proposed method or new developments of similar methods. Most important in this respect are radionuclides that cannot be adequately measured by gamma spectrometry.

In the long term, it is desirable to aim for the inclusion of chemical species analyses into radiochemical separations. This could provide valuable information, even for radionuclides that can easily be measured by gamma spectrometry.

9 Acknowledgements

This study was performed at the Centre for Radiation Protection and Radioecology (Zentrum für Strahlenschutz und Radioökologie, ZSR) at the Leibniz University of Hanover. Therefore, I would like to express my gratitude to Prof. Dr. Rolf Michel for giving me the opportunity to complete my doctoral thesis and providing excellent working facilities at the ZSR.

I am greatly indebted to Dr. Sven Hippler for initiating the research subject, for his never ending inspiration and his willingness to share his competence.

My thanks also include Dr. Steffen Happel and Eichrom Environment in France for the fruitful team work and for the contributions to my work.

The Bundesanstalt für Geowissenschaften und Rohstoffe (BGR) is also thanked for providing the environmental water samples from Mailuu Suu.

I am obliged to Prof. Dr. Carla Vogt and her work group at the Institute for Analytical Chemistry at the Leibniz University of Hanover for the assistance in the ICP-MS measurements.

My warm thanks are owed to all the colleagues at the ZSR, especially Carsten Wanke for his assistance in the field and for the excellent team work. Rüdiger Sachse is especially thanked for his amazing endurance repairing everything that breaks. I would also like to thank the colleagues at the workshop, in particular Frank Koepke and Michael Senft for the competent and reliable technical support.

Last, but not least, I would like to thank Kai Fischer for once again enriching my life with his presence and for his patience with me during the last months of finishing the thesis.

10 Appendices

10.1 Abbreviations

10.2 List of Tables

10.3 List of Figures

10.4 Method: Step-by-step

10.5 Measurement evaluations

10.5.1 Evaluation of the Po-210 alpha measurements

10.5.2 Evaluation of the Pb-210 LSC measurements

10.6 Changeable parameters

10.6.1 Rheinberg

10.6.2 Mailuu Suu

10.1 Abbreviation

ADC	Analog-to-Digital Converter
AMS	Accelerator Mass Spectrometry
BfS	Bundesamt für Strahlenschutz
BGB	Berechnungsgrundlage Bergbau
BGR	Bundesanstalt für Geowissenschaften und Rohstoffe
CEA	Commissariat à l'Energie Atomique
CPM	Counts per Minute
DOE	Department of Energy
DIN	Deutsches Institut für Normung
DJ	Diffused Junction
DOC	Dissolved Organic Carbon
EC	Electron Capture
FCV	Free Column Volume
FWHM	Full Width at Half Maximum
GF-PC	Gas Flow-Proportional Counter
GUM	Guide to the Expression of Uncertainty in Measurement
HPGe	High Purity Germanium
HV	High Voltage
ICP-MS	Inductively Coupled Plasma-Mass Spectrometry
IAEA	International Atomic Energy Agency
ICRP	International Commission on Radiological Protection
ISO	International Organization for Standardisation
LSC	Liquid Scintillation Counting
MCA	Multi-Channel Analyzer
NIST	National Institute of Standards
PC	Personal Computer
PE	Polyethylene
PIPS	Passivated Implanted Planar Silicon
PMT	Photo Multiplier Tube
PSA	Pulse Shape Analysis
PTB	Physikalisch-Technische Bundesanstalt
ROI	Region of Interest
SCR	Sample Channel Ratio
SPE	Solid Phase Extraction
SQP(E)	sample quench parameter of the external standard
SSB	Silicon Surface Barrier
SSK	Strahlenschutzkommission
TID	Total Indicative Dose
UGAB	Ultima Gold™ AB
UNSCEAR	United Nations Scientific Committee on the Effects of Atomic Radiation

UV	Ultraviolet
WHO	World Health Organisation

10.2 List of Tables

10.3 List of Figures

10.4 Method: Step-by-step

Pb-210 and Po-210 in water samples

1. Water sample preparation

1.1 If required, filter the sample through a 0.45 micron filter (preferably performed subsequent to sampling).

1.2 Aliquot 1 kg (1000 ml) of the sample into a 1 l glass beaker. Note the weight.

1.3 Acidify the sample to pH 2, with conc. HNO_3 (about 1 ml per 1000 ml, preferably performed subsequent to sampling).

1.4 Add 0.5 ml of stable lead carrier (10 mg ml^{-1}, preferably performed subsequent to sampling).

1.5 Pipette 1 ml of the sample solution after addition of the carrier and store for the ICP-MS analysis.

1.6 Add an appropriate amount of tracer (Po-208, about 100 mBq).

2. Iron hydroxide co-precipitation

2.1 Add 1 ml of iron carrier (20 mg ml^{-1}) to the sample. Cover beaker with a watch glass and heat at near boiling for an hour.

2.2 Remove watch glass. Add 12 ml conc. ammonium hydroxide to precipitate iron hydroxide. Stir the solution with a glass rod if necessary. Allow beaker to stay on hotplate for another 30 min, with hotplate turned off.

2.3 Let the precipitate settle for at least 2 hours (preferably overnight). Decant the supernatant. Transfer the precipitate into a 30 ml plastic centrifuge tube.

2.4 Centrifuge and discard the supernatant.

2.5 Wash the precipitate with 10 ml water. Centrifuge and discard the supernatant. Repeat twice.

2.6 Dissolve precipitate in 10 ml of 2 M HCl.

3. Set up of Pb cartridge on the vacuum box system

3.1 Place the inner tube rack into the vacuum box with 50 ml glass beakers for collecting the discarded solutions. Fit the lid to the box.

3.2 Place the yellow outer tips into all 24 openings of the lid. Fit in the inner white tip into each yellow tip.

3.3 For each sample solution, fit in the Eichrom *Pb Resin* cartridge on to the inner white tip.

3.4 If necessary, luer lock a membrane filter to the top end of the *Pb Resin* cartridge.

3.5 Luer lock syringe barrels to the top end of the *Pb Resin* cartridge.

4. Lead separation using *Pb Resin* cartridge and the vacuum box system

4.1 Condition a *Pb Resin* cartridge with 10 ml 2 M HCl.

4.2 Load the dissolved precipitate from step 2.6 onto the cartridge. Discard eluent.

4.3 Add 5 ml 2 M HCl to elute bismuth and iron. Record the time and date of this addition. This will be used to calculate the ingrowth of Bi-210. Discard eluent, or keep for further analysis (e.g. uranium or strontium).

4.4 Place a clean, labelled 20 ml LSC glass vial under the cartridge. Add 10 ml 1 M HNO_3 to remove the polonium.

4.5 Add 5 ml 0.1 M HNO_3 to remove all polonium and to lower the nitrate concentration prior to lead elution. This fraction (step 4.4 and 4.5) will be used for the sample preparation for the alpha spectrometry.

4.6 Place a clean, labelled 20 ml LSC glass vial under the cartridge. Add 20 ml of water to elute lead.

5. Sample preparation for Pb-210 counting

5.1 Pipette 5 ml of the lead fraction from step 4.6 into a clean, labelled LSC glass vial. The rest of the solution will be kept for analysis using ICP-MS, in order to determine chemical yield. An aliquot of the fraction can also be used for the determination of Pb-210 by spontaneous deposition of the Po-210 after ingrowth.

5.2 Add 15 ml Ultima Gold AB scintillation cocktail to the vial. Tighten lid and shake to mix.

5.3 Count in LSC, after ingrowth of Bi-210 (30 d).

6. Spontaneous deposition of polonium

6.1 Fill the water bath with about 700 ml of water and heat to 85 °C. Add a small magnetic stirrer.

6.2 Meanwhile, prepare the sample. Add the whole fraction (15 ml) from 4.5 to 185 ml of 0.5 M HCl (total volume: 200 ml) in a 250 ml glass beaker. Add 100 mg of ascorbic acid to the solution. The ascorbic acid will reduce any Fe(III) in the solution and ease the reduction of polonium. Add a magnetic stirrer.

6.3 Remove the foil from a silver disc and rinse with water, ethanol and then acetone. Let it dry in air. When dry, mount in the Teflon holder. Put the holder in the sample solution and put the beaker in the water bath. Deposit for 18 hours.

6.4 After 18 h, demount the Ag disc and rinse it with water, ethanol and then acetone. Let it dry in air.

6.5 To avoid contamination of the detector, the disc should be heated for 15–30 min on a hotplate at 300 °C. Let it cool. Transfer to a labelled Petri dish.

6.6 Count in alpha chamber.

10.5 Measurement evaluations

10.5.1 Evaluation of the Po-210 alpha measurements

Input quantities

The input quantities necessary for the evaluation are listed in Tab. 1. The index »P« denotes the measurement of a sample, the index »B« that of a background measurement. The addition »0« refers to the corresponding blank measurement. In the alpha spectrum the peaks are held apart using the indices »x«, for the radionuclide to be measured and »T« for the tracer respectively.

Tab. 54: Designation of input quantities

Measurement	Measurement time	Number of registered counts (sample peak)	Number of registered counts (tracer peak)
Sample	t_{P}	$n_{\mathrm{x,\,P}}$	$n_{\mathrm{T,\,P}}$
Background (to sample)	$t_{\mathrm{P,\,0}}$	$n_{\mathrm{x,\,P,\,0}}$	$n_{\mathrm{T,\,P,\,0}}$
Blind sample	t_{B}	$n_{\mathrm{x,\,B}}$	$n_{\mathrm{T,\,B}}$
Background (to blind sample)	$t_{\mathrm{B,\,0}}$	$n_{\mathrm{x,\,B,\,0}}$	$n_{\mathrm{T,\,B,\,0}}$

Background correction

The net counts n_{n} of the sample peak (x) and the tracer peak (T) respectively, will be calculated by deducting the measure time corrected background counts from the gross counts of each peak.

$$n_{\mathrm{x,P,n}} = n_{\mathrm{x,P}} - n_{\mathrm{x,P,0}} \frac{t_{\mathrm{P}}}{t_{\mathrm{P,0}}} \tag{10.1}$$

$$n_{\mathrm{T,P,n}} = n_{\mathrm{T,P}} - n_{\mathrm{T,P,0}} \frac{t_{\mathrm{P}}}{t_{\mathrm{P,0}}} \tag{10.2}$$

$$n_{\mathrm{x,B,n}} = n_{\mathrm{x,B}} - n_{\mathrm{x,B,0}} \frac{t_{\mathrm{B}}}{t_{\mathrm{B,0}}} \tag{10.3}$$

$$n_{\mathrm{T,B,n}} = n_{\mathrm{T,B}} - n_{\mathrm{T,B,0}} \frac{t_{\mathrm{B}}}{t_{\mathrm{B,0}}} \tag{10.4}$$

For the uncertainty $u(n)$ of Poisson distributed events n the following dependency

$$u^2(n) = n \tag{10.5}$$

can be applied. By using the basic rules for propagation of uncertainty, the uncertainties of the calculated net counts in (10.1), (10.2), (10.3) and (10.4) are given as

$$u^2\left(n_{\mathrm{x,P,n}}\right) = u^2\left(n_{\mathrm{x,P}} - n_{\mathrm{x,P,0}} \frac{t_{\mathrm{P}}}{t_{\mathrm{P,0}}}\right) = u^2\left(n_{\mathrm{x,P}}\right) + u^2\left(n_{\mathrm{x,P,0}}\right) \frac{t_{\mathrm{P}}}{t_{\mathrm{P,0}}} = n_{\mathrm{x,P}} + n_{\mathrm{x,P,0}} \frac{t_{\mathrm{P}}^2}{t_{\mathrm{P,0}}^2}, \tag{10.6}$$

$$u^2\left(n_{\mathrm{T,P,n}}\right) = u^2\left(n_{\mathrm{T,P}} - n_{\mathrm{T,P,0}} \frac{t_{\mathrm{P}}}{t_{\mathrm{P,0}}}\right) = u^2\left(n_{\mathrm{T,P}}\right) + u^2\left(n_{\mathrm{T,P,0}}\right) \frac{t_{\mathrm{P}}}{t_{\mathrm{P,0}}} = n_{\mathrm{T,P}} + n_{\mathrm{T,P,0}} \frac{t_{\mathrm{P}}^2}{t_{\mathrm{P,0}}^2}, \tag{10.7}$$

$$u^2\left(n_{\mathrm{x,B,n}}\right) = u^2\left(n_{\mathrm{x,B}} - n_{\mathrm{x,B,0}} \frac{t_{\mathrm{B}}}{t_{\mathrm{B,0}}}\right) = u^2\left(n_{\mathrm{x,B}}\right) + u^2\left(n_{\mathrm{x,B,0}}\right) \frac{t_{\mathrm{B}}}{t_{\mathrm{B,0}}} = n_{\mathrm{x,B}} + n_{\mathrm{x,B,0}} \frac{t_{\mathrm{B}}^2}{t_{\mathrm{B,0}}^2} \text{ and} \tag{10.8}$$

$$u^2\left(n_{\mathrm{T,B,n}}\right) = u^2\left(n_{\mathrm{T,B}} - n_{\mathrm{T,B,0}} \frac{t_{\mathrm{B}}}{t_{\mathrm{B,0}}}\right) = u^2\left(n_{\mathrm{T,B}}\right) + u^2\left(n_{\mathrm{T,B,0}}\right) \frac{t_{\mathrm{B}}}{t_{\mathrm{B,0}}} = n_{\mathrm{T,B}} + n_{\mathrm{T,B,0}} \frac{t_{\mathrm{B}}^2}{t_{\mathrm{B,0}}^2} \tag{10.9}$$

respectively.

After the background deduction a critical level test was performed on each peak. In order to prove that a significant contribution (physical effect), adding to the concerned peak in the α-spectrum, was coming from the measured sample, a decision threshold $a^*_{\mathrm{x,P,n}}$ was introduced, where the following requirement

$$n_{\mathrm{x,P,n}} > a^*_{\mathrm{x,P,n}} \tag{10.10}$$

had to be fulfilled. The decision threshold $a^*_{\mathrm{x,P,n}}$ arose from (10.1) and (10.6) for the expected dependency for the true value of the net count $\nu_{\mathrm{x,P,n}}$ and its uncertainty $\tilde{u}(\nu_{\mathrm{x,P,n}})$:

$$\nu_{\mathrm{x,P,n}} = n_{\mathrm{x,P}} - n_{\mathrm{x,P,0}} \frac{t_{\mathrm{P}}}{t_{\mathrm{P,0}}} \tag{10.11}$$

$$\tilde{u}^2(\nu_{\mathrm{x,P,n}}) = n_{\mathrm{x,P}} + n_{\mathrm{x,P,0}} \frac{t_{\mathrm{P}}^2}{t_{\mathrm{P,0}}^2} \tag{10.12}$$

From (10.11) followed

$$n_{\mathrm{x,P}} = \nu_{\mathrm{x,P,n}} + n_{\mathrm{x,P,0}} \frac{t_{\mathrm{P}}}{t_{\mathrm{P,0}}} \tag{10.13}$$

and by inserting (10.13) in (10.12) one gets

$$\tilde{u}(\nu_{\mathrm{x,P,n}}) = \nu_{\mathrm{x,P,n}} + n_{\mathrm{x,P,0}} \frac{t_{\mathrm{P}}}{t_{\mathrm{P,0}}} + n_{\mathrm{x,P,0}} \frac{t_{\mathrm{P}}^2}{t_{\mathrm{P,0}}^2} = \nu_{\mathrm{x,P,n}} + n_{\mathrm{x,P,0}} \frac{t_{\mathrm{P}}}{t_{\mathrm{P,0}}} \left(1 + \frac{t_{\mathrm{P}}}{t_{\mathrm{P,0}}}\right) \tag{10.14}$$

From $\nu_{\mathrm{x,P,n}} = 0$ arose

$$\tilde{u}(0) = n_{\mathrm{x,P,0}} \frac{t_{\mathrm{P}}}{t_{\mathrm{P,0}}} \left(1 + \frac{t_{\mathrm{P}}}{t_{\mathrm{P,0}}}\right). \tag{10.15}$$

In this manner the decision threshold $a^*_{\mathrm{x,P,n}}$ was expressed as

$$a^*_{\mathrm{x,P,n}} = k_{1-\alpha} \cdot \tilde{u}^2(0) = k_{1-\alpha} \sqrt{n_{\mathrm{x,P,0}} \frac{t_{\mathrm{P}}}{t_{\mathrm{P,0}}} \left(1 + \frac{t_{\mathrm{P}}}{t_{\mathrm{P,0}}}\right)}. \tag{10.16}$$

The factor $k_{1-\alpha}$ was a measure of the statistical confidence, which corresponds to the quantile of the standardized normal distribution for the probability $p = 1 - \alpha$. If this decision rule is obeyed, a wrong decision in favour of the presence of the physical effect occurs with a probability not greater than α (error of the first kind).

Mathematical model of evaluation

The general model of evaluation can be expressed as followed:

$$A_{\mathrm{x}} = \frac{A_{\mathrm{T}} \cdot K_{\mathrm{T}}}{K_{\mathrm{x}}} \cdot \frac{n_{\mathrm{x}}}{n_{\mathrm{T}}} \tag{10.17}$$

The for the general model of the evaluation (10.17) necessary number of registered counts n_{x} and n_{T} respectively directly correspond to

$$n_{\mathrm{x}} = n_{\mathrm{x,P,n}} \text{ and} \tag{10.18}$$

$$n_{\mathrm{T}} = n_{\mathrm{T,P,n}} \tag{10.19}$$

respectively. The general decay correction factors K_{T} and K_{x}, for the tracer T and the sample nuclide x respectively, are put together of the specific decay correction factors $k_{\mathrm{w,T}}$ and $k_{\mathrm{w,x}}$, correcting for the decay during the waiting time before the measurement, and $k_{\mathrm{c,T}}$ and $k_{\mathrm{c,x}}$ correcting for decay during the measurement, and can be expressed as:

$$K_{\mathrm{T}} = k_{\mathrm{w,T}} \cdot k_{\mathrm{c,T}} \tag{10.20}$$

$$K_{\mathrm{x}} = k_{\mathrm{w,x}} \cdot k_{\mathrm{c,x}} \tag{10.21}$$

The specific decay correction factors can in turn be expressed as:

$$k_{\mathrm{w,T}} = \exp\left(-\ln 2 \frac{t_{\mathrm{w,T}}}{{}^{\text{Po-208}}t_{1/2}}\right) \tag{10.22}$$

$$k_{\mathrm{c,T}} = \frac{{}^{\text{Po-208}}t_{1/2}}{\ln 2 \cdot t_{\mathrm{c,T}}} \cdot \left(1 - \exp\left(-\ln 2 \frac{t_{\mathrm{c,T}}}{{}^{\text{Po-208}}t_{1/2}}\right)\right) \tag{10.23}$$

$$k_{\mathrm{w,x}} = \exp\left(-\ln 2 \frac{t_{\mathrm{w,x}}}{{}^{\text{Po-210}}t_{1/2}}\right) \tag{10.24}$$

$$k_{\mathrm{c,x}} = \frac{{}^{\text{Po-210}}t_{1/2}}{\ln 2 \cdot t_{\mathrm{c,x}}} \cdot \left(1 - \exp\left(-\ln 2 \frac{t_{\mathrm{c,x}}}{{}^{\text{Po-210}}t_{1/2}}\right)\right) \tag{10.25}$$

By inserting (10.18), (10.19), (10.22), (10.23), (10.24) and (10.25) in the general model of evaluation (10.17) the specific model of evaluation was obtained, as followed

$$A_{\mathrm{x}} = A_{\mathrm{T}} \cdot \frac{\exp\left(-\ln 2 \cdot \frac{t_{\mathrm{w,T}}}{{}^{\text{Po-208}}t_{1/2}}\right)}{\exp\left(-\ln 2 \cdot \frac{t_{\mathrm{w,x}}}{{}^{\text{Po-210}}t_{1/2}}\right)} \cdot \frac{\frac{{}^{\text{Po-208}}t_{1/2}}{\ln 2 \cdot t_{\mathrm{c,T}}} \cdot \left(1 - \exp\left(-\ln 2 \cdot \frac{t_{\mathrm{c,T}}}{{}^{\text{Po-208}}t_{1/2}}\right)\right)}{\frac{{}^{\text{Po-210}}t_{1/2}}{\ln 2 \cdot t_{\mathrm{c,x}}} \cdot \left(1 - \exp\left(-\ln 2 \cdot \frac{t_{\mathrm{c,x}}}{{}^{\text{Po-210}}t_{1/2}}\right)\right)} \cdot \frac{n_{\mathrm{x,P,n}}}{n_{\mathrm{T,P,n}}} \tag{10.22}$$

By inserting (10.1) and (10.2), the above equation could be ascribed to its input quantities(Tab. 52:

$$A_\mathrm{x} = A_\mathrm{T} \cdot \left(\frac{\exp\left(-\ln 2 \cdot \frac{t_{\mathrm{w,T}}}{{}^{\text{Po-208}}t_{1/2}}\right) \cdot \frac{{}^{\text{Po-208}}t_{1/2}}{\ln 2 \cdot t_{\mathrm{c,T}}} \cdot \left(1 - \exp\left(-\ln 2 \cdot \frac{t_{\mathrm{c,T}}}{{}^{\text{Po-208}}t_{1/2}}\right)\right)}{\exp\left(-\ln 2 \cdot \frac{t_{\mathrm{w,x}}}{{}^{\text{Po-210}}t_{1/2}}\right) \cdot \frac{{}^{\text{Po-210}}t_{1/2}}{\ln 2 \cdot t_{\mathrm{c,x}}} \cdot \left(1 - \exp\left(-\ln 2 \cdot \frac{t_{\mathrm{c,x}}}{{}^{\text{Po-210}}t_{1/2}}\right)\right)} \right) \cdot \left(\frac{n_{\mathrm{x,P}} - n_{\mathrm{x,P,0}} \frac{t_\mathrm{P}}{t_{\mathrm{P,0}}}}{n_{\mathrm{T,P}} - n_{\mathrm{T,P,0}} \frac{t_\mathrm{P}}{t_{\mathrm{P,0}}}} \right)$$

(10.23)

Confidence limits

For the uncertainty $u(A_\mathrm{x})$ of the in (10.23) specified activity A_x the following equation could be applied, assuming that the decay correction factor have negligible uncertainties:

$$u^2(A_\mathrm{x}) = u^2\left(A_\mathrm{T} \frac{n_{\mathrm{x,P,n}}}{n_{\mathrm{T,P,n}}} \right) \tag{10.24}$$

According to the basic rules of propagation of uncertainty it followed

$$\begin{aligned} u^2(A_\mathrm{x}) &= u^2(A_\mathrm{T}) \cdot \left(\frac{n_{\mathrm{x,P,n}}}{n_{\mathrm{T,P,n}}} \right)^2 + A_\mathrm{T}^2 \cdot u^2\left(\frac{n_{\mathrm{x,P,n}}}{n_{\mathrm{T,P,n}}} \right) \\ &= u^2(A_\mathrm{T}) \cdot \left(\frac{n_{\mathrm{x,P,n}}}{n_{\mathrm{T,P,n}}} \right)^2 + A_\mathrm{T}^2 \cdot \left(\frac{u^2(n_{\mathrm{x,P,n}})}{n_{\mathrm{T,P,n}}^2} + \frac{n_{\mathrm{x,P,n}}^2 \cdot u^2(n_{\mathrm{T,P,n}})}{n_{\mathrm{T,P,n}}^4} \right) \end{aligned} \tag{10.25}$$

which by inserting (10.1) and (10.2) for the net counts n_n as well as (10.6) and (10.7) for the uncertainties $u(n_\mathrm{n})$ the uncertainty $u(A_\mathrm{x})$ could be ascribed to its input quantities (Tab. 52):

$$\begin{aligned} u^2(A_\mathrm{x}) &= u^2(A_\mathrm{T}) \cdot \left(\frac{n_{\mathrm{x,P}} - n_{\mathrm{x,P,0}} \frac{t_\mathrm{P}}{t_{\mathrm{P,0}}}}{n_{\mathrm{T,P}} - n_{\mathrm{T,P,0}} \frac{t_\mathrm{P}}{t_{\mathrm{P,0}}}} \right)^2 \\ &+ A_\mathrm{T}^2 \cdot \left(\frac{n_{\mathrm{x,P}} - n_{\mathrm{x,P,0}} \frac{t_\mathrm{P}}{t_{\mathrm{P,0}}}}{\left(n_{\mathrm{T,P}} - n_{\mathrm{T,P,0}} \frac{t_\mathrm{P}}{t_{\mathrm{P,0}}} \right)^2} + \frac{\left(n_{\mathrm{x,P}} - n_{\mathrm{x,P,0}} \frac{t_\mathrm{P}}{t_{\mathrm{P,0}}} \right)^2 \cdot n_{\mathrm{T,P}} - n_{\mathrm{T,P,0}} \frac{t_\mathrm{P}^2}{t_{\mathrm{P,0}}^2}}{\left(n_{\mathrm{T,P}} - n_{\mathrm{T,P,0}} \frac{t_\mathrm{P}}{t_{\mathrm{P,0}}} \right)^4} \right) \end{aligned} \tag{10.26}$$

Decision threshold

According to (10.22) the true value of the activity α_x was expected as

$$\alpha_x = A_T \frac{n_{x,P,n}}{n_{T,P,n}}, \tag{10.27}$$

from which directly followed:

$$n_{x,P,n} = n_{T,P,n} \frac{\alpha_x}{A_T} \tag{10.28}$$

By inserting (10.1) in (10.28) the following equation was obtained:

$$n_{x,P} = n_{T,P,n} \frac{\alpha_x}{A_T} + n_{x,P,0} \frac{t_P}{t_{P,0}} \tag{10.29}$$

For the uncertainty $\tilde{u}(\alpha_x)$ (10.25) applied:

$$\tilde{u}(\alpha_x) = u^2(A_T) \cdot \left(\frac{n_{x,P,n}}{n_{T,P,n}} \right)^2 + A_T^2 \cdot \left(\frac{u^2(n_{x,P,n})}{n_{T,P,n}^2} + \frac{n_{x,P,n}^2 \cdot u^2(n_{T,P,n})}{n_{T,P,n}^4} \right) \tag{10.30}$$

By inserting (10.1) instead of $n_{x,P,n}$ and (10.6) instead of $u(n_{x,P,n})$ the following was obtained:

$$\tilde{u}(\alpha_x) = u^2(A_T) \cdot \left(\frac{n_{x,P} - n_{x,P,0} \dfrac{t_P}{t_{P,0}}}{n_{T,P,n}} \right)^2 + A_T^2 \cdot \left[\frac{n_{x,P} + n_{x,P,0} \dfrac{t_P^2}{t_{P,0}^2}}{n_{T,P,n}^2} + \frac{\left(n_{x,P} - n_{x,P,0} \dfrac{t_P}{t_{P,0}} \right)^2 \cdot u^2(n_{T,P,n})}{n_{T,P,n}^4} \right] \tag{10.31}$$

Using (10.29) for $n_{x,P}$ in (10.30) yielded after simplifying

$$\tilde{u}(\alpha_x) = u^2(A_T) \cdot \left(\frac{\alpha_x}{A_T}\right)^2 + A_T^2 \cdot \left[\frac{\alpha_x}{A_T \cdot n_{T,P,n}} + \frac{n_{x,P,0} \frac{t_P}{t_{P,0}} \left(1 + \frac{t_P}{t_{P,0}}\right) + \left(\frac{\alpha_x}{A_T}\right)^2 \cdot u^2(n_{T,P,n})}{n_{T,P,n}^2} \right] \tag{10.32}$$

For a true value of $\alpha_x = 0$ followed:

$$\tilde{u}(0) = \frac{A_T}{n_{T,P,n}} \sqrt{n_{x,P,0} \frac{t_P}{t_{P,0}} \left(1 + \frac{t_P}{t_{P,0}}\right)} \tag{10.33}$$

The decision threshold could thereof be formulated as

$$A_x^* = k_{1-\alpha} \cdot \tilde{u}(0) = k_{1-\alpha} \frac{A_T}{n_{T,P,n}} \sqrt{n_{x,P,0} \frac{t_P}{t_{P,0}} \left(1 + \frac{t_P}{t_{P,0}}\right)} . \tag{10.34}$$

With (10.2) the decision threshold could be ascribed to its input quantities (Tab. 52):

$$A_x^* = k_{1-\alpha} \cdot \tilde{u}(0) = k_{1-\alpha} \frac{A_T}{n_{T,P} - n_{T,P,0} \frac{t_P}{t_{P,0}}} \sqrt{n_{x,P,0} \frac{t_P}{t_{P,0}} \left(1 + \frac{t_P}{t_{P,0}}\right)} \tag{10.35}$$

The value for the statistical confidence was chosen to $k_{1-\alpha} = 1.645$.

Detection limit

The detection limit is defined as

$$\alpha_x^* = A_x^* + k_{1-\beta} \cdot \tilde{u}(\alpha_x^*) \tag{10.36}$$

By inserting (10.32) in (10.36) followed:

$$\alpha_{\mathrm{x}}^{*}=A_{\mathrm{x}}^{*}+k_{1-\beta}\sqrt{\begin{array}{l}u^{2}(A_{\mathrm{T}})\cdot\left(\dfrac{\alpha_{\mathrm{x}}^{*}}{A_{\mathrm{T}}}\right)^{2}\\+A_{\mathrm{T}}^{2}\cdot\left[\dfrac{\alpha_{\mathrm{x}}^{*}}{A_{\mathrm{T}}\cdot n_{\mathrm{T,P,n}}}+\dfrac{n_{\mathrm{x,P,0}}\dfrac{t_{\mathrm{P}}}{t_{\mathrm{P,0}}}\left(1+\dfrac{t_{\mathrm{P}}}{t_{\mathrm{P,0}}}\right)+\left(\dfrac{\alpha_{\mathrm{x}}^{*}}{A_{\mathrm{T}}}\right)^{2}\cdot u^{2}(n_{\mathrm{T,P,n}})}{n_{\mathrm{T,P,n}}^{2}}\right]\end{array}} \tag{10.37}$$

By inserting (10.2) and (10.7) the detection limit could be ascribed to its input quantities (Tab. 52):

$$\alpha_{\mathrm{x}}^{*}=A_{\mathrm{x}}^{*}+k_{1-\beta}\sqrt{\begin{array}{l}u^{2}(A_{\mathrm{T}})\cdot\left(\dfrac{\alpha_{\mathrm{x}}^{*}}{A_{\mathrm{T}}}\right)^{2}\\+A_{\mathrm{T}}^{2}\cdot\left[\begin{array}{l}\dfrac{\alpha_{\mathrm{x}}^{*}}{A_{\mathrm{T}}\cdot n_{\mathrm{T,P}}-n_{\mathrm{T,P,0}}\dfrac{t_{\mathrm{P}}}{t_{\mathrm{P,0}}}}\\+\dfrac{n_{\mathrm{x,P,0}}\dfrac{t_{\mathrm{P}}}{t_{\mathrm{P,0}}}\left(1+\dfrac{t_{\mathrm{P}}}{t_{\mathrm{P,0}}}\right)+\left(\dfrac{\alpha_{\mathrm{x}}^{*}}{A_{\mathrm{T}}}\right)^{2}\cdot\left(n_{\mathrm{T,P}}-n_{\mathrm{T,P,0}}\dfrac{t_{\mathrm{P}}}{t_{\mathrm{P,0}}}\right)}{\left(n_{\mathrm{T,P}}-n_{\mathrm{T,P,0}}\dfrac{t_{\mathrm{P}}}{t_{\mathrm{P,0}}}\right)^{2}}\end{array}\right]\end{array}} \tag{10.38}$$

The statistical confidence factor was set to $k_{1-\beta}=1.645$.

10.5.2 Evaluation of the Pb-210 LSC measurements

Tab. 55: Input quantities for the LSC evaluation

Quantity	Symbol	Unit	Uncertainty symbol
Number of gross counts	N_g	1	$u(N_g)$
Time of gross measurement	t_g	s	
Gross count rate	R_g	s^{-1}	$u(R_g)$
Number of background counts	N_0	1	$u(N_0)$
Time of background measurement	t_0	s	
Background count rate	R_0	s^{-1}	$u(R_0)$
Counting efficiency	ε	$Bq^{-1}\ s^{-1}$	$u(\varepsilon)$
Chemical yield	η	1	$u(\eta)$
Sample volume	V	l	$u(V)$
Aliquot correction factor	f_a	1	$u(f_a)$
Volume of aliquot of the Pb fraction	v_a	l	$u(v_a)$
Volume of the total Pb fraction	v_{Pb}	l	$u(v_{Pb})$
Waiting time	t_w	s^{-1}	
Waiting time correction factor	K_w	1	
Decay constant	λ	s^{-1}	
Activity	A	Bq	$u(A)$
Decision threshold	A^*		
Detection limit	α^*		

Mathematical model of evaluation

The general model of evaluation for the activity concentration can be expressed as followed:

$$A = \frac{R_g - R_0}{\varepsilon \eta V f_a} \cdot K_w \,, \tag{10.39}$$

where $$R_0 = \frac{N_0}{t_0} \tag{10.40}$$

and $$R_g = \frac{N_g}{t_g} \,. \tag{10.41}$$

The aliquot correction factor f_a is put together from

$$f_a = \frac{v_a}{v_{Pb}}. \tag{10.42}$$

Due to the long waiting time for the ingrowth of Bi-210, a waiting time correction factor was applied. Since the sample measurements were short in comparison to the half-life of Pb-210, there was no measurement time correction performed. The uncertainty for the waiting time correction factor was assumed to be negligible. The correction factor can be expressed as:

$$K_w = \frac{\lambda_{Bi}}{\lambda_{Bi} - \lambda_{Pb}} \exp(-\lambda_{Pb} t_w)(1 - \exp(-\lambda_{Bi} - \lambda_{Pb})t_w). \tag{10.43}$$

The specific mathematical model of evaluation can be formulated to:

$$A = \left(\frac{n_g}{t_g} - \frac{n_0}{t_0}\right)\left(\frac{\frac{\lambda_{Bi}}{\lambda_{Bi} - \lambda_{Pb}} \exp(-\lambda_{Pb} t_w)(1 - \exp(-\lambda_{Bi} - \lambda_{Pb})t_w)}{\varepsilon \eta V f_a}\right) \tag{10.44}$$

Confidence limits

$$u(A) = u\left((r_b - r_0)\frac{K_w}{\varepsilon \eta V v}\right) \tag{10.45}$$

$$u^2(A) = u^2\left((r_b - r_0)\frac{K_w}{\varepsilon \eta V v}\right) \tag{10.46}$$

$$\frac{u^2(A)}{A^2} = \frac{u^2(r_b - r_0)}{(r_b - r_0)^2} + \frac{u^2\left(\frac{K_w}{\varepsilon \eta V v}\right)}{\left(\frac{K_w}{\varepsilon \eta V v}\right)^2} \tag{10.47}$$

$$u^2(r_b - r_0) = u^2(r_b) + u^2(r_0) \tag{10.48}$$

$$u^2(r_b) = u^2(n_b)\frac{1}{t_b^2} = n_b \frac{1}{t_b^2} \tag{10.49}$$

$$u^2(r_0) = u^2(n_0)\frac{1}{t_0^2} = n_0 \frac{1}{t_0^2} \tag{10.50}$$

$$\frac{u^2(A)}{A^2} = \frac{n_b \frac{1}{t_b^2} + n_0 \frac{1}{t_0^2}}{\left(\frac{n_b}{t_b} - \frac{n_0}{t_0}\right)^2} + \frac{u^2\left(\frac{K_w}{\varepsilon\eta V\nu}\right)}{\left(\frac{K_w}{\varepsilon\eta V\nu}\right)^2} \quad (10.51)$$

$$u^2(A) = \frac{n_b \frac{1}{t_b^2} + n_0 \frac{1}{t_0^2}}{\left(\frac{n_b}{t_b} - \frac{n_0}{t_0}\right)^2} + \frac{u^2\left(\frac{K_w}{\varepsilon\eta V\nu}\right)}{\left(\frac{K_w}{\varepsilon\eta V\nu}\right)^2}\left(\left(\frac{n_b}{t_b} - \frac{n_0}{t_0}\right)\frac{K_w}{\varepsilon\eta V\nu}\right)^2 \quad (10.52)$$

$$u^2(A) = \left(\frac{n_b \frac{1}{t_b^2} + n_0 \frac{1}{t_0^2}}{\left(\frac{n_b}{t_b} - \frac{n_0}{t_0}\right)^2} + \frac{u^2(\varepsilon)}{\varepsilon^2} + \frac{u^2(\eta)}{\eta^2} + \frac{u^2(V)}{V^2} + \frac{u^2(\nu_a)}{\nu_a^2} + \frac{u^2(\nu_{Pb})}{\nu_{Pb}^2}\right)\left(\left(\frac{n_b}{t_b} - \frac{n_0}{t_0}\right)\frac{K_w}{\varepsilon\eta V\nu}\right)^2 \quad (10.53)$$

Decision threshold

According to (1) the true value of the activity α was expected to be

$$\alpha = (r_b - r_0)\frac{K_w}{\varepsilon\eta V\nu} = (r_b - r_0)\varphi \quad (10.54)$$

$$r_b = \frac{\alpha}{\varphi} + r_0 \quad (10.55)$$

To calculate the uncertainty $\tilde{u}(\alpha)$, equation (10.52) using r_b and r_0 from (10.40) and (10.41) respectively, was applied:

$$\tilde{u}^2(\alpha) = \left(\frac{\frac{r_b}{t_b} + \frac{r_0}{t_0}}{(r_b - r_0)^2} + \frac{u^2(\varphi)}{\varphi^2}\right)(r_b - r_0)^2\varphi^2 \quad (10.56)$$

By inserting (10.55) in (10.56) the following comes out:

$$\tilde{u}^2(\alpha) = \left(\frac{\frac{\frac{\alpha}{\varphi} + r_0}{t_\mathrm{b}} + \frac{r_0}{t_0}}{\left(\frac{\alpha}{\varphi} + r_0 - r_0\right)^2} + \frac{u^2(\varphi)}{\varphi^2} \right) \left(\frac{\alpha}{\varphi} + r_0 - r_0\right)^2 \varphi^2 = \left(\frac{\frac{\frac{\alpha}{\varphi} + r_0}{t_\mathrm{b}} + \frac{r_0}{t_0}}{\left(\frac{\alpha}{\varphi}\right)^2} + \frac{u^2(\varphi)}{\varphi^2} \right) \left(\frac{\alpha}{\varphi}\right)^2 \varphi^2 \quad (10.57)$$

$$\tilde{u}^2(\alpha) = \left(\frac{\frac{\alpha}{\varphi} + r_0}{t_\mathrm{b}} + \frac{r_0}{t_0} + \frac{u^2(\varphi)\alpha^2}{\varphi^4} \right) \varphi^2 \quad (10.58$$

)

For α = 0:

$$\tilde{u}^2(0) = \left(\frac{r_0}{t_\mathrm{b}} + \frac{r_0}{t_0} \right) \varphi^2 = r_0 \left(\frac{1}{t_\mathrm{b}} + \frac{1}{t_0} \right) \varphi^2 \quad (10.59)$$

$$\tilde{u}(0) = \sqrt{r_0 \left(\frac{1}{t_\mathrm{b}} + \frac{1}{t_0} \right)} \cdot \varphi \quad (10.60)$$

$$A^* = k_{1-\alpha} \cdot \tilde{u}(0) = k_{1-\alpha} \sqrt{r_0 \left(\frac{1}{t_\mathrm{b}} + \frac{1}{t_0} \right)} \cdot \varphi \quad (10.61)$$

$$A^* = k_{1-\alpha} \cdot \tilde{u}(0) = k_{1-\alpha} \sqrt{\frac{n_0}{t_0} \left(\frac{1}{t_\mathrm{b}} + \frac{1}{t_0} \right)} \cdot \frac{K_\mathrm{w}}{\varepsilon \eta V \nu} \quad (10.62)$$

Detection limit

The detection limit is defined as

$$\alpha^* = A^* + k_{1-\beta} \cdot \tilde{u}(\alpha^*) \quad (10.63)$$

By inserting (10.58) in (10.62) followed:

$$\alpha^* = A^* + k_{1-\beta} \sqrt{\frac{\frac{\alpha^*}{\varphi} + r_0}{t_\mathrm{b}} + \frac{r_0}{t_0} + \frac{u^2(\varphi) \cdot \alpha^{*2}}{\varphi^4}} \cdot \varphi \quad (10.64)$$

$$\alpha^* = A^* + k_{1-\beta}\left(\sqrt{\frac{\dfrac{\dfrac{\alpha^*}{\left(\dfrac{K_w}{\varepsilon\eta V\nu}\right)}+\dfrac{n_0}{t_0}}{t_b}+n_0+\dfrac{\dfrac{u^2(\varepsilon)}{\varepsilon^2}+\dfrac{u^2(\eta)}{\eta^2}+\dfrac{u^2(V)}{V^2}+\dfrac{u^2(\nu_a)}{\nu_a^2}+\dfrac{u^2(\nu_{Pb})}{\nu_{Pb}^2}\cdot\alpha^{*2}}{\left(\dfrac{K_w}{\varepsilon\eta V\nu}\right)^4}}{}}\right)\left(\frac{K_w}{\varepsilon\eta V\nu}\right) \tag{10.65}$$

10.6 Changeable parameters

10.6.1 Rheinberg

Sampling station	Location description	Temperature (°C)	pH	Conductivity (mS m^{-1})	Redox potential (mV)
1	Hoerstgener Kendel	15.0	7.1	1263	109
2	Schacht Hoerstgen	17.8	7.5	860	232
3	Eyllscher Kendel	20.0	8.0	682	222
4	Rossenray Absetzbecken	28.0	7.2	4400	210
5	GW-Brunnen 2217	16.4	7.1	437	241
6	Rossenray Absetzbecken	25.0	7.5	33100	210
7	GW-Brunnen 1102	14.0	7.4	5.83×10^{-3}	19
8	GW-Brunnen 1017	13.6	7.3	501	–
9	GW-Brunnen 1929H	13.6	7.1	1835	–
10	GW-Brunnen 1647	12.2	7.6	1204	–
11	Rossenray, Einleiter Fossa	28.0	7.6	4090	191
12	Altrhein, Schleuse Ossenberg	18.7	7.8	967	200
13	Jenneckes Gatt	18.4	7.7	1720	197
14	Fossa, in Rheinberg	19.2	7.5	1390	197
15	Krummensteg	21.0	7.5	1613	211

10.6.2 Mailuu Suu

The changeable parameters were measured at the location of sampling in Kyrgyzstan by a member of the BGR.

Station No.	Date of sampling	Temperature (°C)	pH	Conductivity (mS m^{-1})	O_2 saturation (%)	Redox potential (mV)
1-1	21.01.2006	0.3	7.4	240	82.3	243
2-1	21.01.2006	0.9	6.9	234	75.5	93
3-1	21.01.2006	24.1	7.2	449	35	-70
3-2	Oct. 2006	25.7	7.8	433	–	–
4-1	21.01.2006	5	7.1	373	77.5	104
4-2	01.07.2006	15.6	8	577	99	164
5-1	21.01.2006	–	–	–	–	–
6-1	21.01.2006	1.2	7.6	4910	96	
6-2	01.07.2006	22.4	6.6	4640	102.5	110
7-1	21.01.2006	19	7.3	2490	–	-340
7-2	01.07.2006	22.1	7.9	2550	19.6	-305
8-1	21.01.2006	14.7	6.9	1163	51.5	-119
8-2	01.07.2006	–	6.9	1160	109	132
9-1	21.01.2006	11.3	7.1	315	–	-50
9-2	01.07.2006	20.6	6.2	309	100	260
10-1	21.01.2006	9.6	6.8	1575	–	70
10-2	01.07.2006	18.5	6.5	896	69.2	140
11-1	01.07.2006	14.3	8.5	1693	16.4	181
11-3	Oct. 2006	15.8	7.2	2120	–	–
12-1	July 2006	27.2	6.3	11063	58.4	88
13-1	01.07.2006	17.1	7.7	160	98.5	27.1
14-1	01.07.2006	23.3	8.7	9460	87	141
14-2	Oct. 2006	18.8	8.8	12430	101.9	–
15-1	01.07.2006	23.8	7.6	2100	92	184
15-3	Oct. 2006	16.9	7.5	2150	65	220
16-1	01.07.2006	13.1	6.9	1154	21	113
17-1	01.07.2006	17.9	6.7	2350	58.2	82
18-1	Oct. 2006	19.4	8.2	1933	–	–
19-1	Oct. 2006	14.1	8.5	269	–	–
20-1	Oct. 2006	18.4	7.7	3070	–	–

21-1	Oct. 2006	17.2	8.7	896	–	–
24-1	Oct. 2006	14.4	7.2	1023	68.1	171
35-1	April 2007	12.9	7.4	2300	–	–
36-1	April 2007	14.6	7.2	1149	–	–
37-1	April 2007	16.2	7.2	971	–	–
38-1	April 2007	20.5	8.1	1081	–	–
39-1	April 2007	–	–	–	–	–

11 Bibliography

[1] INTERNATIONAL COMMISSION ON RADIOLOGICAL PROTECTION (ICRP): Age-dependent Doses to Members of the Public from Intake of Radionuclides: Part 5, Compilation of Ingestion and Inhalation Coefficients. ICRP Publication 72. In: *Ann. ICRP* 26 (1995) Nr. 1.

[2] SWIFT, B.: Forensic Sci. Int. 98 (1998), p. 119

[3] UNITED NATIONS SCIENTIFIC COMMITTEE ON THE EFFECTS OF ATOMIC RADIATION (UNSCEAR) (Eds.): Sources and Effects of Ionizing Radiation: UNSCEAR 1988, Report the General Assembly, with Annexes. New York, NY: UNSCEAR, 1988

[4] HORWITZ, E. P.; CHIARIZIA, R.; DIETZ, M. L.: A novel strontium-selective extraction chromatographic resin. In: *Solvent Extraction and Ion Exchange.* 10 (1992), Nr. 2, S. 313–336

[5] HORWITZ, E. P.; DIETZ, M. L.; RHOADES, S.; FELINTO, C.; GALE, N. H.; HOUGHTON, J.: A lead-selective extraction chromatographic resin and its application to the isolation of lead from geological samples. In: *Analytica Chimica Acta.* 292 (1994), pp. 263–273

[6] VAJDA, N.; LAROSA, J.; ZEISLER, R.; DANESI, P.; KIS-BENEDEK, GY.: A novel technique for the simultaneous determination of Pb-210 and Po-210 using a crown ether. In: *Journal of Environmental Radioactivity*. 37 (1997), pp. 355–372

[7] EICHROM TECHNOLOGIES (ED): Lead-210 in Water. Rev. 1.8. (OTW01). 2005

[8] CLAYTON, R. F.; BRADLEY, E. J.: A cost-effective method for the determination of Po-210 and Pb-210 in environmental samples. In: *Science of the Total Environment.* 173/174 (1995), pp. 23–28

[9] BECQUEREL, H.: Sur les Radiations Invisibles Émises par les Corps Phosphorescents. In: *C. R. Acad. Sci. Paris* 122 (1896) p. 501

[10] CURIE, M.: Rayons Émis par les Composés de l'Uranium et du Thorium. In: *C. R. Acad. Sci. Paris* 126 (1898), p. 1102

[11] SCHMIDT, G. C.: Über die von Thorium und den Thorverbindungen ausgesandte Strahlung. In: *Verh. Phys. Ges. Berlin* 17 (1898), p. 4

[12] CURIE, P.; SLODOWSKA-CURIE, M.: Sur une Nouvelle Substance Radio-active Contenu dans la Pechblende. In: *C. R. Acad. Sci. Paris* 127 (1898), p. 175

[13] SIEHL, A.: Grundlagen und geowissenschaftliche Aspekte der natürlichen Radioaktivität. In: SIEHL, A. (Ed.): *Umweltradioaktivität.* Berlin: Ernst & Sohn Verlag, 1996. –ISBN 3-433-01813-8

[14] LIESER, K. H.: *Nuclear and Radiochemistry. Fundamentals and Applications.* 2nd Ed. Weinheim: Wiley-VCH, 2001. –ISBN 3-527-30317-0

[15] KEMSKI, J.; KLINGEL, R.; SIEHL, A.: Die terrestrische Strahlung durch natürlich radioaktive Elemente. In: SIEHL, A. (Ed.): *Umweltradioaktivität*. Berlin: Ernst & Sohn Verlag, 1996. –ISBN 3-433-01813-8

[16] PFENNIG, G.; KLEWE-NEBENIUS, H.; SEELMANN-EGGEBERT, W.: Chart of the nuclides, 6th Ed. 1995. Revised reprint 1998

[17] GASCOYNE, M.: Geochemistry of the actinides and their daughters. In: IVANOVICH, M.; HARMON, R. S. (Eds.): *Uranium-series Disequilibrium: Applications to Earth, Marine, and Environmental Sciences*. 2^{nd} Ed. Oxford: Clarendon Press, 1992.

[18] GIBSON, W. M.: The radiochemistry of Lead, NAS-NS Publication 3040, U.S. Atomic Energy Commission, Washington (1961)

[19] ELSTER, J.; GEITEL, H.: Further studies on Becquerel rays. In: *Ann. de Phys.* 69 (1899), p. 83

[20] HEVESY, G.; PANETH, F.: A manual of radioactivity. London: Oxford Univ. Press, 1926.

[21] APPLEBY, P. G.; OLDFIELD, F.: Application of Lead-210 to sedimentation studies. In: IVANOVICH, M.; HARMON, R. S. (Eds.): *Uranium-series Disequilibrium: Applications to Earth, Marine, and Environmental Sciences*. 2^{nd} Ed. Oxford: Clarendon Press, 1992.

[22] NuDat2.4: NuDat database version 2.4, accessed March 2008. http://www.nndc.bnl.gov/nudat2/chartNuc.jsp

[23] BAGNELL, K. W.: *Chemistry of the rare radioelements: Polonium–Actinium*. A.E.R.E., Harwell. London: Butterworths Scientific Publications, 1957.

[24] ATKINS, P. W.; BERAN, J. A.: *General Chemistry*. 2^{nd} Ed. New York: Scientific American Books, 1992. –ISBN 0-7167-2496-0

[25] HOLLEMAN, A. F.: *Lehrbuch der Anorganischen Chemie* / WIBERG, E.; WIBERG, N. (Bearb.) 101^{st} Ed. Berlin: Walter de Gruyter, 1995. –ISBN 3-11-012641-9

[26] SEDLET, J.: Radon and Radium. In: KOLTHOFF; ELVING (Eds.): *Treatise on analytical chemistry. Part II: Analytical chemistry of the elements, vol. 6*. Wiley & Sons, USA, 1964.

[27] GILBERT, T. W.: Lead. In: KOLTHOFF; ELVING (Eds.): *Treatise on analytical chemistry. Part II: Analytical chemistry of the elements, vol. 6*. Wiley & Sons, USA, 1964

[28] SEDLET, J.: Actinium, Astatine, Francium, Polonium, and Protactinium. In: KOLTHOFF; ELVING (Eds.): *Treatise on analytical chemistry. Part II: Analytical chemistry of the elements, vol. 6*. Wiley & Sons, USA, 1964.

[29] UNITED STATES NUCLEAR REGULATORY COMMISION. (2006) Fact Sheet: Polonium-210. In: http://www.nrc.gov/reading-rm/doc-collections/fact-sheets/polonium.pdf

[30] FIGGINS, P. E.: The radiochemistry of Polonium, NAS-NS Publication 3037, U.S. Atomic Energy Commission, Washington (1961)

[31] RHODES, R.: *The making of the atomic bomb*. Simon & Schuster, London, 1986

[32] BROOKS, L. S.: The vapor pressure of polonium. In: *J. Am. Chem. Soc*. 77 (1955), p. 3211

[33] HEALTH PHYSICS SOCIETY: Polonium-210 Information Sheet. http://hps.org

[34] LIDE (Ed.): *Handbook of Physics and Chemistry*. 73rd Edition. CRC Press, Boca Raton, Florida, 1992–1993

[35] DICKIN, A. P.: *Radiogenic Isotope Geology*. Cambridge University Press, Cambridge, UK. 1997. –ISBN: 0-521-43151-4

[36] IVANOVICH, M.; LATHAM, A. G.; KU, T.-L.: Uranium-series disequilibrium applications in geochronology. In: IVANOVICH, M.; HARMON, R. S. (Eds.): *Uranium-series Disequilibrium: Applications to Earth, Marine, and Environmental Sciences*. 2nd Ed. Oxford: Clarendon Press, 1992.

[37] GOLDBERG, E. D.: Geochronology with Pb-210 in radioactive dating. IAEA Vienna (1963), pp. 121–131

[38] OSMOND, J. K.; COWART, J. B.: Groundwater. In: IVANOVICH, M.; HARMON, R. S. (Eds.): *Uranium-series Disequilibrium: Applications to Earth, Marine, and Environmental Sciences*. 2nd Ed. Oxford: Clarendon Press, 1992.

[39] RAMA; KOIDE, M.; GOLDBERG, E. D.: Lead-210 in natural waters. In: *Science* 134 (1961), pp. 98–99

[40] CRAIG, H.; KRISHNASWAMI, S.; SOMAYAJULU, B. L. K.: Lead-210–radium-226. Radioactive disequilibrium in the deep sea. In: *Earth planet. Sci. Lett*. 17 (1973), pp. 295–305

[41] BACON, M. P.; ELZERMAN, A. W.: Enrichment of Pb-210 and Po-210 in the sea surface microlayer. In: *Nature* 284 (1980), pp. 332–334

[42] BENOIT, G.; HEMOND, H. F.: A biogeochemical mass balance of Po-210 and Pb-210 in an oligotrophic lake with seasonally anoxic hypolimnion. In: *Geochim. Cosmochim. Acta* 51 (1987), pp. 1445–1446

[43] BACON, M. P.; SPENCER, D. W.; BREWER, P. G.: Pb-210/Ra-226 and Po-210/Pb-210 disequilibria in seawater and suspended particulate matter. In: *Earth Plant. Sci. Lett*. 27A (1976), pp. 277–296

[44] LETHO, J.; KELOKASKI, P.; VAARAMAA, K.; JAAKKOLA, T.: Soluble and particle bound ^{210}Po and ^{210}Pb in groundwaters. In: *Radiochim. Acta* 85 (1999), pp. 149–155

[45] VESTERBACKA, P.; MÄKELÄINEN, I.; ARVELA, H.: Natural radioactivity in drinking water in private wells in Finland. In: *Radiat. Prot. Dosi.* 113 (2005) 2, pp. 223–232

[46] HARADA, K.; BURNETT, W. C.; LAROCK, P. A.; COWART, J. B.: Polonium in Florida groundwater and its possible relationship to the sulfur cycle and bacteria. In: *Geochim. Cosmochim. Acta*. 53 (1989), pp. 143–150

[47] VREČEK, P.; BENEDIK, L.; PIHLAR, B.: Determination of Pb-210 and Po-210 in sediment and soil leachates and in biological materials using a Sr-resin column and evaluation of column reuse. In: *Appl. Radiat. Isot*. 60 (2004), pp. 717–723

[48] JIA, G.; BELLI, M.; LIU, S.; SANSONE, U.; XU, C.; ROSAMILLA, S.; XIAO, X.; GUADINO, S.; CHEN, L.; YANG, H.: The fractionation and determination procedures for the speciation of Pb-210 and Po-210 in soil samples. In: *Anal. Chim. Acta* 562 (2006), pp. 51–58

[49] KIRCHHEIMER, F.: *Das Uran und seine Geschichte*. E. Stuttgart: Schweizerbart'sche Verlagbuchhandlung, 1963.

[50] SCHWANKNER, R. J.; LIECKFELD G.; LIENERT, D.: Die Frühgeschichte des Urans. In: *Die Geowissenschaften*. 7 (1989), S. 215–224

[51] INTERNATIONAL ATOMIC ENERGY AGENCY (IAEA) (Eds.): Uranium 2005: Resources, Production and Demand (Red Book). Vienna, IAEA. 2005

[52] INTERNATIONAL ATOMIC ENERGY AGENCY (IAEA): Annual Report 1994, under www.iaea.org

[53] INTERNATIONAL ATOMIC ENERGY AGENCY (IAEA): Annual Report 2006, under www.iaea.org

[54] GATZWEILER, R.: Lagerstätten- und produktionsbedingte Umweltauswirkungen des Uranerzbergbaus. In: SIEHL, A. (Ed.): *Umweltradioaktivität*. Berlin: Ernst & Sohn Verlag, 1996. –ISBN 3-433-01813-8

[55] CATCHPOLE, G. J.; KIRCHNER, G.: Restoration of groundwater contaminated by alkaline in-situ leach uranium mining. In: MERKEL, B.; HURST, S.; LÖHNERT, E. P.; STRUCKMEIER, W. (Eds.): *Uranium mining and hydrogeology. Proceedings of the International Conference and Workshop, Freiberg, Germany, October 1995*. Cologne: Sven von Loga Publishing, 1995.

[56] URANERZBERGBAU GMBH: *Kosten der Stilllegung und Sanierung von Urangewinnungsprojekten im internationalen Vergleich – Einflußgrößen und Abhängigkeiten*. Abschlußbericht zum Forschungsauftrag Nr. 37/93 des Bundesministeriums für Wirtschaft; Wessling, 1994

[57] INTERNATIONAL ATOMIC ENERGY AGENCY (IAEA) (Eds.): *Current practices for the management and confinement of uranium mill tailings*. Vienna: IAEA, (Technical Report Series No. 335)

[58] International Energy Association (IEA): Coal information. 2004

[59] United Nations Scientific Committee on the Effects of Atomic Radiation (UNSCEAR) (Eds.): *Sources and Effects of Ionizing Radiation*: UNSCEAR 1993, Report the General Assembly, with Annexes. New York, NY: UNSCEAR, 1993

[60] Koperski, J.: Radiation protection in the mining and milling of mineral sands. Paper submitted to the Bulletin of the Australian Radiation Protection Society, March (1993)

[61] United Nations Scientific Committee on the Effects of Atomic Radiation (UNSCEAR) (Eds.): *Sources and Effects of Ionizing Radiation*: UNSCEAR 2000, Report the General Assembly, with Annexes. New York, NY: UNSCEAR, 2000

[62] Corbett, J. O.: The radiation dose from coal burning: a review of pathways and data. In: *Radiat. Prot. Dosimetry*. 4 (1983), pp. 5–19

[63] Lebecka, J., B. Lukasik and S. Chalupnik. Purification of saline water from coal mines of radium and barium. In: *Pol. Tech. Rev*. 5-6 (1994), pp. 24–27

[64] Kolb, W. A.; Wojcik, M.: Enhanced radioactivity due to natural oil and gas production and related radiological problems. In: *Sci. Total Environ.* 45 (1985), pp. 77–84

[65] Nordic Liason Committee for Atomic Energy (NKA) (Eds.). Project RAS-430. National Institute of Radiation Hygiene, Norway. 1989

[66] Leenhouts, H. P.; Stoop, P.; van Tuinen, S. T.: Non-nuclear industries in the Netherlands and radiological risks. Report no. 610053003. National Institute of Public Health and the Environment, the Netherlands (1996)

[67] Jaworowski, J.: Sources and the global cycle of radium. In: *The environmental behaviour of Radium*. IAEA Technical Report Series No. 10. Vienna, (1990), Chap. 22, pp. 129–142

[68] Bundesamt für Strahlenschutz (Eds.): *Jahresbericht 2002*. Salzgitter, 2003

[69] Arnold, L.: *Windscale 1957. Anatomy of a nuclear accident*. 2nd Ed. Basingstokes and London: Macmillan Press Ltd., 1995.

[70] Garland, J. A.; Wakeford, R.: Atmospheric emissions from the Windscale accident of October 1957. In: *Atmospheric Environment*. DOI: 0:1016/j.atmosenv.2006.12.049 (2007)

[71] Crick, M. J.; Linsley, G. S.: An assessment of the radiological impact of the Windscale reactor fire, October 1957. In: *Int. Radiat. Biol.* 46 (1984) No. 5, pp. 479–506

[72] Austin, T. B.: Pile 1 fire, October 1957–1983: Estimates of polonium and tritium release. Calder Works TR/PLON/4710, available from the corresponding author.

[73] CHAMBERLAIN, A. C.: Emission of fission products and other activities during the accident to Windscale Pile no. 1 in October 1957. Report AERE M-3194. UKAEA, Harwell, 1984.

[74] LIESER, K. H.: Radionuclides in the geosphere: Sources, Mobility, Reactions in natural waters and interactions with solides. In: *Radiochim. Acta* 70/71 (1995), pp. 355–375

[75] MOORE, W. S.: Radionuclides of the uranium and thorium decay series in the estuarine environment. In: IVANOVICH, M.; HARMON, R. S. (Eds.): *Uranium-series Disequilibrium: Applications to Earth, Marine, and Environmental Sciences*. 2nd Ed. Oxford: Clarendon Press, 1992.

[76] STUMM, W.; MORGAN, J. J.: *Aquatic Chemistry: Chemical equilibria and rates in natural waters*. 3rd Ed. New York, N. Y.: John Wiley & Sons, 1996. –ISBN 0-471-51185-4, p. 896

[77] BACON, M. P.; SPENCER, D. W.; BREWER, P. G; MURRAY, J. W.: Lead-210, polonium-210, manganese and iron in the Cariaco Trench. In: *Deep Sea Res*. 27 (1980), pp. 119–135

[78] BENOIT, G.; HEMOND, H. F.: Po-210 and Pb-210 remobilization from lake sediments in relation to iron and manganese cycling. In: *Environ. Sci. Technol.* 24 (1990), pp. 1224–1234

[79] MOMOSHIMA, N.; SONG, L.-X.; OSAKI, S.; MAEDA, Y.: Formation and emission of volatile polonium compound by microbial activity and polonium methylation with methylcobalamin. In: *Environ. Sci. Technol.* 35 (2001), pp. 2956–2960

[80] LAROCK, P.; HYUN, J.-H.; BOUTELLE, S.; BURNETT, W. C.; HULL, C. D.: Bacterial mobilization of polonium. In: *Geochim. Cosmochim. Acta* 60 (1996), pp. 4321–4328

[81] KIM, G.; KIM, S.-J.; HARADA, K.; SCHULTZ, M. K.; BURNETT, W. C.: Enrichment of excess Po-210 in anoxic ponds. In: *Environ. Sci. Technol.* 39 (2005), pp. 4894–4899

[82] SWARZENSKI, P. W.; MCKEE, B. A.; SØRENSEN, K.; TODD, J. F.: Pb-210 and Po-210, manganese and iron cycling across the O_2/H_2S interface of a permanently anoxic fjord: Framvaren, Norway. In: *Marine Chem*. 67 (1999), pp. 199–217

[83] WAHL, A. C.; BONNER, N. A.: *Radioactivity applied to chemistry*. New York: Wiley, 1951.

[84] BROOKINS, D. G.: *Eh-pH Diagrams for Geochemistry*. Berlin Heidelberg New York: Springer-Verlag, 1988. –ISBN 3-540-18485-6

[85] WESTALL, J.; ZACHARA, J. L.; MOREL, F. M. M.: MINEQL, a computer program for the calculation of chemical equilibrium composition of aqueous systems. Technical note 18, Parsons Laboratory, MIT, Cambridge. 1976

[86] WESTALL, J.: MICROQL, A chemical equilibrium program in Basic, Report 86-02, Oregon State University, Corvallis, OR. 1986

[87] CALMANO, W.; LIESER, K. H.: Untersuchungen der Austauschvorgänge con Spurenelementen an Schwebstoffen mit Hilfe der Radionuklidtechnik. In: *Fresenius Z. Anal. Chem.* 307 (1981), p. 356

[88] CHOPPIN, G. R.; ALLARD, B.: Complexes of Actinides with naturally occurring organic compounds. In: FREEMAN, A.J.; KELLER, C. (Eds.): *Handbook on the Physics and Chemistry of the Actinides*. Vol. 3. Amsterdam: Elsevier, 1985. P. 407

[89] KAVANOUGH, M. C.; LECKIE, J. O. (Eds.): Particulates in water. In: *Amer. Chem. Soc.* Advances in Chemistry series 189, Washington D. C. (1980)

[90] NOZAKI, Y.; ZHANG, J.; TAKEDA, A.: ^{210}Pb and ^{210}Po in the equatorial Pacific and the Bering Sea: The effects of biological productivity and boundary scavenging. In: *Deep-Sea Research II.* 44 (1997) No. 9–10, pp. 2203–2220

[91] CHUNG, Y.; LIN, C.; WANG, P.; SU, Y. (2006), Ra-228, Ra-226, Pb-210 and Po-210 variations in the water columns and the surface water plankton in the Luzon Strait and northern South China Sea, *Eos Trans. AGU*, 87 (52), Fall Meet. Suppl., Abstract B53C-0353

[92] FISHER, N. S.; BURNS, K. A.; CHERRY, R. D.; HEYRAUD, M.: Accumulation and cellular distribution of Am-241, Po-210 and Pb-210 in two marine algae. In: *Marine Ecol.* 11 (1983), pp. 233–237

[93] CHERRY, R. D.; FOWLER, S. W.; BEASLEY, T. M.; HEYRAUD, M.: Polonium-210: Its vertical oceanic transport by zooplankton metabolic activity. In: *Marine Chem.* 3 (1975), pp. 105–110

[94] PANETH, F.: Über kolloide Lösungen radioaktiver Substanzen. In: *Colloid and Polymer Science*. 13 (1913), pp. 1–4

[95] MCCARTHY, J. F.; ZACHARA, J. M.: Subsurface transport of contaminants. In: *Environ. Sci. Technol.* 23 (1989) 5, pp. 496–502

[96] HAHN, O.: *Applied radiochemistry*. Ithaca, NY: Cornell University Press, 1936.

[97] SIMON, S. L.; IBRAHIM, S. A.: The plant/soil concentration ratio for calcium, radium, lead, and polonium: Evidence for non-linearity with reference to substrate concentration. In: *J. Environ. Radioactivity* 5 (1987), pp. 123–142

[98] ATHALYE, V. V.; RAMACHANDRAN, V.; D'SOUZA, T. J.: Influence of chelating agents on plant uptake of Cr-51, Pb-210 and Po-210. In: *Environ. Pollution* 89 (1995), pp. 47–53

[99] PIETRZAK–FLIS, Z.; SKOWRONSKA-SMOLAK, M.: Transfer of ^{210}Pb and ^{210}Po to plants via root system and above-ground interception. In: *Sci. Tot. Environ.* 162 (1995), pp. 139–147

[100] INTERNATIONAL ATOMIC ENERGY AGENCY (IAEA) (Eds.): *Handbook of parameter values for the prediction of radionuclide transfer in temperate environments*. Vienna: IAEA, 1994 (Technical Report Series No. 364). –ISBN 92-0-101094-X (STI/DOC/010/364)

[101] VREČEK, P.; BENEDIK, L.: Determination of ^{210}Pb and ^{210}Po in sediments, water, and plants in an area contaminated with mine waste. In: *Mine water and the environ.* 21 (2002), pp. 156–159

[102] CLULOW, F. V.; DAVÉ, N. K.; LIM, T. P.; AVADHANULA, R.: Radionuclides (lead-210, polonium-210, thorium-230, and -232) and thorium and uranium in water, sediments, and fish from lakes near the city of Lake Elliot, Ontario, Canada. In: *Environ. Pollution* 99 (1998), pp. 199–213

[103] BEAK: *Survey of data on the radionuclide content of fish in Canada*. Report prepared for the Atomic Energy Control Board by Beak Consultants Ltd. 1987

[104] WAITE, D. T.; JOSHI, S. R.; SOMMERSTAD, H.: The effect of uranium mine tailings on radionuclide concentrations in Langley Bay, Saskatchewan, Canada. In: *Arch. Environ. Contam. Toxicol.* 17 (1988), pp. 373–380

[105] INTERNATIONAL COMMISSION ON RADIOLOGICAL PROTECTION (ICRP): Dose Coefficients for Intakes of Radionuclides by Workers. ICRP Publication 68. In: *Ann. ICRP* 24 (1994) Issue 4.

[106] INTERNATIONAL COMMISSION ON RADIOLOGICAL PROTECTION (ICRP): Basic Anatomical and Physiological Data for use in Radiological Protection: The Skeleton. ICRP Publication 70. In: *Ann. ICRP* 25 (1995) Issue 2.

[107] INTERNATIONAL COMMISSION ON RADIOLOGICAL PROTECTION (ICRP): Age-dependent Doses to Members of the Public from Intake of Radionuclides: Part 2, Ingestion Dose Coefficients. ICRP Publication 67. In: *Ann. ICRP* 23 (1993) Issue 3/4.

[108] INTERNATIONAL COMMISSION ON RADIOLOGICAL PROTECTION (ICRP): Age-dependent Doses to Members of the Public from Intake of Radionuclides: Part 3, Ingestion Dose Coefficients. ICRP Publication 69. In: *Ann. ICRP* 25 (1995) Issue 1.

[109] GAMOV, G. Z.: In: *Phys.* 51, 204 (1928)

[110] CANBERRA INDUSTRIES (Ed.): *Genie 2000 Spectroscopy System: Operations*. Meriden, CT: Canberra Industries, 2001

[111] CANBERRA INDUSTRIES (Ed.): *Model S509 Genie-2000 Alpha Analyst: User's Manual.* Meriden, CT: Canberra Industries, 2001

[112] CANBERRA INDUSTRIES (Ed.): *Model S570 Genie-2000 Alpha Analyst: User's Manual*. Meriden, CT: Canberra Industries, 2001

[113] CANBERRA INDUSTRIES (Ed.): *Model S570 Genie-2000 Alpha Analyst: Installation Guide*. Meriden, CT: Canberra Industries, 2001

[114] SILL, C. W.; OLSEN, D. G.: Sources and Prevention of recoil contamination of solid-state alpha detectors. In: *Anal. Chem.* 42 (1970), pp. 1596–1607

[115] RODRIGUEZ, P. B.; SANCHEZ, M. A.; VERA TOMÉ, F.: Experimental studies of self-absorption and backscattering in Alpha-particle sources. In: *Appl. Radiat. Isot*. 9 (1997), pp. 1215–1220

[116] JOHANSSON, L.; SIBBENS, G.; ALTZITZOGLOU, T.; DENECKE, B.: Self-absorption correction in standardisation of Tl-204. In: *Appl. Radiat. Isot*. 56 (2002), pp. 199–203

[117] PACKARD INSTRUMENT COMPANY (Ed.): High throughput screening of samples containing alpha and beta radionuclides: An overview of methods. Alpha Beta Application Note ABA-005. Meriden, CT: Packard Instrument Company, 1992

[118] HORROCKS, D. L.: *Applications of Liquid Scintillation Counting*. New York and London: Academic Press, Inc., 1974. –ISBN 0-12-356240-6

[119] A young physicist at seventy: Hartmut Kallmann. In: *Phys. Today* 19 (1966), pp. 51–54

[120] ELLIOTT, J. C.: Effect of vial composition and diameter on the determination of efficiency, background, and quench curves in liquid scintillation counting. In: *Anal. Chem.* 56 (1984), pp. 758–761

[121] WIEL, J. T.; HEGGE, T.: Advances in scintillation cocktails. In: *Liquid scintillation counting and organic scintillators*. 1992, pp. 51–59.

[122] L'ANNUNZIATA, M. F. (Ed.): *Handbook of radioactivity analysis*. 2nd Ed. San Diego, CA: Academic Press, 2003. –ISBN: 0-12-436603-1

[123] KNOLL; G. F.: *Radiation, detection and measurement.* 3rd Edition. Hoboken, NJ: John Wiley & Sons, 1999.

[124] THOMSON, J.: *Use and preparation of quench curves*. Liquid scintillation application note. Perkin Elmer Life Sciences, Inc. 2002

[125] BIRKS, J. B.: In: The theory and practice of scintillation counting. Pergamon, Oxford, 1964. pp. 219–227

[126] VOLTZ, R.; LAUSTRIAT, G.; COCHE, A. In: *Journal de Physique (Paris)*. 29 (1968), p. 159

[127] VOLTZ, R.; DUPONT, H.; LAUSTRIAT, G. In: *Journal de Physique (Paris)*. 29 (1968), p. 297

[128] BIRKS, J. B. In: *IEEE Transactions on Nuclear Science*. NS7-2 (1960), p. 2

[129] RODRIGUEZ BARQUERO, L.; GRAU CARLES, A.: The influence of the primary solute on alpha/beta discrimination. In: *Appl. Radiat. Isot*. 49 (1998), pp. 1065–1068

[130] KATZLBERGER, C.; WALLNER, G.; IRLWECK, K.: Determination of Pb-210, Bi-210 and Po-210 in drinking water. In: *J. Radioanal. Nucl. Chem*. 249 (2001) 1, pp. 191–196

[131] WALLNER, G.: Simultaneous determination of Pb-210 and Pb-212 progenies by liquid scintillation counting. In: *Appl. Radiat. Isot*. 48 (1997) 4, pp. 511–514

[132] GRAHEK, Ž.; ROŽMARIĆ MAČEFAT, M.; LULIĆ, S.: Isolation of lead from water samples and determination of Pb-210. In: *Anal. Chim. Acta* 560 (2006), pp. 84–93

[133] VILLA, M.; HURTADO, S.; MANJÓN, G.; GARCÍA-TENORIO, R.: Calibration and measurement of Pb-210 using two independent techniques. In: *Radiat. Meas*. 42 (2007), pp. 1552–1560

[134] DER BUNDESMINISTER FÜR UMWELT, NATURSCHUTZ UND REAKTORSICHERHEIT (Ed.): *Messanleitungen für die Überwachung der Radioaktivität in der Umwelt und zur Erfassung radioaktiver Emissionen aus kerntechnischen Anlagen*. (Pb-210-TWASS-01). München: Elsevier, 2001. –Losebl. Ausg., Lfg. 7. Stand: 03.2006

[135] UNITED STATES DEPARTMENT OF ENERGY (DOE): Determination of Lead-210 in water using extraction chromatography. RP280. 1997

[136] AL-MASRI, M. S.; HAMWI, A.; MIKHLALLATY, H.: Radiochemical determination of lead-210 in environmnetal water samples using Cerenkov counting. In: *J. Radioanal. Nucl. Chem*. 219 (1997), pp. 73–75

[137] VESTERBACKA, P.; IKÄHEIMONEN, T. K.: Optimization of Pb-210 determination via spontaneous deposition of Po-210 on a silver disk. In: *Anal. Chim. Acta* 545 (2005), pp. 252–261

[138] MIURA, T.; HAYANO, K.; NAKAYAMA, K.: Determination of Pb-210 and Po-210 in environmental samples by alpha ray spectroscopy using an extraction chromatographic resin. In: *Analytical sciences.* 15 (1999), pp. 23–28

[139] BECKER, J. S.; DIETZE, H. J.; MCLEAN, J. A.; MONTASER, A.: In: *Anal. Chem*. 71 (1999), p. 3077

[140] ZORIY, M. V.; PICKHARDT, C.; OSTAPCZUK, P.; HILLE, R.; BECKER, J.S.: In: *Int. J. Mass Spectrom.* 232 (2004) p. 217

[141] LARIVIÈRE, D.; EPOV, V. N.; REIBER, K.M.; CORNETT, R. J.; EVANS, R. D.: In: *Anal. Chim. Acta* 528 (2005), pp. 175

[142] LARIVIÈRE, D.; REIBER, K.M.; EVANS, R. D.; CORNETT, R. J.: Determination of Pb-210 at ultra-trace levels in water by ICP-MS. In: *Anal. Chim. Acta* 549 (2005), pp. 188–196

[143] NORM DIN 38402, Ed. 1986-07. *Probenahme aus Fließgewässern* (A 15) – Part 15: Allgemeine Angaben, Gruppe A.

[144] HAHN, O.: *Vom Radiothor zur Uranspaltung. Eine wissenschaftliche Selbstbiographie.* Braunschweig: Fried. Vieweg & Sohn, 1962.

[145] CASE, G. N.; MCDOWELL, W. J.: An improved sensitive assay for Po-210 by use of a background-rejecting extractive liquid-scintillation method. In: *Talanta* 29 (1982), pp. 845–848

[146] JIA, G.; TORRI, G.; PETRUZZI, M.: Distribution coefficients of polonium between 5 % TOPO in toluene and aqueous hydrochloric and nitric acids. In: *Appl. Radiat. Isot.* (2004), pp. 279–282

[147] CHEN, Q.; HOU, X.; DAHLGAARD, H.; NIELSEN, S. P.; AARKROG, A.: A rapid method for the separation of Po-210 from Pb-210 by TIOA extraction. In: *J. Radioanal. Nucl. Chem.* 249 (2001), pp. 587–593

[148] IBRAHIM, S. A.; WHICKER, F. W.: Plant accumulation and plant/soil concentration ratios of Pb-210 and Po-210 at various sites within a uranium mining and milling operation. In: *Env. Exp. Bot.* 27 (1987), pp. 203–213

[149] REISCHMANN, F.-J.; TRAUTMANN, N.; HERRMANN, G.: Chemistry at low concentrations: polonium at a level of 108 to 105 atoms. In: *Radiochimica Acta*. 36 (1984), pp. 139–143

[150] MOSER, R. N.: A comparison of methods for the determination of the dating-nuclides Pb-210 and Ra-226. In: *J. Radioanal. Nucl. Chem*. 173 (1993), pp. 283–292

[151] CHURCH, T. M.; HUSSEIN, N.; FERDELMAN, T.G.; FOWLER, S. W.: An efficient quantitative technique fort he simultaneous analysis of radon daughters Pb-210, Bi-210 and Po-210. In: *Talanta*. 41 (1994), pp. 243–249

[152] PACER, R.A.: The role of Cherenkov and liquid scintillation counting in evaluating the anion-exchange separation of ^{210}Pb–^{210}Bi–^{210}Po. In: *J. Radioanal. Chem.* 77 (1983), pp. 19–28

[153] SKWARZEC, B.; STRUMINSKA, D. I.; BORYLO, A.: The radionuclides U-234, U-238 and Po-210 in drinking water in Gdansk agglomeration (Poland). In: *J. Radioana. Nucl. Chem.* 250 (2001), pp. 315–318

[154] HORWITZ, E. P.; DIETZ, M. L.; FISHER, D. E.: Correlation of the extraction of strontium nitrate by a crown ether with water content of the organic phase. In: *Solvent Extr. Ion Exch*. 8 (1990), pp. 199–208

[155] HORWITZ, E. P.; DIETZ, M. L.; CHIARIZIA, R.; DIAMOND, H.; MAXWELL S. L.; NELSON, M. R.: Separation and preconcentration of actinides by extraction chromatography using a supported liquid anion exchanger: application to the characterization of high-level nuclear waste solutions. In: *Anal. Chim. Acta.* 310 (1995), pp. 63–78

[156] CHEN, J. H.; WASSERBURG, G. J.: The isotopic composition of uranium and lead in Allende inclusions and meteoritic phosphates. In: *Earth and Planetary Science Letters*. 52 (1981), pp. 1–15

[157] INTERNATIONAL ORGANISATION FOR STANDARDISATION (ISO): *Conical fittings with a 6 % (Luer) taper for syringes, needles and certain other medical equipment. Part 1: General requirements.* ISO 594-1:1986 (Geneva: ISO) (1986)

[158] SILL, C. W.: Determination of radium-226 in ores, nuclear wastes and environmental samples by high-resolution alpha spectrometry. In: *Nucl. Chem. Waste Management*. (1987) 7, pp. 239–256

[159] THAKKAR, A. H.; FERN, M. J.; MCCURDY, D.: A rapid determination of Ra-226 and Ra-224 using extraction chromatography. In: WARWICK, P. (Ed.): *Environmental radiochemical analysis II*. A collection of refereed papers presented at the 9th International Symposium on Environmental Radiochemical Analysis held in Maidstone, Kent, UK in September 2002. London: RSC Publishing, 2003. –ISBN 978-0-85404-263-0

[160] LALLY, A. E.; GLOVER, K. M.: Source preparation in alpha spectrometry. In: *Nucl. Inst. Meth.* 223 (1984), No. 2–3, pp. 259–265

[161] Tracerlab method: Analysis: Pb-210 in water. www.tracerlab.com

[162] CURIE, I. In: *J. Chim. Phys.* (1925) 22, p. 471

[163] FLYNN, W. W.: The determination of low levels of polonium-210 in environmental materials. In: *Anal. Chim. Acta*. (1968) 43, pp. 221–227

[164] SMITH, J. D.; HAMILTON, T. F.: Improved technique for recovery and measurement of polonium-210 from environmental materials. In: *Anal. Chim. Acta*. (1984) 160, pp. 69–77

[165] HÄSÄNEN, E.: Dating of sediments, based on Po-210 measurements. In: *Radiochem. Radioanal. Letters.* (1977) 31, No. 4–5, pp. 207–214

[166] FLEER, A. P.; BACON, M. P.: Determination of Pb-210 and Po-210 in seawater and marine particulate matter. In: *Nucl. Instruments and Methods in Physics Research*. (1984) 223, pp. 243–249

[167] BENEDIK, L.; VREČEK, P.: Determination of Pb-210 and Po-210 in environmental samples. In: *Acta Chim. Slov.* (2001) 48, pp. 199–213

[168] BLANCHARD, R. L.: Rapid determination of lead-210 and polonium-210 in environ mental samples by deposition on nickel. In: *Anal. Chem.* (1966) 38, pp. 189–192

[169] EHINGER, S. C.; PACER, R. A.; ROMINES, F. L.: Separation of the radioelements Pb-210, Bi-210 and Po-210 by spontaneous deposition onto noble metals and verifi

cation by Cerenkov and liquid scintillation counting. In: *J. Radioanal. Nucl. Chem.* (1986) 98, pp. 221–227

[170] INTERNATIONAL ORGANISATION FOR STANDARDISATION (ISO): *Determination of the detection limit and decision threshold for ionizing radiation measurements – Part 7: Fundamentals and general applications*. ISO 11929-7 (Geneva: ISO) (2005)

[171] INTERNATIONAL ORGANIZATION FOR STANDARDISATION (ISO): *Guide to the expression of uncertainty in measurement* (GUM) (Geneva: ISO) (1993), corrected reprint (1995) – ISBN 92-67-10188-9

[172] WEISE, K.; HÜBEL, K.; ROSE, E.; SCHLÄGER, M.; TÄSCHNER, M.; MICHEL, R.: Bayesian decision threshold, detection limit and confidence limits in ionising radiation measurement. In: *Radiat. Prot. Dosi.* 121 (2006), pp. 52–63

[173] GANS, I.; FUSBAN, H. U.; WOLLENHAUPT, H.; KIEFER, J.; GLÖBEL, B.; BERLICH, J.; PORSTENDÖRFER, J.: *Ra-226 und andere Radionuklide im Trinkwasser und in Getränken in der Bundesrepublik Deutschland*. Schriftenreihe des Instituts für Wasser-, Boden- und Lufthygiene des Bundesgesundheitsamtes, WaBoLu-Heft 4/1987

[174] VANDENHOVE, H.; PARIDAENS, J.; AITKULOV, A.; IMANAKUNOV, S.; NARAVAGOV, A.; SAVOSIN, M.; TORGOEV, I.; MIRZACHEV, M.; MOMBEKOV, O.; ZEEVAERT, TH.; VANMARCKE, H.: 2002. Mailuu Suu tailings problems and options for remediation. In: MERKEL, B.J., PLANER-FRIEDRICH, B.; WOLKERSDORFER, C. (Eds.): *Uranium in aquatic environment: Proceedings of the international conference on uranium mining and hydrology III and the international mine water association symposium, Freiberg, Germany 15–21 Sept 2002*. Berlin, Springer, pp. 821–829.

[175] VANDENHOVE, H.; QUARCH, H.; CLERC, J. J.; LEJEUNU, J. M.; SWEECK, L.; SILLEN, X.; MALLANTS, D.; ZEEVAERT, TH.: Final report in frame of EC-TACIS project N° SCRE1/N° 38 remediation of uranium mining and milling tailing in Mailuu-Suu District Kyrgyzstan, R-3721. SCK CEN, Mol, Belgium (2003)

[176] VANDENHOVE, H.; SWEECK, L.; MALLANTS, D.; VANMARCKE, H.; AITKULOV, A.; SADYROV, M.; SAVOSIN, M.; TOLONGUTOV, B.; MIRZACHEV, M.; CLERC, J. J.; QUARCH, H.; AITALIEV, A.: Assessment of radiation exposure in the uranium mining and milling area of Mailuu Suu, Kyrgyzstan. In: *J. Environ. Radioactivity.* 88 (2006), pp. 118–139

[177] KRIŽMAN, M.; BYRNE, A. R.; BENEDIK, L.: Distribution of ^{230}Th in milling wastes from the Zirovski vhr Uranium mine (Slovenia), and its radioecological implications. In: *J. Environ. Radioactivity.* 26 (1995), pp. 223–235

[178] BERECHNUNGSGRUNDLAGEN ZUR ERMITTLUNG DER STRAHLENEXPOSITION INFOLGE BERGBAULICHER UMWELTRADIOAKTIVITÄT (Berechnungsgrundlage Bergbau), Stand 30.07.1999

[179] STRAHLENSCHUTZVERORDNUNG (StrlSchV), 20.06.2001, Anlage VII

[180] COUNCIL OF THE EUROPEAN UNION: Council Directive 98/83/EC of 3 November 1998, On the quality of water intended for human consumption

[181] WORLD HEALTH ORGANISATION (WHO): Guidelines for drinking water quality. 3rd Ed. Geneva (WHO): 2004

[182] GELLERMANN, R. *et al.*: *Radiologische Bewertung der Grubenwässer-Einleitungen des Steinkohlebergbaus im Bereich Fossa-Eugeniana – Abschlussbericht*. HGN Hydrogeologie GmbH, Madgeburg. 31.03.2006

[183] WANKE, C.: *Erhöhte Strahlenexpositionen der allgemeinen Bevölkerung als Folge bergbaulicher Aktivitäten*. Hannover, Gottfried Wilhelm Leibniz Universität, Fachbereich Physik, Dissertation, 2008